Thermo-Mechanical Behaviour of A Novel Lightweight Concrete and Its Application In Masonry Walls

A thesis submitted to the University of Manchester for the degree of

Doctor of Philosophy

in the Faculty of Engineering and Physical Sciences

2012

Adnan Flayih Hassan Al-Sibahy

School of Mechanical, Aerospace and Civil Engineering

Abstract

Thermo-mechanical behaviour of a novel lightweight concrete and its application in masonry walls

Adnan Flayih Hassan Al-Sibahy, 2012

Doctor of Philosophy, The University of Manchester

The development of lightweight concretes has made a contribution to advances in structural design. It would be useful to further improve the mechanical properties of lightweight concrete formulations whilst enhancing their resistance to fire degradation and reduced thermal conductivity. Improving the sustainability of any new proposed lightweight concrete formulation is desirable, for example by the inclusion of waste stream components into the formulation.

This thesis describes an investigation of the mechanical, thermal and fire resistance properties of a new type of expanded clay lightweight concrete formulation in which varying quantities of sand are replaced by crushed glass aggregate, in conjunction with the addition of metakaolin (which may be available as a waste component from the manufacture of paper) as a partial replacement for the cement. The investigation involved short and long-term laboratory testing of a range of mechanical and thermal properties of individual concrete formulations and small scale structural elements consisting of masonry blocks made from these formulations (so called wallettes). An extensive programme of Finite Element Analysis using Abaqus was also performed.

The results obtained show that it is possible to produce a structural expanded clay lightweight concrete that possesses good thermal properties by incorporating of ground glass and metakaolin. Compressive and splitting tensile strengths, as well as the modulus of elasticity, increased with an increase in the metakaolin content, while concrete density decreased. Reductions in thermal conductivity and improvements in fire resistance criteria were also observed in comparison with conventional lightweight concrete mixtures. For example, measured thermal conductivity values ranged from 0.092 W/m.K to 0.177 W/m.K, and the insulation criterion (an indicator of resistance to fire) reached up to 110 minutes for a concrete member with a thickness of 29 mm. The highest resistance to the effects of high temperatures was observed for concrete mixes containing either 15% or 30% recycled glass with 10% metakaolin.

The maximum axial loads at failure were 474 kN and 558 kN for reference and modified wallettes respectively, implying corresponding bearing capacities of 7.1 MPa and 8.3 MPa. The critical path of the failure mode was similar for all of the wallettes tested and normally began underneath the load point, then passed through the concrete blocks and head joint to reach the toe of the wallette. The masonry wallettes formulated using reference lightweight concrete blocks exhibited failure due to explosive spalling at 400 ^{o}C with no applied mechanical load, whereas the second type of masonry wallettes (the modified wallettes) did not show such behaviour.

The results of Finite Element Analysis showed that the coefficient of thermal convection had the most influence upon the insulation criterion. From a structural perspective, the key parameters were the value of penalty stiffness and imperfections in wallette construction. In general, a close agreement between the measured and simulated results was observed for both the thermal and structural finite element models at ambient and high temperatures.

Declaration

No portion of the work referred to in the thesis has been submitted in support of an application for another degree or qualification of this or any other university or other institute of learning.

Copyright Statement

To the soul of my father

To my mother, who spent sleepless nights in order to grant me such devotion

To my sincere wife, brothers and sisters for their help and support

To my young daughters Abrar and Hawraa

Adnan

Acknowledgements

The author would like to offer heartfelt thanks to Dr. Rodger Edwards for his supervision and professional guidance throughout the whole period of study here at the University of Manchester. His helpful comments and continued support had an essential role in completing this thesis. The technical assistance of the laboratory staff at the University of Manchester is greatly appreciated especially that provided by John Mason, Paul Nedwell, Paul Townsend, Phil Oakes and Gordon Lester. Many thanks to Prof. Hana Yousif at the University of Akron, US for her scientific comments and advice during the period of writing the first article for publication.

The author is grateful for the scholarship awarded by the Iraqi Ministry of Higher Education and Scientific Research. Special thanks to the Plasmor Concrete Product Company for providing the expanded clay and technical guidance.

The sincere fraternity, help and encouragement of Drs Jalal Al-Obaedi, Khalid Al-Farhany, Tumadhir Borhan, Hathaim Al-Thairy, Ahmed Majhool and Basim Al-Humeidawi are greatly appreciated. Many thanks also for the encouragement provided by the Iraqi students at both Manchester and Salford Universities.

Publication and submitted papers

The following is a list of the author's publications and submitted papers relating to the context of the current thesis; see Appendix (A).

Journal papers

1. Al-Sibahy A., Edwards R. Mechanical and thermal properties of novel lightweight concrete mixtures containing recycled glass and metakaolin. *Construction and Building Materials*, 31: 157-167, 2012.

2. Al-Sibahy A., Edwards R. Thermal behaviour of novel lightweight concrete at ambient and elevated temperatures: Experimental, modelling and parametric studies. *Construction and Building Materials*, 31: 174-187, 2012.

3. Al-Sibahy A., Edwards R. Behaviour of masonry wallettes made from a new concrete formulation under combination of axial compression load and heat exposure: experimental approach. *Engineering Structures*, 48: 193-204, 2013.

4. Al-Sibahy A., Edwards R. Behaviour of masonry wallettes made from a new concrete formulation under compression loads at ambient temperatures: Testing and modelling *(Submitted to Engineering Structures on 3 May 2012)*.

Conference papers

1. Al-Sibahy A., Edwards R. *Structural behaviour of new developed lightweight concrete masonry walls*. 12th SPARC Conference, The University of Salford, May 2012.

2. Al-Sibahy A., Edwards R. *Structural behaviour of new masonry lightweight concrete wallettes at high temperatures*. Postgraduate Research Conference, The University of Manchester, December 2011: 1-2.

3. Al-Sibahy A., Edwards R. *Thermo-mechanical behaviour of new combination of lightweight aggregate concrete mixtures*. Conference of Engineering Sciences. Iraqi Cultural Attaché-London, October 2011.

4. Al-Sibahy A., Edwards R. *Thermo-mechanical behaviour of new combination of lightweight aggregate concrete mixtures*. 31st Cement and Concrete Science Conference (Novel Devel-

opments and Innovations in Cementitious Materials). Imperial College London, September 2011: PP8.

5. Al-Sibahy A., Edwards R. *Mechanical behaviour of high metakaolin lightweight aggregate*. International Conference of Computational Methods and Experimental Measurements XV. Wessex Institute of Technology, May 2011: 85-96.

6. Al-Sibahy A., Edwards R. *A new method of producing lightweight aggregate concrete*. Postgraduate Research Conference, The University of Manchester, July 2010: 43.

Contents

List of Figures

List of Tables

Nomenclature

Except for the symbols which are defined in their places when they appear in the text and for those with a clear meaning, the following list defines the Roman and Greek symbols in addition to the Abbreviations used throughout the thesis. The basic units are given for their corresponding Roman and Greek symbols.

Roman Symbols

A_c	Compression area	mm^2
$A_{\theta 1}$	Area of masonry up to temperature of $\theta 1$	mm^2
$A_{\theta 2}$	Area of masonry up to temperature of $\theta 2$	mm^2
c	Constant obtained from stress-strain tests at elevated temperatures	-
D	Diameter of the cylindrical sample	mm
d_c	The degradation of the elastic stiffness in compression state	mm
d_t	The degradation of the elastic stiffness in tension state	mm
E_c	Modulus of elasticity	GPa
F	Maximum load at failure	N
f_c	Compressive strength	MPa
f_t	Splitting tensile strength	MPa
$f_{d\theta 1}$	Design compressive strength of masonry up to $\theta 1$	MPa
$f_{d\theta 2}$	Design compressive strength of masonry between $\theta 1$ and $\theta 2$, taken as $cf_{d\theta 1}$	MPa
h	Initial height of wall	mm
h_{ef}	Effective height of wall	mm
$\dot{h}_{net,c}$	Net convective heat flux component	W/m^2
$\dot{h}_{net,r}$	Net radiative heat flux component	W/m^2
k	Thermal conductivity	W/m.K

L	Diameter of the cylindrical sample	mm
x	Thickness	mm

Greek Symbols

ε	Strain	-
σ_a	Upper loading stress	MPa
σ_b	Basic stress	MPa
ε_a	Mean strain under the upper loading stress	-
ε_b	Mean strain under the basic stress	-
$\varepsilon_{Lateral}$	Lateral strain	-
$\varepsilon_{Vertical}$	Vertical strain	-
ε_m	Surface emissivity of the member	-
ε_f	Emissivity of fire	-
θ	Temperature	^{o}C
θ_g	Temperature of gas in the vicinity of the member exposed to fire	^{o}C
θ_m	Surface temperature of the member	^{o}C
θ_r	Effective radiation temperature of the fire environment	^{o}C
$\theta 1$	Temperature up to which the cold strength of the masonry wall may be used	^{o}C
$\theta 2$	Temperature above which the material has no residual strength	^{o}C
σ	Stefan Boltzmann constant	W/m^{2}K^4
α_c	Coefficient of convection heat transfer	W/m^{2}K
ϕ	Capacity reduction factor in the middle of the wall	-
ρ	Density	kg/m^3

Abbreviations

G	Recycled glass
MK	Metakaolin
R	Reference concrete mix without recycled glass and metakaolin

M	Modified concrete mix incorporating recycled glass and metakaolin
45%G+0%MK	Concrete mix containing 45% recycled glass and 0% metakaolin
15%G+5%MK	Concrete mix containing 15% recycled glass and 5% metakaolin
30%G+5%MK	Concrete mix containing 30% recycled glass and 5% metakaolin
45%G+5%MK	Concrete mix containing 45% recycled glass and 5% metakaolin
15%G+10%MK	Concrete mix containing 15% recycled glass and 10% metakaolin
30%G+10%MK	Concrete mix containing 30% recycled glass and 10% metakaolin
45%G+10%MK	Concrete mix containing 45% recycled glass and 10% metakaolin

Chapter 1

Introduction

1.1 Background

Lightweight concrete has been widely used in different structural applications and its consumption grows every year on a global basis [1]. The reason for this is that using lightweight concrete has many advantages. These include: a reduction in the dead load of the building, which minimizes the dimensions of structural members; the production of lighter and smaller pre-cast elements with inexpensive casting, handling and transportation operations; the provision of more space due to the reduction in size of the structural members; a reduction in the risk of earthquake damage; and increased thermal insulation and fire resistance [1–3].

Among the multiple construction applications, masonry structures form the largest proportion of the uses of lightweight concrete. In the UK, the total production of concrete blocks intended for the construction of masonry walls reached about 54648 thousand square metres in 2011, 30% of which were lightweight varieties [4]. Such utilization provides improved thermal insulation and fire resistance, thereby it is considered an effective approach not only in fire protection but also in reducing the U-values of structures.

Lightweight concrete can be produced in a apractical range of densities between about 300 and 1850 kg/m^3, using three methods. The first is so-called no fines, where the fine portion (sand particles) of the total concrete aggregate is omitted. The second method is by introducing stable air bubbles inside the concrete body through mechanical foaming and chemical admixture.

This type of concrete is known as aerated, cellular or gas concrete. The third and most popular method is by using lightweight aggregate. This may come from either a natural or an artificial source [5]. The third method is addressed in this thesis by means of the use of expanded clay.

Expanded clay is one example of an artificial lightweight aggregate. It has fragile, closed internal micro-cavities, which enhance thermal insulation properties [6].

During the last decade, the trend towards environmentally friendly construction has grown, and with a wide range of associated research. Part of this research activity has involved the exploration of possible uses for recycled material streams. For example, waste glass forms one of the primary sources which affects the environment. Each year in the UK, households throw away over 29.1 million tonnes of waste, 4.2% of which is glass [7]. Recycling glass therefore makes an important contribution to overall sustainability. In the case of construction, there are several options for making use of waste glass and other by-product materials in concretes.

In practice, the inclusion of crushed or ground glass in concrete mixes as an entire or partial replacement for aggregate is of growing interest. This operation reduces the demand on natural resources for construction materials and provides multiple alternatives to the traditional ingredients of concrete mixes [6, 8, 9].

However, in many applications involving recycled waste glass, a slight increase in the expansion of the concrete was observed, due to the alkali-silica reaction triggered in this process. It has also been observed that if pozzolanic additions are made to mixes containing glass, the alkali-silica reaction is significantly diminished [6].

Some studies have reported that metakaolin is a versatile mineral admixture [10, 11]. It has high pozzolanic activity and can be produced by the calcination of waste sludge from the paper recycling industry [12].

To date, several developments in the field of construction materials have emphasised the importance of improving the thermo-mechanical behaviour of concrete elements. However, no work seems to have been conducted that is concerned with the behaviour of lightweight concrete formulated using the by-product materials glass and metakaolin in conjunction with expanded clay aggregate. Nor has the application of this formulation been investigated in load-bearing masonry walls at either ambient or elevated temperatures.

1.2 Research objectives

This study aims to investigate the thermal and mechanical properties of a new combination of structural lightweight concrete and its application as load-bearing masonry walls at ambient and high temperatures, using both experimental and modelling approaches. This kind of lightweight concrete contains different percentages of recycled glass and metakaolin as a partial replacement for natural sand and Portland cement respectively. In order to achieve the main aim of this research, the objectives are identified in detail below:

1. Investigate the enhancement of the mechanical strength of the reference (expanded clay) lightweight concrete when recycled glass and metakaolin are added at both ambient and high temperature conditions through an experimental programme. This investigation is associated with an evaluation of the key factors governing the overall mechanical behaviour of the formulated lightweight concrete mixes. A comparison with some standard expressions for predicting the mechanical behaviour of lightweight concrete will also be included in this investigation.

2. Investigate, through an experimental programme, the improvement of the thermal behaviour of the reference lightweight concrete in terms of its thermal insulation and durability against the effect of high temperatures by the inclusion of different percentages of recycled glass and metakaolin materials.

3. Investigate the ultimate amount of by-product materials (recycled glass and metakaolin) which can be used to produce the modified lightweight concrete mixes without adversely affecting their thermo-mechanical behaviour at both ambient and elevated temperatures.

4. Develop a reliable finite element model to simulate the thermal behaviour of both the reference and modified lightweight concrete mixes. This allows for the evaluation of the most influential parameters on heat transfer through these types of lightweight concrete

mixes at high temperatures.

5. Investigate, through an experimental programme, the structural application of the reference and developed lightweight concrete mixes as load-bearing masonry walls in terms of load-bearing capacity, deformation and failure mode criteria under axial compression loads at both ambient and high temperatures.

6. Evaluate, through numerical modelling, the key parameters which affect the behaviour of masonry walls under axial compression loads at both ambient and high temperatures. This evaluation will be based upon a developed finite element model which will be validated against the experimental measurements.

1.3 Outline of the thesis

This thesis is divided into eleven chapters. Following this introductory chapter, Chapter 2 provides a review of the literature relevant to the research presented within this thesis. Specifically, there is a review of the mechanical and thermal behaviour of lightweight aggregate concretes at both ambient and high temperatures. Replacement techniques for concrete constituents and thermo-mechanical behaviour of masonry walls have also been addressed, as well as the numerical simulation of thermal and structural behaviours.

Chapter 3 presents the strategies for selection of the appropriate reference expanded clay structural lightweight concrete and the development approaches for producing the modified lightweight concrete mixes using by-product materials. This process is based upon mix design methodology and trial mixes. It should be noted that most of the technical content of this chapter has already been published within the Journal of Construction and Building Materials [13] as well as within the International Conference of Computational Methods and Experimental Measurements XV [14].

Chapter 4 deals with the experimental investigation of the mechanical properties of the reference and modified lightweight concrete mixes at ambient temperatures. The results obtained are then discussed to identify the overall mechanical behaviour of these mixes. This part of the thesis has been published within the Journal of Construction and Building Materials [13].

Chapter 5 deals with the thermal properties of the lightweight concrete mixes at temperatures ranged from 20 ^{o}C to 800 ^{o}C. The main thermal properties such as density, thermal conductivity, specific heat and heat flow are measured experimentally and discussed in detail. The findings presented within this chapter have been published within the Journal of Construction and Building Materials [15] and within the 31st Cement and Concrete Science Conference "Novel Development and Innovation in Cementitious Materials" [16].

The development of a reliable finite element model to simulate the thermal behaviour of the lightweight concrete mixes is presented in Chapter 6. The main constituents of the numerical model are described and its implementations are then investigated. Most of the findings described within this chapter have been published within the Journal of Construction and Building Materials [15].

In Chapter 7, a strategy for optimising the modified lightweight concrete mixes and its structural applications is developed and applied. This achieved through the selection of masonry wallettes as an appropriate structural element to be adopted in this research. The findings described within Chapter 7 have been submitted to the Journal of Engineering Structures.

The behaviour of the reference and modified masonry wallette samples under conditions of ambient temperature and axial compression load is addressed in Chapter 8. This involves conducting a wide experimental programme to evaluate the load-bearing capacity, deformation and failure mode criteria. The findings presented in this chapter have been submitted to the Journal of Engineering Structures. In addition, some parts of this chapter have been presented and published within the Postgraduate Research Conference [17] as well as within the SPARC 12 Conference [18].

Chapter 9 describes an experimental methodology for the investigation of the behaviour of reference and modified masonry wallette samples under conditions of high temperatures and axial compression loads, together with the results obtained. Significant parts of Chapter 9 have been published within the Journal of Engineering Structures [19]. Moreover, some parts of this chapter are also presented and published in the Postgraduate Research Conference [17].

The numerical simulation of the structural behaviour of the masonry wallettes under conditions of axial compression loads at both ambient and high temperatures are presented in Chapter 10. The pure thermal behaviour of the masonry wallettes is also simulated through individual numerical model. In both structural and pure thermal models, the strategy for developing a reliable numerical simulation approaches are described and discussed. Most of the findings within this chapter have been submitted to the Journal of Engineering Structures. In addition, some parts of this research has also been presented and published in the Postgraduate Research Conference [17] and the SPARC 12 Conference [18].

Finally, Chapter 11 covers the main conclusions which emerge throughout this study. The limitations and conditions of this research and the suggestions for further studies are also presented in this chapter.

Chapter 2

Literature review

2.1 Introduction

A review of the literature relevant to the context of the main topics raised throughout this thesis is presented in this chapter. Eight categories of subject matter are identified in order to describe their fundamental concepts. These include the mechanical and thermal behaviours of lightweight aggregate concretes at ambient and high temperatures, replacement techniques for the concrete constituents, the behaviour of masonry walls as load-bearing structural members when exposed to various temperatures as well as the numerical simulation of both the thermal and structural behaviours of lightweight concrete and masonry walls. The main conclusions derived from previous studies are then reported at the end of the chapter.

2.2 Mechanical behaviour of lightweight aggregate concrete

A considerable amount of literature has been published on the mechanical properties of lightweight concrete. These studies covered a wide range of lightweight concretes used in practical applications. Most of the general principles were drawn up based upon experimental investigations.

Unlike normal weight aggregate, lightweight aggregate has a tendency to absorb large amounts of water. Such behaviour affectes the density of lightweight concrete due to the resultant increase in the specific gravity of the aggregate when it absorbs the water [5]. For the purposes of producing lightweight concretes and mix design, the quantity of water absorbed by aggregate particles should be calculated. Consequently, the water/cement ratio is defined by the effective water content in the mix.

Lightweight concrete usually has a lower mechanical strength than normal weight concrete. This is related to the nature of aggregate being used in the lightweight concrete, which is characterised by low strength. In addition, at a specific level of compressive strength, lightweight concrete needs a high cement content in comparison with normal weight concrete. This behaviour becomes more pronounced at higher values of compressive strength, as shown in Figure 2.1.

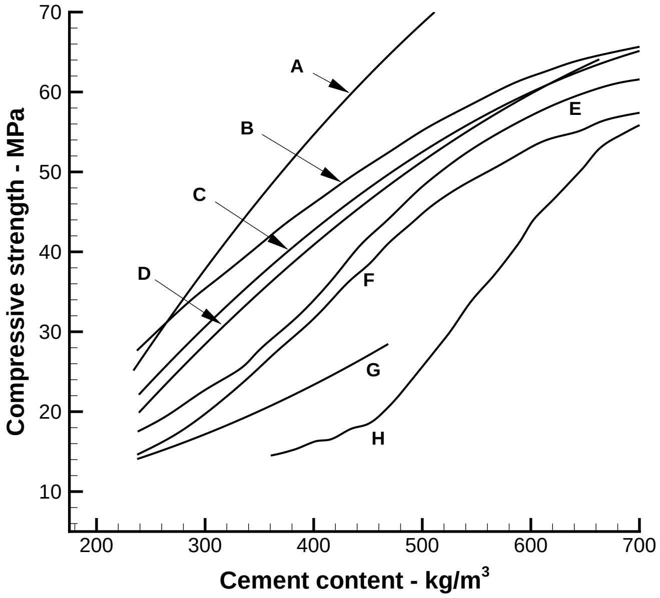

Figure 2.1: The relationship between compressive strength and cement content at 28 days age for normal weight and various lightweight aggregate concretes with a slump of 50 mm: (A) normal weight concrete determined according to the British design method for uncrushed aggregate with a maximum size of 20mm [20]; (B) sintered fly ash and normal weight fine aggregate; (C) pelletized blastfurnace slag and normal weight fine aggregate; (D) sintered fly ash; (E) sintered shale; (F) expanded slate; (G) expanded clay and sand; (H) expanded slag [5]

The effect of particle size of lightweight aggregate on mechanical strength is not as apparent as in normal weight concrete. In addition to the strength of cement mortar which is similar in the cases of both concretes, the volume fraction of lightweight aggregate has an important effect on the role of particle size. Chen et al. [21] have found that the compressive strength of the expanded shale lightweight concrete increases as the maximum size of the aggregate particles decreases. This increase can be as much as 40% when a particle size of 12.5 mm is used instead of 19 mm for the lightweight concrete mix, with a density ranging from 500 to 800 kg/m^3. Whatever the case, this increase is limited by the total porosity (volume fraction) of lightweight aggregate within the concrete mix [22]. When the amount of porosity becomes close to 25%, no significant effect is observed. This behaviour may be explained by the lower stiffness of lightweight aggregate phase compared with the mortar matrix, which is equal to approximately one quarter of the stiffness of the latter [45]. However, some studies stated that using a combination of 40% medium (4-8mm) and 30% of both fine (0-4mm) and coarse (8-16mm) particle sizes produces the highest value of compressive strength [23].

The pores of the interfacial zone between the cement paste and aggregate phase have a noteworthy influence on the mechanical strength of lightweight concrete. As the number of pores increase, so the mechanical strength decreases. This is related to the bond strength of the interfacial zone, which is affected by an increasing number of pores [24]. Previous studies have reported that the bond strength between the cement paste and aggregate phase is higher for lightweight concrete than for normal concrete. This behaviour results from the ability of lightweight aggregate to permit the infiltration of some cement paste into the open surface pores [5].

In general, the influence of interfacial zone pores is governed by two parameters, namely the size of the lightweight aggregate particles and the water/cement ratio. Tommy et al. [24] conducted an experimental programme to investigate the influence of the aforementioned parameters. Pelletized lightweight aggregates from heated clay with three particle sizes of 5 mm, 15 mm and 25 mm were used. The particles had corresponding crushing strengths of 4.27 MPa, 5.79 MPa and 1.69 MPa respectively. Three different W/C ratios were used to produce the lightweight concrete mixes, namely 0.4, 0.44 and 0.48. The results obtained are presented in Figure 2.2.

The authors pointed out that the number of pores for the concrete mixes with particle sizes of 5 mm and 25 mm increase with the W/C ratio due to remaining air voids after the consumption of water. Except for the behaviour of the concrete mix containing particles size of

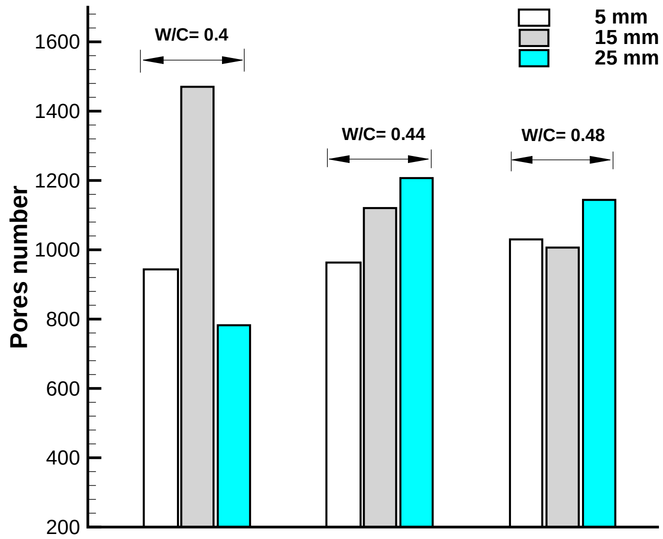

Figure 2.2: The effect of aggregate particle size and W/C ratio on the number of pores within the interfacial zone [24]

15 mm with W/C=0.4, no clear explanation was made for decreasing the number of pores within the interfacial zone of the concrete mix containing aggregate particles of the same size at W/C ratios of 0.44 and 0.48. However, one possible explanation can be offered. This is by taking into consideration both the pore system of the lightweight aggregate and the volume/surface ratio of the aggregate particles [5]. These features have a notable influence on the composite structure of lightweight concrete and normally decrease with increasing crushing strength of the lightweight aggregate.

Commonly, both the tensile strength and modulus of elasticity of lightweight concrete are expressed as a function of compressive strength. Some empirical relationships were derived based upon the level of compressive strength and the type of lightweight aggregate used. For example, Rossignolo et al. [25] performed an experimental study to investigate the mechanical behaviour of high performance expanded clay lightweight concrete. The results obtained showed that the ratios of tensile strength and modulus of elasticity to compressive strength were lower than those of normal weight concrete. The following equations were reported as relations between the aforementioned features.

$$f_t = 0.1 f_c - 1.2 \tag{2.1}$$

$$E_c = 0.12 f_c + 7.5 \tag{2.2}$$

Occasionally, the modulus of elasticity is defined by both the density and compressive strength of lightweight concrete. Such an approach is related to the interactive relationship between these aspects. Smadi and Migdady [26] have found Equation 2.3 to have the best correlation for fitting the test results of tuff lightweight concrete.

$$E_c = (0.08 + 0.03\sqrt{f_c})\rho^{1.5} \tag{2.3}$$

In general, the failure of the lightweight concrete under splitting tensile load takes place within the lightweight aggregate phase, whereas it usually occurs at the interfacial zone for normal weight concrete [5]. This is an indication of the strong bond between the cement paste and lightweight aggregate, as mentioned earlier.

2.3 Replacement techniques for concrete constituents

Recently, different approaches have been fostered in order to develop the constituents of traditional concrete. Replacing one or more of the ingredients of lightweight concrete is one of these approaches. The motivation of such an approach is to modify a specific property, to enhance environmental credentials, or both. Several attempts have been made to evaluate the mechanical behaviour of concrete mixes produced by this formulation.

In terms of normal weight concrete, Limbachiya [27] investigated the possibility of using washed glass as a partial substitute for natural sand up to 50% with a glass particle size of less than 5 mm. The source of crushed waste glass was a melange of different glass colours with a relative density of between 8% and 13% less than that of natural sand. All other constituents were held constant. Both fresh and hardened properties of concrete mixes were experimentally examined. The test results showed that the addition of crushed glass reduces the workability of fresh concrete; nevertheless, it was within the acceptable range of 25 mm (slump). The compressive strength decreases with an increase in glass content of more than 20%, as shown in Figure 2.3a. This behaviour was explained by means of a weak interfacial bond of the crushed glass-cement matrix in addition to the development of cracks within the glass phase. The same approach was also followed by Ismail and Al-Hashmi [28], but the upper limit of the amount of natural sand that could be replaced by recycled glass was 20% and the glass particle size was about 1.2 mm. The results obtained confirmed the reduction in the workability of fresh concrete observed by Limbachiya [27]. However, in the case of compressive strength, except at an age of 14 days, contrasting behaviour was noted, where the compressive strength increased when the 20% glass content was used, as shown in Figure 2.3b. The percentage increases were about 8%, 2% and 4.5% at ages of 3, 7 and 28 days respectively. The reason for this was attributed to the pozzolanic activity of the fine glass particles. The same cannot be said for the case of large glass particles (5 mm) which had already been used by Limbachiya [27].

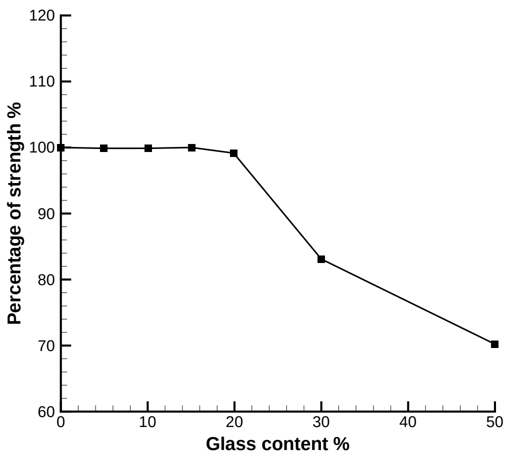

(a)

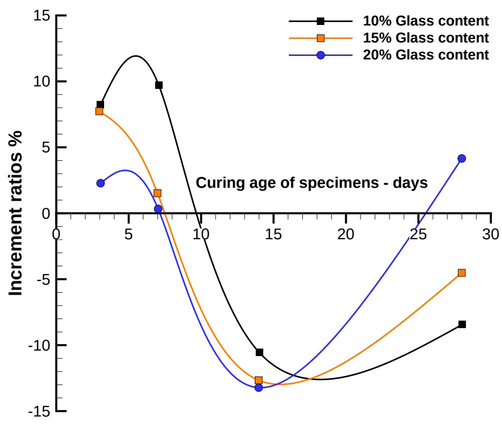

(b)

Figure 2.3: The effect of using recycled glass as a partial replacement for natural sand on the mechanical strength of normal weight concrete: (a) compressive strength at 28 days age [27]; (b) increment ratios in compressive strength at various ages[28]

Except for the research of Petrella et al. [6], there was no published study regarding the use of recycled glass in the applications of lightweight concretes. In the aforementioned research, two particle sizes of recycled glass were used as an aggregate to produce the lightweight concrete mixes, namely 0.5-2 mm and 2-16 mm. The volume fraction of the fine aggregate phase (0.5-2 mm) was divided to be in equal amounts of nominal particle size of 0.5-1 mm and 1-2 mm. The coarse aggregate phase (2-16 mm) was fabricated as a mixed volume fraction. In addition to recycled glass, expanded clay and gravel were also used as aggregate constituents with a similar particle size to that of the recycled glass. Based upon the type of aggregate used and the particle size, six series of lightweight concrete mixes were investigated, as shown in Table 2.1.

Table 2.1: Details of the lightweight concrete mixes [6]

Lightweight concrete code	Fine aggregate with particle size of 0.5-2 mm	Coarse aggregate with particle size of 2-16 mm
A	Waste glass	Waste glass
B	Waste glass	Gravel
C	Expanded clay	Expanded clay
D	Expanded clay	Gravel
E	Waste glass	Expanded clay
F	Expanded clay	Waste glass

The results obtained indicated that the strength level was in descending order for the concrete samples C, E, F and A. The corresponding compressive strength values at 28 days age were 17.9 MPa, 13.5 MPa, 7.4 MPa and 4.2 MPa respectively. The density of both concrete samples type B and D exceeded the limit required for lightweight concrete (1850 kg/m^3), hence they behaved like a normal weight concrete. The enhanced strength level resulting from the combination of recycled glass and/or expanded clay was attributed to the pozzolanic role of these materials which was enhanced at finer particle sizes. Nevertheless, the pozzolanic activity was higher for the expanded clay grains. On the whole, the role of recycled glass in the lightweight concrete was identical to that observed in normal weight concrete.

The issue of alkali-silica reaction (ASR) is worthy of research when the recycled glass is used as a full or partial substitute for fine or coarse aggregate. This reaction takes place between the alkali components of cement (Na_2O or K_2O) and the active silica constituent of the aggregate.

It may cause the aggregate particles to debond from the surrounding cement paste due to the high expansion which occurs within the aggregate particles [5].

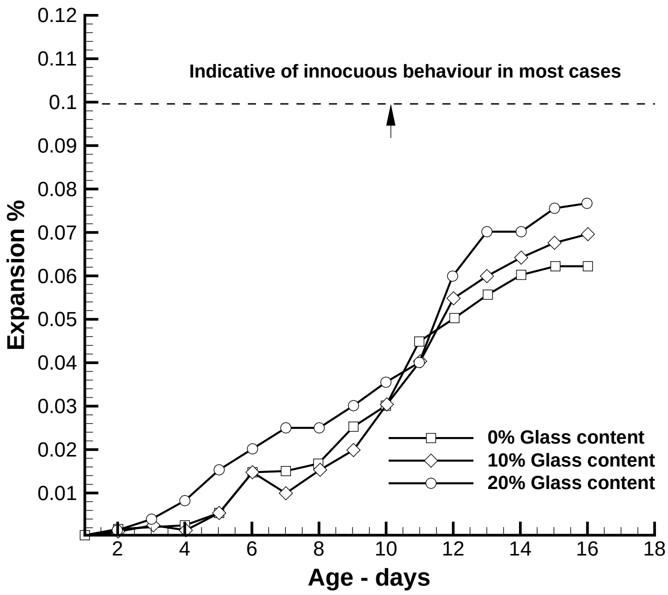

Figure 2.4: The effect of recycled glass on the expansion of the mortar bar [27]

The DD 249:1999 [29] set limits for such expansion as no more than 0.1% of the initial length for a mortar bar specimen. Based upon the aforementioned specification, in his study of a normal weight concrete, Limbachiya [27] found that the expansion of a mortar bar below that limit would not exhibit deleterious swelling (0.1%) due to ASR, as shown in Figure 2.4. Very similar results were also observed by Ismail and Al-Hashmi [28].

In order to identify the actual influence of recycled glass on ASR, Xie et al. [30] conducted a comprehensive experimental study by replacing 10% of the natural sand content with recycled glass. The results obtained revealed that the substitution of finer particles of natural sand with an equivalent particle size of recycled glass kept the expansion of the mortar bar lower than the specified limit of no more than 0.1% . Identical behaviour was also observed by Rajabipour et al. [31]. Such behaviour was explained by the pozzolanic role of the fine glass particles [30]. In early work, it was speculated that ASR only occurs in the presence of Ca^{++} ions [5]. On this basis, pozzolanic materials are preferable in such cases as they tend to mitigate the concentration of calcium ions in the hydration products.

Due to its high pozzolanic potential, metakaolin material is usually classified as a possible mineral admixture for concrete mixes [10]. Several improvements in the characteristics of produced concrete can be achieved when this material is used [32]. Normally, the inclusion of metakaolin is intended as a partial replacement for cement [10, 32, 33] .

Previous studies have reported that the metakaolin is manufactured by the calcination of kaolinitic clay ($Al_2Si_2O_7$) at temperature between 650 ^oC-800 ^oC [9–11, 32, 33] or the calcinations of waste sludge from the paper recycling industry [11, 12]. Typically, it has a surface area about 15 times that of Portland cement with a specific gravity of 2.4 g/cm^3 [10].

Some research works were performed in order to investigate the influence of the addition of metakaolin on the mechanical behaviour of concrete mixes. Parande et al. [10] concluded that the filler effect, the acceleration of cement hydration and a pozzolanic reaction with calcium hydroxide are the main factors influencing the contribution that metakaolin makes to strength when it is used as a partial replacement for cement in concrete. The relative importance of each of the three factors changed with age during the curing process. An instantaneous effect was observed for the filler role, followed by the acceleration of cement hydration during the first day after the concrete was cast. Thereafter, an increasing and significant contribution from the pozzolanic reaction took place which may continue for over the long-term. Parande et al. [10] highlighted that the conclusions made by Wild et al. [34] indicated that the positive contribution of metakaolin in increasing the strength of concrete was limited in the first 14 days following casting.

However, the former review of Parande et al. [10] does correlate with what was accurately explained by Wild et al. [34]. Wild et al. [34] state that the optimum metakaolin content which enhanced the compressive strength between the ages of 1 day to 90 days was 20%, with a light increase in the compressive strength of concrete mixes beyond 14 days. This increase reached about 20% at 90 days age when both 15% and 20% metakaolin contents were used, whereas it was about 32% at an age of 14 days, as shown in Figure 2.5.

Many experimental studies, for example [35–37], showed that the optimum content of metakaolin material which produced the highest increase in the mechanical strength of the concrete mix is

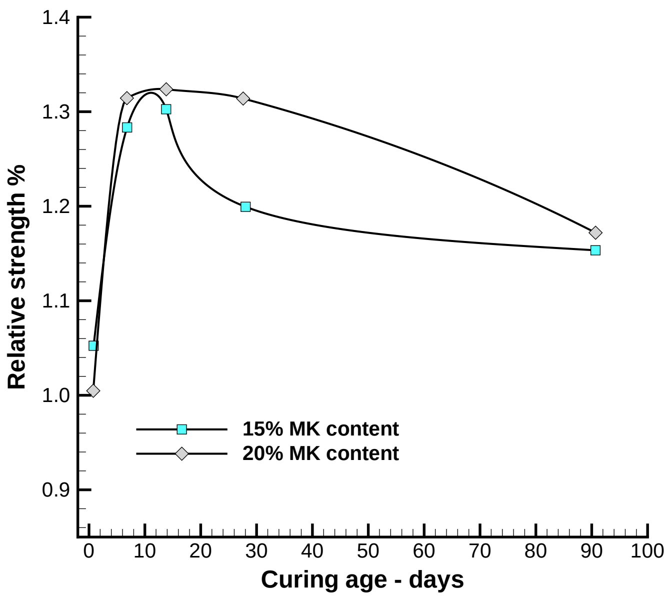

Figure 2.5: The effect of metakaolin content on the strength of concrete in relation to the control mix [34]

equivalent to 10% by weight of Portland cement. Another important note is that the metakaolin material has a major role in reducing the amount of $Ca(OH)_2$ released during the hydration of cement. $Ca(OH)_2$ is responsible for promotion of the ASR, as previously mentioned.

In terms of comparison with other mineral admixtures, Justice et al. [38] conducted an experimental investigation of the behaviour of concrete samples containing silica fume and two types of metakaolin. The latter had different surface area values (25.4 m^2/g and 11.1 m^2/g respectively). All of the mineral additives were used as a partial replacement for cement with a percentage of 8%. The results obtained demonstrated clear improvements in the mechanical and integrity characteristics of the metakaolin concrete mixes over those of silica fume. The percentage increase in strength reached as much as 25% at 28 days age. Such behaviour was attributed to the fine size of the metakaolin particles, resulting in higher pozzolanic activity.

2.4 Thermal behaviour of lightweight concrete

The relevant literature shows that the overall thermal behaviour of concrete is governed by the thermal properties of its components, namely cement paste and aggregate. Because it forms

50% of the volume of the concrete (or more in some cases), the mineralogical characteristics of aggregate have the greater influence on the thermal properties of concrete. On the other hand, a minor role was observed for the cement paste [5].

In general, much published research about the thermal properties of lightweight concrete has been concerned with thermal conductivity. The reason for this is that thermal conductivity is a good indicator of the likely thermal performance of concrete. Unlike normal weight concrete that exhibits thermal behaviour which is independent of density, many studies have pointed out that the thermal conductivity of lightweight concrete varied with the density. This is normally due to the lower thermal conductivity of air, which occupies a considerable mass within lightweight concrete [5].

In terms of systematically modifying the lightweight concrete composition using by-product materials, several studies have set out to evaluate the thermal behaviour of such a field of research. Demirboga and Gul [39] investigated the effect of substitution pumice aggregate with expanded perlite on the thermal conductivity of lightweight concrete. The additions of expanded perlite were in the range of 0% to 100% by weight of the pumice. In addition, three percentages of fly ash and silica fume were used as a partial replacement for Portland cement, namely 10%, 20% and 30%. The results obtained showed that the thermal conductivity of the formulated concrete decreases with an increase in the expanded perlite content. Further reduction in thermal conductivity was also observed when the fly ash and silica fume were used. This behaviour was mainly due to the relatively low conductivity of expanded perlite and both fly ash and silica fume admixtures which consequently led to lower thermal conductivity for the lightweight concrete produced. Among the different lightweight concrete mixes examined throughout this study, the concrete mix containing 100% expanded perlite and 30% fly ash showed the lowest thermal conductivity at about 0.15 W/mK. Identical results for the thermal behaviour of expanded perlite were observed by Demir and Serhat [40].

Demirbas [41] critically evaluated the findings of Demirboga and Gul [39] and made the following observations:

1. No clear relationship was demonstrated between density and the thermal conductivity of

lightweight concrete.

2. The influence of both temperature load and water content was not considered. These parameters have a significant effect on the thermal conductivity of lightweight concrete.

3. There was no discussion of the role of emitted gases which are usually generated during the heating of concrete and in cases of decomposition of $Ca(OH)_2$, calcium silicate hydrates and calcium carbonation. Such behaviour may cause cracks to propagate within the concrete due to local overpressure in the porous system.

However, the author of this thesis supports the original findings, because the methodology of the experimental programme adopted by Demirboga and Gul [39] allowed for drying the concrete samples at a nominal oven temperature of 110 ± 10 ^{o}C. Thereafter, all concrete samples were weighed at 24-hour intervals until the weight loss did not exceed 1%. Based upon this technique, the decomposition of both calcium silicate hydrates and calcium hydroxide cannot take place at this temperature level (110 ± 10 ^{o}C). Previous studies [42–44] have reported that the aforementioned decomposition may occur at about 500 ^{o}C. It was also noted that the relationship between the density and thermal conductivity of lightweight concrete already exists, as shown in Figure 2.6.

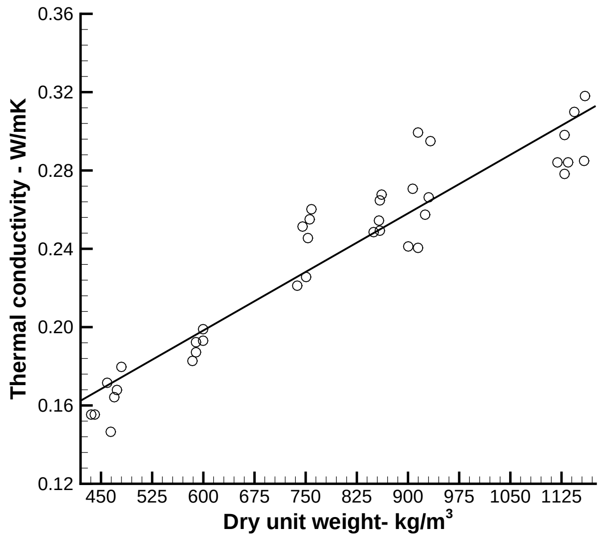

Figure 2.6: The relationship between dry unit weight and thermal conductivity [39]

The effect of aggregate particle size on the thermal behaviour was demonstrated by the study conducted by Unal and et al. [3]. Based upon the results obtained, they concluded that an increase in fine particles causes a notable increase in thermal conductivity with variation of cement content, whereas an essentially constant thermal conductivity value was observed for all cases when the proportion of the medium sized particles increases, as shown in Figure 2.7. This behaviour may be explained by the role of cement paste, which becomes more apparent as the number of fine aggregate particles increases. Consequently, a dense concrete mix will be obtained due to the occupation of most air voids by cement paste.

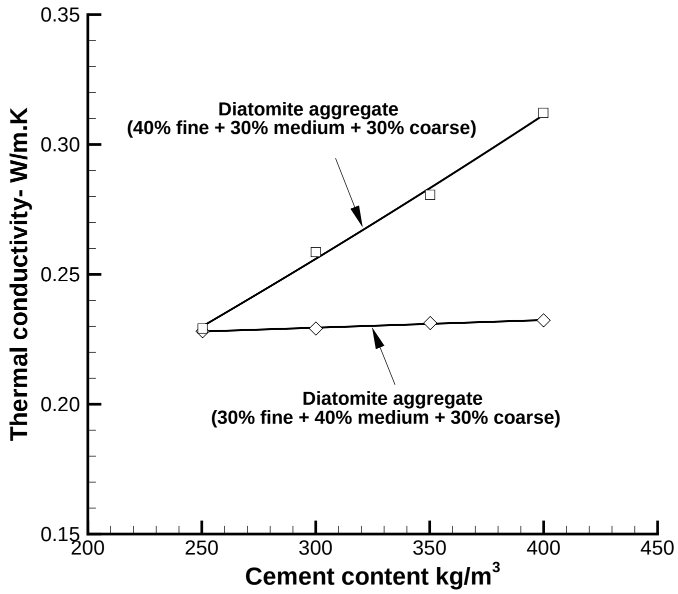

Figure 2.7: The effect of particle size on thermal conductivity at various cement contents [3]

The thermal properties of lightweight concrete made with expanded clay and/or recycled glass aggregate were also evaluated in the experimental programme conducted by Petrella et al. [6]. The results showed that the thermal conductivities of the concrete mix types A, C, E and F (see Table 2.1) were 0.158 W/mK, 0.285 W/mK, 0.236 W/mK and 0.192 W/mK respectively. This behaviour marks the positive effect of recycled glass on the increase of thermal insulation due to its lower thermal conductivity in comparison with the other constituents of concrete. In addition, the pozzolanic activity of recycled glass may have a noticeable influence upon this issue.

2.5 Behaviour of lightweight concrete at high temperatures

When a concrete element is exposed to high temperatures, both its mechanical and thermal properties are affected in various forms. On the whole, these forms are manifested either in a loss of strength or in cracking or spalling. Many factors can influence the significance of this issue, such as the duration of exposure to high temperatures, the maximum temperature applied, the type of aggregate used and the moisture content of the concrete mix [5, 45].

In comparison with normal weight concrete, lightweight concrete exhibits less strength loss and a lower tendency to cracking under the effect of high temperatures, as shown in Figure 2.8 [46]. The reasons for this are the lower thermal conductivity, diffusivity and expansion of lightweight aggregate in comparison with normal weight aggregate [45]. From Figure 2.8, it can be seen that the lightweight concrete retains its original strength up to about 300 ^{o}C. At 800 ^{o}C, the reduction in compressive strength reaches about 60%. For the case of normal weight concrete, the reduction begins at about 100 ^{o}C and reaches as much as 80% at around 800 ^{o}C. Similar behaviour to that of compressive strength was also reported for the tensile behaviour at high temperatures [5].

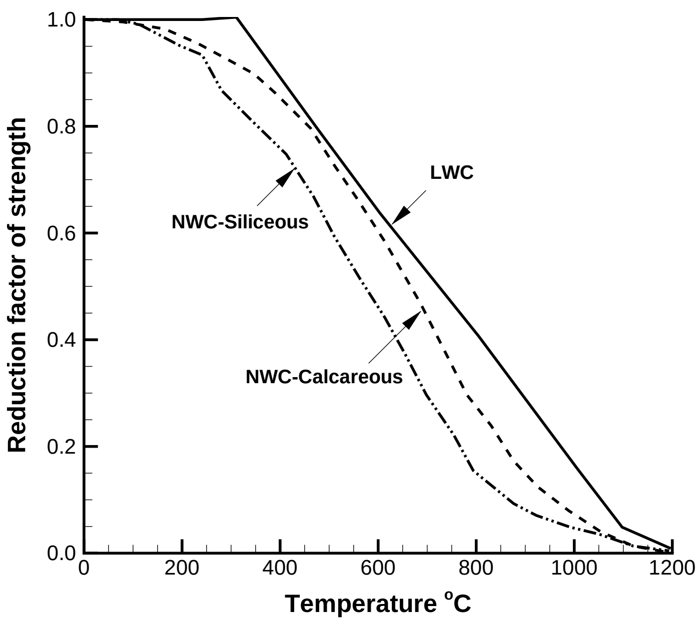

Figure 2.8: The reduction factor of compressive strength at high temperatures [46]

The effect of using fly ash as a partial replacement for cement on the behaviour of pumice structural lightweight concrete at high temperatures was investigated by Tanyildizi and Coskun [47]. Three different percentages of fly ash were used, namely 10%, 20% and 30%. A steady state heat exposure regime was followed throughout the experimental programme. The results obtained showed that both compressive and splitting tensile strength decrease with the temperature. This reduction takes place at about 200 ^{o}C. In all cases, the addition of fly ash mitigated the reduction in the strength of the concrete samples at high temperatures. This behaviour was explained by the formulation of a tobermorite component which enhanced the strength of the concrete. The latter component is a result of the lime-fly ash reaction at high temperatures.

Early research has reported that the flexural strength of lightweight concrete decreases sharply at about 90 ^{o}C, then it recovers its original strength and even exceeds it above 400 ^{o}C [48]. However, more recent experimental data for a wide range of lightweight concretes does not confirm these findings: rather, a continuous decrease in flexural strength was observed with temperatures [5].

The most serious effect of exposing concrete to high temperatures is spalling. This phenomenon causes the ejection of fragments from the heated surface of the concrete. This occurrence can take place at temperatures above 100 ^{o}C when the heating rate is high. The main mechanism for spalling is the breaking up of the concrete surface due to the generation of high mechanical forces resulting from steam pressure within the concrete pores [49]. The common types of spalling are surface, aggregate and explosive. The latter can lead to the entire collapse of a structure [50].

Previous studies have summarised the main parameters which may influence the risk of explosive spalling in concrete as follows [51, 52]:

1. Heating rate: If the heating rate is above 3 ^{o}C/min, spalling may occur. The severity of spalling increases as the heating rate increases.

2. Permeability of concrete: The probability of explosive spalling increases with the decreasing permeability of concrete. Because of their high density and lower permeability, high

strength concretes and (to a lesser degree) normal concretes have a greater susceptibility to explosive spalling than lightweight concrete [53, 54].

3. Pore saturation level: Explosive spalling may occur if the moisture content is more than 2-3% of the weight of the concrete. This level of moisture forms the critical amount for the propagation of steam pressure.

4. Element section size: Both thick and thin sections have a lower tendency for explosive spalling than medium-sized sections. The reason for this is that the moisture can escape rapidly from thin sections so that there is no chance for the critical steam pressure to be generated. No clear explanation has been offered for the behaviour of thick sections. However, it could be related to the wide cover which enhances the tensile strength of the concrete surface against the steam pressures generated.

5. Level of external load: The restraint of a high compressive load increases the possibility of explosive spalling due to induced high levels of thermal expansion.

6. Presence of cracking: Internal cracks work as accommodation for the generation of steam pressure which promotes explosive spalling.

In terms of the thermal behaviour of lightweight concrete at high temperatures, early studies [5] have mentioned that thermal conductivity slightly increases at about 50 ^{o}C; thereafter, a considerable decrease takes place at about 120 ^{o}C. Eventually, the value of thermal conductivity at 800 ^{o}C reached about half of that observed at ambient temperature. Recently, BS EN 1992-1-2 [46] pointed out that the thermal conductivity of lightweight concrete exhibits a continuous decrease with temperatures up to 800 ^{o}C, followed by a stabilisation behaviour, as shown in Figure 2.9a. However, the author of this thesis noted that BS EN 1996-1-2 [55] describes different behaviour from [46], as shown in Figure 2.9b. A greater increase in the value of thermal conductivity was observed at about 100 ^{o}C due to the evaporation of moisture from the concrete sample. Above about 400 ^{o}C, a constant thermal conductivity value was measured. As a result, the variation in the thermal conductivity of lightweight concrete with temperature can be considered a complex behaviour and is mainly dependent upon the type of aggregate used. Similar behaviour was also observed for specific heat but with a proportionally greater increase in the limit of the evaporation temperature than that observed for thermal conductivity [55].

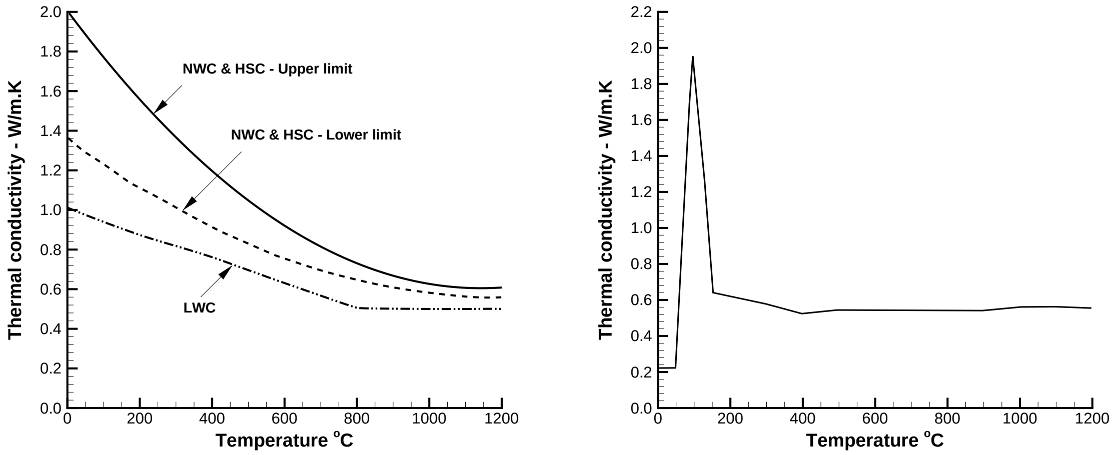

(a) (b)

Figure 2.9: The variation in thermal conductivity with temperature (a) for normal and lightweight concretes [46]; (b) for pumice lightweight concrete [55]

2.6 Numerical modelling of the thermal behaviour of lightweight concrete

Numerical modelling of thermal behaviour deals with heat transfer analysis, which is based upon the thermal response of a material in terms of its temperature profile. This analytical approach has significant applications in the construction field; for example, in the determination of the ability of a structure to withstand elevated temperatures, as might be experienced during a fire, and also to predict thermally generated stress regimes under the same conditions. The first application represents pure heat transfer analysis, while the second application incorporates a coupled response (thermal-stress analysis)[56].

Heat transfer occurs by means of any one or a combination of the following modes: conduction, convection and radiation. In conduction mode, the heat transfer takes place within the matter at the atomic/molecular level. This process is most significant in solids. The movement of a heated fluid (gas or liquid) is the cause of thermal energy transferred by the mode of convection. The third mode (radiation) involves the direct transfer of energy by means of electromagnetic radiation [57].

The fire resistance of lightweight aggregate concrete samples has been studied by Chow and Chan [58]. Essentially, they assumed that the fire resistance of a material is a thermal conduction problem. A numerical simulation approach was followed using the LIBRA finite element package to calculate the temperature distribution at specified nodes. The results obtained were then validated against the experimental measurements. The applied thermal load complied with the requirement of BS 476: Part 20 [59] and was applied in two cases, namely unidirectional and three directional exposures. Both convection and radiation heat transfer were considered at the exposed and unexposed sides of the concrete samples, with different coefficient values. The results of the simulation indicated that the element size has no effect on the simulation outputs. In addition, a notable variation of about 20% was observed between the predicted and measured temperature values for the unexposed side of the lightweight concrete samples. This variation was explained by the effect of a phase change which may take place within this range of temperature exposures. Similar results were also obtained by Conner et al. [60] who found that the predicted combined convection and radiation modes on both sides of the lightweight concrete element give good agreement with the experimental measurements.

2.7 Mechanical behaviour of masonry walls at ambient temperatures

Masonry walls are the most ancient structural elements and have been used for more than 10 thousand years. Some examples of great masonry constructions still exist from this era, such as Ziggurat at Ur (2600 B.C) and the Pyramids in Egypt (2580 B.C). These structures are evidence of the efficiency, ease of use and wide availability of the raw materials for such a type of construction. Over time, many developments have taken place, both in terms of the materials used and the methods of construction [61].

A masonry wall can be defined as a composite element of units and mortar (and in some cases grout and reinforcement). In order to understand the global behaviour of masonry walls, the behaviour of their components and their interaction with each other should first be addressed [62, 63]. This approach saves both time and cost. However, some cases require detailed evaluation using an assemblage wall.

In practice, the classification of a masonry wall depends upon whether it is loaded or not. If the wall contributes in supporting the applied loads, it is considered to be a load bearing wall, otherwise it is regarded as a so-called partition (non-load bearing) wall. The latter is usually used to satisfy the considerations of thermal and sound insulation [55, 64].

For load bearing masonry walls, the mechanical strength is affected by many factors, such as the geometry and strength of the unit, the height of the wall, the thickness and the strength of the mortar [62, 63].

When a perforated unit (a unit with coring) is used, the ratio of wall strength to unit strength decreases compared with that observed for solid units. Such a reduction can be as much as 40% for a wall constructed with a mortar joint thickness of 10 mm for 70% solid units. This behaviour is related to the magnitude of the available net area for resisting the lateral tensile stress propagated within the units at the failure. Decreasing the height of the unit causes a decrease in the strength of the wall due to an appreciable increase in the transverse stresses on the unit, resulting from the confining effects of the mortar joints. A distinct relationship between both the unit and wall strengths was reported, which almost behaves as a linear correlation [62].

A clear reduction in the strength of a masonry wall was noted with increasing effective height (relative to effective thickness). The main cause of this behaviour is attributed to the buckling failure which emerged in such cases. If this case is associated with eccentric loads, a further decrease in the strength of the masonry wall will take place, as shown in Figure 2.10 [65].

With reference to the effect of mortar, a notable increase in strength of masonry wall was indicated when high strength mortar is used and vice versa. However, the former effect becomes weaker when high strength units are used. The thicker mortar joint produces a lower strength for the masonry walls, as shown in Figure 2.11. Such behaviour had a major pronounced effect

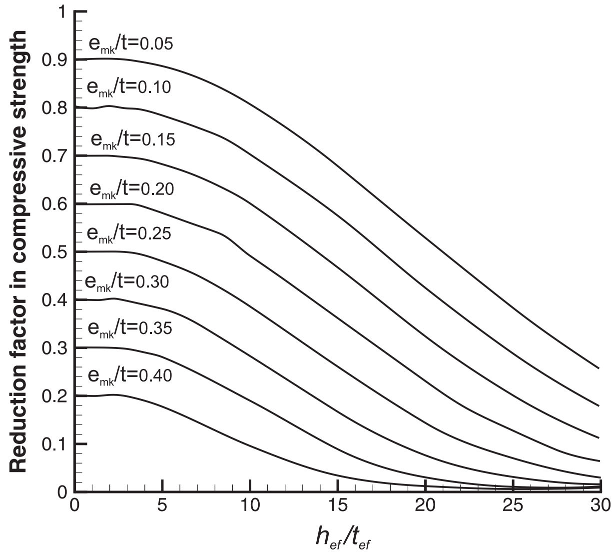

Figure 2.10: The capacity reduction factor in strength of a masonry wall as a function of both slenderness ratio (h_{ef}/t_{ef}) and eccentricity of loads based on $E = 700f_k$ [65]

in perforated brick units [62]. Previous studies [63, 65] have mentioned that the standard joint thickness is 10 mm.

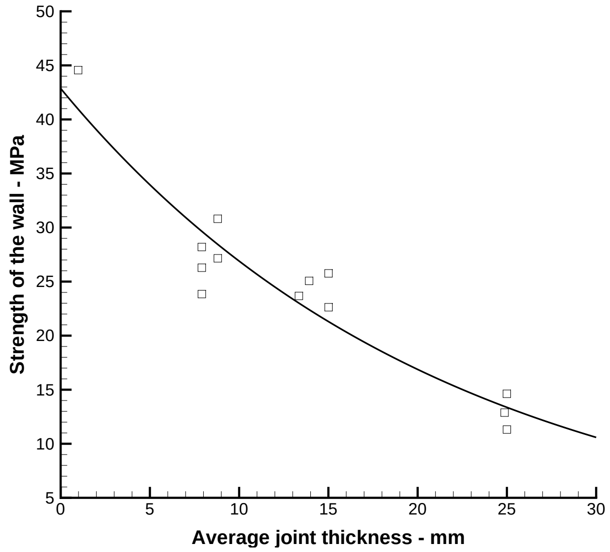

Figure 2.11: The effect of mortar joint thickness on the compressive strength of a masonry wall using brick units with a strength of 55.7 MPa [62]

In addition to the above factors, it has been noted that the size of the wall specimen and the end confinement have an important effect upon the behaviour of masonry walls under uniaxial loads. Using a sufficient number of bed joints for prism samples (wallettes) is necessary to represent the whole failure mode of a full-scale wall with a correct strength value. The experimental evidence has shown that a prism sample at least three units high is required to satisfy the former requirement. If an appropriate end platen restraint is used, the crack pattern is similar to that of an actual wall [62, 66, 67].

Brencich and Felice [68] conducted an experimental study to address most of the aforementioned factors using brickwork masonry prisms. Masonry prisms of two different geometries were formulated using two types of brick units with different dimensions and strength levels. In addition, three types of mortar were used to provide the bonding strength between the units. The applied load was designed to comprise both concentric and eccentric conditions, as shown in Figure 2.12.

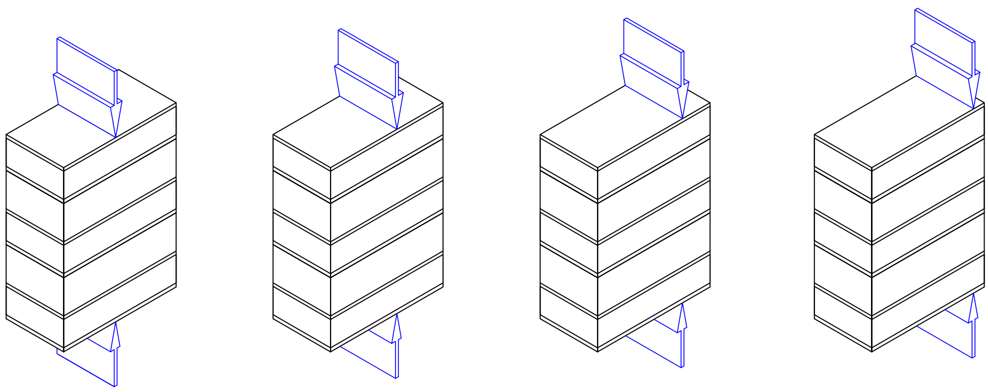

Figure 2.12: Concentric and eccentric load conditions used in the experimental programme [68]

The prism dimensions measured $270 \times 250 \times 110$ mm ($h \times l \times t$)(sample 1) and $280 \times 200 \times 140$ mm ($h \times l \times t$) (sample 2). The compressive strengths of the brick units were 19.7 MPa for brick 1 and 30 MPa for brick 2. For both brick 1 and brick 2, the dimensions were either $240 \times 110 \times 55$ mm or $280 \times 140 \times 55$ mm ($l \times w \times t$). Cement-lime (mortar 1), white cement-lime (mortar 2) and hydraulic lime (mortar 3) mortars were the main categories used throughout the experimental programme. The latter mortar type (mortar 3) and the brick unit with dimensions of $280 \times 140 \times 55$ mm ($l \times w \times t$) were only used to formulate prism sample 3, whilst both mortar 1 and mortar 2 were adopted in prism samples 1 and 2.

The results obtained of the uniaxial compressive strength revealed that the roles of the masonry components and the loading conditions were both significant. In all tested cases, the prism sample with the highest compressive strength was constructed from the stronger brick unit. The masonry prism sample 3 exhibited approximately one-half the compressive strength of that observed for sampe 1. The reason for this was the lower strength value of mortar 3 compared to those used to formulate prism sample 1 (mortar 1 and mortar 2). The reduction in strength due to applying eccentric loads ranged from 27% to 50%. However, less reduction was noted for sample 3 when it was tested under an eccentric load. This behaviour may be explained by the higher ductile response of hydraulic lime mortar when exposed to compression loads.

The failure modes of the tested samples showed different crack paths, as shown in Figure 2.13. In general, a uniform crushing failure mechanism was judged for the concentric loading condition. On the other hand, collapse occurred under eccentric loading conditions at the compressed zone at the same time as horizontal cracks appeared within the brick-mortar interface in the opposite (tension) zone. However, in both loading conditions, the concentration of tensile stresses within the brick units was a major reason for the initiation of the failure mechanism.

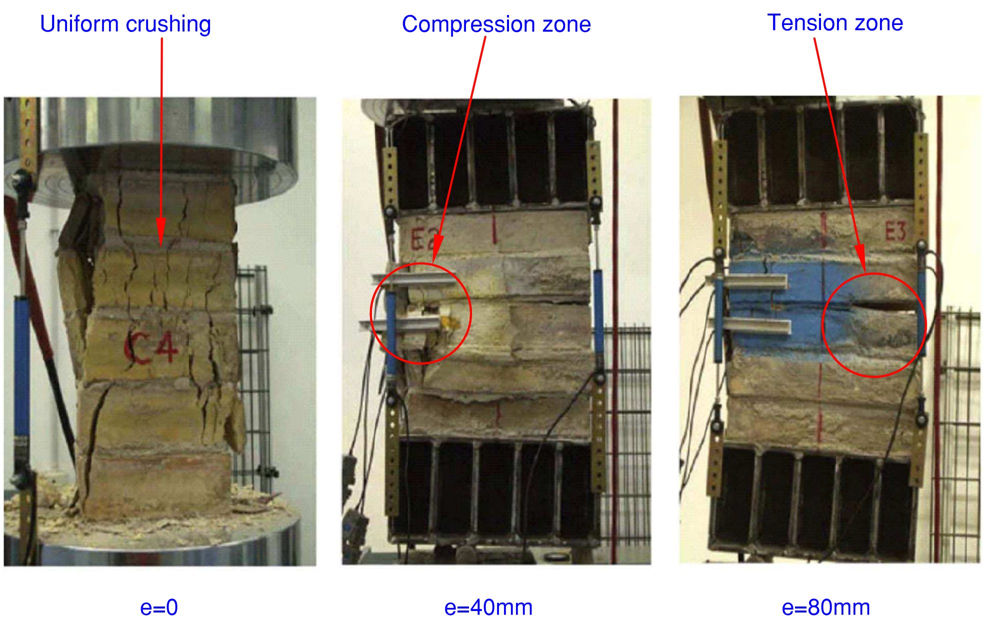

Figure 2.13: Failure modes of prisms sample 3 under concentric and eccentric load conditions [68]

A similar failure mode was also observed by Lourenco et al. [69] for vertically perforated clay brick masonry under concentric compression loads but with more severe distortion in the brick units. This is due to the effect of coring which tends to reduce the net cross-section of the unit, thereby the lateral tensile stresses are concentrated and the failure takes place shortly afterwards.

2.8 Behaviour of masonry walls at high temperatures

Special consideration is required when attempting to evaluate the behaviour of masonry walls under the combined effects of load and high temperatures because of the complexity of the interaction between these two conditions. BS EN Standards [55, 70] summarised the structural requirements of masonry walls under the effects of both mechanical load and high temperatures by means of three main criteria: insulation, integrity and load bearing capacity. The insulation criterion represents the time elapsed from the beginning of exposure to elevated temperatures during which the wall specimen maintained its separation function so that the average temperature at the unexposed surface does not exceed the initial average temperature plus 140 ^{o}C. In addition, the developing temperature of an unexposed surface at any location does not exceed the initial average temperature plus 180 ^{o}C. The integrity criterion refers to the ability of the masonry wall to preserve its separation role without causing ignition of the cotton pad, permitting penetration of a standard gauge or resulting in flame for more than 10s at the unexposed face. The criterion of load bearing capacity represents the ability of a masonry wall to withstand the applied loads during exposure to high temperatures so that the following limitations are satisfied:

1. Limiting vertical contraction (c) in (mm)

$$c = \frac{h}{100} \tag{2.4}$$

2. Limiting rate of vertical contraction ($\dot{c}$) in (mm/min)

$$\dot{c} = \frac{3h}{1000} \tag{2.5}$$

However, all of the above requirements are based upon the results of a standard fire test in which heat is applied in a transit condition with a unidirectional formulation. For the case of steady state conditions, Russo and Sciarretta [71] performed an experimental investigation to evaluate the behaviour of masonry walls made from hand-made clay bricks under the unidirectional effect of two temperature levels, namely 300 ^oC and 600 ^oC, for about an hour. The total dimensions of the masonry prism were $510 \times 510 \times 250$ mm ($h \times l \times t$). Firstly, all samples were exposed to pure heat from one side. Thereafter, the samples were removed from the furnace in order to conduct the concentric compression test. The results obtained for the temperature profile at three different locations (the unexposed face and the exposed face both at the mortar joint and at the brick) are shown in Figure 2.14.

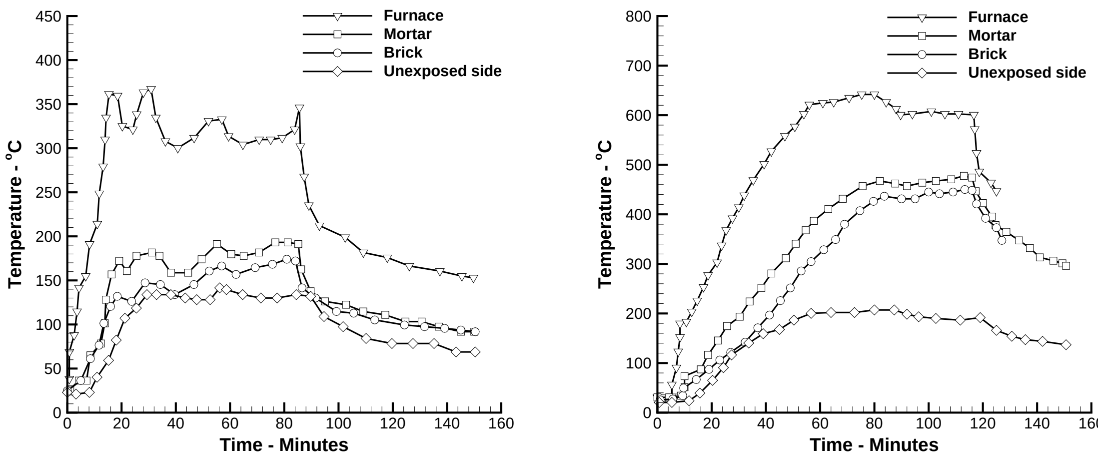

(at 300 ^oC) (at 300 ^oC)

Figure 2.14: Temperature profile for the masonry prism samples after exposure to high temperatures [71]

Except for noting the difference between the temperatures of the furnace and the unexposed side of the masonry prism, which reached about 400 ^oC when exposed to 600 ^oC, no further conclusions were drawn from these results. However, it can be seen that the steady state condition for both desired temperature levels was not satisfied due to the notable variation in the furnace temperature which exceeded the permissible limit ($\pm$ 5 ^oC) indicated by the BS EN Standard [70]. Another important point to note is that the insulation criterion is required for evaluation and this mainly depends upon the differences between the temperatures of the exposed and unexposed sides of the masonry prism. In addition, no explanation was offered regarding the temperature variation between the brick and mortar joint.

In conclusion, the study highlighted the decay associated with the effect of high temperatures which occurred in the form of the propagation of micro-cracks and detachments at the brick-mortar interface. Such effects become more apparent at 600 ^{o}C.

In terms of mechanical behaviour, the results obtained showed that the compressive strength of the masonry prism exhibited a slight increase of about 4% at 300 ^{o}C compared with the reference sample at ambient temperature. At 600 ^{o}C, the compressive strength showed a decrease of as much as 9%. Similar behaviour to that of compressive strength was also observed for the modulus of elasticity.

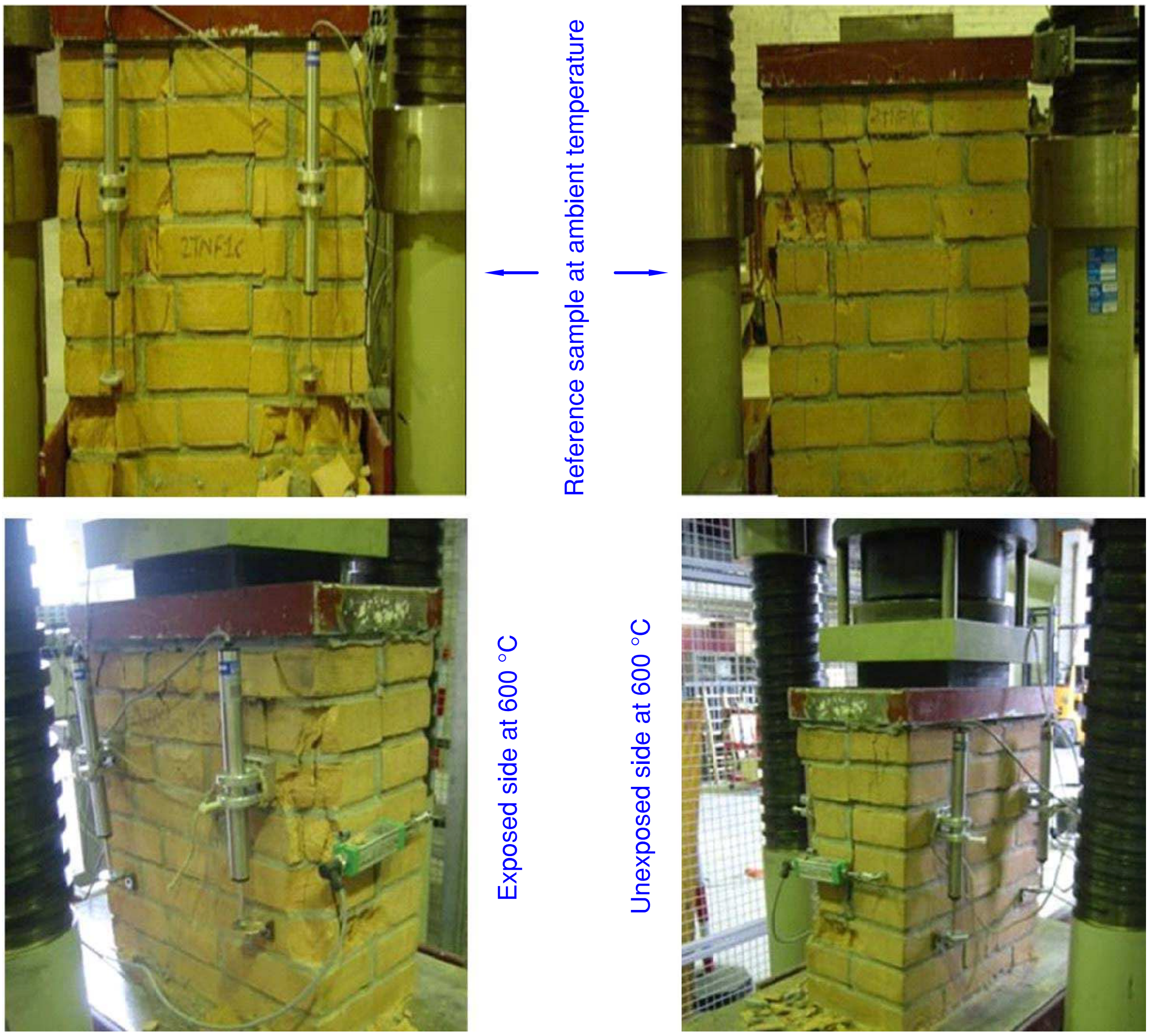

Figure 2.15: Failure mode of reference prism samples at ambient temperature and after exposure to 600 ^{o}C; both sides of the samples are visible [71]

Based upon the failure mode, visual inspection indicated that the crack initiation of the heated samples first occurred on the exposed side. The failure path exhibited both vertical and horizontal cracks, as shown in Figure 2.15. Less damage was observed on the unexposed side than on the exposed side. In general, the decay due to the combined effect of heat and compression loads was slightly higher than that observed for the reference samples at ambient temperatures.

The behaviour of block-work masonry prisms (wallettes) under compression loads at both ambient and high temperatures was investigated by Ruvalcaba [67]. An all around steady state heat regime was used, with temperatures ranging from 20 ^oC to 800 ^oC. The concrete blocks tested contained furnace bottom ash in their composition (with unspecified content). The dimensions of the wallettes were 685 × 670 × 100 mm ($h \times l \times t$). The results obtained showed that the compressive strength decreases with an increase in temperature, with the percentage reduction reaching about 80% at 800 ^oC. In addition, the corresponding percentage reduction in the modulus of elasticity reached up to 97%. The major cause of such behaviours is deterioration of the strength of both constituents of the wallette (blocks and mortar) at high temperatures.

(a) at 400 ^oC (b) at 600 ^oC

Figure 2.16: Failure modes of block-work masonry wallettes at high temperatures [67]

With respect to thermal behaviour, the results indicated that the time required to reach the stabilisation temperature (steady state condition) increases with an increase in the level of applied temperature. The failure mode of the tested samples revealed spalling at temperature levels of 400 ^{o}C and beyond. The intensity of spalling increases as the temperature increases, as shown in Figure 2.16. For all of the test cases, the failure was due to a combination of spalling and the compression loads.

2.9 Numerical modelling of the structural behaviour of masonry walls

Several constitutive models are available to simulate the structural behaviour of masonry walls. The constitutive concept and the complexity are the base for identifying each model. Linear elastic, plastic and nonlinear behaviours are the most common models used for the prediction of the material response in terms of the stress-strain feature [61]. In a linear constitutive model, the material is treated as being infinitely elastic in both compression and tension. This assumption is valid for materials possessing high tensile strength or in circumstances where the material is being subjected to stress values lower than the elastic limit. Because masonry structures are typically very weak in tension due to their interfacial joints, and because they also support massive mechanical loads, this modelling approach is not appropriate for handling the structural response of the masonry walls [61, 72]. A plastic model, on the other hand, is intended to predict the maximum load that can be withstood by a structure. This means that a plastic model must simultaneously satisfy two requirements, namely that the maximum load at failure has been achieved and that the material exhibits ductile behaviour. When the total deformation of the wall goes beyond the ductility of masonry walls, the second condition is no longer met. Unlike linear elastic and plastic models, nonlinear models can reflect the full range of behaviour of the masonry walls from the linear elastic range up to the failure stage [61].

Previous studies [73, 74] reported that even at the allowable loading, the global behaviour of masonry walls is nonlinear due to its combination of different constituents (masonry units and mortar joints). From this viewpoint, the nonlinear formulation is an adequate approach to simulate the response of the masonry walls under different loading situations. However, in the contrast to linear elastic and plastic models, the nonlinear model needs more input data and is more time consuming.

The most commonly used constituent theory for representing nonlinear behaviour is that of the damage mechanism. In this theory, the transformation from a linear to a nonlinear response is mainly attributed to a decrease in the elastic stiffness of a material, resulting from damage (or degradation) in tension or in compression [61, 75].

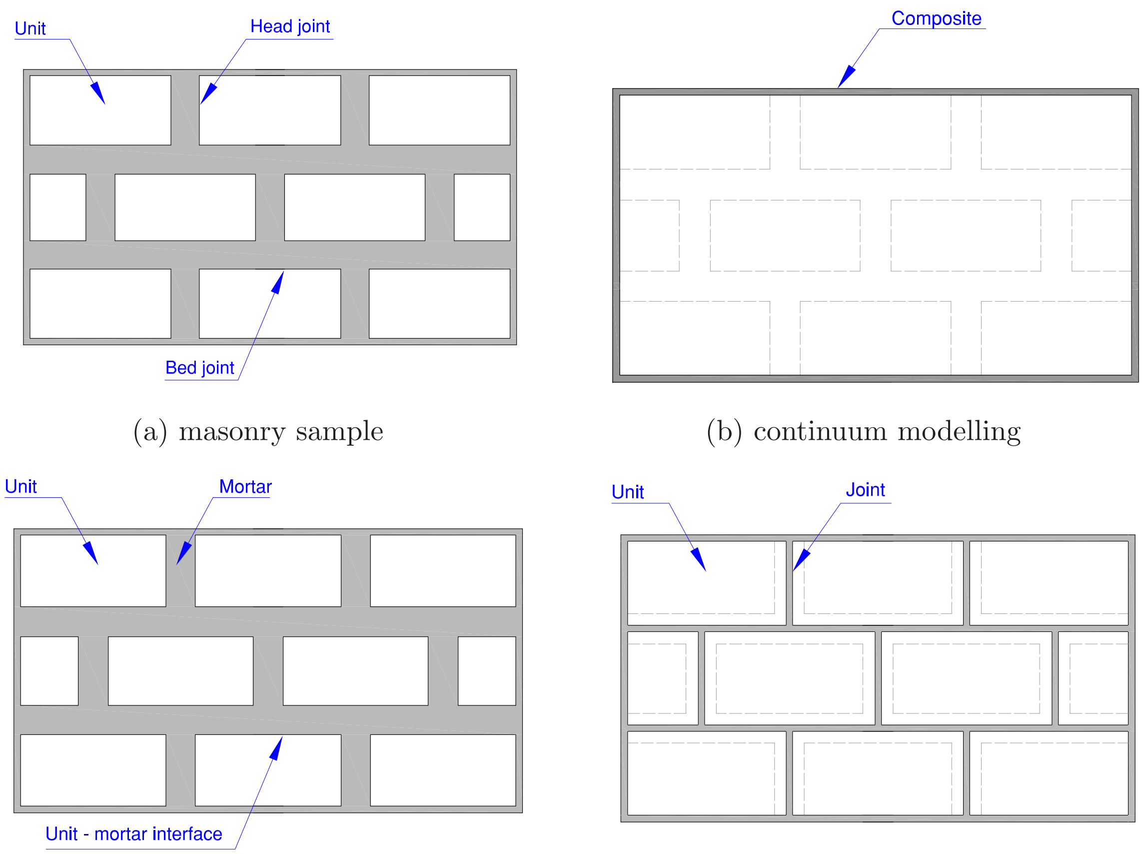

(a) masonry sample (b) continuum modelling

(c) detailed micro-modelling (d) simplified micro-modelling

Figure 2.17: Modelling techniques for masonry [72]

Previous studies [61, 72, 76] have proposed different techniques to simulate the structural behaviour of masonry using either continuum (so called "smeared-crack") models or discontinuum (so called "discrete-crack") models. In continuum models, all of the masonry units, mortar joints and unit-mortar interfaces are treated as homogenous isotropic continuum elements, as shown in Figure 2.17b. This approach gives a global view for the behaviour of masonry with a smaller number of elements required for modelling. The continuum model approach is suitable for modelling the macro-level behaviour of large structures, where the economic issue is the most governing parameter in the analysis.

Discontinuum models, on the other hand, are used to predict the nonlinear micro-level behaviour of small structures in situations where a higher degree of computational accuracy is required. There are two variants of this technique, namely simplified and detailed. The detailed micro-level approach describes both masonry units and mortar joints as continuum elements, while the unit-mortar interface is simulated as a discontinuum element, as shown in Figure 2.17c. In the simplified approach, both the mortar joint and the unit-mortar interface are merged into discontinuum line interface elements, whilst the masonry unit is simulated as a continuum element and extended in order to compensate for the change in geometry, as shown in Figure 2.17d. In terms of the accuracy of the two approaches, as might be expected, the detailed micro-level approach produces more highly refined results than those of the simplified one. The reason for this is that the Poisson's ratio of the mortar joint is not taken into account in the simplified approach [61]. However, the detailed approach is highly computational resource intensive and this must be borne in mind. Selection of the most appropriate approach depends on a number of parameters such as the level of accuracy required, availability of data and capacity of computational resources.

2.10 Summary

Based upon the previous studies presented in this chapter, some conclusions are drawn in this summary. The density feature is indicative of the level of both the mechanical and thermal performance of lightweight concrete. In general, the mechanical strength increases with increasing density, whereas contrasting behaviour is observed for the thermal conductivity in the same conditions. A major effect was noted for the mix proportions and the characteristics of the materials used on the behaviour of lightweight concrete. It would therefore be interesting to select the proper constituents and mix composition to meet the intended purpose of using the lightweight concrete.

Industrial by-products and recycled waste materials can be used as alternatives for one or more ingredients of lightweight concrete, offering some benefits in terms of both cost and performance. Normally, the ASR was lower than the specified nocuous limit when the recycled glass was incorporated as a partial replacement for natural sand. A further reduction in ASR was also indicated when the pozzolanic materials were simultaneously used. The geometry and strength of both the masonry unit and mortar, in addition to the geometry of the wall and the locations of the applied load were the most influential parameters on the behaviour of load-bearing masonry walls. In the event of a fire , the structural requirements of masonry walls should be considered in terms of insulation, integrity and load bearing capacity.

Chapter 3

Developing a new type of structural lightweight concrete mixture

3.1 Introduction

Recent developments in the field of construction materials have emphasised the importance of improving the thermo-mechanical behaviour of concrete elements. Nevertheless, the need for further research has become increasingly apparent. In this chapter, a strategy is described for the development of a new type of lightweight concrete produced using by-product materials. The following issues are discussed in detail: selection of the lightweight concrete combination; specification of the materials used; design of the reference lightweight concrete mix; trial mixes; design of the modified lightweight concrete mixes; the test programme and the mixing, casting and curing of concrete samples.

3.2 Selection of the lightweight concrete combination

Different ratios of by-product materials, namely recycled waste glass and metakaolin powder, were selected in conjunction with expanded clay to produce the lightweight concrete mixtures. According to the available data presented in Chapter 2, the aforementioned combination has not been previously studied.

The motivations for choosing the above materials can be summarised as follows:

1. Using recycled waste glass as a partial replacement for natural sand reduces the total density and improves the thermal insulation properties of the concrete. Also, it is considered a feasible practical solution for mitigating the environmental problem of waste glass disposal [6, 27, 28].

2. Metakaolin is a by-product material of paper manufacture. It acts as a pozzolanic material and reduces the effect of the alkali-silica reaction between Portland cement and the particles of glass aggregate. In addition, it can be used to improve concrete strength and to reduce the amount of cement used [11, 12, 34, 37].

3. Unlike most other lightweight aggregates, the expanded clay content could be formulated to achieve the strength level of structural lightweight concrete with good thermal behaviour. It is available in a wide range of particle sizes to suit many construction applications [6].

3.3 Details of the experimental programme

3.3.1 The specification of materials used

All of the lightweight concrete mixtures were produced using ordinary Portland cement compliant with BS EN 197-1 [77] as manufactured by the Lafarge Company. A medium grade 8-5R expanded clay type (Techni Clay) was used as a coarse aggregate. This aggregate was provided by the Plasmor Concrete Products Company [78]. It has a mean bulk density, typical moisture content and particle density of 330 kg/m^3, 20% w/w and 550 kg/m^3 respectively. Natural sand for building purposes was used as a fine aggregate in this study. Equal amounts of recycled waste glass with particle sizes of 0.5-1 and 1-2 mm were used as a partial replacement for natural sand. The specific gravity of the recycled glass was 2.52 [79]. Metakaolin (MK) material type Metastar 501 as supplied by the WhitChem Company [80] was adopted as a partial replacement for ordinary Portland cement. Figure 3.1 shows the grading for the expanded clay, natural sand and modified sands incorporating recycled glass at different ratios, while Figures 3.2a to 3.2d show the main ingredients of the lightweight concrete mixtures investigated in this study. The physical and chemical properties of the main materials used are presented in Table 3.1.

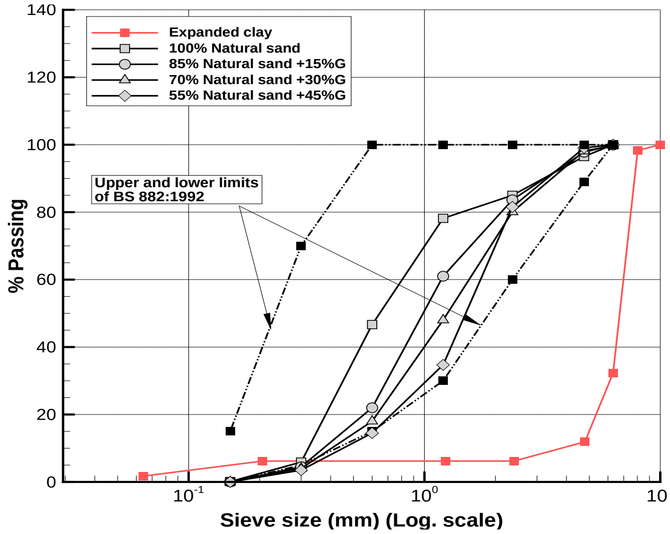

Figure 3.1: Grading of the expanded clay, natural sand and modified sands incorporating recycled glass at different ratios

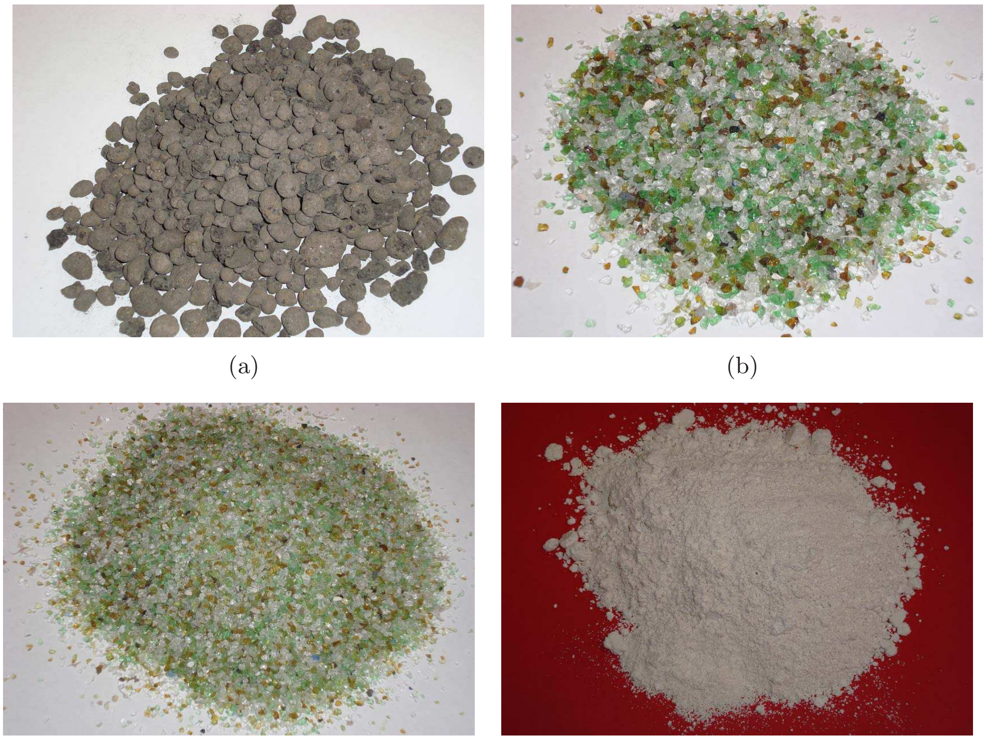

(a) (b) (c) (d)

Figure 3.2: The main ingredients of the lightweight concrete mixtures: (a) expanded clay; (b) recycled glass 1-2 mm; (c) recycled glass 0.5-1 mm; (d) metakaolin material

Table 3.1: Chemical compositions and physical properties of the Portland cement, expanded clay, metakaolin and recycled glass [77–80]

Property	Cement	Expanded clay	Property	Metakaolin	Property	Recycled glass
SiO_2 (%)	31.135	60	Colour	White	Composition	Produced from mixed colour recycled container glass
Al_2O_3 (%)	10.29	20	ISO Brightness	> 82.5	Particle Shape	Sub-angular granular
Fe_2O_3 (%)	4.295	8	-2μ (mass %)	> 60	Colour	Mixed colour-light green
CaO (%)	48.5	3	+325 mesh (mass%)	< 0.03	Bulk Density	1.45 tonnes per cubic metre
MgO (%)	2.27	3	Moisture (mass%)	< 1	Hardness	6-7 (Moh's Scale)
SO_3 (%)	2.49	0.5	Aerated powder density (kg/m^3)	320	SiO_2 (%)	72.2
K_2O (%)	0.835	3	Tapped powder density (kg/m^3)	620	Na_2O (%)	13.3
TiO_2 (%)	-	1	Surface area (m^2/g)	14	CaO (%)	10.9
Na_2O(%)	0.22	-	Pozzolanic reactivity (mg $Ca(OH)_2$/g)	> 950	MgO(%)	1.65
Eq. Na_2O(%)	0.765	-			$Al2O_3$ (%)	1.5
L.O.I (%)	1.98	< 0.5				
Other	-	1				

3.3.2 Design of the reference lightweight concrete mixture

The objective of the experimental programme was to produce a structural lightweight aggregate concrete consistent with classes D1.6 and LC16/18 of the BS EN 206-1 [81] classification of density and compressive strength. According to this classification, the concrete samples should have a dry density of no more than 1800 kg/m^3 with a minimum characteristic cube strength of 18 MPa at 28 days age. Consequently, a reference lightweight concrete mixture was designed to satisfy these requirements.

The calculations of the mix design were carried out based upon the procedure suggested by Chandra and Berntsson [82], which consists of the nine steps listed below:

1. Determine the mean compressive strength given by Equation 3.1:

$$m \geq f_{ck} + \lambda . S_n \tag{3.1}$$

where m is the mean strength of a set of samples; f_{ck} is the specific characteristic strength of the concrete in MPa; λ is a factor depending on the number of samples in the set of statistical analysis; and S_n is the standard deviation of the set of strength results from the samples.

According to the number of samples in the set (more than 30), S_n and λ were taken as 7% and 1.48 respectively [82].

2. Calculate the strength of the lightweight aggregate particles (f_{la}) using Equation 3.2:

$$f_{la} = a.10^{b\rho/1000} \tag{3.2}$$

where a and b are coefficients of the strength of the lightweight aggregate particles which depend on the type of aggregate, as shown in Table 3.2, and ρ is the particle density in kg/m^3. The equivalent aggregate number for the expanded clay with a bulk density of 330 kg/m^3 used in this research is No.3 [82]. So, the values of a and b were taken as 1 and 1.25 respectively (see Table 3.2).

3. Calculate the strength of the cement mortar by applying the following expression:

$$log\ f_m = (log\ f_c - v_{la}\ log f_{la})/(1 - v_{la}) \tag{3.3}$$

where:

f_m is the strength of the mortar (MPa); f_c is the strength of the concrete (MPa); f_{la} is the strength of the lightweight aggregate (MPa); and v_{la} is the volume of the lightweight aggregate particles (m^3).

Table 3.2: Coefficients a and b of the strength of the lightweight aggregate particles [82]

Aggregate No.	a	b
1	1.52	1.14
2	1.12	1.22
3	1.00	1.25
4	0.89	1.28

4. The volume of the lightweight aggregate particles is chosen to be in the range of 40%-45%, as recommended by Chandra and Berntsson [82].

5. The water/cement ratio was calculated using Equation 3.4.

$$W/C = log(140/f_m)/0.87 \tag{3.4}$$

6. Select the volume of cement paste (v_p) which is recommended to be 30% of the total volume of the concrete [82] .

7. Determine the cement content (C) using Equation 3.5.

$$C = 1000v_p/(0.31 + W/C) \tag{3.5}$$

8. The volume of natural sand (v_S) was calculated from Equation 3.6.

$$v_S = 1 - (v_p + v_{la} + v_{air}) \tag{3.6}$$

where v_p is the volume of the cement paste (m^3) and v_{air} is the volume of air which is assumed to be 2% of the total concrete volume [5, 82]

9. Determine the water absorbed by the lightweight aggregate particles which is recommended to be around 3% [78].

The results obtained for 1 m^3 of the reference lightweight concrete mix design (dry materials) are presented in Table 3.3. However, these results were verified by means of trial mixes, as explained in Section 3.3.3.

Table 3.3: Composition of 1 m^3 of the designed reference lightweight concrete mix

Ingredient	Weight kg/m^3	Volume m^3
Ordinary PC	390	0.120
Effective water	179.4	0.179
Absorbed water	7.425	-
Natural sand	598	0.280
Expanded clay	247.5	0.400
Air	-	0.020

3.3.3 Trial mixes

In order to verify the result obtained from the mix design for the reference lightweight concrete, five trial mixes were formulated, as shown in Table 3.4. Three concrete mixes incorporated a superplasticizer admixture type sulfonated naphthalene-formaldehyde condensates (SNF). The other two mixes were produced without superplastizer admixture.

Two contrasting issues can be achieved when the superplasticizer admixture is used: it may increase the workability of the mix while the strength level is kept constant, or vice versa [5]. The second role was considered throughout this experimental programme. This implies a reduction in the total mixing water. On this basis, the content of the superplasticizer was adjusted based upon the fluidity aspect of the reference lightweight concrete. To maintain a similar fluidity in each mixture, the equivalent water/cement ratio for the lightweight concrete mix containing the superplasticizer admixture was calculated using Equation 3.7 [83].

$$\text{W/C of SP}_{mix} = \text{W/C of R}_{mix} \times \frac{(100 - \text{percentage water reduction})}{100} \tag{3.7}$$

where SP_{mix} and R_{mix} are , respectively, the lightweight concrete mix containing superplasticizer and the equivalent concrete mix without the superplasticizer admixture.

The main criteria for evaluating the above five trial mixes are the values of compressive strength and density of concrete mix as well as the fluidity aspect. As mentioned in Section 3.3.2, the first two criteria were intended to be within the classes D1.6 and LC16/18 of the structural lightweight concrete classification [81]. They were therefore experimentally measured at 28 days age. The fluidity aspect refers to the concrete mix being of an adequate workability to suit the practical application. The workability characteristic is indicative of the available time for mixing, transportation, casting and compaction operations of concrete mixes [5]. It was selected to be 50 $\pm$5 mm slump for the fresh concrete state [20].

The results obtained for the aforementioned criteria are presented in Table 3.4. It can be seen that all of the trial mixes met the strength level of the structural lightweight concrete. However, from the point of view of workability, only trial mixes No.2 and No.3 satisfied the necessary requirements. Interestingly, all of the concrete mixes containing the superplasticizer admixture exhibited either worst or collapse workability.

In comparison with trial mix No.3, trial mix No.2 can be formulated with a smaller amount of sand. In addition, this mix had a lower dry density than trial mix No.3. As a result, trial mix No.2 was selected as the reference lightweight concrete mix to be used throughout this study. The values of the dry density and compressive strength of this mix were 1678.3 kg/m^3 and 18.53 MPa at 28 days age respectively. Moreover, the fluidity aspect was 47 mm using the slump test.

Table 3.4: Mix proportions, density, compressive strength and the slump results of the trial mixes

Mix marker	Ingredients							Results of fresh concrete	Results of 28 days	
	Portland PC kg/m^3	Effective water kg/m^3	Natural sand kg/m^3	Expanded clay kg/m^3	Absorbed water kg/m^3	Super-plasticizer (%)	W/C ratio (%)	Slump mm	Density kg/m^3	Strength MPa
Trial mix (1)	392.07	150.87	598	247.5	7.425	1.5	0.384	Collapse	1687.1	19.57
Trial mix (2)	392.07	176.56	598	247.5	7.425	0	0.45	47	1678.33	18.53
Trial mix (3)	390	179.40	728	220	6.6	0	0.46	47	1752.7	21.47
Trial mix (4)	454.37	151.57	598	247.5	7.425	0.75	0.333	10	1724.33	22.71
Trial mix (5)	392.07	141.14	598	247.5	7.425	2	0.36	40	1661.75	18.96

3.3.4 Design of the modified lightweight concrete mixtures

In order to achieve a lightweight concrete mixture with good stability, integrity and insulation properties, the composition of the selected reference lightweight concrete from Section 3.3.3 was systematically modified using by-product materials. Both recycled glass and metakaolin materials were added to the reference lightweight concrete in different percentages. It is important that these percentages be adequately identified. All other constituents of the reference lightweight concrete were kept the same. The obtained concrete mixes were so-called "modified concrete mixes".

Previous studies [35–37] reported that the optimum percentage of metakaolin is 10% by weight of cement. The former percentage was taken as a guide for selection of the metakaolin additions. On this basis, another two sets of metakaolin material (5% and 15%) were also taken into consideration. However, the higher metakaolin percentage (15%) exhibited inferior workability. This behaviour may be explained by the higher surface area of metakaolin particles compared to ordinary Portland cement. Such an issue causes a higher tendency to absorb the mixing water, thereby the cement will become hydrated at a faster rate, and may cause an increase in the micro-hardness of the paste-aggregate interfacial zones [14]. As a result, this percentage was omitted from the experimental scheme of this study. In other words, the adopted percentages of metakaolin were 5% and 10%. In the case of recycled glass, three ratios were selected to be used as a partial replacement for the natural sand, namely 15%, 30% and 45% by volume. This range of replacements was chosen based upon the previous studies [27, 28] to give the best compromise between the substitution of more recycled glass and developing or keeping the thermo-mechanical behaviour of the produced lightweight concrete mix. To evaluate the effect of metakaolin alone on the behaviour of the concrete mix containing a specific ratio of recycled glass, an additional lightweight concrete mix was also considered. This mix contained 45% glass without metakaolin. This allows for a relative comparison with the concrete mix containing a combination of 45% recycled glass with different ratios of metakaolin. As a result, a total of seven modified lightweight concrete mixes were used in the experimental programme. The details of all the above lightweight concrete mixes are presented in Table 3.5.

Table 3.5: Details of reference and modified lightweight concrete mixes

Ingredients	Reference lightweight mix kg/m^3	Modified lightweight concrete mixes						
		15G+5MK kg/m^3	30G+5MK kg/m^3	45G+5MK kg/m^3	15G+10MK kg/m^3	30G+10MK kg/m^3	45G+10MK kg/m^3	45G+0MK kg/m^3
Ordinary PC.	392.07	372.47	372.47	372.47	352.84	352.84	352.84	392.07
Metakaolin	0.00	19.60	19.60	19.60	39.20	39.20	39.20	0.00
Effective water	176.56	176.56	176.56	176.56	176.56	176.56	176.56	176.56
Natural sand	598	508.28	418.59	328.87	508.28	418.59	328.87	328.87
Glass aggregate 0.5-1 mm	0.00	43.46	86.93	130.40	43.46	86.93	130.40	130.40
Glass aggregate 1-2 mm	0.00	43.46	86.93	130.40	43.46	86.93	130.40	130.40
Expanded clay	247.50	247.50	247.50	247.50	247.50	247.50	247.50	247.50
Water due to absorption	7.42	7.42	7.42	7.42	7.42	7.42	7.42	7.42
W/C	0.45	0.45	0.45	0.45	0.45	0.45	0.45	0.45
Total water	183.98	183.98	183.98	183.98	183.98	183.98	183.98	183.98

3.3.5 Test programme

The strategy of the experimental investigation for the developed lightweight concrete mixtures was designed to cover the objective of this research. On this basis, the test programme was divided into two parts. The first part addresses the short- and long-term mechanical behaviour tests of both the reference and modified lightweight concrete samples. These tests are described in detail within Chapter 4. The second part deals with the thermal properties of both lightweight concrete mixtures at ambient and elevated temperatures, as described in detail in Chapter 5. Since the expansion caused by the alkali-silica reaction is normally below the nocuous limit especially when a pozzolanic material (metakaolin) is used as an additive to the concrete mix [11, 12, 34, 37], no experimental test was included to address this issue.

3.3.6 Mixing, casting and curing of concrete samples

Before beginning the casting operation, all specimen moulds were prepared according to BS EN 12390-1 [84]. Each mould was carefully cleaned firstly by removing any residual pieces of concrete. All joints and internal faces were then coated with a thin layer of oil to achieve water-tightness and prevent the concrete from becoming adhered to the mould.

To ensure the homogeneity of the constituents of each mix, the dry ingredients of the concrete mix were pre-mixed for about 2 minutes using a 0.1 m^3 vertical portable mixer in accordance with BS EN 12390-2 [85]. The required amount of mixing water was then slowly added during the mixing process until a suitable consistency was achieved.

The fresh concrete was then cast into the moulds in three layers. Each layer was compacted using a vibrating table until there was no further appearance of large air bubbles on the surface of the concrete. The excess concrete above the upper edge of the mould was removed using a steel trowel to achieve a relatively smooth surface.

After casting, the samples were stored in the laboratory and covered with a nylon sheet to ensure a supply of humid air around the specimens. After 24 hours the samples were demoulded, marked and immersed in a tank of water at a temperature of 20 ± 2 ^oC until the date of the test. Figure 3.3 shows the curing operation of the concrete specimens in water.

Figure 3.3: Curing of concrete specimens in tanks of water

3.4 Summary

A strategy for developing a new structural lightweight concrete has been presented in this chapter. The results obtained show that the volumetric mix proportions of the designed lightweight concrete were 1:2.3:3.3 (cement:sand:expanded clay) which is equivalent to 1:1.5:0.63 by weight. The concrete mix with density, compressive strength and slump of 1678.33 kg/m^3, 18.53 MPa and 47 mm receptivity adequately met the requirements necessary for the structural lightweight concrete of classes D1.6 and LC16/18 as specified by BS EN 206-1 [81] and was considered a reference lightweight concrete. Due to the worst workability associated with their fresh concrete mixes, both the superplasticizer admixture and the mixes with high metakaolin content (15%) were inappropriate for use in formulating the reference and modified lightweight concrete mixes respectively. The development scheme of the modified lightweight concrete mixes indicated two series of metakaolin replacement, namely 5% and 10%, whereas recycled glass was included at three percentages, namely 15%, 30% and 45%.

Chapter 4

Mechanical behaviour of the lightweight concrete mixes

4.1 Introduction

Measurement of the mechanical properties of concrete samples is an important stage in the identification of the global behaviour of the structural elements being produced. Since the research described in this thesis deals with a new formulation of lightweight aggregate concrete, it would be inappropriate if the commonly quoted standard values of the material properties were directly used to reflect the mechanical properties of this kind of concrete.

In this chapter, the mechanical behaviour of both the reference and modified lightweight concrete mixes are experimentally investigated. The test procedures are described in accordance with the relevant BS EN Standards. The results obtained are discussed in detail and compared with some standard expressions for the prediction of a range of mechanical properties. The main conclusions are then summarised at the end of this chapter.

4.2 Mechanical properties of the concrete

In general, the mechanical behaviour of concrete is summarised in terms of its mechanical strength. The strength of concrete is indicative of its load bearing capacity, as well as being a sign of the quality of concrete [5, 82]. In practice, the most common loads are either compressive or tensile (or shear, in some cases) in nature. When a concrete element is subjected to applied loads, it shows some deformation in different directions until failure takes place [5]. In order to evaluate this, uniaxial compressive or tensile loads are normally used.

Previous studies [5, 82] have highlighted that concrete is a complex material. This is because the hydrated cement paste is a function of time, whilst the aggregate phase is a function of its mineralogy. Such conflicting behaviour of the concrete ingredients is the most influential parameter in determining the overall mechanical strength of concrete.

Based upon the aforementioned criteria, a comprehensive experimental programme was designed to evaluate both the reference and modified lightweight concretes mixes. Short and long-term mechanical properties were investigated to give a broader understanding of the actual performance of different concrete mixes.

As density is a critical factor in the lightweight concrete [26], it was also evaluated throughout the experimental programme.

4.3 Details of the experimental programme

4.3.1 Density of concrete

These tests were performed according to BS EN 12390-7 [86]. The average density of three cubic samples with dimensions of 100 mm was determined. To achieve the saturation surface dry condition, the samples were removed from the basin of water, wiped and left to dry in the laboratory for one hour and then weighed using a scale with an accuracy of 1 gram. Due to the unevenness of the top surface of the samples, the volume of the cubes were determined using the actual dimensions of each face. Basically, the density of the concrete was recorded as $mass/volume$ in units of kg/m^3. Since this test was non-destructive, the density was also checked using 100×200 mm cylindrical samples. This test was repeated when the samples were 7, 28, 90 and 180 days old.

4.3.2 Compressive strength

The compressive strengths of the concrete mixes were measured for the 100 mm cube specimens in accordance with BS EN 12390-3 [87] using a digitally controlled compression machine with a maximum load capacity of 2000 kN. Before starting the test, any visible moisture was removed from the specimens. Thereafter, any loose grit or any other materials that could be in contact with the loading plate were cleaned from the specimens' surfaces. The specimens were then placed in the testing machine perpendicular to the axis of the concrete cast. A constant loading rate of 0.3 MPa/s was used throughout the tests. The load and vertical displacement were recorded until the specimen failed and the maximum load in kN was recorded. These tests were carried out for both the reference and modified concrete mixes at ages of 7, 28, 90 and 180 days. Figure 4.1 shows the testing machine and the concrete specimens after the test. The compressive strength (f_c) is given by the following equation:

$$f_c = \frac{F}{A_c} \tag{4.1}$$

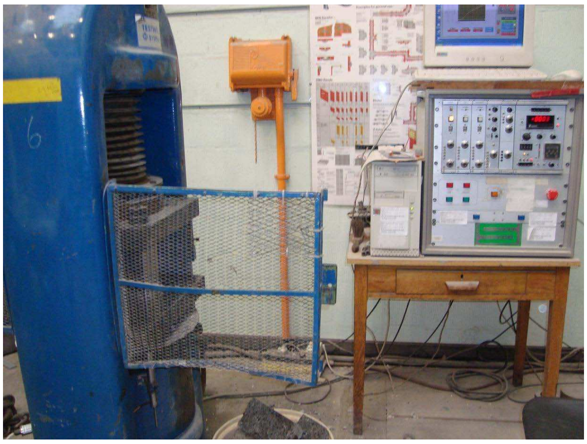

(a) Testing machine

(b) Cube specimens after the test

Figure 4.1: Compression-testing machine and cube specimens after the test

4.3.3 Splitting tensile strength

The indirect tensile strength was measured by means of a splitting tensile strength test according to BS EN 12390-6 [88]. Cylindrical specimens with dimensions of 100 × 200 mm were tested.

Two wooden packing strips with dimensions of $200 \times 15 \times 3$ mm ($l \times w \times t$) were fixed to the upper and lower surfaces of the specimens in order to ensure a uniformly distributed applied load, as shown in Figure 4.2a. The assembly of the steel rig and the concrete specimen was placed in the compression-testing machine, and an axial load was then applied at a constant rate of 1.5 kN/s, as shown in Figure 4.2b. Following this, the maximum failure load was recorded and the splitting tensile strength (f_t) was calculated using Equation 4.2. The result for each case was taken as the mean of three values. Due to time constraints, this test was carried out at ages of 120 and 180 days.

$$f_t = \frac{2F}{\pi DL} \tag{4.2}$$

(a) The steel rig and cylindrical specimen

(b) Testing machine

Figure 4.2: Set-up of the splitting tensile test

4.3.4 Modulus of elasticity and Poisson's ratio

These tests were carried out according to BS ISO 1920-10 [89] using cylindrical specimens with dimensions of 100×200 mm. The average result of the two tests was taken to determine the static modulus of elasticity. The specimens had been taken out of the water two weeks previously in order to attach the vertical and lateral strain gauges, as shown in Figure 4.3a. For more accurate readings, linear potentiometer with a length of 85 mm were attached vertically to the specimen on two sides. The specimens were then placed in the compression machine and the axial load was applied at a constant rate of 0.3 MPa/s, as shown in Figure 4.3b. The values of the load, vertical and lateral displacements were digitally recorded. The test was conducted at a sample age of 140 days. The modulus of elasticity (E_c) and Poisson's ratio (v) were calculated using Equations 4.3 and 4.4 respectively.

$$E_c = \frac{\Delta_\sigma}{\Delta_\varepsilon} = \frac{\sigma_a - \sigma_b}{\varepsilon_a - \varepsilon_b} \tag{4.3}$$

where $\sigma_a = f_c/3$ and $\sigma_b = 0.5$.

$$v = -\frac{\Delta\varepsilon_{Lateral}}{\Delta\varepsilon_{Vertical}} \tag{4.4}$$

(a) Fitting the strain gauges

(b) Application of the compression load

Figure 4.3: Static modulus of elasticity test using cylindrical specimens

4.4 Test results and discussion

4.4.1 Density of concrete mixes

Figures 4.4a to 4.4f show the results obtained of the density measurements. It can be seen that the modified concrete mixes exhibited lower densities than the reference mix for all ages of the test samples. This was to be expected, as the specific gravity of recycled glass, at 2.52, is less than that for natural sand, at 2.65. The substitution of sand for glass particles was done by volume, meaning that the obtained density would be lower than for those of the reference concrete mix. This observation is in agreement with the results of Ismail and Al-Hashmi [28].

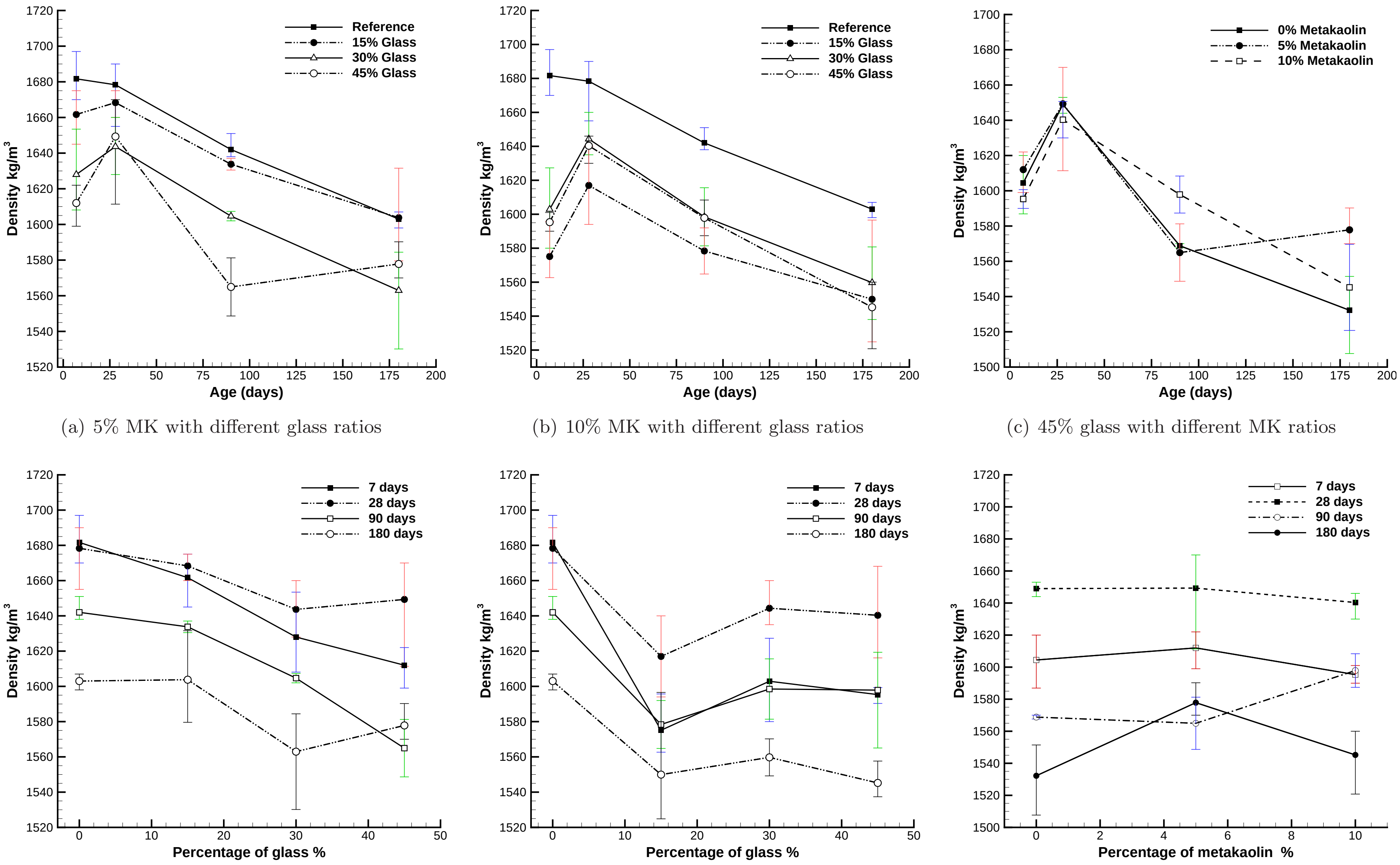

(a) 5% MK with different glass ratios

(b) 10% MK with different glass ratios

(c) 45% glass with different MK ratios

(d) 5% MK at different test ages

(e) 10% MK at different test ages

(f) 45% glass at different test ages

Figure 4.4: Density of the reference and modified concrete mixes

In general, all of the lightweight concrete mixes exhibited a continuous decrease in density beyond 28 days curing, as shown in Figures 4.4a to 4.4c. There are several possible explanations for this observation. These are: the consumption of the water available to generate the chemical reactions during the hydration processes [82]; the removal of evaporable water existing in the capillary pores when the ambient relative humidity falls below about 45%, leaving empty pores and the interlayer or zeolitic water which is usually held between the surfaces of certain planes in a crystal may contribute to the decrease in density [5]. Increases in the density of the modified concrete mixes at 28 days age compared with those at 7 days were also observed by Courard et al. [90].

For concrete mixes containing 5% metakaolin, a reduction in density values caused by the addition of glass was observed. Since glass possesses a lower specific gravity than natural sand, the magnitude of this reduction increased as the glass content increased. However, the concrete mix containing 45% glass showed a slight increase in density at 28 and 180 days when compared to the mix containing 30% glass, as shown in Figures 4.4a and 4.4d. The reason for this might be the smooth surface texture of the glass particles and their reduced tendency to absorb water in comparison with sand, thereby increasing the amount of water confined in the interior pores of the concrete mix at the higher glass ratio (45%) and thus resulting in an increase in the concrete density [6, 8, 9]. A decrease in density was observed for the concrete mix containing 45% glass content at 90 days age. The reason for this observation is unclear.

The high metakaolin content (10%) was shown to have an appreciable effect upon density, as can be seen in Figures 4.4b and 4.4e. The highest reduction in density was observed in the case of the concrete mix with 15% glass, followed by the mixes with 45% and 30% glass respectively. These seemingly contradictory results may be related to the role of the metakaolin material in the hydration of cement. It causes acceleration of the hydration process and increases the quantity of water consumed, as Parande et al. noted [10]. This phenomenon becomes more visible when the percentage of metakaolin replacement is increased to 10%, leading to a reduction in the density of the concrete mix. However, this role diminishes with increasing glass content.

Figures 4.4c and 4.4f show the effect of metakaolin additions on the density of concrete mixes containing 45% glass. It can be seen that an increase in metakaolin content leads to a decrease in the density of concrete at earlier ages (7 and 28 days). Similar results were also reported by Wild et al. [34] and are consistent with the accelerated rate of hydration due to metakaolin. After that, the density increased with increasing metakaolin content.

4.4.2 Compressive strength

The results of the compressive strength behaviour of the reference and modified concrete mixes at various metakaolin ratios and test ages are presented in Figures 4.5a to 4.5f. These results indicate that the modified concrete mixes possessed higher compressive strength values than the reference mix and exceeded the required strength level of structural lightweight concrete by as much as 11%. It is likely that these results are due to the role of the metakaolin material in the pozzolanic reaction, filler function and acceleration of the cement hydration process [10], resulting in improved compressive strength.

Due to the high silica content of the pozzolanic material (metakaolin), it has the capability to react with the calcium hydroxide generated from the hydration process to produce a gel of calcium silicate hydrate (C-S-H), as shown below. The C-S-H content has an important effect on the strength of concrete [10–12, 33].

$$SiO_2 + Ca(OH)_2 \rightarrow CSH$$

It was observed that the highest compressive strength with 5% metakaolin content was achieved in the case of the mix with 30% glass content for ages up to 90 days, as shown in Figures 4.5a and 4.5d. After this sample age, the 15% glass content samples showed higher compressive strength. However, there was a slight decrease in the compressive strength of the concrete mix containing 45% glass at later ages when compared with the reference concrete. This may be attributed to only partial elimination of $Ca(OH)_2$ being achieved (due to insufficient metakaolin being present), with the negative effect of the glass aggregate on the compressive strength [8, 9].

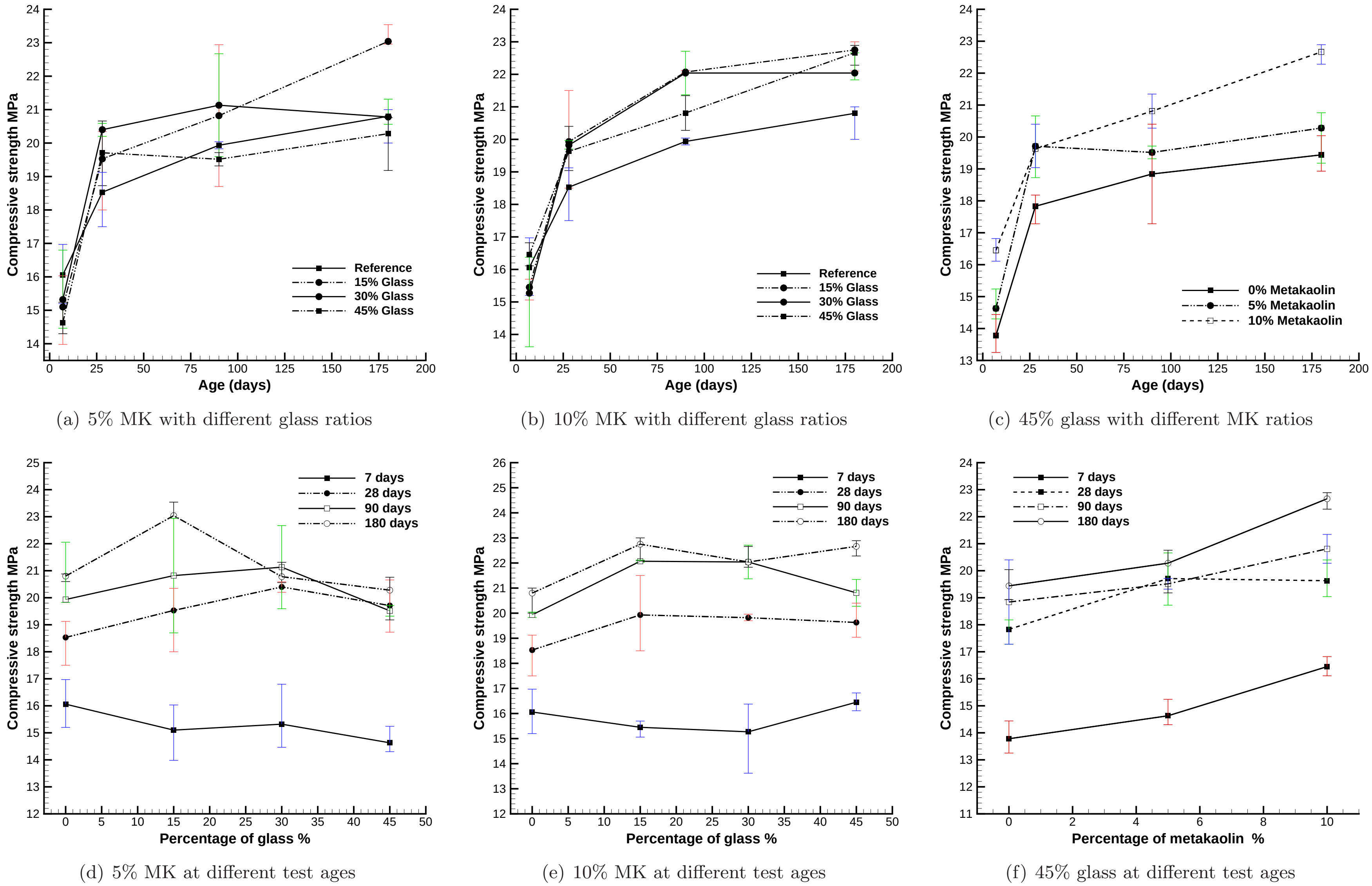

(a) 5% MK with different glass ratios

(b) 10% MK with different glass ratios

(c) 45% glass with different MK ratios

(d) 5% MK at different test ages

(e) 10% MK at different test ages

(f) 45% glass at different test ages

Figure 4.5: Compressive strength of the reference and modified concrete mixes

Clear improvements in compressive strength were observed for the modified concrete mixes compared to the reference mix at all ages of the test when 10% metakaolin was used, as shown in Figures 4.5b and 4.5e.

It was noted that the compressive strength of the concrete samples containing 30% recycled glass with both levels of metakaolin replacements (5% and 10%) indicated a slight decrease at later ages (180 days), as shown in Figures 4.5a and 4.5b. The reason for this decrease is not clear, but is thought to be related to the amount of metakaolin required to fully coat the glass particles.

Generally, it can be said that the most influential parameter governing the compressive strength of modified concrete mixes containing various glass contents is the ratio of metakaolin to glass. A high metakaolin to glass ratio improves the strength up to a ratio value of about 22%, as shown in Figure 4.6, while low ratio values produce concrete mixes with lower strength capacity. If the ratio increases above 22%, inconsistent behaviour is observed up to 33%, and then no appreciable change in compressive strength can be considered when the ratio of metakaolin to glass increases above 33%.

In the case of fixed glass content (45%), an increase in metakaolin content improves the compressive strength for all testing ages, as shown in Figures 4.5c and 4.5f.

The expression suggested by BS EN 1992-1-1 [91] for estimating the compressive strength at time (t) for concrete of a normal weight has been validated using SPSS statistical software to investigate its consistency with the obtained compressive strength results of the lightweight concrete mixtures. The expression is as below:

$$f_{cm}(t) = \beta_{cc}(t) f_{cm} \tag{4.5}$$

and

$$\beta_{cc}(t) = exp\left\{ s\left[1 - (\frac{28}{t})^{1/2}\right]\right\} \tag{4.6}$$

where f_{cm} is the mean compressive strength (MPa) at 28 days; t is the age of the concrete sample in days and s is a coefficient whose value depends on the type of cement and is typically in the range of 0.2-0.38 for normal weight concretes.

In this study, one type of cement was used to produce all of the concrete mixes as mentioned in Section 3.3.1, so a difference in s value might be considered to give an indication of the effect of recycled glass and metakaolin materials on the compressive strength.

The results of the nonlinear regression analysis showed that the value of s coefficient for the reference concrete is located out of the standard limits at 0.16, while it was consistent with the above limits for the concrete mixes containing 15% and 30% recycled glass with 10% metakaolin content with values of 0.24 and 0.22 respectively.

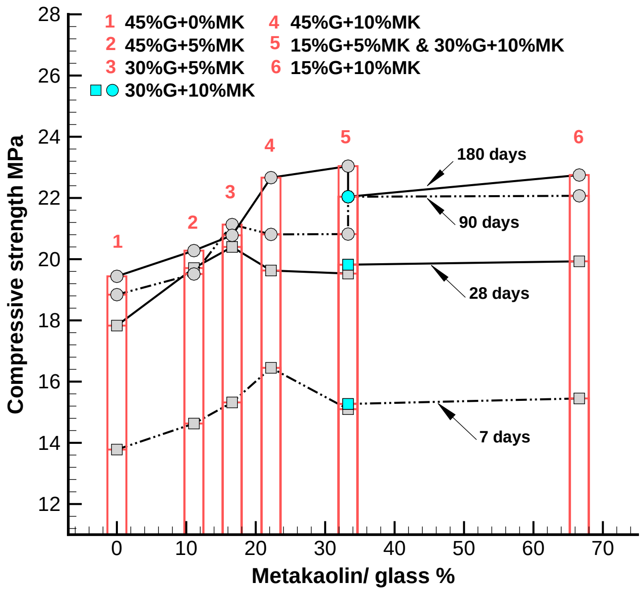

Figure 4.6: The effect of metakaolin/glass ratio on the compressive strength of the modified lightweight concrete mixes containing various percentages of glass

4.4.3 Splitting tensile strength

The results of the splitting tensile strength tests are presented in Figures 4.7a to 4.7c. Improvements in splitting tensile strength were observed for the modified concrete mixtures in relation to the reference concrete. These improvements may be related to an increase in the compressive strength of the concrete mixtures resulting from the pozzolanic action of the metakaolin material. The same behaviour was also reported by Qian and Li [92].

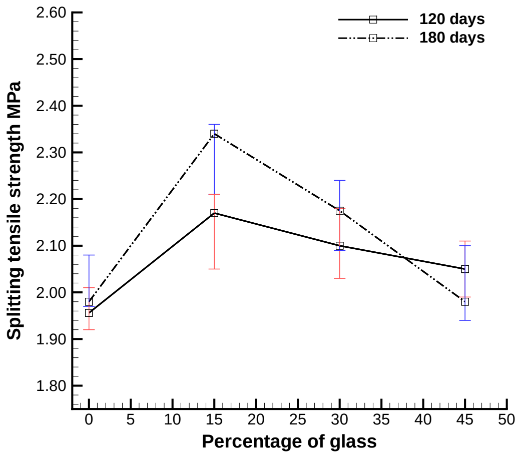

(a) 5% MK at various glass ratios

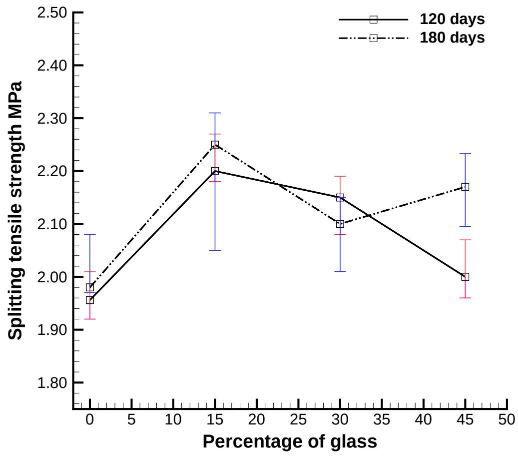

(b) 10% MK at various glass ratios

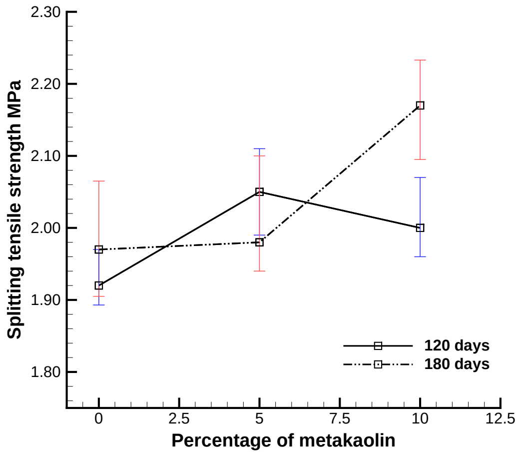

(c) 45% glass at different MK ratios

Figure 4.7: The splitting tensile strength of the reference and modified lightweight concrete mixes

The effect of the glass ratio with 5% metakaolin content on splitting tensile strength is shown in Figure 4.7a. It can be seen that the concrete mix containing a 15% glass ratio exhibits the highest tensile strength value for both test ages. This behaviour is consistent with the measured compressive strengths of these mixes. A slight decrease in splitting tensile strength was seen for mixes with 30% and 45% glass ratios. A similar tendency for the splitting tensile strength feature of the concrete mixes containing 10% metakaolin to those containing 5% metakaolin was also observed, as shown in Figure 4.7b. These observations may be explained by the presence of flaws at higher glass contents, leading to high stress concentrations in very small volumes of specimen associated with micro-fracture. These flaws vary in size and could be caused by shrinkage within the hydrated cement paste and a weaker bond in the transition zone between the paste and aggregate [5].

The effect of metakaolin content on the splitting tensile strength of the concrete mixes containing a 45% glass ratio is shown in Figure 4.7c. Overall, a noticeable improvement in splitting tensile strength can be achieved when metakaolin is added to a concrete mix containing a high percentage of glass.

BS EN 1992-1-1 [91] uses the following expression to predict the tensile strength of lightweight concrete according to its density and the characteristics of normal weight concrete.

$$f_{lctm} = f_{ctm} . \eta_1 \tag{4.7}$$

$$f_{ctm} = 0.3 f_{ck}^{2/3} \tag{4.8}$$

where f_{lctm} and f_{ctm} are the tensile strength of the light and normal weight concrete respectively in MPa ; f_{ck} is the compressive strength of normal weight concrete in MPa; η_1 is a coefficient that can be obtained from the following equation.

$$\eta_1 = 0.4 + 0.6\rho/2200 \tag{4.9}$$

where ρ is the density of lightweight concrete in kg/m^3.

Using regression analysis of the results obtained in this study, Equations 4.10 and 4.11 were derived to compute the splitting tensile strength of lightweight concrete mixtures directly from their compressive strength values, with R^2 values of 0.76 and 0.88 for 5% and 10% metakaolin replacement respectively.

$$f_{lctm} = 0.1 f_{lck} \tag{4.10}$$

$$f_{lctm} = 0.096 f_{lck} \tag{4.11}$$

where f_{lck} is the compressive strength of lightweight concrete in MPa.

4.4.4 Stress-strain behaviour

The values for both lateral and vertical strains with their corresponding stresses for the reference and modified lightweight concrete mixes are presented in Figures 4.8a to 4.8c.

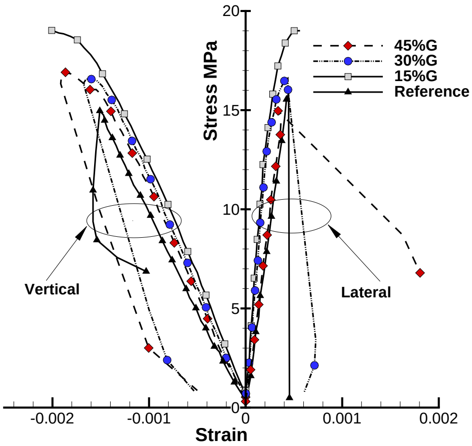

(a) 5% MK at various glass ratios

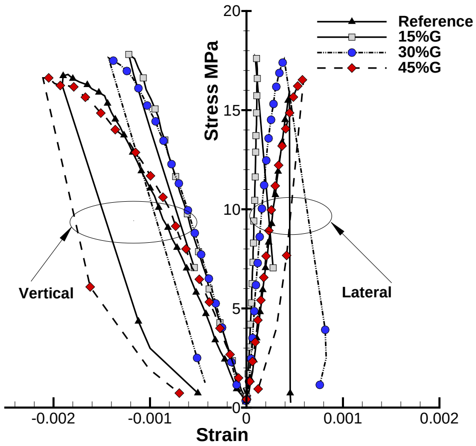

(b) 10% MK at various glass ratios

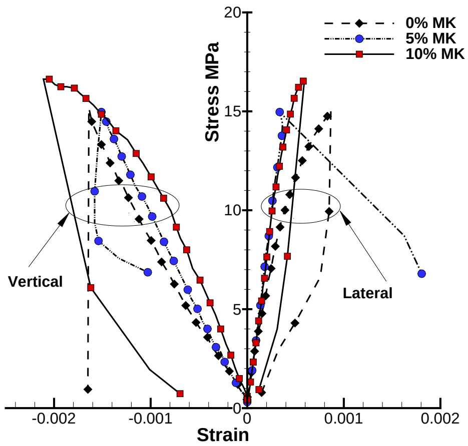

(c) 45% glass at different MK ratios

Figure 4.8: Stress-strain curves of the reference and modified concrete mixes

It can be seen that the stronger concrete mix possesses a steeper post peak part of the stress-strain curve than the other mixes. In other words, the stronger lightweight concrete mix shows the most brittle behaviour, while the less steep post peak part of the stress-strain curve represents behaviour which is more ductile.

The maximum lateral and vertical strains were 0.00168 and 0.0021 for the concrete mixes containing 45% glass, with 5% and 10% metakaolin respectively.

All measured compressive stress values for the concrete mixtures were lower than those derived using the cube samples. This is well understood when using cylindrical specimens to measure compressive strength. Cube specimens exhibit more lateral restriction than cylindrical ones, due to their geometrical shape; thereby the measured compressive strength is higher [5].

For both quantities of metakaolin replacement, with the exception of the concrete mixes containing 45% glass, the reference concrete mix showed a lower stress magnitude, while the concrete mix containing 15% glass exhibited a higher stress level, as shown in Figures 4.8a and 4.8b. Furthermore, at a specific stress level, the stronger concrete mixture has a lower strain value.

The effect of the metakaolin ratio on the stress-strain behaviour of the concrete mixes containing 45% glass is shown in Figure 4.8c. From this figure, there is a clear trend that the high metakaolin content (10%) enhances the load-bearing capacity of a concrete mixture.

4.4.5 Static modulus of elasticity and Poisson's ratio

The results of static modulus of elasticity and Poisson's ratio at 140 days age are illustrated in Figures 4.9 and 4.10.

These figures show that the greatest modulus of elasticity for concrete mixes containing 5% metakaolin was observed for a mix containing 15% glass, while a mix containing 30% glass demonstrated the highest modulus of elasticity for the set of concretes containing 10% metakaolin replacement. This is consistent with compressive strength behaviour which is affected by the coating of the metakaolin material around the glass aggregate particles.

All of the modified concrete mixes (except the mix containing 45% glass with 5% metakaolin) showed improvements in the modulus of elasticity when compared with the reference concrete.

The increase in the modulus of elasticity for the concrete mix containing 30% glass with 10% metakaolin was about 43%.

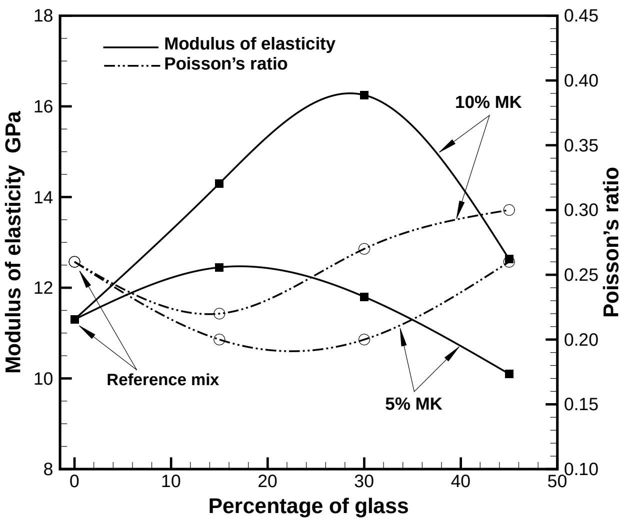

Figure 4.9: Modulus of elasticity and Poisson's ratio of the reference and modified concrete mixes

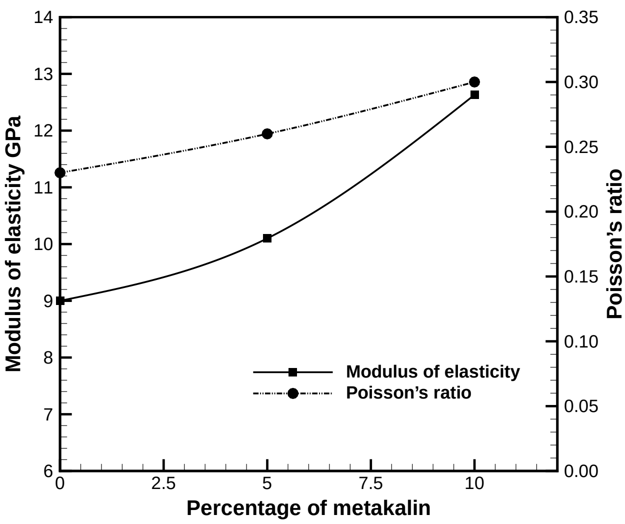

Figure 4.10: The effect of metakaolin material on the modulus of elasticity and Poisson's ratio of the concrete mix containing 45% glass

The results of the Poisson's ratio measurements indicate that the concrete mixes containing 45% glass give higher values for both amounts of metakaolin replacement.

A semi-linear relationship was observed between the characteristics of the modulus of elasticity and the Poisson's ratio with the percentage of metakaolin for the concrete mixes containing a 45% glass replacement, as shown in Figure 4.10.

4.5 Summary

The short and long-term mechanical properties of both reference and modified lightweight concrete mixes were experimentally measured. The results obtained show that when the recycled glass materials are used in conjunction with metakaolin additions and expanded clay, it is possible to produce a structural lightweight concrete with compressive strength and density of up to 20.4 MPa and 1617 kg/m^3 respectively at 28 days age. The inclusion of recycled glass particles results in a decrease in the density values of modified concrete mixes by as much as 6% compared to the reference mix. This reduction was observed at all curing times. Improvements in the value of the compressive strength in both the short- and long-term behaviours were achieved when metakaolin was used as a partial replacement for cement. The ratio of metakaolin to recycled glass influences the overall strength development of the modified concrete mixes, with the maximum increase in compressive strength being observed at a metakaolin:glass ratio of 22%. Improvements in splitting tensile strength were observed at all curing times and these correlated with observed increases in compressive strength. An increased metakaolin content improves the modulus of elasticity of the modified concrete mixes by as much as 43%.

Chapter 5

Thermal behaviour of the lightweight concrete mixes

5.1 Introduction

In the event of a fire or exposure to high temperatures, thermal stresses play a significant role in the deterioration of concrete structures, and the outcome is greatly affected by the thermal properties of the concrete being used. As part of the research objectives, the thermal behaviour of the produced lightweight concrete mixes needs for evaluation.

This chapter describes an experimental investigation carried out in this important area. The behaviour of concrete at elevated temperatures is described. The details of the experimental programme are then presented. Thereafter, the results obtained are discussed followed by a summary of the main conclusions raised in this chapter.

5.2 Behaviour of concrete at elevated temperatures

When concrete is exposed to high temperatures, some physical and chemical changes take place. Previous studies have described these changes in several forms [42–44, 93]. Free water evaporates at around 100 ^{o}C and is completely removed at 120 ^{o}C. Above approximately 150 ^{o}C, there is a loss of the water chemically bound in hydrated calcium silicate, with a peak rate of loss at 270

^{o}C. The propagation of micro-cracks begins after 300 ^{o}C and mechanical strength and thermal conductivity are degraded at this stage, with some associated expansion taking place. Between 400 ^{o}C and 600 ^{o}C, complete desiccation occurs and crystals of calcium hydroxide decompose into their original components (calcium oxide and water), producing weakened concrete. Further decomposition of hydrated calcium silicate takes place above 600 ^{o}C, and spalling behaviour is observed. The cement paste is transformed into a glass phase above 1150 ^{o}C.

As mentioned in Chapter 2, spalling reduces the integrity of concrete members and may cause the complete collapse of a structure. It occurs at elevated temperatures when the pore pressure and thermal stresses exceed the tensile strength of the concrete. The most influential parameters governing this phenomenon are the permeability of the concrete and the continuity of its pore system. If the concrete has a low permeability with a close pore network, the pore pressure begins to build up. This increasing pressure produces stresses on the interior structure of the concrete. The intensity of pore pressure increases with increasing temperature [53, 54].

5.3 Details of the experimental programme

Unit weight (density), thermal conductivity, specific heat and heat flow characteristics were investigated at ambient and elevated temperatures according to the relevant BS EN Standards. The temperature exposure ranged from 20 ^{o}C to 800 ^{o}C. The former range represents the most critical conditions in which the phase changes may occur [42, 44, 64] . The same mix proportions as those mentioned in Section 3.3.4 were used to formulate the reference and modified lightweight concrete mixes. However, because the casting operation was carried out during the summer season, the amount of water absorbed by the expanded clay particles was revised to overcome the drying out of the particle surfaces during the storing period. It was adjusted to be 12%.

5.3.1 Density at elevated temperatures

The densities of the concrete mixes at elevated temperatures were measured in accordance with BS EN 12390-7 [86] using $200 \times 100 \times 50$ mm prism specimens. This test aimed to evaluate the effect of moisture content on the thermal performance of the concrete mixes. The prism samples were removed from the water and wiped using a clean piece of cloth and kept in the laboratory air conditions for about one hour. A manually controlled furnace with a heating capability of up to 1000 ^oC was used to apply a heating rate of about 10 ^oC/minute, as shown in Figure 5.1. The tests were conducted at a specimen age of 90 days.

Figure 5.1: The manually controlled furnace used to generate higher temperatures for the density test

5.3.2 Thermal conductivity test

The hot wire method described in BS EN 993-15 [94] was used to measure the thermal conductivity of 200 × 100 × 50 mm brick concrete samples. Nichrome wire with a diameter of 1.6 mm and 0.537 ohms per metre resistance was used as a hot wire.

Three type K thermocouples with a wire diameter of 1.6 mm were used simultaneously to measure the temperature increase within the furnace and within the reference and measurement specimens. The hot wire and measurement thermocouple were fixed in parallel to the top surface of the lower concrete sample (the measurement specimen) at a distance of 15 mm during the casting operation of the concrete, as shown in Figures 5.2a and 5.2b. A reference thermocouple was attached to the upper concrete sample (the reference specimen) using TBS, a thermal bonding compound. Three support pieces and a top cover from the same concrete mix were used, with dimensions of 125 × 10 × 20 mm and 125 × 100 × 20 mm respectively, as shown in Figure 5.2c.

The test assembly was placed inside the furnace and the hot wire was connected to a digital

(a) Preparation of the moulds

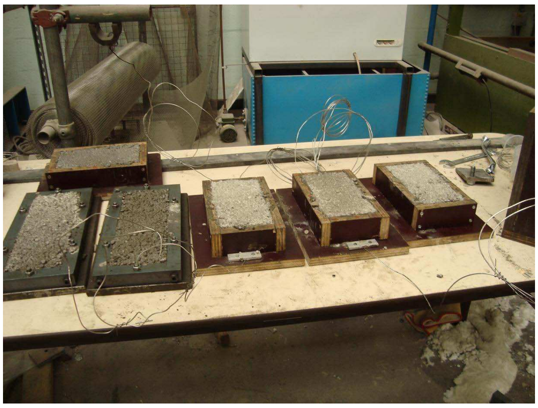

(b) Casting of the concrete samples with hot wire

(c) Test assembly in the furnace

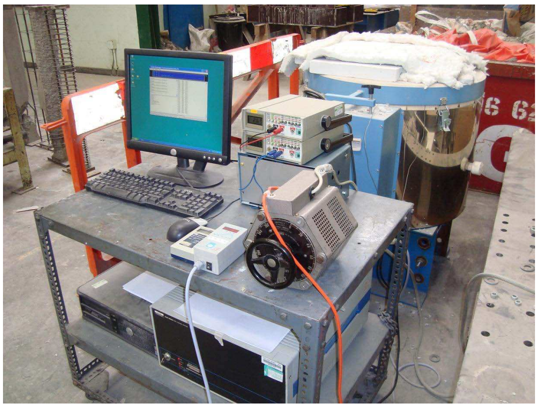

(d) Furnace and multimeter

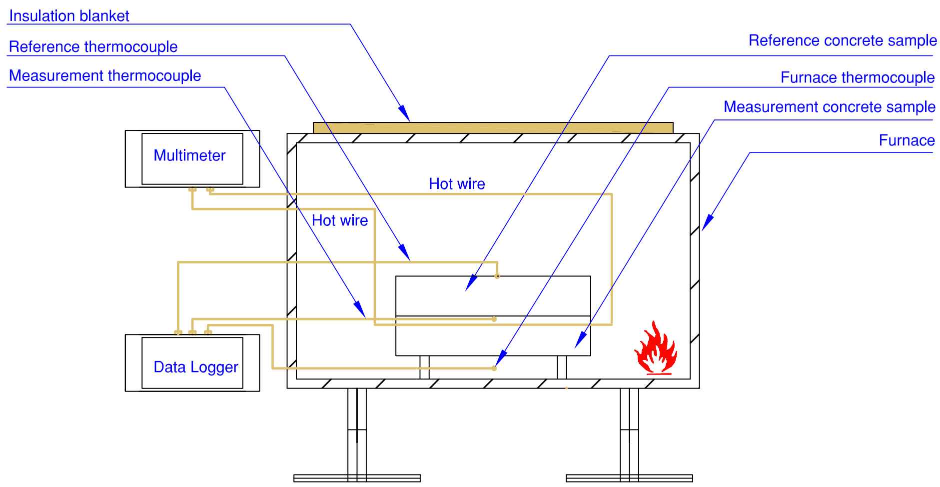

(e) A schematic for the thermal conductivity test

Figure 5.2: Preparation and set-up of the thermal conductivity test

multimeter in order to measure the current and voltage drop along it, as shown in Figures 5.2d and 5.2e. The furnace was then heated to the specific test temperature at a heating rate of

300 ^{o}C/h. This test was carried out at a sample age of 90 days and at a range of temperatures between 20 ^{o}C and 800 ^{o}C. The test was conducted twice at each temperature and the average of the two values was taken. Thermal conductivity (λ) was determined using the following equation:

$$\lambda = \frac{P}{4\pi l} \times \frac{-Ei(\frac{-r^2}{4at})}{\Delta\theta(t)} \tag{5.1}$$

where P is the rate of energy transfer in W, l is the length of the hot wire (=0.2 m), r is the distance between the hot wire and the measurement thermocouple (=0.015 m), t is the time in seconds elapsed from the heating circuit was switched on, and a is the thermal diffusivity in m^2/s. The term $-Ei(-r^2/4at)$ is an exponential integration depending on the temperature-time difference [94].

5.3.3 Heat flow test

Unidirectional heat flow tests were carried out according to BS EN 1363-1 [70], using prism specimens measuring 300 $\times$ 100 $\times$ 29 mm. The heat was supplied by a digitally controlled furnace with a heating rate of 300 ^{o}C/h. The heating chamber of the furnace had an internal diameter of 648 mm and a height of 534 mm, as shown in Figure 5.3a. Each specimen was placed over the upper opening of the furnace. Three type K thermocouples of 1.6 mm diameter were used to measure the temperature rise in the furnace and on the exposed and unexposed surfaces of the concrete sample. These thermocouples were attached using tie wire and the thermal bonding compound, as shown in Figure 5.3b. The same approach was also used by Borhan [95]. All of the sides of the concrete specimen were covered with an insulation blanket.

Thereafter, the furnace temperature was increased to 800^{o}C and kept at this temperature for about 25 minutes. The temperature of the furnace and of both the exposed and unexposed surfaces of the concrete samples were recorded simultaneously every 15 seconds. In addition, a thermal camera was used to check the temperature of the unexposed surface. This test was conducted at a sample age of 90 days. Figure 5.3c shows the unidirectional heat flow regime.

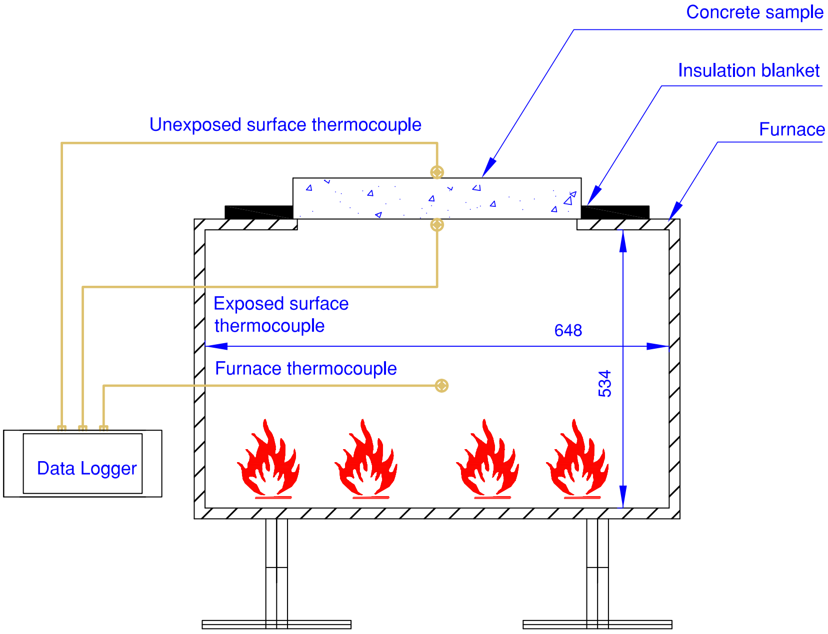

(a) Digitally controlled furnace (all dimensions in mm)

(b) Attached the thermocouples

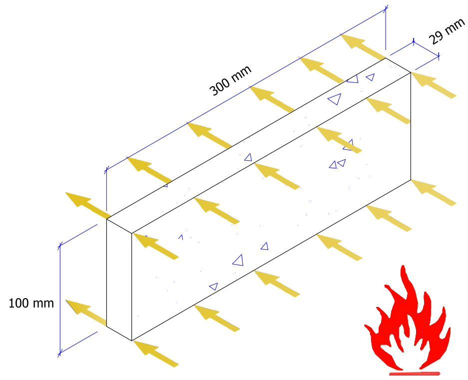

(c) Unidirectional heat flow regime (rotated 90^o)

Figure 5.3: Details of the unidirectional heat flow test

5.3.4 Specific heat calculation

The specific heat (c_p) of the reference and modified concrete mixes was calculated at ambient and elevated temperatures based upon the results of the thermal conductivity and density features, using the following equations [96]:

$$c_p = \frac{\lambda}{\rho.a} \tag{5.2}$$

$$a = cr^2 exp[\frac{4\pi \Delta T \lambda}{Q}]/(4t) \tag{5.3}$$

where c is the Euler's constant = 1.781; Q is the power per unit length (W/m) and ΔT is the temperature difference in K.

5.4 Test results and discussion

5.4.1 Density at elevated temperatures

The results of the density measurements at elevated temperatures for the reference and modified concrete mixes are illustrated in Figures 5.4a to 5.4c.

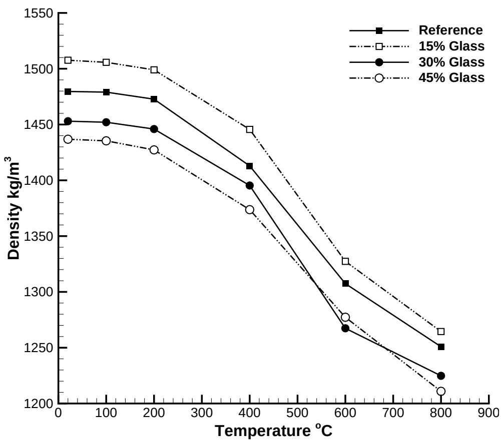

(a) 5% MK with various glass ratios

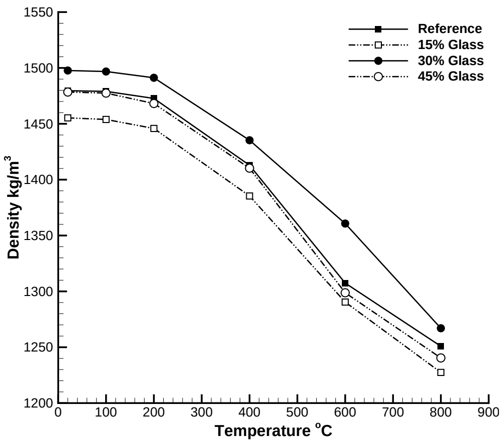

(b) 10% MK with various glass ratios

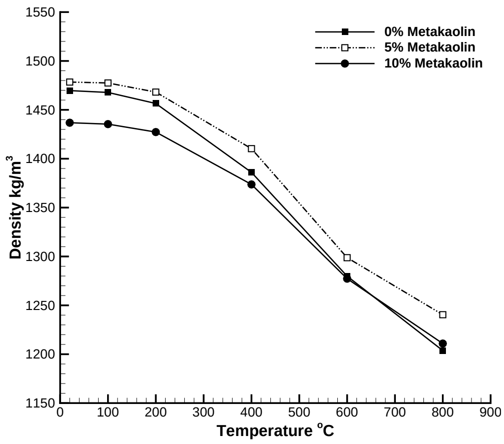

(c) 45% glass with various MK ratios

Figure 5.4: The effect of elevated temperatures on the density value of the reference and modified concrete mixes

In general, the density of concrete mixes trended to decrease with an increase in temperature. This behaviour is due to the elimination of the free water from the capillary pores by evaporation, in addition to the loss of chemically bound water [42–44, 93]. The decrease in density at 800 ^{o}C compared to the density measured at ambient temperature was about 20% for both the reference and modified concrete mixes.

Different density values were observed for the lightweight concrete mixes at temperature of 20 ^{o}C measured in this experimental part compared to those observed during the mechanical properties programme described in Chapter 4. This may be attributed to the effect of the surface conditions of the expanded clay particles and the time of casting. Particles with dry surface conditions can absorb a lot of water and this can consequently affect the density. This behaviour indicates the reason for classifying the lightweight concrete into a range of density classes, as each class has an upper and a lower density limit [81].

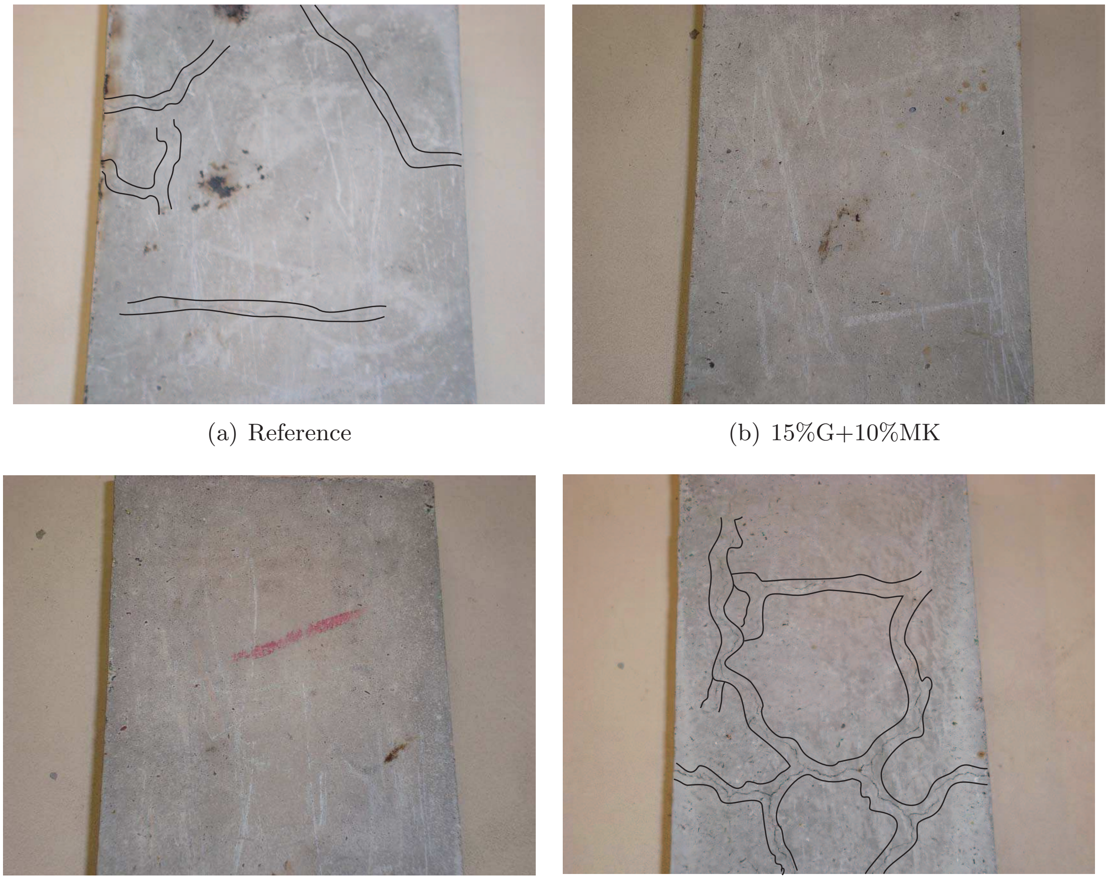

(a) Reference

(b) 15%G+10%MK

(c) 30%G+10%MK

(d) 45%G+0%MK

Figure 5.5: Reference and several modified concrete samples after heating to 800 ^{o}C

Visual inspection of the reference concrete mix and the mix containing 45% glass without metakaolin revealed that several cracks had formed at higher temperatures. Conversely, the metakaolin replacement improved the durability of the modified concrete mixes against high temperatures, as shown in Figures 5.5a to 5.5d. However, the mixes with high glass content (45%) exhibited spalling at 800 ^{o}C, regardless of the presence of metakaolin. It seems likely that this behaviour was due to the large temperature variation between the outer and inner surfaces of the concrete samples, associated with a higher heating rate. These factors combined to produce a higher internal pressure exceeding the tensile strength of the concrete sample [53, 54].

The experimental tests also showed that the concrete mixes exhibited a colour change at elevated temperatures. The colour change was from dark grey to a white colour.

5.4.2 Thermal conductivity and specific heat

Figures 5.6a to 5.7c show the results of thermal conductivity and specific heat measurements for the reference and modified concrete mixes at ambient and elevated temperatures.

It can be seen that all of the modified concrete mixes showed superior thermal behaviour, with their measured thermal conductivity values up to 42% lower than those of the reference concrete mix. A possible explanation for this behaviour is the fact that glass and metakaolin have lower thermal conductivities than natural sand and Portland cement which they partially replaced, thereby reducing the thermal conductivity of the modified mixes. However, between 20 ^{o}C and 400 ^{o}C, the decrease in thermal conductivity of the concrete mix containing 30% glass was less than for the mix containing 15% glass, as shown in Figures 5.6a and 5.6b, meaning that another factor influenced the thermal conductivity of the concrete mixes. This could be related to the distribution of air voids throughout the concrete sample [5].

The percentage decreases in thermal conductivity at ambient temperature for the concrete mixes containing 15%, 30% and 45% glass ratios with 5% metakaolin were 37%, 32% and 16.5% respectively, when measured in relation to the value of the reference concrete. The corresponding percentage decreases for the 10% metakaolin replacement were 31%, 30% and 42% respectively.

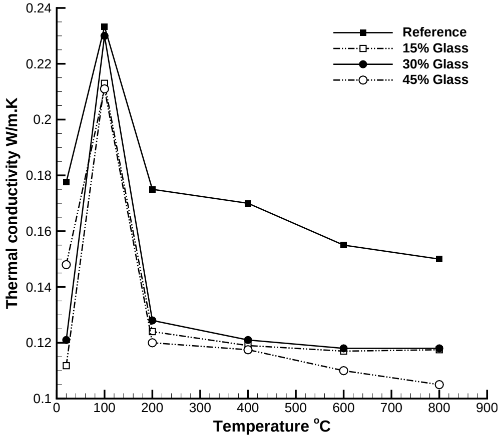

(a) 5% MK with various glass ratios

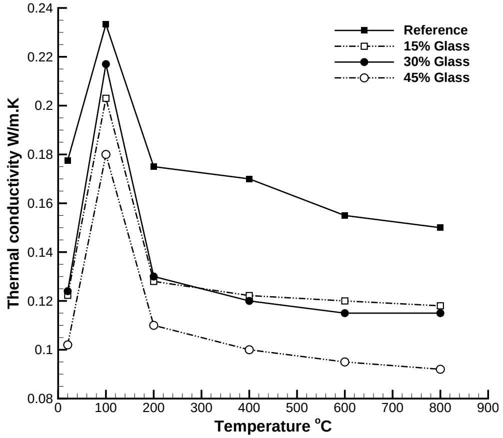

(b) 10% MK with various glass ratios

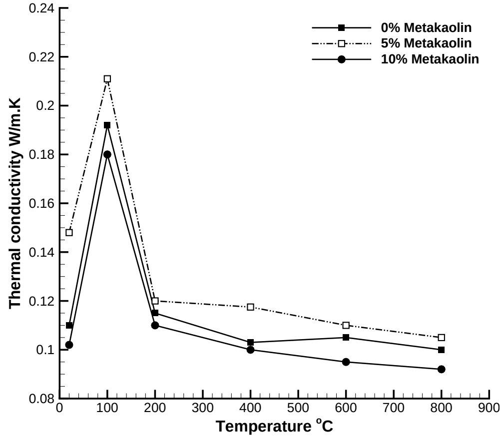

(c) 45% glass with various MK ratios

Figure 5.6: Thermal conductivity of the reference and modified lightweight concrete mixes at elevated temperatures

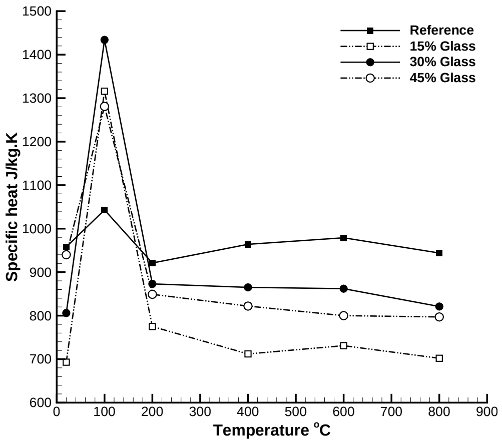

(a) 5% MK with various glass ratios

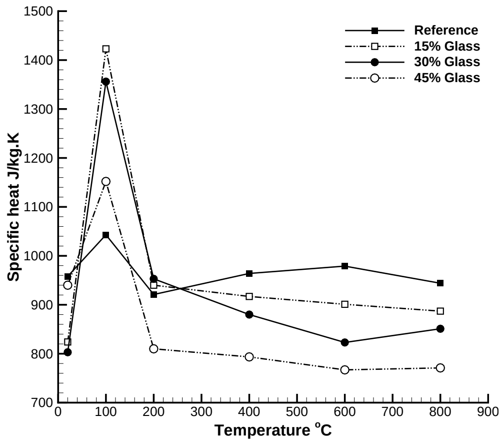

(b) 10% MK with various glass ratios

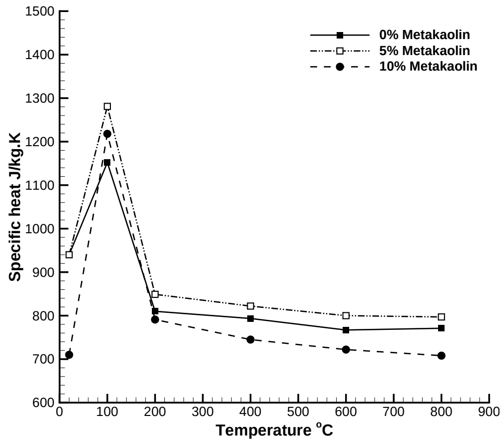

(c) 45% glass with various MK ratios

Figure 5.7: Specific heat of the reference and modified concrete mixes at elevated temperatures

In the case of exposure to high temperatures (800 ^{o}C), the aforementioned percentages were 21%, 21% and 30% for the set of concretes containing 5% metakaolin and 21%, 23% and 38% for those containing 10% metakaolin.

For all of the concrete mixes, the value of thermal conductivity was higher at 100 ^{o}C than at ambient temperature, due to the evaporation of free water associated with loss of latent heat of vaporisation, as shown in Figures 5.6a to 5.6c. Once the free water was completely removed, the thermal conductivity decreased as the temperature increased. The same behaviour is mentioned in BS EN 1996-1-2 [55].

A positive effect was observed for the 10% metakaolin content on reducing the thermal conductivity of the concrete samples containing 45% glass content, as shown in Figure 5.6c. However, the same cannot be said in the case of the lower percentage of metakaolin (5%), where higher thermal conductivity values have been observed. The reason for this contrast in the behaviour of the metakaolin is not clear, but it may be linked to the internal structure of the concrete mix.

Except at 100 ^{o}C, the calculated values of specific heat for the modified concrete were lower than those of the reference samples, as shown in Figures 5.7a to 5.7c. This may be attributed to the lower thermal conductivity of these mixes when compared to the reference concrete. At 100 ^{o}C, the modified concrete mixes held excessive amounts of water in the interior pores, which caused an increase in the specific heat at this temperature, whereas a smaller increase was recorded for the reference samples at this temperature.

Nguyen and et al. [64] used the following expression to predict the variation of specific heat at 100^{o}C.

$$\Delta C_p^{peak} = \frac{wH_{vap}}{2\Delta T} \tag{5.4}$$

where C_p^{peak} is the specific heat variation at 100^{o}C , w is the water content, H_{vap} is the latent heat of vaporisation (=2260 KJ/kg), and ΔT is half of the evaporation temperature interval (= 5 ^{o}C). Figure 5.8 shows the variation of specific heat with temperature.

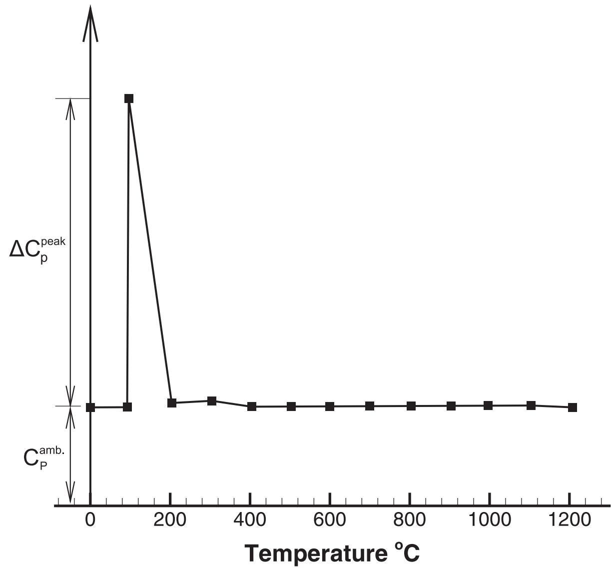

Figure 5.8: Variation of specific heat with temperature [64]

The experimental results for specific heat at 100 ^oC were verified against the above expression and the results obtained are summarised in Table 5.1. It can be seen that the reference mix exhibited same specific heat value for both measured and calculated cases, while the measured specific heat values of modified concrete mixes were higher than those calculated using Eq. 5.4. In general, these indicate that the modified concrete mixes confined more water within their pore network and needed a longer time to dry out than the reference mix. These findings reinforce the earlier conclusions regarding thermal conductivity and specific heat of the modified concrete mixes at 100 ^oC.

Table 5.1: Verification of specific heat test results with the expression used by Nguyen et al.[64]

Mix Name	Calculated specific heat at 100 ^oC using Eq. 5.4	Specific heat test result at 100 ^oC
Reference	1089.5	1043
15%G+5MK	1014.2	1316
30%G+5MK	1009.4	1434
45%G+5MK	1150.18	1281
15%G+10MK	1248.8	1423
30%G+10MK	1015.4	1356
45%G+10MK	1033.18	1218
45%G+0MK	1364.8	1152

The effect of metakaolin content on the value of specific heat for concrete mixes containing 45% glass at elevated temperatures indicates a positive role of the 10% metakaolin replacement on reducing the value of specific heat, as shown in Figure 5.7c. This result is consistent with those obtained for thermal conductivity.

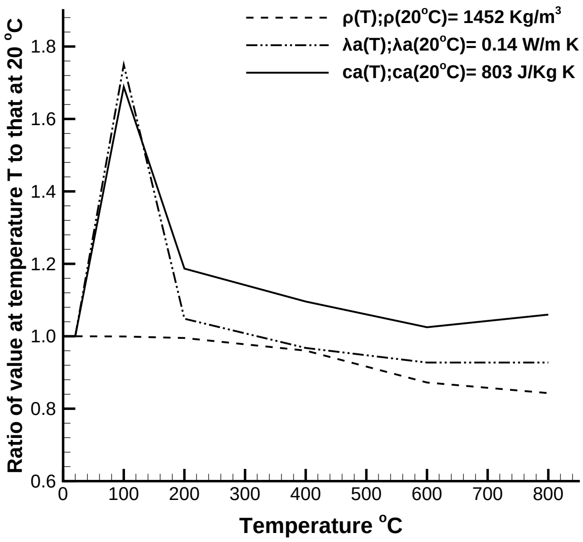

Figure 5.9: Temperature-dependent properties of the present research of the modified concrete mix containing 30% glass with 10% metakaolin

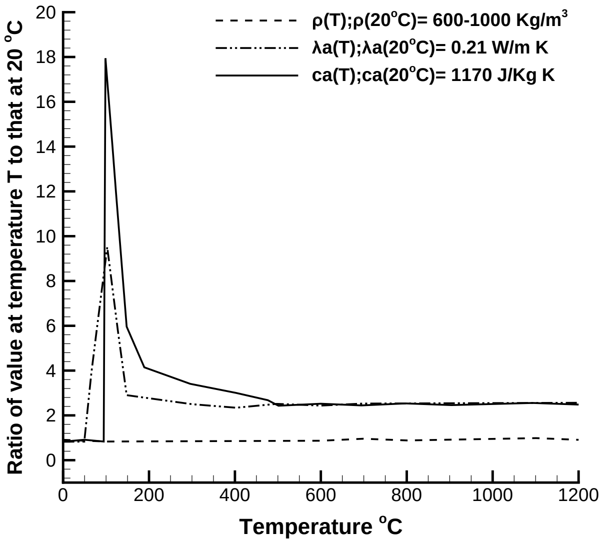

Figure 5.10: Temperature-dependent properties of pumice lightweight aggregate concrete units with a density range of 600-1000 kg/m^3 [55]

It would be relevant to compare the results obtained for the modified concrete mix (30% G +10% MK) in this research with the other lightweight concretes (pumice) listed in BS EN 1996-1-2 [55], as shown in Figures 5.9 and 5.10.

It can be seen that the present research results showed superior thermal performance than that of pumice lightweight concrete. Less variation in thermal conductivity and specific heat at 100 ^{o}C was observed for the modified concrete mix. This reached about 1.7% for both features, whereas the corresponding variation for the pumice lightweight concrete reached about 9.5% and 18% for the thermal conductivity and specific heat respectively. At temperatures exceeding 100^{o}C, both features settled down to about 1.1% and 3.5% for the current modified mix and pumice lightweight concrete respectively.

The presentation of temperature-materials properties according to BS EN 1996-1-2 [55] must be commented upon. It does not clearly show the effect of elevated temperatures on the density of a material. The density appeared as a straight line due to the small variation in its value compared to the values of thermal conductivity and specific heat, as shown in Figure 5.10. It would therefore be more suitable if each of the aforementioned properties is plotted separately.

5.4.3 Heat flow

The results of the heat flow test and the temperature differences between the exposed (hot) and unexposed (cold) surfaces of the concrete samples are shown in Figures 5.11a to 5.12c. A lower temperature difference implies a higher rate of heat flow.

From Figures 5.12a to 5.12c, it can be seen that the temperature differences were greater for the modified mixes than for the reference concrete, thus showing that the heat flow rate was lower in the modified mixes. This behaviour can be explained by the combined roles of metakaolin and glass in improving the thermal properties of the concrete samples. In addition, increasing the metakaolin and glass content reduced the amount of heat transferred due to the coating function. This is consistent with the lower measured thermal conductivities of these mixes, as mentioned in Section 5.4.2.

In all of the lightweight concrete mixes, there was a slight jump in the temperature value of the unexposed surface at about 150 ^{o}C. The latter is equivalent to a temperature of about 550 ^{o}C for the exposed surface, as shown in Figures 5.11a to 5.11h. This behaviour might be explained by the phase change due to the decomposition of the crystals of calcium hydroxide into their original components. Moreover, the thermal pounded compound is debonded at this range of heat exposure, causing a slight increase in the thermocouple reading. In the case of the exposed surface, the time-temperature relationship for all of the lightweight concrete mixes was approximately linear and followed the imposed temperature curve.

Figures 5.12a to 5.12c showed that the maximum temperature differences for both sets of the metakaolin replacement were achieved for the concrete mix with a glass content of 45% followed by those with a glass content of 30% and 15% respectively.

The reference concrete samples showed significant cracking and bowing towards the heat source. The mix containing 45% glass without metakaolin exhibited less cracking and bowing, while the other concrete mixes had excellent resistance against the effect of high temperature, with no visible cracking, as shown in Figures 5.13a to 5.13d.

In terms of acceptable performance as stated in the BS EN Standards [55, 70], the insulation property should satisfy the following requirements:

$$T_{ave.} \leq T_{ini.} + 140 \text{ K} \tag{5.5}$$

$$T_{max.} \leq T_{ini.} + 180 \text{ K} \tag{5.6}$$

where $T_{ave.}$, $T_{max.}$ and $T_{ini.}$ are the average, maximum and initial temperatures of the unexposed surface in K. When Equations 5.5 and 5.6 are applied, the concrete mix containing 45% glass and 10% metakaolin had the longest period of thermal insulation, which was 110 minutes.

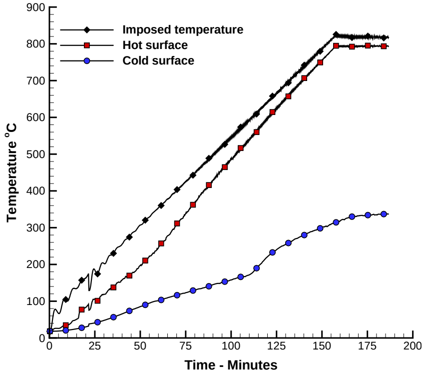

(a) Reference

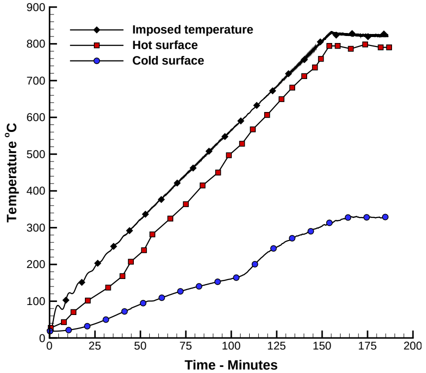

(b) 15%G+5%MK

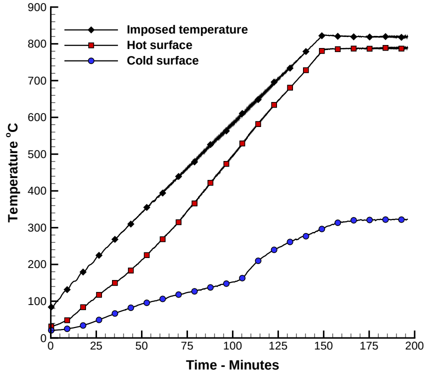

(c) 30%G+5%MK

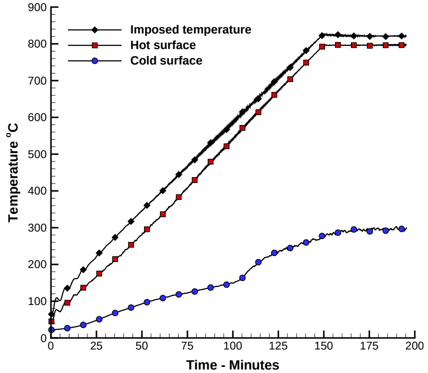

(d) 45%G+5%MK

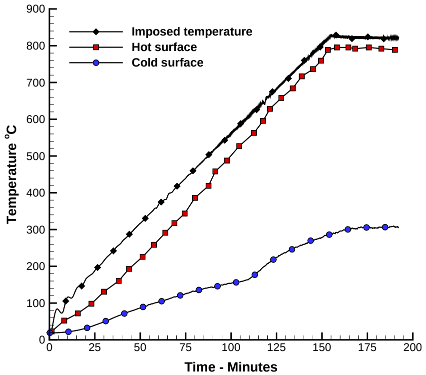

(e) 15%G+10%MK

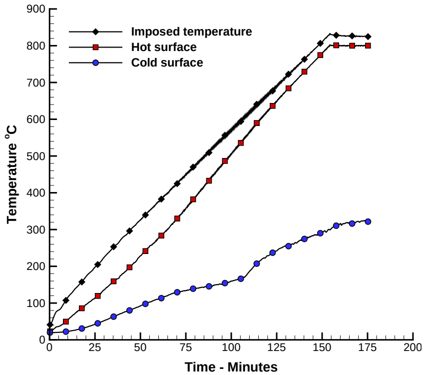

(f) 30%G+10%MK

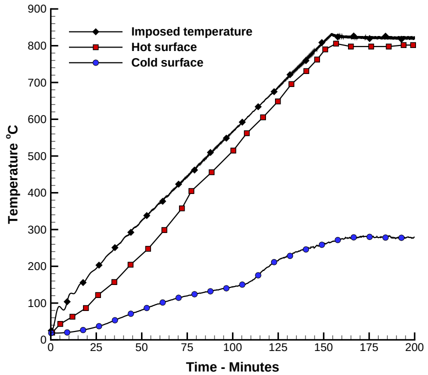

(g) 45%G+10%MK

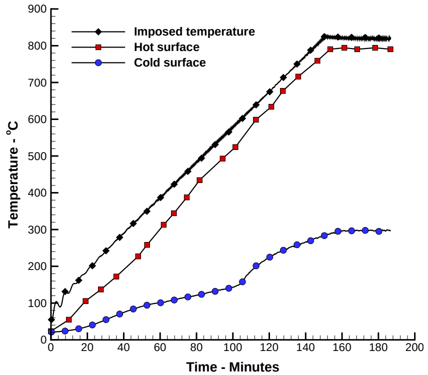

(h) 45%G+0%MK

Figure 5.11: The heat flow test results of the reference and modified concrete mixes

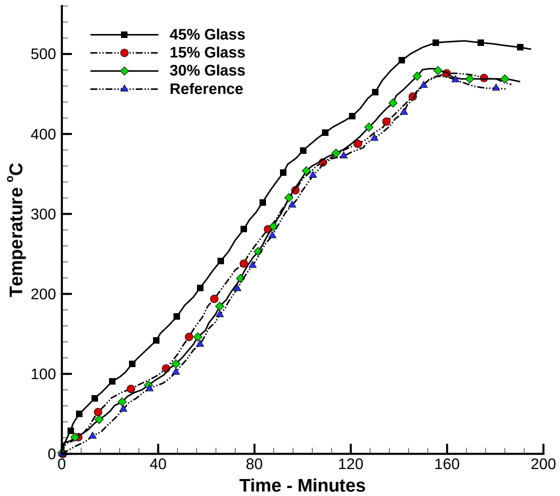

(a) 5% MK with various glass ratios

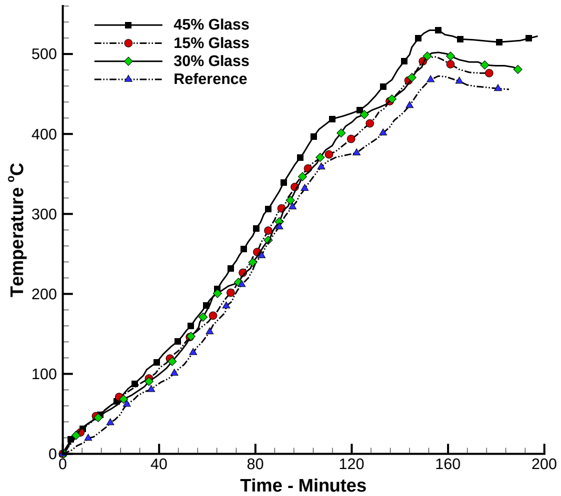

(b) 10% MK with various glass ratios

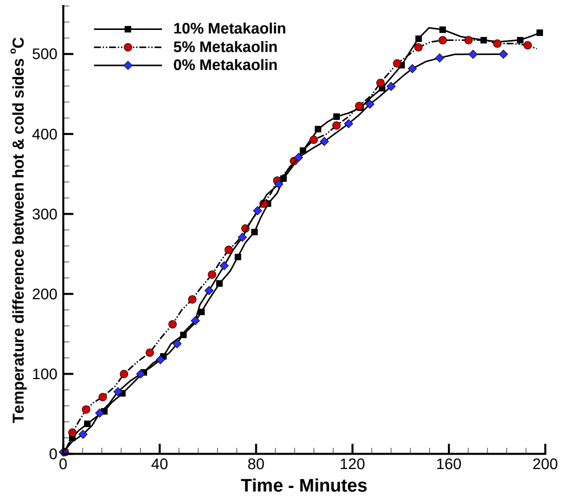

(c) 45% glass with various MK ratios

Figure 5.12: The temperature difference between the exposed and unexposed surfaces

(a) Reference

(b) 15%G+10%MK

(c) 30%G+10%MK

(d) 45%G+0%MK

Figure 5.13: The effect of unidirectional heat exposure on some lightweight concrete mixes

5.5 Summary

A detailed experimental investigation of the thermal properties of lightweight concrete was described in this chapter. The results obtained revealed that both the reference and modified concrete mixes showed reductions in density with an increase in temperature. Similar percentage decreases were recorded for both the reference and modified concrete mixes, reaching levels of around 20% when the concrete mixes were heated to 800 ^{o}C.

The addition of metakaolin improved the durability of the lightweight concrete mixes at elevated temperatures and the greatest enhancement was for the mix with 10% metakaolin content, while the samples of the reference concrete and of the concrete mix without metakaolin exhibited failure due to severe cracking. Samples with high glass content (45%) showed a tendency to deteriorate at elevated temperatures due to spalling, while the lower glass ratios were shown to confer improvements in fire resistance. Reductions in thermal conductivity were observed, which demonstrated the effects of varying both the recycled glass and metakaolin contents. The modified concrete mixes exhibited a greater increase in specific heat at 100 ^{o}C relative than did the reference concrete, due to the confinement of excessive water inside the pore system. Improved thermal insulation times were recorded for the modified concrete mixes, the best value being 110 minutes for the samples containing 45% glass and 10% metakaolin.

Chapter 6

Numerical simulation of the thermal behaviour of the lightweight concrete samples

6.1 Introduction

In order to evaluate different cases of heat exposure and geometries of lightweight concrete samples, it is necessary to develop a robust and reliable finite element model. This chapter describes and discusses the strategy developed for the numerical simulation of the pure heat transfer problem using the Abaqus/Standard 6.10-1 finite element package. Firstly, heat transfer analysis and the development of non-linear thermal behaviour is addressed, followed by calibration and validation issues. Finally, some applications are described which intend to explore the effects of different parameters on the results of the developed finite element model.

6.2 Heat transfer analysis

As mentioned in Chapter 2, there are two approaches to the application of heat transfer analysis, namely thermal-stress analysis and pure thermal analysis. This chapter considers the second type of analysis which mainly aims to identify the temperature profile within a given material.

With reference to the case of heat exposure investigated in Chapter 5, unidirectional heat transfer was assumed in order to evaluate the thermal behaviour of a range of selected lightweight concrete mixes. Such an exposure condition is governed by the following equation [57]:

$$c_p \frac{\partial \theta}{\partial t} = k \frac{\partial^2 \theta}{\partial x^2} \tag{6.1}$$

The above thermal behaviour was simulated through a developed finite element model, as explained in this chapter. In order to simplify and reduce the computational processes, the effect of hygral modelling released from the mass transfer of fluid within a partial saturated porous media (concrete) was disregarded. The latter effect might be needed in order to account the temperature variation within the concrete sample. Nevertheless, it is considered an expensive process. The same approach was also followed by Nguyen and et al. [64].

6.3 Numerical simulation technique

In a pure heat transfer problem, the main components of the finite element model are the element type, material model, thermal load and boundary conditions in addition to the selected solution procedure. All of these components are discussed in the context of their place within the Abaqus/Standard finite element package [56] in the following sections.

6.3.1 Element type

From the Abaqus/Standard element library [97], an eight-node linear interpolation diffusion heat transfer brick (DC3D8) element was selected to simulate the heat flow through the concrete specimens. This is a solid segment three dimensional element and has the capability to formulate the geometry of a concrete sample. The basic variable at the nodes of this element (degree of freedom) is the scalar temperature, which is denoted as a nodal variable (NT11). The non-linear behaviour of the material properties is considered at the integration points by assigning a solid homogenous section for the element's entire geometry.

6.3.2 Material model

The material model of the heat transfer analysis consists of three major properties which govern the overall thermal behaviour of the lightweight concrete samples. These are thermal conductivity, specific heat and density. The thermal conductivity represents how easily heat flows through the material [57]. It was treated as an isotropic property for all of the lightweight concrete samples. This characteristic was observed during the experimental investigation described in Chapter 5.

Specific heat is a property which represents the capacity of a material to store heat[57]. The Abaqus/Standard represents the specific heat of materials as the rate of the increase in internal thermal energy.

The thermal properties of all of the lightweight concrete samples investigated in this study vary with the change in temperature, which makes the heat transfer analysis non-linear. To resolve this issue, the Abaqus/Standard provides an option to define any temperature-dependent data items required. Since the thermal conductivity, density and specific heat of the lightweight concrete specimens were measured at temperatures ranging from 20 ^{o}C to 800 ^{o}C, their values were tabulated in the Abaqus/Standard material model as functions of temperature changes.

6.3.3 Thermal load and boundary conditions

Thermal load and boundary conditions are required in order to define the effective modes of heat transfer. The Abaqus/Standard allows such definition through what is referred to as the interaction model. In the interaction model, both the film condition and surface radiation, in conjunction with the environment temperature, are assumed to be responsible for the change in temperature of the surfaces and inside of the concrete sample. This means that thermal action is defined by net heat flux ($\dot{h}_{net}$), which is expressed by Equations 6.2 to 6.4 [98].

$$\dot{h}_{net} = \dot{h}_{net,c} + \dot{h}_{net,r} \tag{6.2}$$

$$\dot{h}_{net,c} = \alpha_c(\theta_g - \theta_m) \tag{6.3}$$

$$\dot{h}_{net,r} = \varepsilon_m \varepsilon_f \ \sigma[(\theta_r + 273)^4 - (\theta_r + 273)^4] \tag{6.4}$$

According to the test set-up, the geometry of each concrete sample was divided into two surface conditions, namely the exposed (hot) surface and the unexposed (cold) surface, as shown in Figure 6.1. The remaining surfaces were considered unexposed as they were insulated from the effects of the heat, as described in Chapter 5.

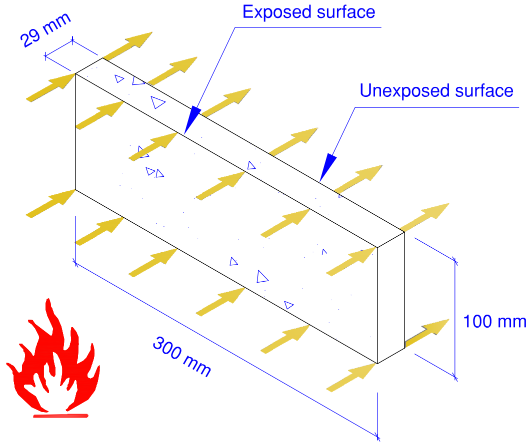

Figure 6.1: Boundary conditions for the concrete samples under unidirectional heat exposure

Initially, the temperature of the whole system was defined as being equal to ambient temperature (in this case 20 ^{o}C) using a predefined file option. Thereafter, radiation and/or convection heat transfer were considered as a thermal action on both surfaces of the concrete samples using an interaction model. The formulation of the convection and radiation heat effects were calibrated in terms of the coefficient of convection (film condition) and the value of surface emissivity, as described in Section 6.4. In all of the heat exposure formulations, the imposed temperature (in this case the furnace temperature) was tabulated as an amplitude file. For the whole model, the value of the Stefan-Boltzmann constant (σ) was defined as (5.67×10^{-8} W m^{-2} K^{-4}) using the model attributes.

6.3.4 Procedure of the finite element solution

It was mentioned in Section 6.3.2 that non-linearity variation of the material properties with the temperature variation makes the numerical simulation non-linear. Consequently, this had to be taken into account within the finite element solution. Because of the imposed temperature changes with time, a transient heat transfer method was used to simulate the thermal behaviour of the lightweight concrete samples. This method is governed by the maximum allowable temperature and emissivity changes per increment. On this basis, the numerical analysis comprised three main steps, as follows:

1. Establish the initial temperature condition.

2. Apply a transient heat transfer step containing an interaction model with both surface film condition and surface radiation.

3. Release the interaction model in the previous step and then apply two boundary conditions for the hot and cold surfaces according to the result obtained in step 2.

Step 3 was used in order to overcome the notable divergence in the results of the numerical simulation in relation to those obtained in the experimental measurements at the end of the heat exposure period. The former divergence was observed in the results of the unexposed surface temperature, as presented in previous published research work [15].

Both of the latter steps (steps 2 and 3) were divided into small time increments. The sizes of initial, minimum and maximum time increments have significant influences upon the simulation results. When the initial time increment is selected, the Abaqus/Standard automatically adjusts the size of the rest of the increments. Equation 6.5 provides the minimum feasible initial time increment (Δt) [56].

$$\Delta t \geq \frac{\rho \ c_p}{6\lambda} \Delta l^2 \tag{6.5}$$

where Δl is the distance between the nodes for the element near the surface with the highest temperature gradient.

At each increment, the Abaqus/Standard follows the Newton-Raphson equilibrium iterations to solve the linearized system of Equation 6.6 [56]. These iterations provide convergence at the end of each time increment within the temperature tolerance limits.

$$Kc = R \tag{6.6}$$

where K is the tangent stiffness matrix, R is the residual flux vector and c is the solution correction.

6.4 Calibration of the finite element model

In order to adjust the accuracy of the finite element model, the parameters which may have the most influence on the results obtained were investigated. These include the element mesh size, the coefficient of convection and the surface emissivity. The calibration technique was based upon the comparison with the measured results of the reference lightweight concrete (unless stated) using the following data: $10 \times 8 \times 8$ ($l \times h \times t$) element mesh size, 0.85 surface emissivity and 4-25 coefficient of convection (film condition). The latter data were chosen for the aforementioned parameters after a sensitivity analysis for a range of selected practical limits, as described in the next sections.

6.4.1 Element mesh size

Three different mesh sizes were investigated; the first comprised ($5 \times 2 \times 2$) ($l \times h \times t$) elements and hereafter referred to as the "coarse" mesh size. The second was formulated with ($10 \times 8 \times 8$) ($l \times h \times t$) elements and referred to as the "medium" mesh size. On the other hand, the third involved ($20 \times 16 \times 16$) ($l \times h \times t$) elements and so-called "fine" mesh size. In all of these cases, the concrete sample was divided in a similar manner so that the element geometry obtained was approximately cubic in shape, as shown in Figure 6.2. The results obtained for the sensitivity analysis of the mesh size are presented in Figure 6.3a to 6.3c.

It can be seen that the temperature profile is similar in all cases, implying that the mesh size has minimal effect on the results of numerical model. This behaviour may be explained by the uniformity of the heating action upon the exposed surface resulting from the unidirectional regime. In addition, the isotropic behaviour of the thermal conductivity feature may cause a uniform heat transfer within the internal lightweight concrete sample. Similar results were also observed by Chow and Chan [58]. On this basis, in order to reduce the computational intensity of the analysis, the medium mesh size was selected to perform the whole numerical simulation.

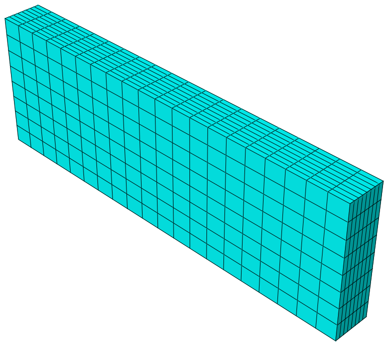

Figure 6.2: Formulation of the fine mesh size

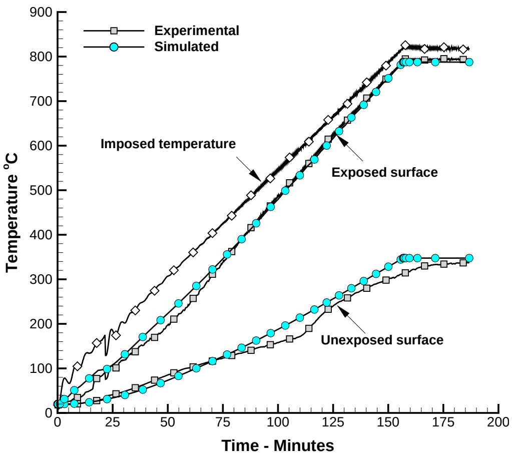

(a) Coarse mesh size

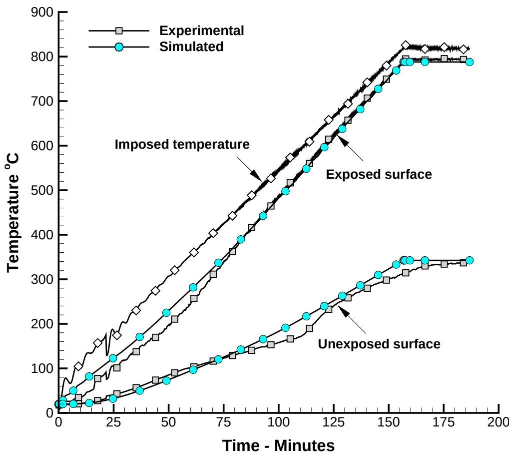

(b) Medium mesh size

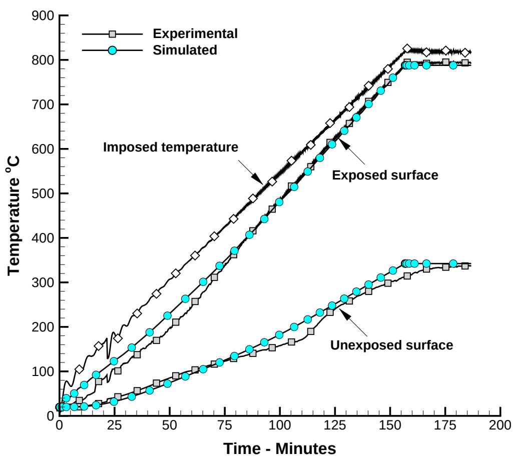

(c) Fine mesh size

Figure 6.3: The effect of element mesh size on the results of numerical simulation

6.4.2 Coefficient of convection

The combined effect of convection and radiation is the major source of heat transfer from the furnace environment to the exposed surface of the concrete sample and from the unexposed surface to the atmosphere. Previous studies [58, 98] have pointed out different approaches to the convection and radiation actions during exposure to high temperatures. These can be summarised as follows:

- Case 1: Considering the effects of convection and radiation on both of the sample surfaces with values of coefficient of convection (film condition) as 25 W/m^2K and 9 W/m^2K for the hot and cold surfaces respectively [98].
- Case 2: Applying the effects of both convection and radiation to the hot surface, while the cold surface is subjected only to the convection effect. In this case, the corresponding values of the film condition are taken as 25 W/m^2K and 4 W/m^2K for the hot and cold surfaces respectively [98].
- Case 3: Same as in Case 1, but with a range of film condition between 7.5-9.5 W/m^2K and 4.5 W/m^2K for the hot and cold surfaces respectively [58].

All of the above cases were investigated and the results obtained for the reference lightweight concrete samples are shown in Figures 6.4a to 6.4c. It can be seen that the Case 2 showed more reliable results for both the hot and cold surface temperatures than the other cases and the outcome was in agreement with the overall measured results.

If the modified lightweight concrete samples are taken into account, Cases 1 and 3 showed a clear variation in the cold surface temperatures compared to the measured results (see for example Figures 6.5a and 6.5b for the concrete mix containing 30% glass and 10% metakaolin). On the other hand, Case 2 confirmed its reliable results, as shown in Figure 6.7f. On this basis, Case 2 was considered in the subsequent numerical simulation processes.

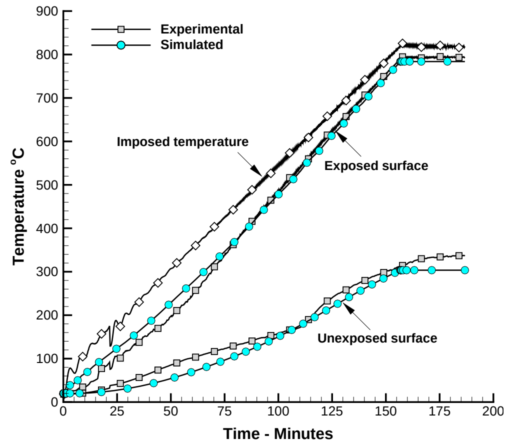

(a) Case 1

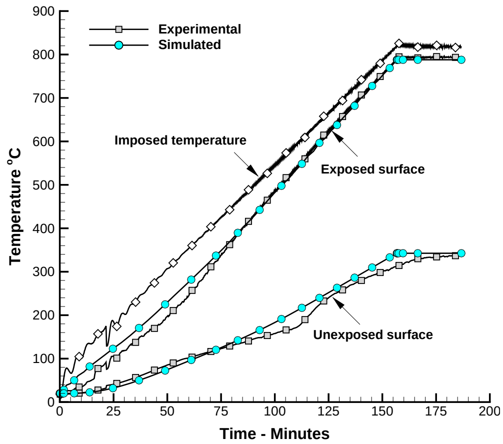

(b) Case 2

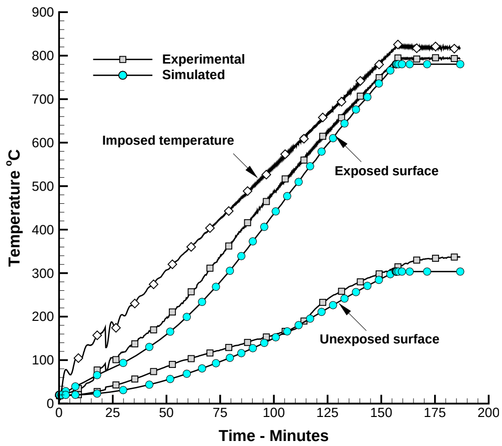

(c) Case 3

Figure 6.4: The effect of the film condition on the results of numerical simulation for the reference lightweight concrete samples

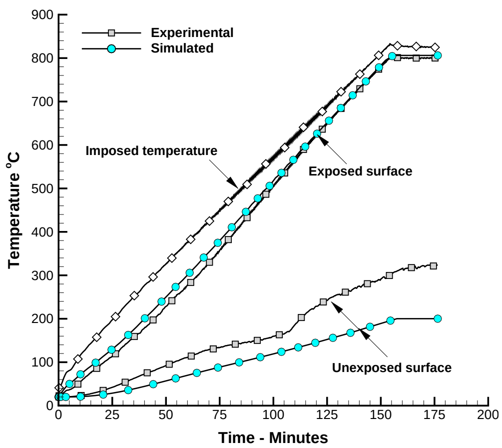

(a) Case 1

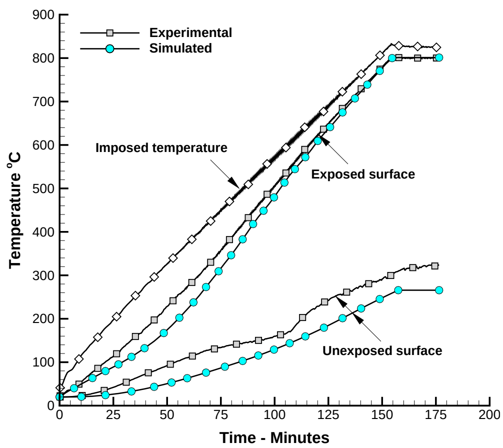

(b) Case 3

Figure 6.5: The effect of the film condition on the results of numerical simulation for the modified lightweight concrete samples containing 30% glass and 10% metakaolin

6.4.3 Surface emissivity

In order to evaluate the effect of radiation, the surface emissivity of the lightweight concrete samples was investigated. As mentioned in the previous section, the effect of radiation was only considered on the hot surface, implying that emissivity had no effect on the cold surface. Three different values forming a practical range of surface emissivity for the various lightweight concretes were selected. These were 0.8, 0.85 and 0.9.

The results of the sensitivity analysis for the former surface emissivity values in terms of the time-temperature profile of the hot surface are presented in Figure 6.6. Similar behaviour was observed for all the cases investigated, indicating a lesser effect of this range of emissivity values on the overall thermal behaviour of the lightweight concrete samples. This is consistent with the results obtained by Viskanta [99]. As a result, the value of 0.85 was selected as an emissivity for the hot surface, as it represents the mean of the examined values.

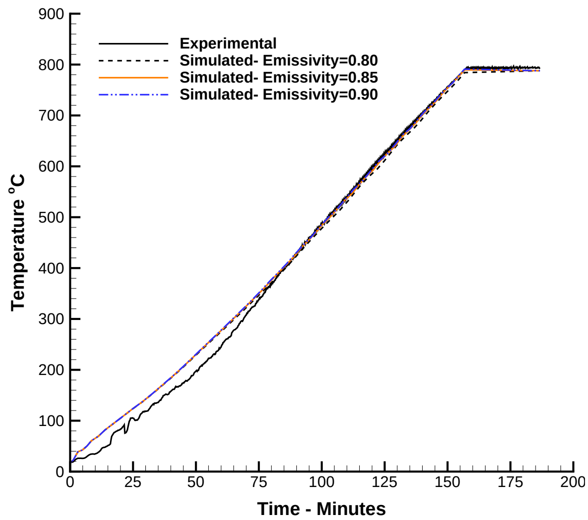

Figure 6.6: The effect of emissivity value on the simulation results of the hot surface

6.5 Validation of the finite element model

After a wide investigation for the main parameters of the finite element model, the data used in the numerical simulation are summarised in Table 6.1. Some of these data were adopted from the direct test results performed in Chapter 5.

Table 6.1: Data used in the numerical simulation

No.	Property	Value
1	Coefficient of convection (film condition) of the exposed surface (W/m^2K)	25
2	Coefficient of convection (film condition) of the unexposed surface (W/m^2K)	4
3	Surface emissivity of the exposed surface	0.85
4	Density at exposure to various temperatures (kg/m^3)	From test results, see Section 5.4.1
5	Specific heat at exposure to various temperatures (J/ kg.K)	From test results, see Section 5.4.2
6	Thermal conductivity at exposure to various temperatures (W/ m.K)	From test results, see Section 5.4.2

To check the reliability of the developed numerical model, it was necessary to validate the results generated by its use with those obtained in the experimental phase. Figures 6.7a to 6.7h show the numerical simulation results for the reference and modified lightweight concrete samples with their corresponding test results in terms of time-temperature aspect.

In general, a close agreement between the measured and simulated results was observed for both the exposed and unexposed surfaces for all of the concrete samples. The simulated results closely followed the experimental measurements from the transient state to the steady state condition. However, there were slight variations in the temperature of the cold surface (and, in some cases, the hot surface). This may be explained by two assumptions made as part of the simulation conditions, namely of a linear value for the coefficient of convection heat transfer and of pure unidirectional heat flow. The chemical phase change at the high temperatures may also have had some effect on the thermal behaviour of the concrete samples. The latter took place at about 550 ^{o}C, at which the temperature decomposition of the calcium hydroxide into its original components would be expected [43].

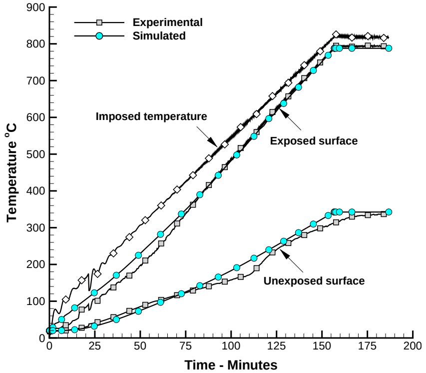

(a) Reference

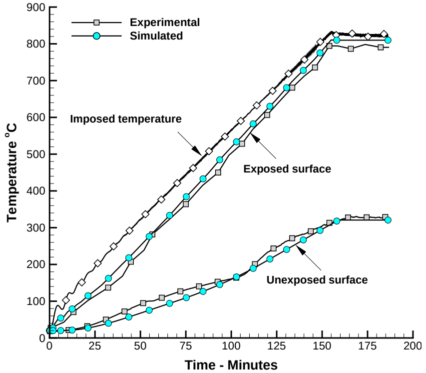

(b) 15%G+5%MK

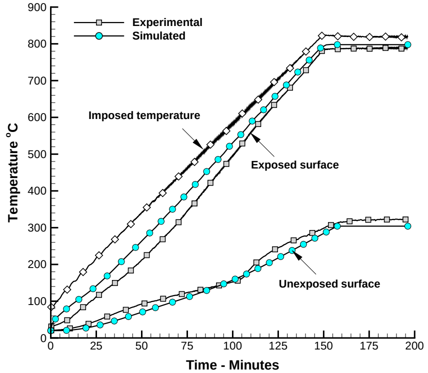

(c) 30%G+5%MK

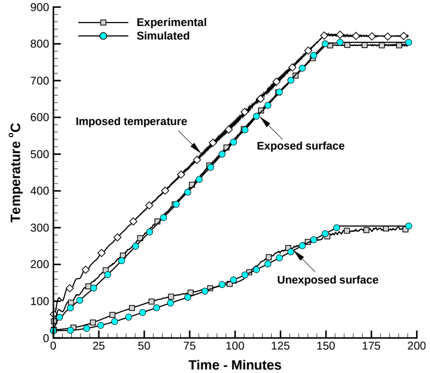

(d) 45%G+5%MK

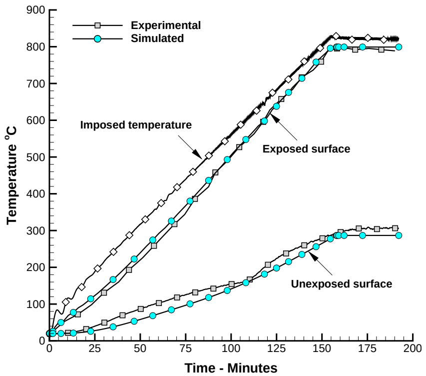

(e) 15%G+10%MK

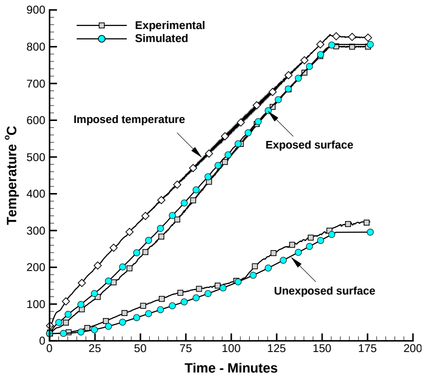

(f) 30%G+10%MK

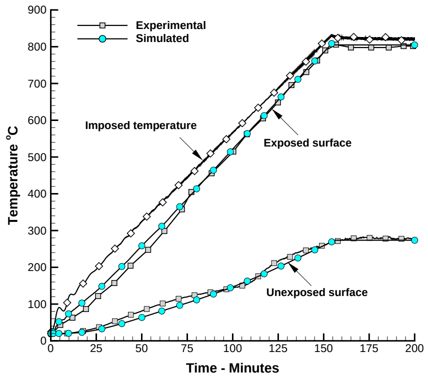

(g) 45%G+10%MK

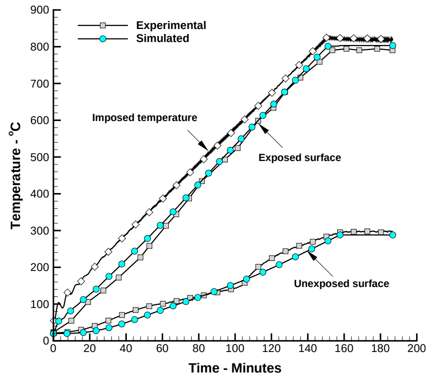

(h) 45%G+0%MK

Figure 6.7: The results of numerical simulation with their corresponding measurements for the reference and modified lightweight concrete mixes

Figures 6.8 and 6.9 show the temperature distribution throughout the thickness of the samples when exposed to heat for different lengths of time and the temperature profile as contour lines for the reference concrete and one example of the modified lightweight concrete mixes (30% G + 10% MK). It can be seen that the difference between the hot and cold surface temperatures reached about 445 ^{o}C and 510 ^{o}C for the reference and (30% G + 10% MK) mixes respectively at the end of their exposure to heat (157 minutes). This implies an improvement in the thermal insulation by as much as 65 ^{o}C. Such behaviour was also observed in the experimental phase.

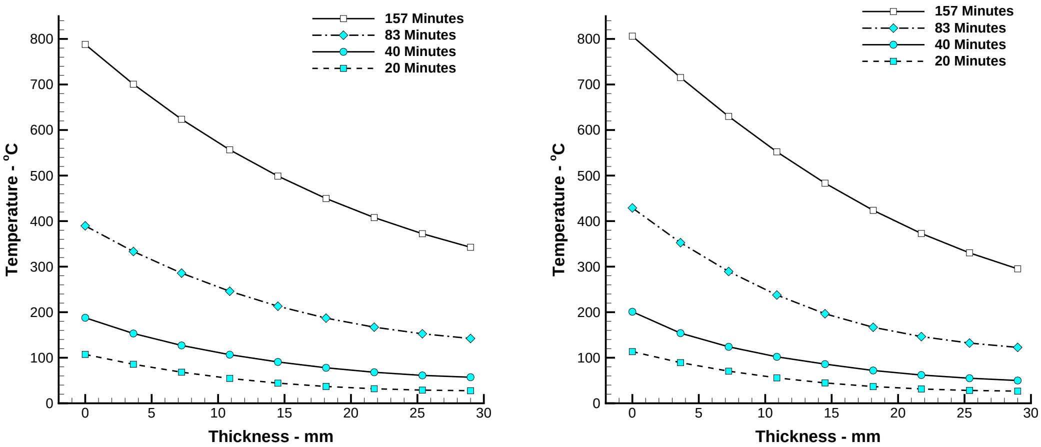

(a) Reference (b) 30%G+10%MK

Figure 6.8: Distribution of temperature through the thickness of some of the lightweight concrete samples when exposed to heat for different lengths of time

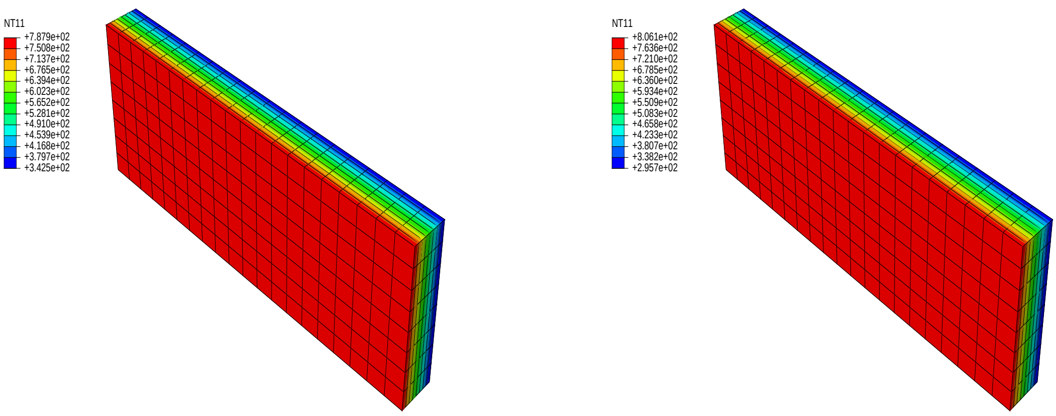

(a) Reference (b) 30%G+10%MK

Figure 6.9: Contour lines of the temperature profiles of some of the lightweight concrete samples

6.6 Parametric study

The thermal behaviour of the reference and modified lightweight concrete samples may vary from one category to another within the same concrete mix depending upon several factors. For this reason, three parameters that commonly influence thermal performance were investigated in terms of their effect on the insulation criteria. These parameters can be classified as:

1. Material properties: variations in the values of thermal conductivity and specific heat.
2. Environmental properties: changing the coefficient of convection heat transfer.
3. Geometric properties: variations in the thickness of the concrete samples.

The values of thermal conductivity, specific heat, the coefficient of thermal convection at the unexposed surface and the thickness of the concrete samples were selected as λ = 0.1 to 0.45 W/m.K, c_p= 600 to 1400 J/kg.K, α_c = 4 to 15 W/m^2.K and t = 29 to 200 mm respectively. These limits represent the means of the commonly adopted values for lightweight concrete used for insulation purposes [64]. All of the former parameter variations were applied at steps 2 and 3 of the main solution steps described in Section 6.3.4. The insulation criterion was calculated according to Equations 5.5 and 5.6. The results indicate that the unexposed surface temperature should not be allowed to exceed 160 ^{o}C. The parametric study was based upon the thermal model described in Section 6.3, which was validated against the experimental results. The feature of temperature-dependent data of the material model was adjusted by means of the systematic variation of each property at ambient temperature while keeping the other properties constant. The influence of variations in sample thickness was investigated by predicting the temperature of the unexposed surface after 165 minutes exposure to heat. This regime was chosen because the insulation property did not indicate the thermal behaviour when the value of the sample thickness was increased, meaning that the higher thickness values required longer exposure to heat in order to achieve the desired standard insulation criteria.

Figures 10a to 13c show the results obtained for the parametric study of the reference and modified concrete mixes. In general, the results indicate that the coefficient of thermal convection had the largest influence on the insulation criteria, followed by specific heat and thermal conductivity. A positive linear relationship was recorded for the coefficient of thermal convection and specific heat versus insulation property, as shown in Figures 6.11a to 6.12c, while a counteractive behaviour was noted for the effect of thermal conductivity. Increasing the thickness of the concrete samples was associated with a reduction in the temperature of the unexposed surface, as shown in Figures 6.13a to 6.13c.

The modified concrete mixes exhibited superior thermal separation behaviour with increasing values of the governing parameters (except thermal conductivity). The concrete mix with 10% MK and 45% glass replacements showed the longest insulation period of all the concrete mixes, reaching as long as 195 minutes, as shown in Figures 6.12b and 6.12c. This is consistent with its superior thermal conductivity resulting from the combined effect of metakaolin and recycled glass, as mentioned in Chapter 5. The former concrete mix exhibited a more pronounced increase in the insulation criterion at the higher values of the coefficient of convection (15 W/m^2K). This behaviour may be explained by a smaller difference between the coefficients of convection for the exposed and unexposed surfaces, implying that less heat was transferred between these surfaces.

The results observed for thermal conductivity showed a longer insulation criterion for the reference concrete in comparison with those of the modified concrete samples, as shown in Figures 6.10a to 6.10c. This behaviour could be related to the assumption of fixed values of the other parameters with the variation of thermal conductivity. Indeed, this regime has a noticeable effect on the overall thermal behaviour of this parameter. For instance, the density and specific heat have an inverse relation with the thermal conductivity feature (see Eq. 5.2).

The temperature of the unexposed surface of the modified concrete samples was approximately 30 ^oC when the sample thickness was 100 mm, as shown in Figures 13a to 13c. This is close to ambient temperature, so from an economical point of view, 100 mm may be considered an adequate thickness for these concrete mixes to resist heat exposure. At the lower thickness values, the difference in temperature of the unexposed surfaces of the reference and modified concrete mixes was more appreciable and reached about 55 ^oC for a concrete sample 50 mm thick. However, the aforementioned difference becomes limited as the concrete thickness is increased.

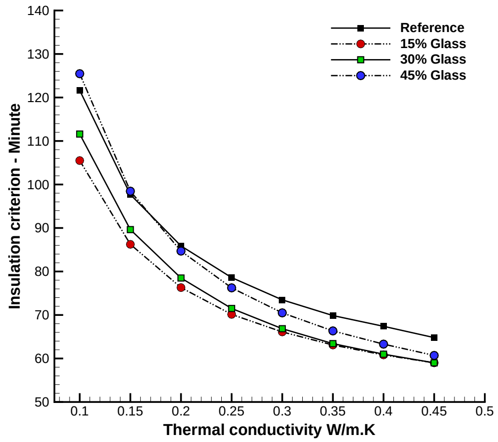

(a) 5% MK with various glass ratios

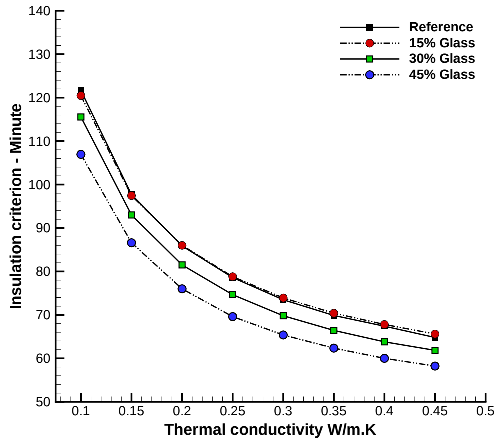

(b) 10% MK with various glass ratios

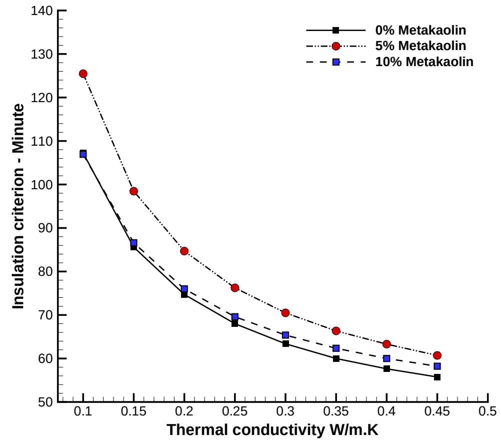

(c) 45% glass with various MK ratios

Figure 6.10: The effect of thermal conductivity on the insulation property of different lightweight concrete mixes

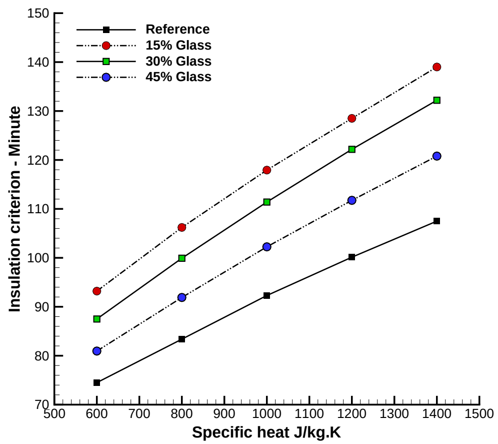

(a) 5% MK with various glass ratios

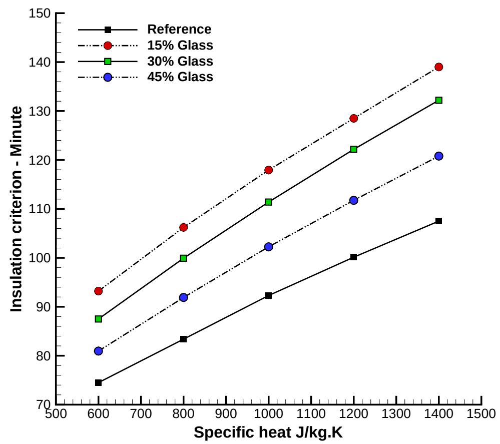

(b) 10% MK with various glass ratios

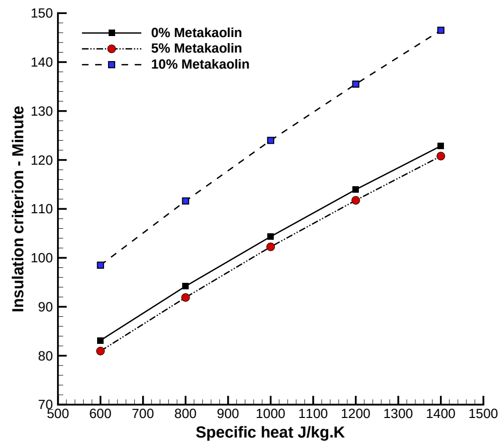

(c) 45% glass with various MK ratios

Figure 6.11: The effect of specific heat on the insulation property of different lightweight concrete mixes

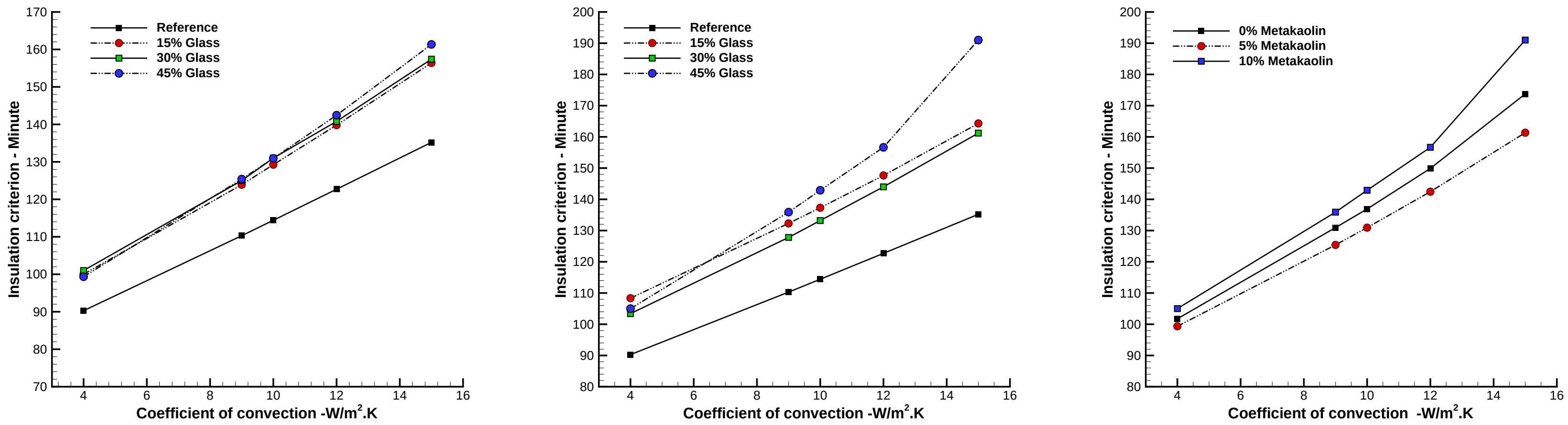

(a) 5% MK with various glass ratios (b) 10% MK with various glass ratios (c) 45% glass with various MK ratios

Figure 6.12: The effect of the coefficient of thermal convection on the insulation property of different lightweight concrete mixes

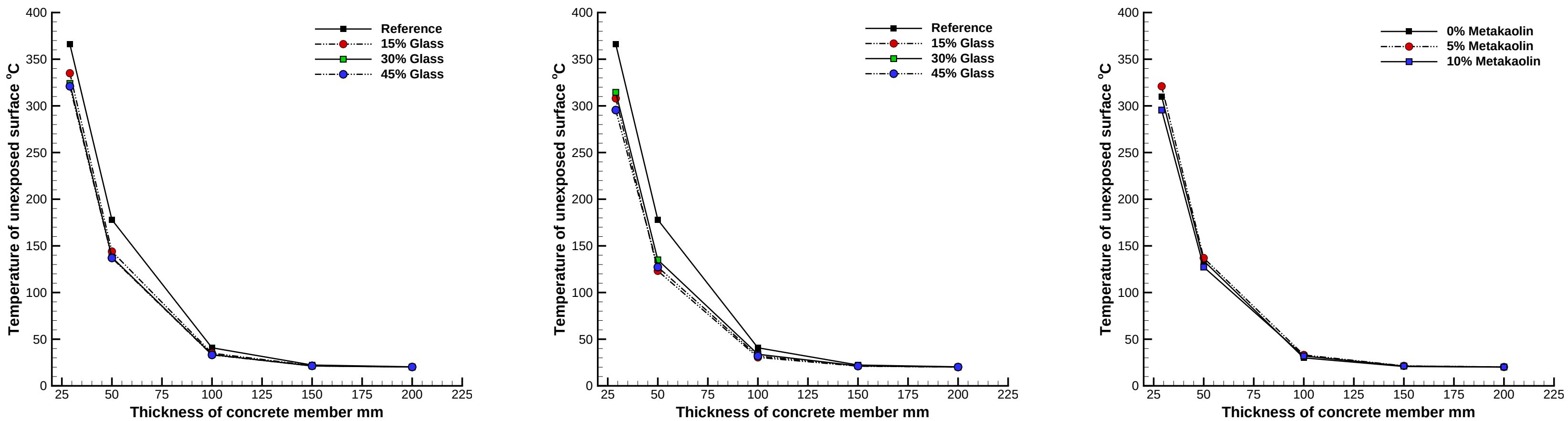

(a) 5% MK with various glass ratios (b) 10% MK with various glass ratios (c) 45% glass with various MK ratios

Figure 6.13: The effect of the thickness of the concrete member on the unexposed surface temperature of different concrete mixes

6.7 Summary

A finite element model was designed to predict the temperature distribution within the lightweight concrete samples. Incorporating the non-linear material properties caused by temperature variation into the model was essential in order to understand the global thermal behaviour of the lightweight concrete samples. Thermal convection and radiation governed the heat transfer between the furnace environment and the exposed surface of the sample. On the unexposed surface, the finite element model was consistent with the suggestion of omitting the effect of thermal radiation. The effects of both the mesh size and the value of surface emissivity were negligible in terms of the overall numerical results.

In general, the finite element model developed in the present study was reliable in predicting the time-temperature behaviour of all of the concrete mixes. The parametric study showed that the coefficient of thermal convection had the most influential role on the insulation criterion.

Chapter 7

Structural applications of the developed lightweight concrete mixes

7.1 Introduction

Previous chapters have described the fundamental mechanical and thermal properties of a range of selected lightweight concrete mixes which incorporated different percentages of by-product materials. However, in order to give a broader picture, their practical application as structural elements needs detailed evaluation. This chapter describes and discusses the optimisation of the modified lightweight concrete mixes, the selection strategy for a given structural element (masonry wall) and the design scheme for this structural element.

7.2 Selection of the optimum modified concrete mix

To move forward with the practical application, an optimisation methodology is required for the selection of the most adequate modified lightweight concrete mix which can be used in the field of construction. This optimisation methodology is based upon the fulfilment of the main objectives of this study, namely improving the thermo-mechanical behaviour of the concrete mixes and allowing for the use of more by-product materials. After a comprehensive experimental investigation for the aforementioned parameters in Chapters 3 to 5, the results obtained highlighted the following key points:

1. The strength requirements for use as a structural lightweight concrete were achieved at both levels of metakaolin addition. The strength value was in ascending order for the concrete mixes containing 45%, 30% and 15% glass respectively. At the same time, with the exception of the concrete mixes containing 45% glass, a significant increase in the strength of the modified concrete mixes was achieved in comparison with the reference concrete.

2. The thermal criteria generally improved with the largest improvements observed for the concrete mixes containing 10% metakaolin.

3. Thermal conductivity decreased as the glass content increased.

4. When the concrete mixes were exposed to high temperatures, explosive spalling consistently occurred when the glass content was above 30%.

The global trends in the behaviour of modified concrete mixes in comparison with the reference concrete are summarised in Table 7.1. It is important that the thermo-mechanical properties of the modified concrete mix used be as least as good as the traditional ones. It is also important that resistance to the effects of fire and heat is not adversely affected, as this would have serious implications for safety. It is therefore necessary to evaluate the optimum concrete mix among those examined during the experimental programme.

It can be seen from Table 7.1 that the concrete mix containing 30% recycled glass with 10% metakaolin met all the necessary requirements and that is possible to use this concrete mix without any deterioration in thermal or mechanical properties. Furthermore, considerable amounts of by-product materials were incorporated to produce this lightweight concrete with a better thermo-mechanical behaviour. On this basis, this concrete mix was considered throughout the structural application described in this thesis.

Table 7.1: Global behaviour of the modified concrete mixes in terms of mechanical strength, thermal criteria, resistance to heat and amount of recycled materials used in comparison with the reference concrete mix

No.	Mix code	Mechanical strength		Thermal insulation		Resistance to heat		Amount of recycled materials	
		Better than (R)	Worse than (R)	Better than (R)	Worse than (R)	Durable	Non-durable	MK (%)	G (%)
1	5%MK+15%G	√		√		√		5	15
2	5%MK+30%G	√		√		√		5	30
3	5%MK+45%G		√	√			√	5	45
4	10%MK+15%G	√		√		√		10	15
5	10%MK+30%G	√		√		√		10	30
6	10%MK+45%G		√	√			√	10	45
7	0%MK+45%G		√	√			√	0	45

7.3 Selection of the structural member for testing

In previous laboratory work, the testing programme was performed on small specimens which normally varied in their shape depending on the relevant procedure of BS EN standards. This work provided many of the fundamental properties of the lightweight concrete mixes. However, in practice, it becomes difficult to ignore the structural application of the produced lightweight concrete, as this application is more indicative of the real behaviour of the concrete samples after geometrical magnification and interaction with other structural parts. Consequently, exploring the behaviour of the reference and optimum modified concrete mixes as structural elements is extremely useful.

Any structural building consists of a combination of different elements. Each element is designed to perform its intended function within the whole system. In general, these elements can be classified as slabs, beams, columns, masonry walls and foundations. The first four elements form the components of the so-called super-structure, while the foundation element refers to the sub-structure part of the building. Indeed, at least half of the total volume of the structural elements in the domestic buildings is composed of the masonry walls [62]. On this basis, it would be of great value if the lightweight concrete developed during this research could be used for the construction of masonry walls.

In terms of constructional applications, masonry walls may make both a structural contribution and serve thermal separation functions or else may only be required to fulfil the (non load-bearing) separation role [55, 64]. The former type of masonry wall, which is intended to support applied loads and provide insulation, is considered throughout the next chapters in terms of experimental investigation and analytical simulation.

Depending on the method of construction, several categories of masonry walls are available. The most commonly used are single-leaf, cavity and composite walls. In the case of single-leaf walls, the thickness of the wall represents the width of the masonry unit, as shown in Figure 7.1a. It could be fabricated to suit both the applications of load bearing and non-load bearing. Cavity walls are constructed with double leafs and incorporate a separation cavity between them, as shown in Figure 7.1b. The type of material and the geometry of the masonry units used in the construction of the leafs varies greatly. To connect these leafs together, two techniques are usually followed: header units or metal ties. The first technique was used in ancient constructions, while the metal tie connection method is relatively modern. Due to its ability to enhance the support of applied loads and to decrease the penetrated water, the major application of cavity walls is as exterior walls. Except the number of leafs being used, which could be two (or more), the construction of composite walls is similar to that of cavity walls, as shown in Figure 7.1c. It should also be mentioned that the cavity between the leafs in composite walls is solidly filled with mortar or grout, while it is left empty in the case of cavity walls. However, to provide the composite action, composite walls require more headers or metal ties to connect the wythes sufficiently [62, 63].

All of the above masonry walls can be found with either light or high reinforcement. The reinforcements could be placed horizontally through the bed joint, or vertically through the grouted cavity or the units' holes [62].

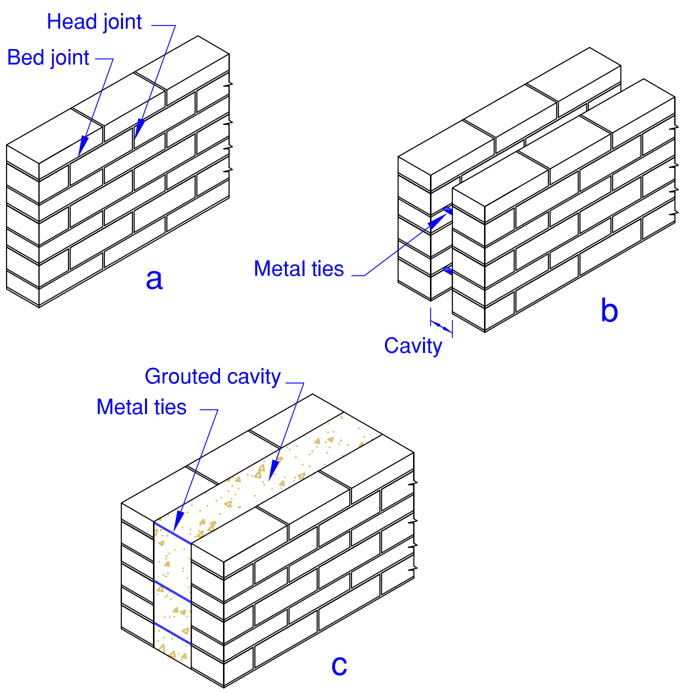

Figure 7.1: Types of masonry walls: (a) single leaf wall; (b) cavity wall; (c) composite wall [62]

Different masonry units made from a range of materials are available to construct these types of walls. The most common types are clay, calcium silicate and concrete units [63]. These are produced in a variety of geometries. If the dimensions of a masonry unit are less than or equal to 337.5 × 225 × 112.5 mm ($l \times w \times t$), it is classified as a brick. If any dimensions exceed the aforementioned limits then according to BS 6073: Part 1 [100] the unit is considered a block. Concrete masonry units are commonly produced in dimensions suitable for block applications. The main classes of standard-size concrete blocks are solid, cellular and hollow, as shown in Figure 7.2 [63].

As unreinforced single leaf masonry walls constructed with solid concrete blocks are the most used in commercial applications [62, 63], this kind of walls is considered in the next phase of the research work described in this thesis.

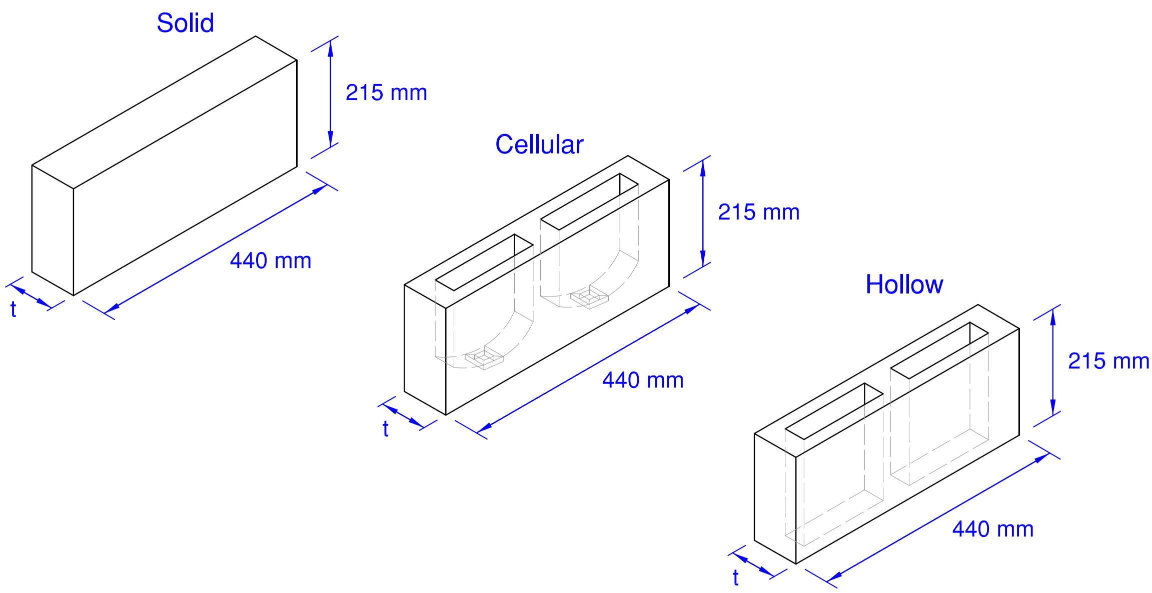

Figure 7.2: Types of concrete blocks [63]

7.4 Selection of the dimensions of the masonry blocks

According to British Standard BS BS EN 771-3 [101] which classifies the standard sizes of masonry units, solid concrete blocks with dimensions of 440×215×100 mm ($l\times w\times t$) were chosen. To produce these blocks, plywood moulds were designed with total dimensions of 815 × 490 × 120 mm ($l\times w\times t$), as shown in Figure 7.3. Each mould was designed to produce three solid concrete blocks per casting cycle. The measured dimensional deviations for each mould complied with the permitted values given in BS EN 771-3 [101].

(a)

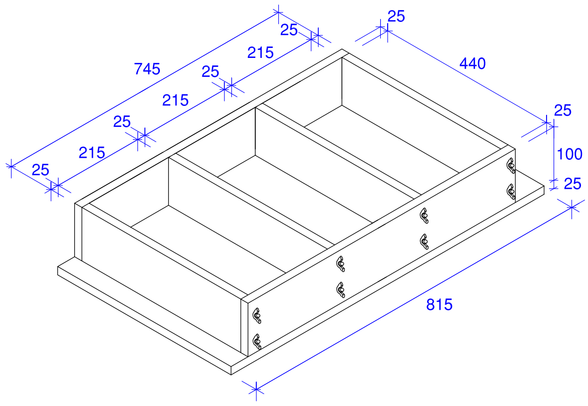

(b)

Figure 7.3: Details of the wooden moulds (all dimensions in mm)

7.5 Casting the concrete blocks

Before the casting process, all moulds were cleaned and painted with two perpendicular oil layers in order to prevent the adhesion of concrete. Two different types of solid concrete blocks were produced in this experimental part, one made from the reference mix and the other made from the optimum modified concrete (30%G+10%MK). Identical mix proportions to that of the first experimental phase described in Chapter 3 were used for both concrete blocks. The mixing procedure described in BS EN 12390-2 [85] was followed using a 0.17 m^3 portable electric mixer. The casting of the fresh concrete mix was performed in three layers. Each layer was completely compacted using a vibrating table until there was no further appearance of large air bubbles on the surface of the concrete. The upper edge of the mould was levelled by removing the excess concrete using an aluminium rod which was passed across the total width of the mould. A trowel was then used to smooth the upper surface, as shown in Figure 7.4. The samples were stored in the laboratory and covered with a plastic sheet to ensure the circulation of humid air around the specimens. After 24 hours, the samples were demoulded, marked and cured in water at a temperature of $20 \pm 2\ ^{o}$C for about six months, as shown in Figure 7.5. This longer curing time was not by design, but rather due to a delay in access to the experimental apparatus. Thereafter, all concrete blocks were removed from the water and left to dry in the laboratory in ambient conditions before running the test two weeks.

In addition to the concrete blocks, three 100 mm cubic and ten 100×200 mm cylindrical specimens of each concrete mix were casted in order to measure the compressive strength and modulus of elasticity respectively.

Figure 7.4: Casting the concrete blocks

(a) (b)

Figure 7.5: Curing process for (a) concrete blocks; (b) cubic and cylindrical concrete samples

7.6 Compressive strength of the concrete blocks

In accordance with EN 772-1 [102], by adopting a shape factor (δ), using the results obtained for 100 mm cubic test samples can give an indication of the compressive strength of different geometries of masonry units. The magnitude of δ depends on the width and height values of the masonry unit. On this basis, the compressive strength of both concrete blocks can be determined. When the former specifications are followed, the corresponding shape factor δ for the selected block dimensions is 1.38, as shown in Table 7.2.

Figure 7.6 shows the compressive strength test results for both concrete mixes at six months of age. It can be seen that the optimum modified concrete displays greater compressive strength than the reference mix. The average value of compressive strength for the three 100 mm cubic samples were 20.58 MPa and 21.93 MPa for the reference and modified lightweight concrete respectively. These results comply with the findings of the first experimental phase and imply corresponding compressive strength values for the reference and optimum modified concrete blocks of 14.9 MPa and 15.9 MPa respectively.

Table 7.2: Value of shape factor (δ) according to EN 772-1 [102][a]

Height of unit (mm)	Least horizontal dimension of unit (mm)				
	50	100	150	200	250 or greater
50	0.85	0.75	0.7	-	-
65	0.95	0.85	0.75	0.70	0.65
100	1.15	1.00	0.90	0.80	0.75
150	1.30	1.20	1.10	1.00	0.95
200	1.45	1.35	1.25	1.15	1.10
250 or greater	1.55	1.45	1.35	1.25	1.15

[a]Linear interpolation is permitted

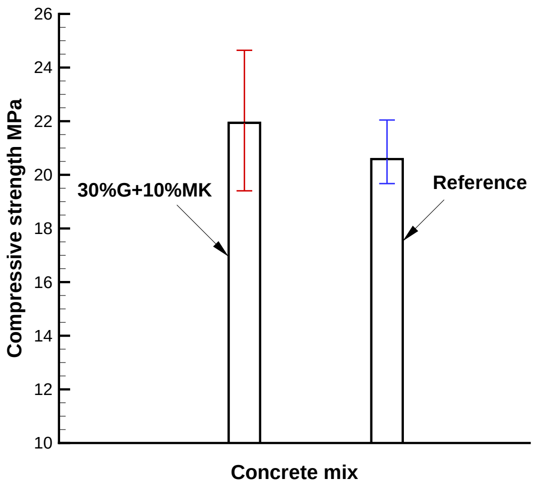

Figure 7.6: The compressive strength of the reference and optimum modified concrete mixes at six months age

7.7 Selection of the masonry mortar

To achieve the desired target of this section of the research, general purpose site-made masonry mortar was used to provide the bonding strength between the masonry units. Normally, masonry mortars are classified according to their compressive strength and referred to by the letter M followed by the value of their compressive strength. The BS 5628-1 [103] denotes four main mortar classes, (i) to (iv). The character (i) corresponds to M12, while (iv) corresponds to M2. If a load-bearing masonry wall is intended to construct, M12 is preferable to other mortars. The reason for this is the higher strength level of this mortar class, which can enhance the bearing capacity of masonry walls. In accordance with this, M12 was used as a base for the design calculations of the masonry mortar.

Two masonry mortars with different constituents were investigated throughout this experimental work. The first consisted of sand and cement ingredients, while the other was incorporated lime in conjunction with sand and cement. Table 7.3 shows the mix proportions of the two masonry mortars.

Table 7.3: Details of the mix proportions of the cement mortars

General name of mortar (by volume)	Cement (kg/m^3)	Sand (kg/m^3)	Water (kg/m^3)	Lime (kg/m^3)	W/Cm	Slump (mm)
1:3	369	1320	315	0.00	0.85	50
1:0.5:4.5	235	1538	369	54	1.27	60

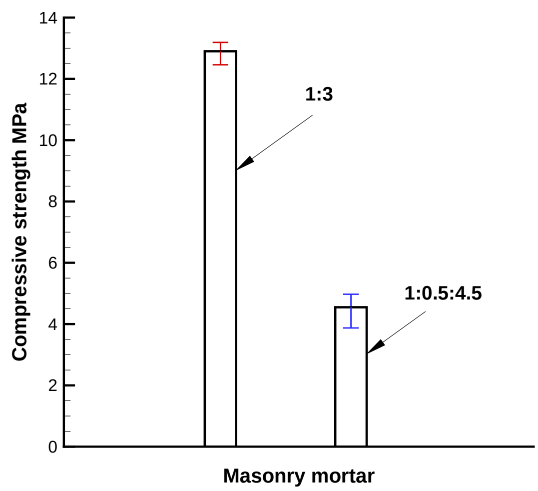

Figure 7.7: The results of compressive strength measurements at 28 days age for different cement mortars

A quantity of water was added to produce a suitable mortar consistency (slump 50-60 mm). As the main criterion for evaluating masonry mortar is its compressive strength, three cubic specimens were taken from each mortar mix and the compressive strength was then measured at 28 days age. The results obtained are illustrated in Figure 7.7. It can be seen that the cement-sand mortar exhibited higher compressive strength than the one with lime incorporated within its constituents, falling in the range of the M12 classification. On the other hand, the lowest strength value was noted for the masonry mortar with lime. Thus, the latter mortar cannot provide a sufficiently strong bond between masonry units desired for load-bearing walls and because of this the cement-sand mortar was selected to formulate the masonry walls.

7.8 The geometrical design of the masonry wall test samples

After the selection of appropriate blocks and mortar in terms of the dimensions and constituents aspects which explained in previous sections, it was necessary to consider the geometrical design of masonry walls. The major function of masonry walls is to provide sufficient support for the external loads of the structure. Previous studies [62, 63] have demonstrated that the criterion of the load-bearing capacity of masonry walls against the axial loads is the most influential parameter by which to assess their overall performance. Consequently, the behaviour of masonry walls under axially applied compression loads is considered in this phase of the experimental programme.

To evaluate the compression behaviour of masonry walls, it would be more practical to follow the idea of small scale wall sections (wallettes), as this saves both time and cost of investigation and, in any case, gives results that are representative of the behaviour of large scale masonry walls [62, 66, 67].

According to BS EN 1052-1 [104], the preparation of the wallettes for testing their compressive strength should satisfy the following requirements:

1. The length of the wallette (l_w) $\geq 1.5 \times$ length of the unit(l_u)
2. The thickness of the wallette (t_w) $\geq$ thickness of the unit(t_u)
3. The height of the wallette (h_w) $\geq 3 \times$ height of the unit (h_u), $\geq 3 \times$ thickness of the wallette (t_w), $\geq$ length of the wallette (l_w) and $\leq 15 \times$ thickness of the wallette (t_w)

BS EN 1996-1-1 [65] also specifies a minimum net area on plan of 0.04 m^2. The above items were taken into consideration in designing the geometry of wallettes, as shown in Figure 7.8a.

7.9 Building the masonry wallettes

To achieve the geometric shape of the wallettes described in Section 7.8, some of the concrete blocks were cut in half using a special clipper-diamond tipped cutting wheel. Wooden plates of a suitable size were prepared to be used as a flat base upon which to stand the masonry wallettes, as shown in Figure 7.8b. These plates were covered with a thick plastic sheet along their upper face and coated with oil, thus permitting the lifting of the masonry wallettes without them becoming adhered to the wooden plate. The total dimensions of the wallettes were 670 × 685 × 100 mm ($l \times h \times t$) constructed with three courses of blocks. Each course contains one and a half solid lightweight concrete blocks. Four horizontal bed joints and three perpendicular head joints were used for each wallette. The magnitude of the overlap between the concrete blocks was compliant with the limits of BS EN 1996-1-1 [65] which defined it as greater than or equal to 0.2 times the block height or 100 mm, whichever is greater. The top bed joint was capped to adjust the horizontal level using a glass sheet, as shown in Figure 7.8c. This regime permits the application of a uniformly distributed load upon the wallettes. A total of 16 masonry wallettes were built in the same manner, as shown in Figure 7.8d. Following this process, all of the wallette samples were covered with a polythene sheet for 28 days to achieve the desired bonding strength of the mortar, as shown in Figure 7.9.

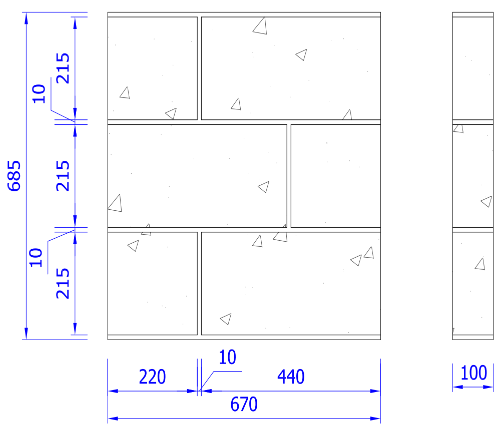

(a)

(b)

(c) (d)

Figure 7.8: Geometric shape and details of the construction of the masonry wallettes (all dimensions in mm)

Figure 7.9: Curing of the masonry wallettes in the laboratory

7.10 Prediction of the compressive strength of the masonry wallettes

For the purpose of the preliminary prediction of the characteristic compressive strength of the masonry walls under compression loads from the strength of their components, the Eurocode 6 [65] suggested the following equation:

$$f_k = K f_b^{\alpha} f_m^{\beta} \tag{7.1}$$

where f_k is the characteristic compressive strength of masonry walls, in MPa; K is a constant depending on the types of unit and mortar being used; α and β are constants; and f_b and f_m are the normalised mean strength of a unit in the direction of the applied action and the compressive strength of the mortar.

To generalise the above formula for use with different unit geometries, British Standard BS EN 1996-1-1 [65] incorporated the shape factor δ mentioned in Section 7.6. Furthermore, this standard specified the values of α and β constants for most structural applications, as 0.7 and 0.3 respectively.

Applying Equation 7.1 by taking K= 0.55 which corresponds to the use of a solid masonry units and general purpose mortar and δ=1.38, the predicted characteristic compressive strengths are 6 MPa and 6.3 MPa for the masonry wallettes constructed with units of the reference and optimum modified concrete mixes respectively. These predicted values were verified against the experimental measurements, as explained in Chapter 8.

7.11 Summary

This chapter has discussed a methodology for exploring the practical application of the lightweight concrete mixes produced in the preceding experimental work as a structural member. The outcomes involved the selection of the mix of (30%G+10%MK) as an optimum modified concrete mix and load-bearing masonry walls as a suitable structural member to be used for practical application. Solid concrete blocks with dimensions of 440 × 215 × 100 mm and M12-class general purpose cement mortar were the proposed constituents of the masonry walls. The geometrical design illustrated that the small scale masonry walls (wallettes) with dimensions of 685 × 670 × 100 mm meets the requirements of the relevant BS EN standards. A prediction of the characterised compressive strength of the masonry wallettes showed that the reference and optimum modified wallettes can support 6 MPa and 6.3 MPa of compression stress respectively.

Chapter 8

Structural behaviour of the masonry wallettes under compression loads

8.1 Introduction

Masonry walls normally act as structural members to resist floor and (in some cases) beam loads. Axial compression forces form a significant part of the total live and dead loads applied upon the masonry walls. Following the research strategy mentioned in Chapter 7, this chapter is concerned with the structural evaluation of both types of masonry wallette samples under conditions of axial compression load at ambient temperature. Firstly, the behaviour of masonry walls subjected to a concentrated load is described, and then a design for an appropriate experimental programme is explained in detail. Next, the measurement of the modulus of elasticity for the constituents of both wallettes is discussed, followed by the results and discussion of the wallette tests. Finally, a brief summary of the main findings of this chapter is presented.

8.2 Behaviour of the masonry walls subjected to concentrated loads

In practice, unlike homogenous materials, the properties of which may be relatively easily assessed, the behaviour of masonry walls under concentrated loads is complex because they incorporate mortar joints. Usually, these joints have a lower strength value than those of units, thereby acting as planes of weakness within the wall system [72]. The restraining effect, on the other hand, increases as the applied loads increase, and enhances the strength of the area underneath the region of the load action. The source of this enhancement is the upholding of the less confined surrounding parts of the wall [65, 105].

The degree of enhancement (γ) is defined as the ratio of the average stress underneath the load plate to the stress in the wall if the load was applied over its full width. The value of γ essentially depends on the ratio of the loaded area ($\grave{a}/a$), the position of the applied load in relation to the end of the wall (d/a), and the aspect ratio of the wall (a/h), as presented in Figure 8.1. However, when the wall is subjected to a load over its full thickness, the effect of the degree of enhancement can be neglected. The wall is therefore treated as in plane stress [105].

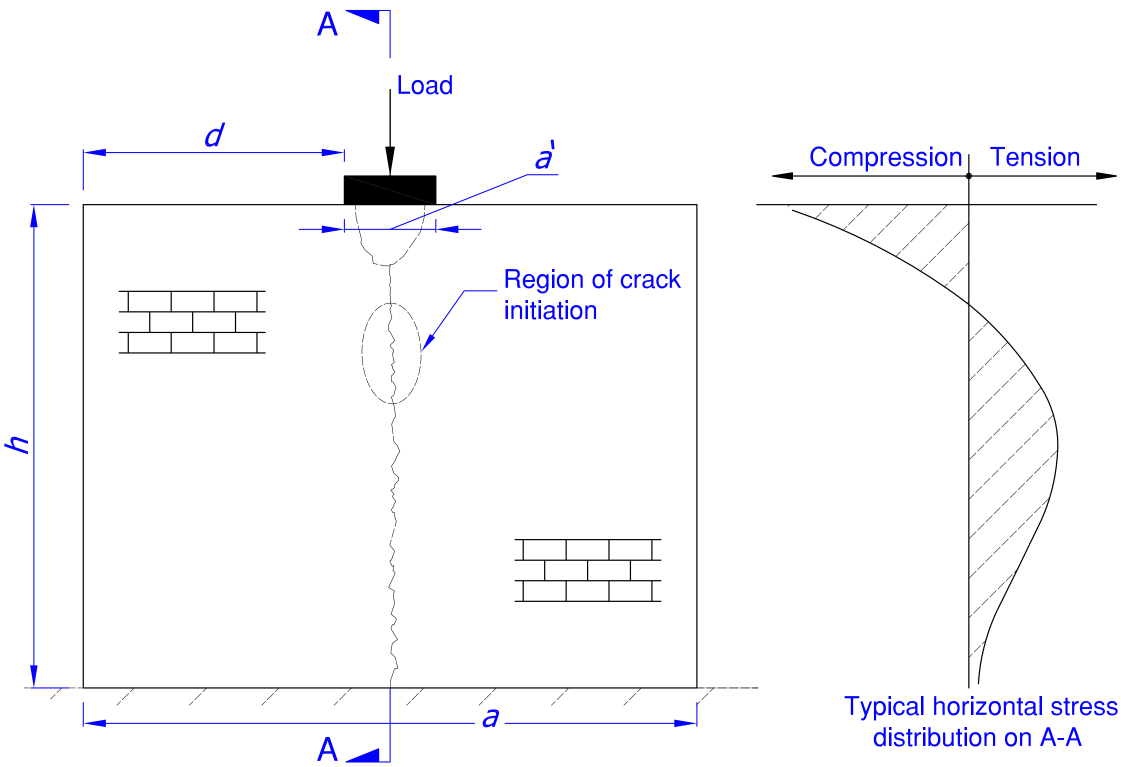

Figure 8.1: Masonry walls subjected to a concentrated load [105]

The failure of a wall can be caused by either debonding of the mortar joint, or cracking or crushing in one or both of the wall constituents (units and mortar joints). As a result, the cracks start to take place underneath the point where the load is applied in which the lateral stresses are high. Thereafter, vertical cracks propagate along the wall height, as shown in Figure 8.1.

As full thickness loading is the most commonly applied condition for evaluating the behaviour of masonry walls and reflecting their practical applications within a structural building, this formulation is addressed later in the thesis. In order to achieve the aforementioned condition and to assess the bearing capacity of both masonry wallette samples, concentric axial loads were applied above a stiff steel plate covering the whole thickness of the wallette, as explained in the following sections.

8.3 Details of the experimental programme

8.3.1 Preparations for the test

The masonry wallettes were lifted from their places to the testing rig [67] using a special technique to keep them safe from collapsing under their gravity load or from cracking the mortar joints. This technique consists of attaching two U-section steel columns along the vertical edges of the masonry wallettes, as shown in Figure 8.2a. The total height of the U-section steel column was 670 mm, while the web and flange cross-section details were 200×10 mm ($h \times t$) and 100×20 mm ($l \times t$) respectively. The former columns were connected together using four 20 mm diameter horizontal tension bars. In order to accommodate the tension bars, two small steel stiffeners with dimensions of ($40 \times 30 \times 10$) mm ($l \times h \times t$) with a 25 mm diameter central hole were welded to the upper and lower edges of each column web. The tension bars were then tightened sufficiently to produce confinement of the composite wallette-steel frame system while in transit to the test equipment. To reduce the risk of excessive tightening which may cause the wallettes to be crushed, a thin layer of plastic was inserted between the wallette and the steel columns. Thereafter, a crane and a stiff steel chain with two hooks was used to lift the wallettes, as shown in Figure 8.2b.

(a) (b)

Figure 8.2: Lifting the masonry wallettes: (a) the steel frame; (b) crane with steel chain and hooks

8.3.2 The test rig

To ensure the stability of the frame during the application of loads, the test rig was constructed from a heavy steel frame. Two universal I-section steel columns with 200×20 mm web and flange dimensions were firmly connected to two universal U-section beams, as shown in Figure 8.3a. The cross-section dimensions of the beam were 300×20 mm and 100×20 mm for the flange and web respectively. The universal steel beam carried the loading system midway along its length. The loading system included a hydraulic jack with a capacity of 1000 kN which stood upon a load cell. Two 20 mm diameter tension bars were incorporated to carry a steel beam with dimensions of 670×100×60 mm, as shown in Figure 8.3b. The purpose of using the steel beam was to uniformly distribute the applied loads over the upper surface of the wallette. Each tension bar was fitted with two scroll disks which allowed for raising or lowering the steel beam. To eliminate bending and/or twisting, the tension bars were passed through a stiff steel plate located between the hydraulic jack and the load cell. The mechanism of applying the loads in this test rig was manually controlled. In order to record the variation in the load, the output signal from the load cell was connected to a data logger.

(a)

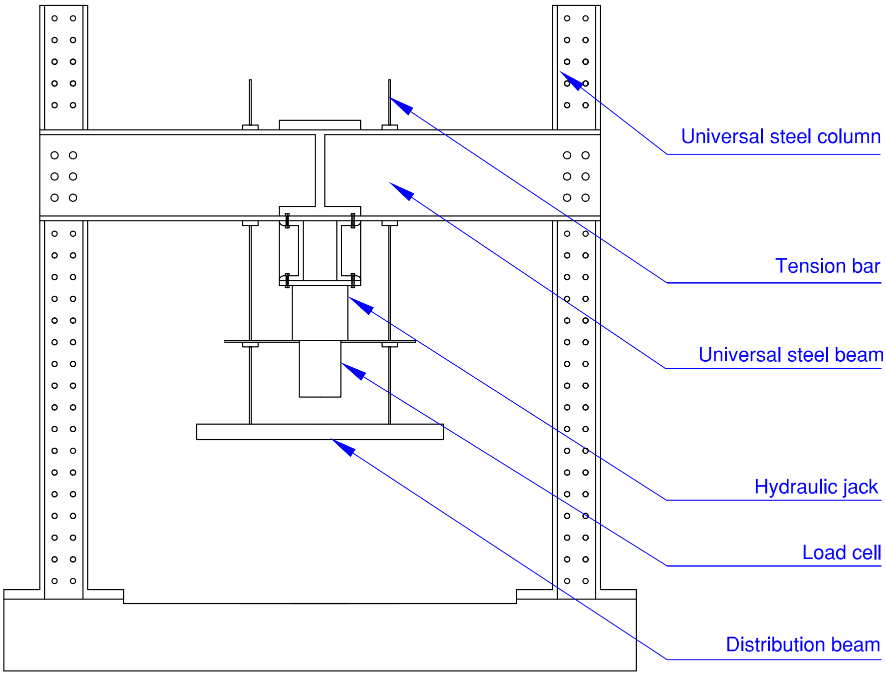

(b)

Figure 8.3: Details of the test rig: (a) the actual rig; (b) schematic details

8.3.3 Stress-strain behaviour and modulus of elasticity test

At this stage, data is needed for the stress-strain and modulus of elasticity of both the reference and optimum modified concrete block samples. In addition, the same data for cement mortar are required in order to model the response of the masonry wallettes to axial compression loading. Although these measurements were carried out for both types of concrete during the early experimental investigation (Chapter 4), the results would be more representative if the tested concrete samples were taken from the same mixes which were used to produce the concrete blocks. These tests were conducted for the cement mortar for the first time. The same procedure described in BS ISO 1920-10 [89] was followed using cylindrical specimens with dimensions of 100 mm diameter and 200 mm length, as shown in Figure 8.4. The average value of the results for the two samples was taken. Except for the cement mortar samples (which only involved vertical strain gauges), the other concrete samples were fitted with both vertical and horizontal strain gauges.

Figure 8.4: Preparation of the concrete samples for the modulus of elasticity test

8.3.4 Set-up of the compressive strength and deformation tests of the masonry wallettes

In order to implement the intended strategy of this investigation, all of the wallette samples characterised for testing at ambient temperature were subjected to technical preparation. Firstly, the load cell was calibrated to justify the load reading by multiplying its value by the correction factor, which was 1.48. Secondly, the wallette samples were placed in the test rig using the lifting method explained in Section 8.3.1. The deformation behaviour of the masonry wallettes was then determined in terms of the displacement measured at five different positions, as shown in Figures 8.5 and 8.6. Two reading points (points 1 and 2) representing the vertical displacement were measured using a position sensor. A linear potentiometer was used to measure the out of plane (lateral) displacement at three different points (points 3, 4 and 5) along the height of the wallette. These lateral displacement gauges were located at the top, centre and bottom of the wallette face, as shown in Figure 8.6. Furthermore, two additional linear potentiometers were placed along the horizontal centre line of the wallette (points $\grave{4}$ and $\grave{\grave{4}}$) in order to verify the accuracy of the central reading (point 4). The data logger was programmed to record the load-displacement values every second, indicated in kN and mm respectively. The average values for two wallettes were taken for each type of wallette.

Figure 8.5: Set-up of the compressive strength test (the displacement sensors are visible)

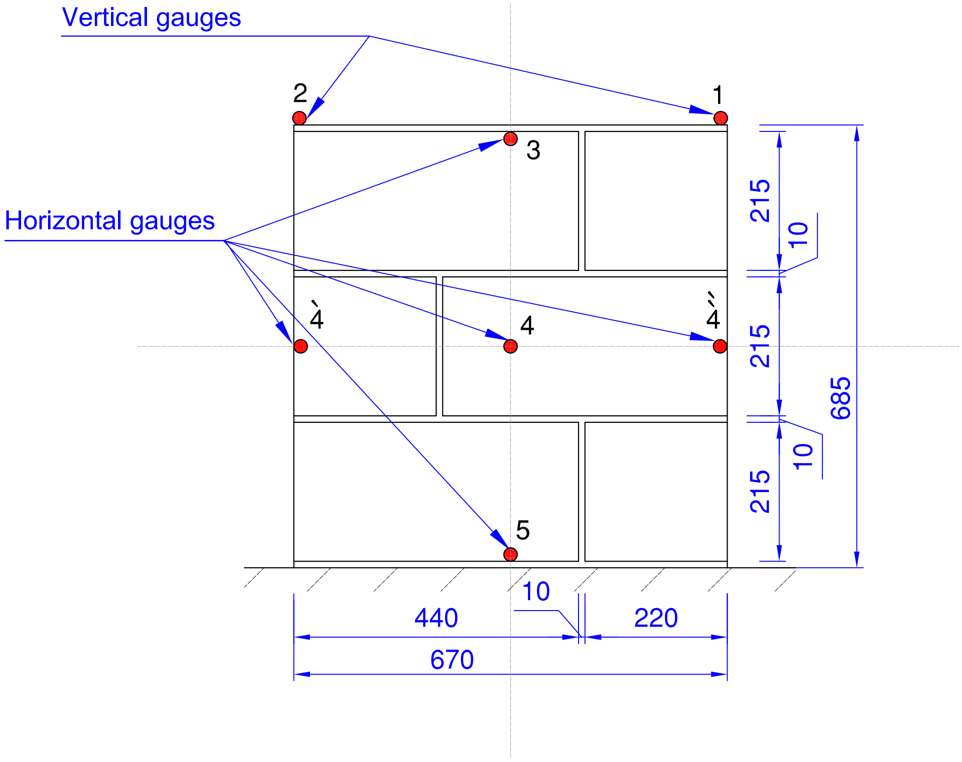

Figure 8.6: Locations of the position sensors and linear potentiometers used in the compressive strength test

8.4 Test results and discussion

8.4.1 Stress-strain curve and modulus of elasticity

Figures 8.7a to 8.9b show the results obtained for the stress-strain and modulus of elasticity tests of both the lightweight concrete mixes and cement mortar.

A rarher similar stress-strain curve for both concrete mixes can be seen in Figure 8.7a. This behaviour indicates a convergent strength level and deformation criterion under compression loads for these concrete mixes. Nevertheless, a remarkable variation in the vertical deformation was observed between the former concrete mixes during the early investigation in the first experimental part (Chapter 4). This variation reached about 22% at the maximum stress, as shown in Figure 8.7b, while the corresponding ratio of the present test results was about 3%. In many experimental works, such differences may occur due to many circumstances such as variation in casting time, humidity and temperatures. The differences between the early and present test results can therefore be considered limited. However, a consistent tendency was observed for the modulus of elasticity and Poisson's ratio aspects in both experimental phases, as shown in Figures 8.9a and 8.9b. These results provide further evidence for the early conclusions suggested in Sections 4.4.4 and 4.4.5 which referred to the higher modulus of elasticity and compressive strength of the optimum modified concrete mix in comparison with the reference concrete.

For the mortar samples, the cylindrical specimens exhibited higher stress values than the cubic specimens which were used in the compressive strength tests (Section 7.7), as shown in Figures 7.7 and 8.8. This behaviour is the opposite to that noted for both of the concrete mixes. The reason for this occurrence may be attributed to the effects of restriction and the presence of micro-cracks in the transition zone between the cement paste and aggregate. The latter effect is mostly present within the concrete samples as opposed to in the cement mortar [5]. The effect of the restriction of the specimen edges depends upon the geometry of the specimen and is similar for both of the concrete mixes and the cement mortar.

For the purpose of performing the analytical modelling of structural behaviour of the wallettes which is addressed later in the thesis, the present test results are considered to reflect the material properties of both types of concrete blocks and the cement mortar.

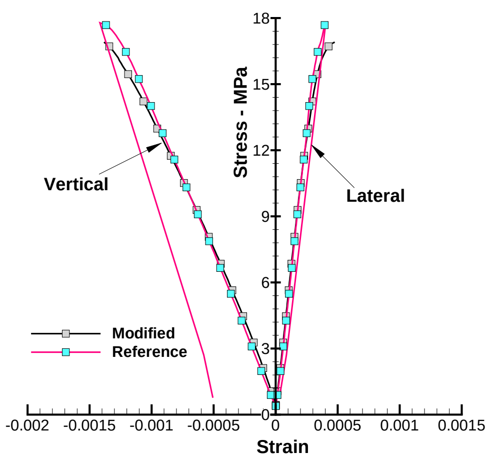

(a)

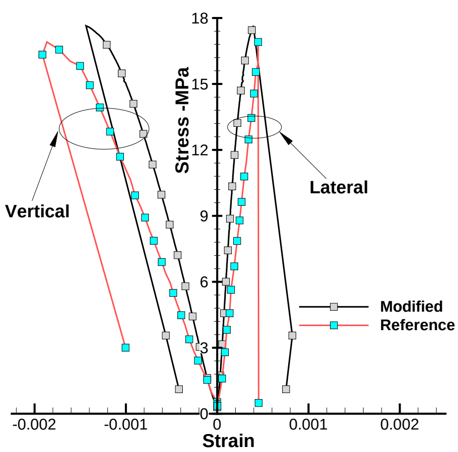

(b)

Figure 8.7: Stress-strain curves of both concrete mixes: (a) present test results; (b) results of the first experimental part

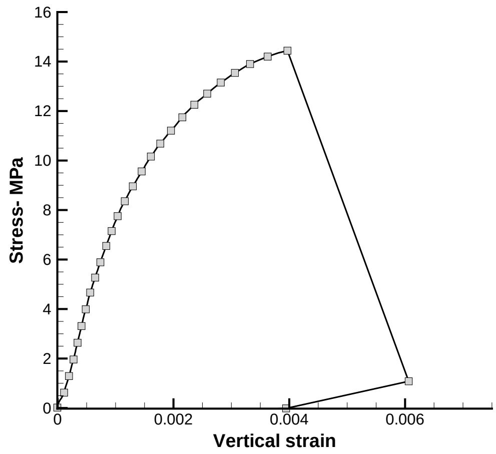

Figure 8.8: Stress-vertical strain curve of the cement mortar

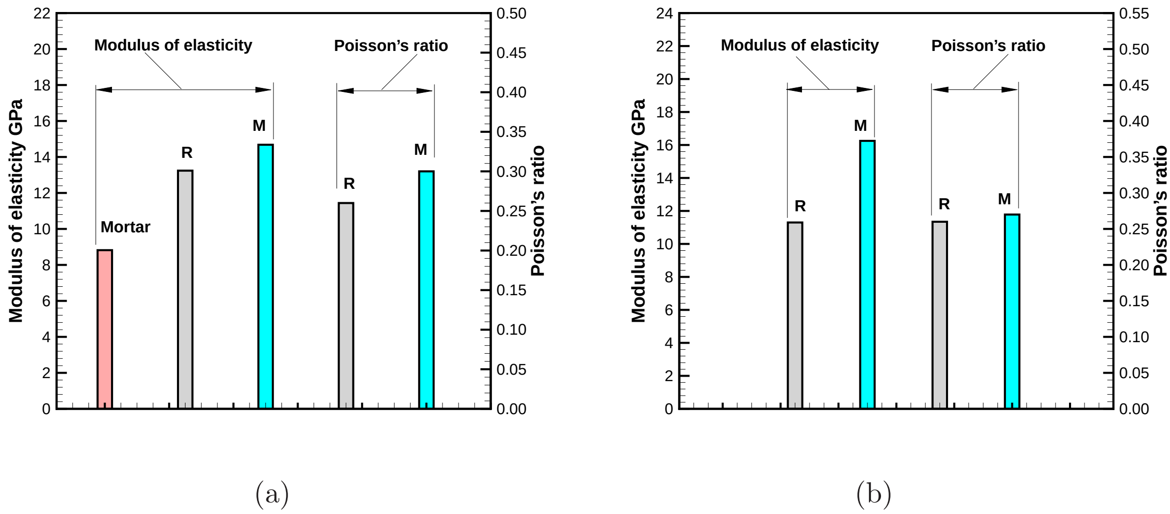

Figure 8.9: Modulus of elasticity and Poisson's ratio: (a) present test results; (b) results of the first experimental part

8.4.2 Compressive strength and deformation behaviour of the masonry wallettes

The results obtained for the axial compression tests of the reference and optimum modified masonry wallettes in terms of the load-displacement feature are illustrated in Figure 8.10.

It can be seen that the maximum axial loads at failure were 474 kN and 558 kN for the reference and optimum modified wallettes respectively, implying a corresponding ultimate compressive strength of 7.1 MPa and 8.3 MPa. This indicates an increase in load-bearing capacity of as much as 17% more for the optimum modified wallettes than that of the reference specimens. Such behaviour can be explained by the higher compressive strength of the optimum modified concrete blocks, whereas the characteristic compressive strength of masonry wallettes is a function of the strength of both the blocks and the cement mortar. As the strength of the cement mortar was the same for both types of wallette, this implies an increase in the compressive strength of the optimum modified wallettes due to the properties of the blocks.

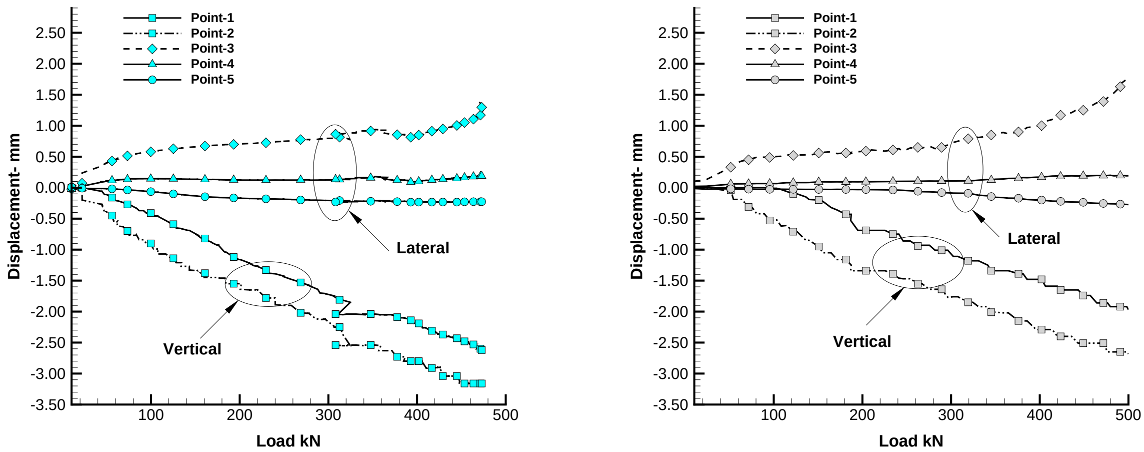

(a) (b)

Figure 8.10: Load-vertical and lateral displacement curves: (a) reference wallettes; (b) optimum modified wallettes

It is worthy of note that the characteristic compressive strength values of the masonry wallettes which were predicted in Chapter 7 were consistently lower than the corresponding measured values. The percentage deviations were about 16% and 24% for the reference and optimum modified masonry wallettes respectively. A possible explanation for this is the lower value of the K constant (0.55) suggested by Eurocode 6 [65]. However, if the upper limit value of K is used (0.6), then the predicted values will be 6.6 MPa and 7 MPa for the reference and optimum modified wallettes respectively, which is much closer to the measured results. In practice, this suggests that the K values given in [65] are not appropriate for the lightweight concrete blocks used in this study.

From Figure 8.10, it can be seen that the masonry wallettes acted as a cantilever column, whereas the top end (point 3) moves laterally away from its original position to give the largest deflection value along the height of the wallette. This behaviour follows the overall boundary conditions of the test set-up, in which there was no restriction against the lateral movement at the top end. Followed the top end, a deflection was caused at the centre of the wallette (point 4), with a value proportional to its relative height. In contrast to the top end and centre point, the base of the wallette (point 5) tended to move in the opposite direction. The behaviour of the base of the wallette reveals the capability of the lower support to resist the global motion of the wallette, thus providing overall stability.

Figures 8.11 and 8.12 show the failure modes of both masonry wallettes. Two masonry wallettes were observed for each set of tests. Approximately similar failure modes were noted for all tested samples, due largely to a combined compression-shear effect, leading to splitting failure. In addition, behaviour akin to crushing failure was perceptible in both of the optimum modified wallettes, as shown in Figure 8.12. In general, the cracking path can be characterised as follows: vertical cracking started from about the midpoint of the upper cement mortar layer (local point of the load application), crossing the top concrete block then passing through the head joint (centre core) and eventually ending near the left lower corner (toe of the wallette). Some of the wallette samples experienced cracking at the top right corner, while the second sample of the optimum modified wallettes showed severe cracking that began in the top left region, crossing the mid left core until the toe of the wallette. However, the vertical cracks propagated in the reference wallettes and continued up to the point of failure, allowing more time for cracks to develop. Sudden vertical cracking associated with failure was observed in the case of the optimum modified wallettes. This behaviour explains the perceived brittleness of the latter wallettes. Based upon the above observations, the most critical regions of the masonry wallettes under the effect of compression loads were diagnosed, as shown in Figure 8.13.

The failure mechanisms of the axial compression wallettes can be explained by the following mechanism, which has been suggested by other researchers [62, 63]. When the strength of the cement mortar is lower than that of the masonry unit (block) and the ratio of height to thickness of the wall is greater than 2:1, which is similar to the case examined in the current study, the cement mortar tends to expand under an axial compression load. This expansion is restricted by the concrete block, which induces a kind of confinement of the cement mortar. This confinement involves a triaxial compression state which enhanced the allowable compression capacity of the cement mortar. The wall system tends to overcome this deformation, maintaining overall stability against the compression stresses. This occurrence exposes the concrete block to a state of biaxial tension from both sides of the bed cement mortar joint. As the axial compression loads increase, the combination of the biaxial tension-axial compression stresses reaches the failure envelope. As a result, vertical cracking through the concrete blocks takes place. In contrast, the cement mortar maintains its integrity without cracking.

(a)

(b)

(c)

Figure 8.11: Failure modes of the reference masonry wallettes: (a) crack propagation; (b) first sample; (c) second sample

(a) (b)

Figure 8.12: Failure modes of the optimum modified masonry wallettes: (a) first sample; (b) second sample

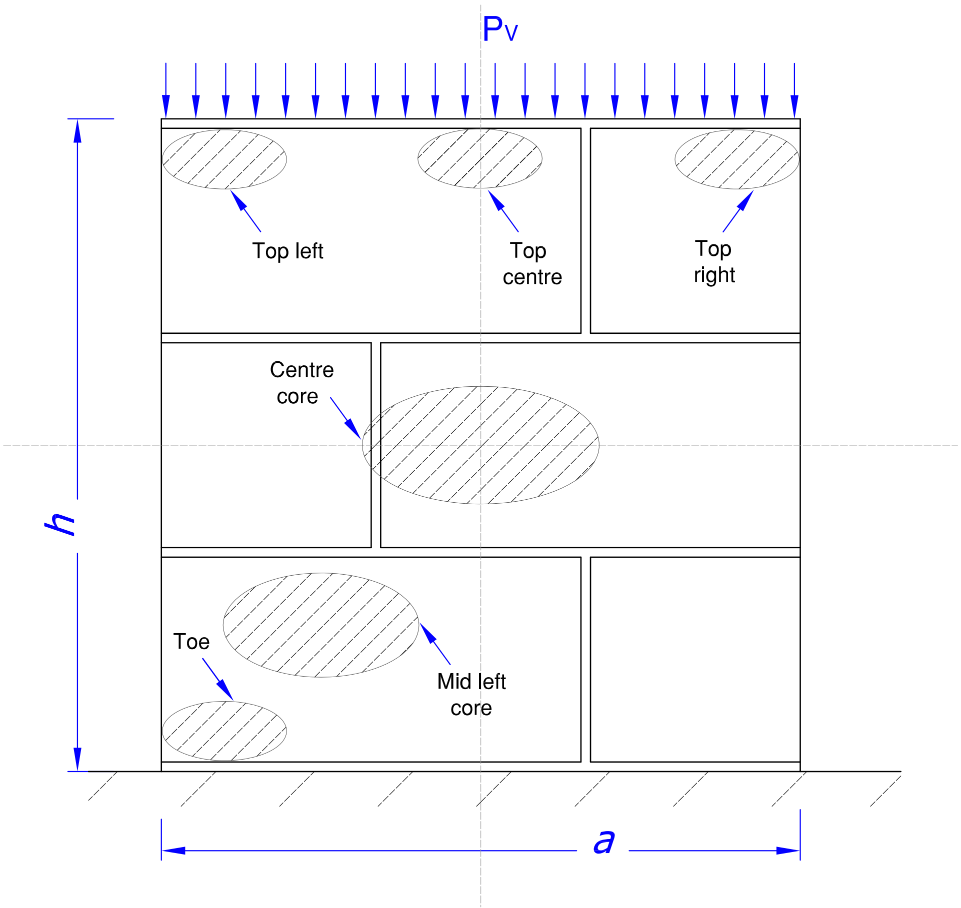

Figure 8.13: The main critical regions of the wallettes' failure modes under axial compression loads

8.4.3 Modulus of elasticity of the masonry wallettes

Consideration of the stress-strain characteristics of the masonry wallettes described in Section 8.4.2, the modulus of elasticity can be calculated. To achieve this, the average vertical strains and their corresponding compression stresses were considered for each masonry wallette. The strain value was calculated by dividing the average vertical displacement over the total height of the wallette, and the results obtained are presented in Figure 8.14. Following the expression given by BS ISO 1920-10 (Equation 4.3) [89], the results obtained showed that the values of the modulus of elasticity of the reference and optimum modified wallettes were 1375 MPa and 1795 MPa respectively.

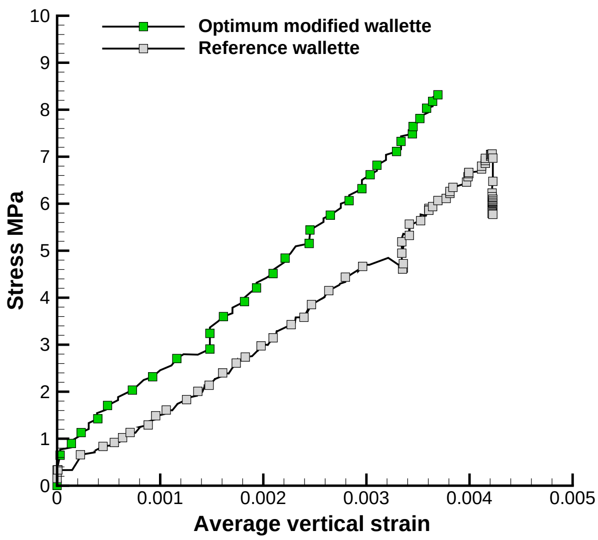

Figure 8.14: Stress versus vertical compression strain of both masonry wallettes

The Eurocode 6 [65] suggested the following formula to determine the value of the modulus of elasticity (E) to be used for the structural analysis of the masonry walls:

$$E = K_E f_k \tag{8.1}$$

where K_E is a constant which is recommended to be 1000 and f_k is the compressive strength of the masonry wallette. On the other hand, BS 5628-1 [103] suggested that the value of K_E should be 700.

In contrast with the results of this research, both of these suggested values produced a higher E value. To match the measured values, the value of K_E must be of the order of 200. This result is an indication that the approach given in [65, 103] is not entirely appropriate for the lightweight concrete blocks studied in this thesis.

It should be mentioned that the ratio between the modulus of elasticity of the optimum modified wallette to that of the reference wallette is equal to about 1.3. This is consistent with the corresponding ratio of their constituent concrete blocks which was about 1.2. Such behaviour provides a further support for the aforementioned discussion of the behaviour of masonry wallettes under axial compression loads in Section 8.4.2.

8.5 Summary

The strength features of the wallette constituents were consistent with the results for the reference and optimum modified concrete mixes which were obtained in the first experimental phase. A greater load-bearing capacity was observed for the optimum modified wallettes than for that of the reference wallettes. All of the wallettes tested tended to behave as columns and failed by means of splitting cracking. The critical path of the propagation of failure was approximately similar for all tested wallettes, normally starting from underneath the load point and passing through the concrete blocks and head joint to reach the toe of the wallette. More brittle behaviour was noted for the optimum modified wallettes, associated with rapid crushing failure. Conversely, relatively ductile behaviour with slow crack evolution was observed for the reference wallettes. Both of the BS EN Standards limits [65, 103] which were suggested to predict the characteristic compressive strength and modulus of elasticity of masonry walls were not found to be appropriate for use with these kinds of masonry wallettes and required adjustment.

Chapter 9

Structural behaviour of the masonry wallette samples under axial compression loads and high temperatures

9.1 Introduction

This chapter forms the second stage of the experimental work on the structural behaviour of the wallette samples examined in this study. It deals with the thermo-structural behaviour of the masonry wallettes at high temperatures. In order to explore the actual performance of the samples, a preliminary investigation was carried out to evaluate the mechanical strength of the masonry constituents at different temperatures. A comprehensive investigation was then carried out for both types of masonry wallettes to determine the most critical thermo-mechanical parameters governing the overall behaviour under a combination of axial compression load and exposure to heat. These parameters are discussed and compared with other relevant studies. A summary of the main findings is provided at the end of the chapter.

9.2 Behaviour of the masonry walls at high temperatures

Practice codes define the requirements for the behaviour of load-bearing masonry walls at high temperatures by specifying the minimum wall thickness necessary to resist the effects of fire for a specific period of time [55, 70]. The period of fire resistance of a given wall element depends upon several parameters, such as the type of masonry unit, the type of mortar, the density of the units, the type of wall construction, the slenderness ratio of the wall and the eccentricity of the load. All of these parameters are relevant to the standard fire test described in BS EN 1365-1 [106], in which the heat applied to the test sample is assumed to be unidirectional in nature.

A simplified calculation model is also suggested by BS EN 1996-1-2 Annex C [55] for predicting the load-bearing capacity of a wall element. This calculation model depends on the limit state for the fire situation in which:

$$N_{Ed} \leq N_{Rd,fi(\theta i} \tag{9.1}$$

where N_{Ed} is the design value of the vertical load applied to the wall, $N_{Rd,fi(\theta i}$ is the design value of the vertical resistance of the wall which is given by:

$$N_{Rd,fi(\theta i} = \phi(f_{d\theta 1}A_{\theta 1} + f_{d\theta 2}A_{\theta 2}) \tag{9.2}$$

However, the above calculation model is valid for masonry walls exposured to standard fire in which the time-temperature curve is given by Equation 9.3 [59]:

$$T = 345\ log(8t + 1) + 20 \tag{9.3}$$

where T is the temperature in ^{o}C and t is the elapsed time in minutes.

For other cases of heat exposure, the practical codes [55, 70] reported that the assessment of masonry walls should be addressed by the results of experimental tests. Because the all around heat exposure for the wallette surfaces forms the most severe case, this regime is considered as a base for the experimental programme running in this chapter, with a linear time-temperature heat exposure to reach the steady state condition ranging from 20 ^{o}C to 400 ^{o}C.

9.3 Details of the experimental programme

9.3.1 The heating system

The applied heating load was provided by a digitally-controlled furnace. This furnace had a total height of 750 mm and consisted of three combined panels, each panel measuring 250 mm in height and 80 mm thick, as shown in Figure 9.1a. The central internal dimensions of the furnace were 1190 × 872 mm ($l \times w$), while its internal end dimensions were 1100 × 770 mm, as shown in Figure 9.1b. The upper and lower ends were opened, thus permitting the laying of the furnace over the base of the rig and providing uniform heat exposure to all surfaces of the wallette samples. Before assembling the furnace, the base plate was insulated using an Isofrax blanket complying with BS EN 1094-1 [107]. A special thick lid was designed using a composite steel frame and Calsil insulation board, as shown in Figure 9.2. For ease of movement, the lid was in two parts, each part with dimensions of 1200 × 700 mm ($l \times w$). Two additional layers of Isofrax insulation blanket were placed on top of the lid of the furnace.

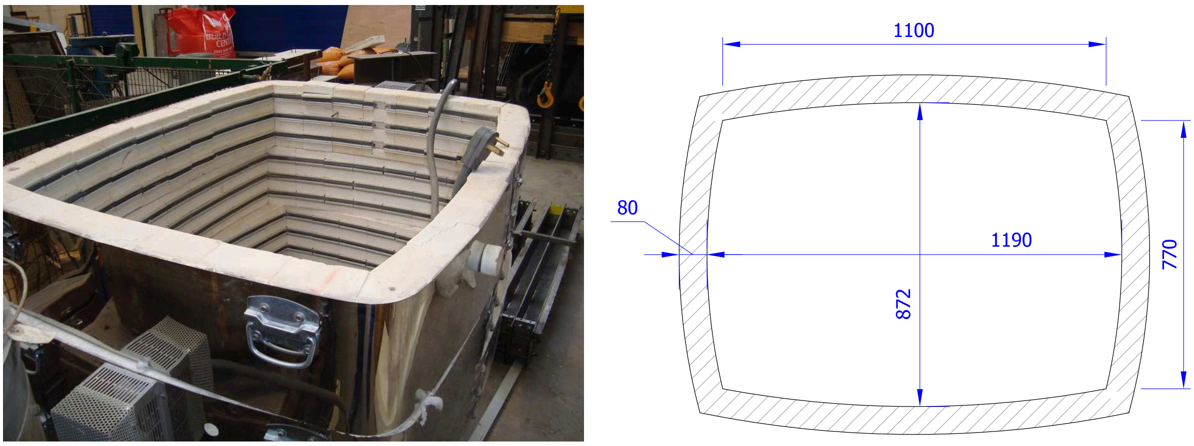

(a) (b)

Figure 9.1: Details of the digitally-controlled furnace used in the test (all dimensions in mm)

Before starting the tests, the temperature stability of the furnace heating was verified. This was done using three type K thermocouple wires arranged at the upper, middle and lower parts of the furnace. The furnace was then heated up to 400 ^{o}C with no sample inside at a heating rate of 300 ^{o}C/h. The furnace temperature was held at a nominal 400^{o}C for about 4 hours. The temperature variation between the thermocouple readings did not exceed 5 ^{o}C.

9.3.2 The loading system

Special arrangements were needed so that the wallette loading system [67] described in Chapter 8 could be used in conjunction with the furnace. In particular, it was important to protect the load cell from any heat damage. This protection was achieved by insulating all around the load cell with an Isofrax blanket layer and by keeping it away from the effect of heat gains from the distribution beam by provision of a sufficient separation space.

Figure 9.2: Details of the loading system and methods of protection of the load cell

Once the wallette temperature reached the specified test temperature, two 100 mm cubic steel blocks were inserted to fill the gap between the load cell and the distribution beam, as shown in Figure 9.2. The weights of the distribution beam and steel blocks were added to the total value of the load at failure.

In all of the experimental tests, a steady state regime was followed. This involved applying the mechanical load when the temperature of the masonry wallettes reached the specified test temperature. Both the load-deformation and temperature variation readings were recorded using a data logger system every second and three minutes respectively.

9.3.3 The measured parameters

In the event of a major fire, some masonry walls are exposed to heat from all sides. This eventuality poses the most serious risk of deterioration. If such an exposed wall is load-bearing, then the combined effect of load and temperature will govern its overall behaviour. On this basis, both types of masonry wallettes were subjected to a combined axial compression load and all around heat effect.

Three major parameters were investigated in this part of experimental work. These were the vertical deformation (displacement), temperature distribution and failure mode of the masonry wallettes.

Both vertical edges of the wallette (points 1 and 2) were monitored using position sensors, as shown in Figure 9.3. These sensors were fastened to the distribution beam using a thin steel wire passing through a steel pulley, and considered to represent the vertical deformation of the wallette samples. Six type K thermocouples with a wire diameter of 1.6 mm were used to measure the temperature within the furnace and also at five locations within the masonry wallette. The locations of the wallette thermocouples were two at the front face (points B and C) and one on the back face (point E), in addition to the head and bed joint thermocouples (points A and D) which passed through the central depth of the wallette, as shown in Figure 9.3. The latter two thermocouples were fixed in their positions using 3 mm-diameter drilled holes. All thermocouples and position sensors were calibrated before performing each test. The test was carried out for both types of masonry wallettes at three temperatures levels: 200 ^oC, 300 ^oC and 400 ^oC. The average reading of two samples was taken for each test result.

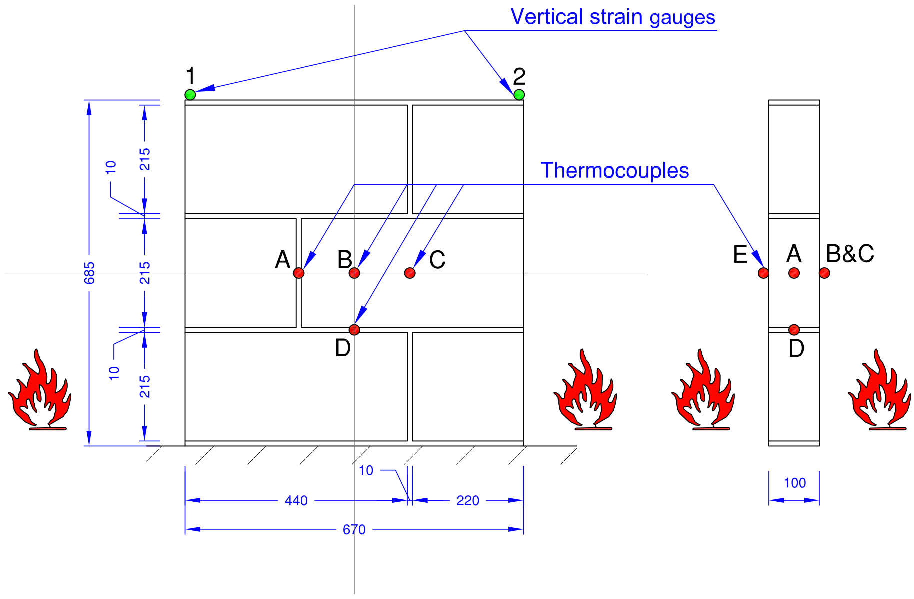

Figure 9.3: Locations of position sensors and thermocouples

9.3.4 Effects of shrinkage and moisture content

Before starting the tests, the top mortar layer of some of the masonry wallettes showed shrinkage. This was due to water loss from the cement mortar after the relatively long curing time in unsaturated air (the laboratory atmosphere) [5]. This shrinkage resulted in an inclined surface. In order to restore the original level of the surface, the affected wallettes were capped again with a mortar formulated from rapid-setting cement. The hardening of this kind of cement takes place within 10 minutes.

When the first test was conducted on the reference wallette sample at 400 ^{o}C, an explosive spalling phenomenon occurred. The initial explanation mooted for this behaviour is the higher liquid moisture content of the concrete blocks [108]. As they were immersed in water for a long time, it was suggested that the period of air drying in the laboratory environment was not sufficient to remove the excessive water confined within the concrete blocks, as shown in Figure 9.4. To overcome this problem, the actual moisture contents of both types of wallettes was calculated using small pieces of the concrete blocks. This was done by drying out the concrete pieces in an electric oven at a temperature of about 70 ^{o}C, then measuring their weight losses at 24 hour intervals for a period of 4 days. The inside temperature of the block pieces was indicated through one type K thermocouple, as shown in Figure 9.5a. The results obtained are illustrated in Figure 9.5b. The variation in the oven temperature for each 24 hour period noted in Figure 9.5a, was due to opening the oven door when picking up the samples for weighing, resulting in a reduction in the average oven temperature.

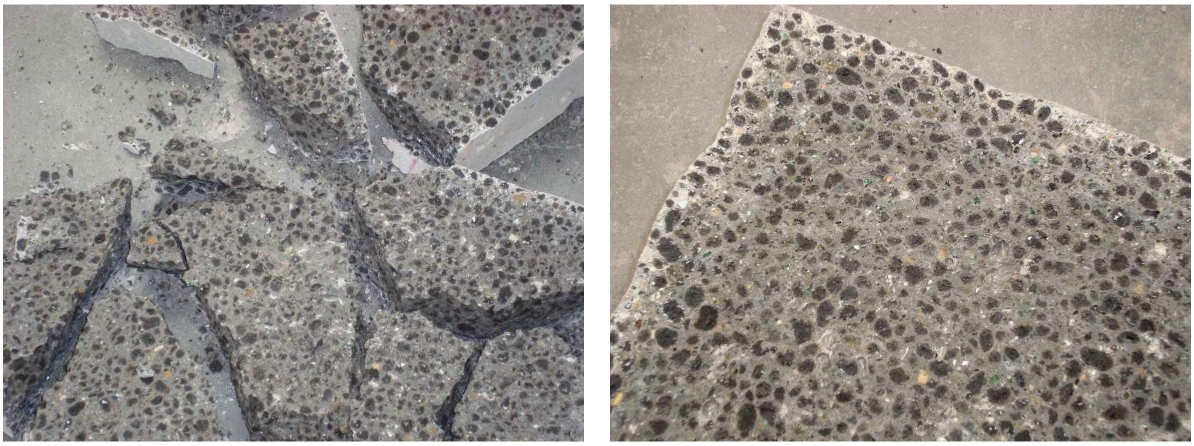

(a) Reference concrete blocks　　(b) Optimum modified concrete blocks

Figure 9.4: Moisture confined within the concrete blocks

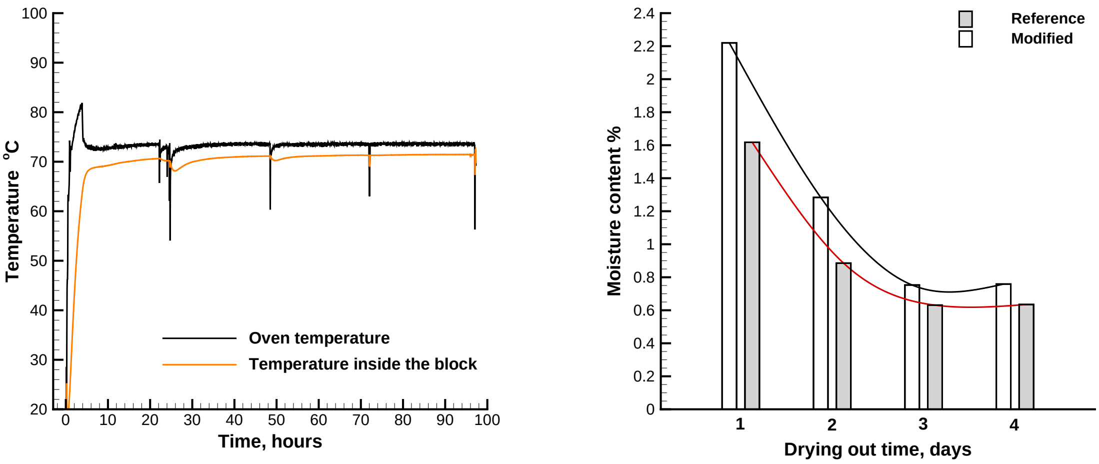

(a)　　(b)

Figure 9.5: Details of the moisture content test: (a) temperature profile of the oven and block samples; (b) the moisture content against the drying out time.

It can be seen from Figure 9.5b that the moisture content of the modified block samples was higher than the reference samples. Both concrete samples exhibited reductions in their moisture content with an increase in the duration of drying. Approximately constant moisture contents were observed after three days for both concrete samples. The residual water content forms the normal limit of air curing. Following these results, all of the wallette samples were initially dried out for 3 days at an oven temperature of 70 ^{o}C before the high temperature test was performed.

9.3.5 Stress-strain and modulus of elasticity tests at high temperatures

In order to provide the required material properties which are essential for numerical simulation, the stress-strain behaviour and modulus of elasticity of the cement mortar and both types of concrete blocks were measured at high temperatures. Cylindrical specimens taken from the same blocks and mortar mixes were tested at an age consistent with that of the relevant wallette samples. The loading system mentioned in Section 9.3.2 was used, with one furnace panel to be compatible with the cylinders height.

Figure 9.6: Set-up of the modulus of elasticity test at high temperatures

The hydraulic jack, load cell and their accessories were moved down to touch the top surface of the sample. A circular steel plate with a diameter of 120 mm and a thickness of 25 mm was placed underneath the distribution beam to provide a uniform compression load above the samples, as shown in Figure 9.6. Three type K thermocouples were used simultaneously to measure the temperatures within the furnace and within the surface and centre of the cylindrical samples, as shown in Figure 9.7a. The heating rate was 300 $^oC/h$. When the temperature equilibrium for all thermocouple readings had been achieved (the specified test temperature $\pm$ 5 ^oC), the axial compression load was then applied.

As the cylindrical samples were located at the centre of the loading system and the vertical position sensors were connected to the ends of distribution beam, the average displacement readings of both sensors was taken for each test, as shown in Figure 9.7b. The test was repeated twice for each set of concrete or cement mortar, at temperatures of 200 ^oC, 300 ^oC and 400 ^oC.

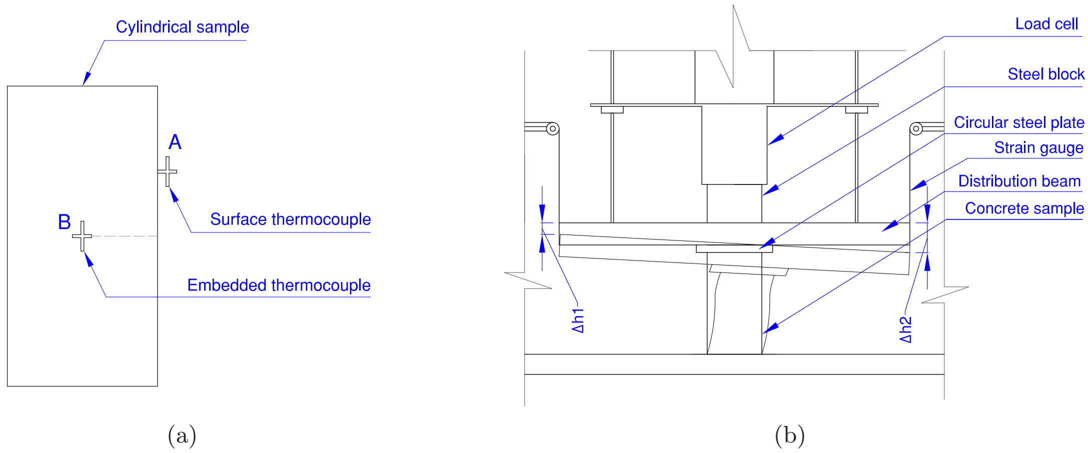

Figure 9.7: Details of the temperature and displacement measurements: (a) locations of the thermocouples; (b) determination of the mean vertical displacement

9.4 Test results and discussion

9.4.1 Stress-strain curves and modulus of elasticity of cylindrical specimens

The results obtained for the stress-strain tests of both types of concrete and the cement mortar at high temperatures are shown in Figures 9.8a to 9.8c.

It can be seen that the vertical strain values increase with an increase in the applied temperature. This is indicative of a progressive reduction in the integrity of the concrete and cement mortar samples when they are exposed to a combined load-temperature regime. In comparison with the results obtained at ambient temperature described in Chapter 8, the percentage increase in vertical strain at maximum stress for both concrete samples was about 400% (see Figure 8.7a). On the whole, these results confirm pervious research findings [109]. Such behaviour can be explained by the presence of new strain components within the loading regime. In addition to strain-related stress, the transient and thermal strain components are now part of the combined load-temperature effect. These additional strain terms represent the largest contribution to the total amount of strain [110, 111].

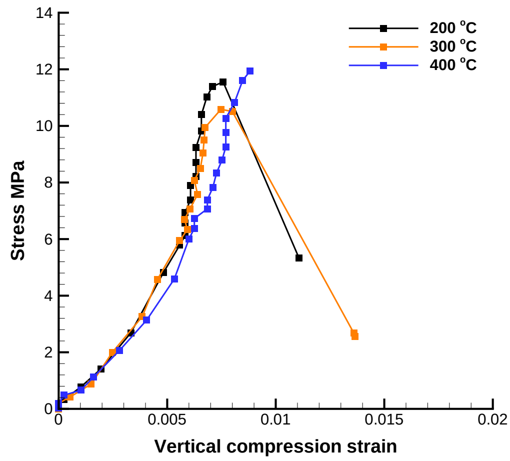

(a)

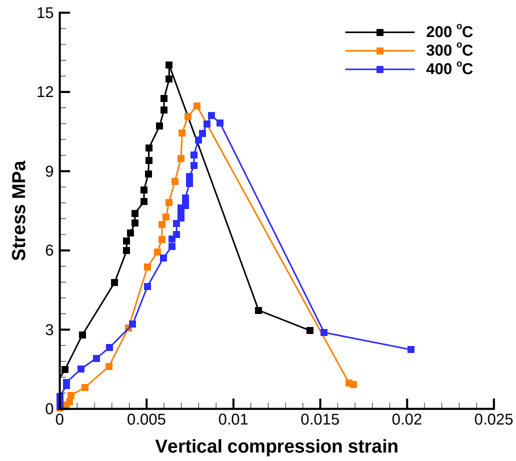

(b)

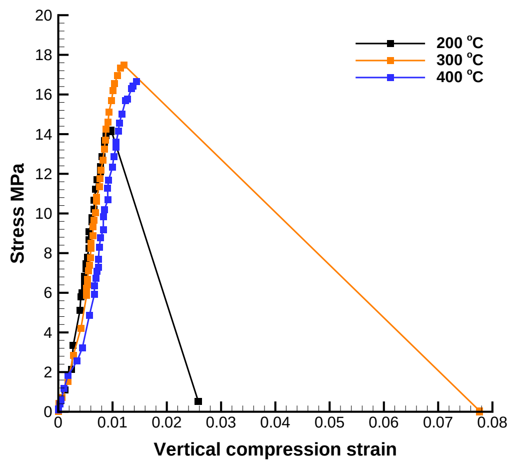

(c)

Figure 9.8: Stress-vertical compression strain curves at exposure to various temperatures: (a) reference concrete; (b) optimum modified concrete; (c) cement mortar

In the case of the cement mortar, the corresponding percentage increase was about 200%, as shown in Figures 9.8c (and 8.8). However, in all of the above cases, if the comparison was based on the strain value at complete failure, the percentage increase would be considerably higher.

Except at 200 ^oC, both the reference and optimum modified concrete samples showed approximately similar stress-strain curves at other testing temperatures. This is consistent with their behaviour at ambient temperatures. At 200 ^oC, the optimum modified mix exhibited a much steeper stress-strain curve, with a lower strain magnitude at a specific stress value than the reference samples, as shown in Figure 9.8b. This behaviour may be related to the modified samples' enhanced resistance to applied heat in this temperature range.

At all of the test temperatures, both of the concrete samples showed a reduction in the value of compressive stress at failure relative to that at ambient temperature. The ratio of strength at temperature T to that at 20 ^oC was about 65% at 400 ^oC. This behaviour is likely to be due to the propagation of micro-cracks with some associated expansion, with a consequent reduction in the strength of the concrete [93].

In contrast, the cement mortar samples showed higher compressive stress values at elevated temperatures in comparison with those at ambient temperature. The percentage increase was as much as 22% at 300 ^oC. The same behaviour was noted in some previous studies [112]. The reasons for this are twofold: firstly, a decrease in applied pressure takes place when drying under heat, which increases Van der Waals forces, resulting in a closer configuration of capillary pores. Secondly, supplemental hydration of cement paste resulting in enhancing the compressive strength [113].

It is of interest to compare the results obtained for the stress-strain curve of the modified concrete samples with those given in BS EN 1996-1-2 [55] for pumice lightweight concrete units. Figure 9.9 compares the results between both behaviours. A reduction in strength of approximately 30% was observed for the optimum modified concrete samples when they were exposed to higher temperatures, while the corresponding percentage for the pumice units was about 20%. On the other hand, the vertical strain value of the pumice units at failure was observed to be double that of the modified concrete samples.

In the case of the modulus of elasticity, the measured values for both the concrete samples and

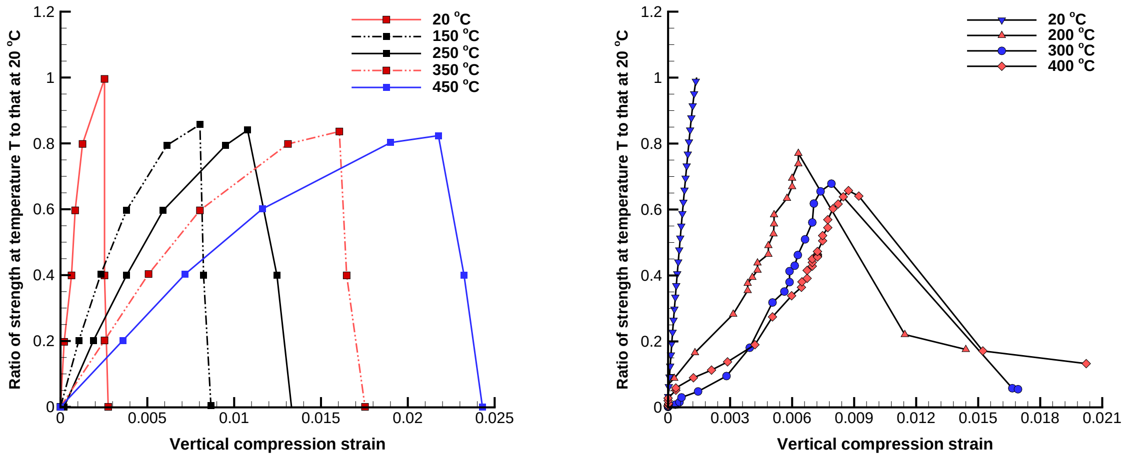

(a) (b)

Figure 9.9: Comparison between the temperature dependent stress-strain curves of pumice units and the optimum modified concrete samples: (a) pumice units with a unit strength of 4-6 MPa and with density of up to 1000 Kg/m^3 [55]; (b) optimum modified concrete samples with a sample strength of 18 MPa

cement mortar were calculated in accordance with BS ISO 1920-10 [89] and the results obtained are illustrated in Table 9.1. Significant reductions in the values of modulus of elasticity were observed when the lightweight concrete and mortar samples were exposed to high temperatures. The residual ratio of modulus of elasticity was in the range of 7%-17%. Among the tested samples, the set of cement mortar samples exhibited the lowest reduction in modulus of elasticity, whilst both lightweight concrete samples were approximately at the same level of deterioration.

Table 9.1: Modulus of elasticity (E) of both concrete samples and cement mortar at high temperatures

	Reference concrete			Modified concrete			Cement mortar		
E (MPa)	200 ^{o}C	300 ^{o}C	400 ^{o}C	200 ^{o}C	300 ^{o}C	400 ^{o}C	200 ^{o}C	300 ^{o}C	400 ^{o}C
	1051.8	1005	861.2	1555	1064	958	1405	1244	971
Reduction in E(%) relative to that at 20 ^{o}C	92.00	92.40	93.45	89.40	92.75	93.47	83.00	84.95	88.25

The failure modes for all of the tested samples are presented in Figures 9.10a to 9.10i. It can be seen that the combined effect of load-temperature is more pronounced at high temperatures. Except for the cement mortar samples, the cylindrical samples failed by means of vertical cracking which took place from the the point of the applied load, associated with the crushing of some affected zones. More brittle behaviour with instantaneous failure was noted for the modified samples compared to the reference samples. The cement mortar, on the other hand, showed a type of shear failure without vertical cracking or crushed zones, as shown in Figures 8.10g to 9.10i.

(a) R-200 ^{o}C

(b) R-300 ^{o}C

(c) R-400 ^{o}C

(d) M-200 ^{o}C

(e) M-300 ^{o}C

(f) M-400 ^{o}C

(g) Mortar-200 ^{o}C

(h) Mortar-300 ^{o}C

(i) Mortar-400 ^{o}C

Figure 9.10: Failure modes of both lightweight concrete and cement mortar cylinder samples at various temperatures

9.4.2 Thermal behaviour of the masonry wallettes

The temperature profile results for both kinds of masonry wallettes when exposed to different temperatures are shown in Figures 9.11a to 9.11e. The key profile was the time-temperature aspect. Due to the difficulties experienced with spalling, no thermal results have been obtained for the reference wallettes at 400 ^{o}C. Further discussion of this case is presented in Section 9.4.3.

It can be seen from the above figures that the duration required for achieving the steady state condition was grater for the optimum modified wallettes than for the reference samples. The difference between the elapsed time to reach a stable (constant) temperature was as much as 1.35 hours more for the optimum modified wallettes in comparison to the reference wallettes. These findings corroborate the previous results obtained for the thermal performance of the modified concrete samples, which were discussed in Chapter 5.

Despite the value of imposed temperature, the stability times for the temperature of the overall system (the temperature of the furnace, wall surfaces and interior wall joints) of the reference wallette samples were convergent. At a lower imposed temperature, a longer time was required for the optimum modified wallettes to satisfy the state of stability. Indeed, at 200 ^{o}C, the temperatures measured of the interior thermocouples for the optimum modified wallettes were about 190 ^{o}C, as shown in Figure 9.11b. This is because the maximum duration of any single test was restricted to 9.6 hours due to health and safety restrictions on the use of the laboratory facilities. With an increase in the imposed temperature, the reduced time taken to achieve the equilibrium condition might be explained by the consideration of the heat transfer processes. Rapid thermal diffusion is associated with the zones of hottest temperature [57]. Generally, all of the time-temperature curves showed two phases of temperature distribution, namely linear and nonlinear parts, as shown in Figure 9.11f. The duration for each part depended upon the imposed temperature and the thermal properties of the wallette being tested. The maximum offset between the temperature curves for the surface and inside joints was at the point of nonlinear interchange of the surface temperature curve. Thereafter, a convergence between the aforementioned temperatures took place. This convergence reached its highest intensity at the end of the equilibrium.

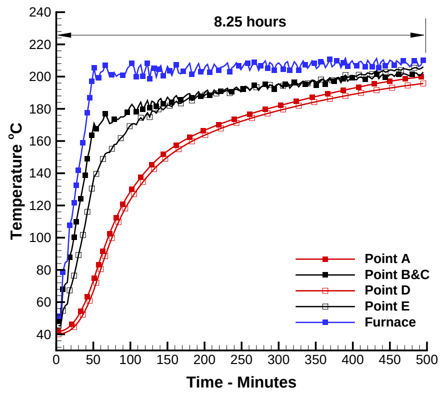

(a) R wallette at 200 ^{o}C

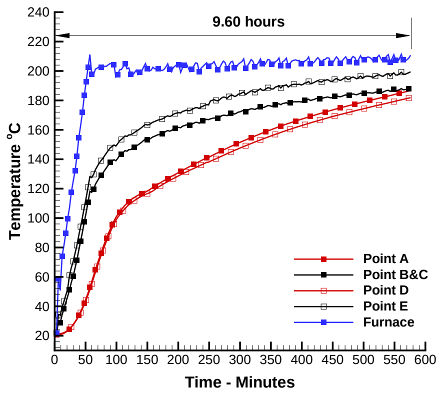

(b) M wallette at 200 ^{o}C

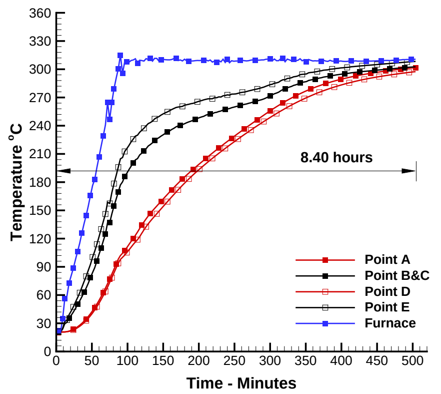

(c) R wallette at 300 ^{o}C

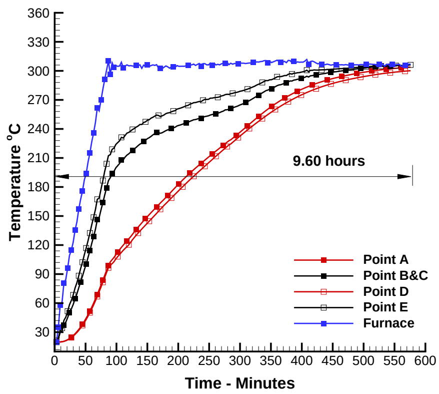

(d) M wallette at 300 ^{o}C

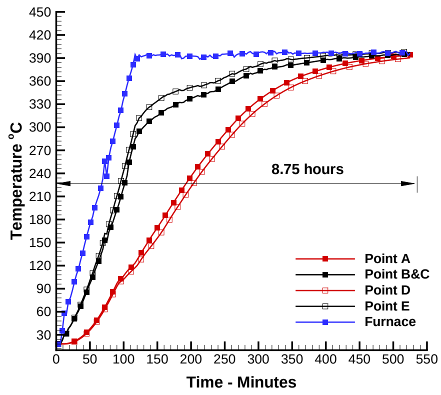

(e) M wallette at 400 ^{o}C

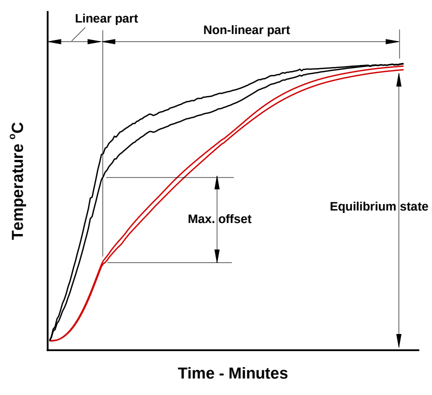

(f) details of the time-temp. curves

Figure 9.11: Time-temperature profiles of the masonry wallettes during exposure to different temperatures

In all of the masonry wallette samples, the experimental results exhibited a noticeable variation in the temperatures of the front and back surfaces (points E, B & C). This behaviour could be related to thermal convection inside the furnace and heat absorption by the wallette mass. The thermocouple readings of the front face (points B & C) were identical, implying a uniform temperature along their positions. A slight variation was observed between the temperatures of the bed and head joints (points A and D). Except for the case of reference wallettes at 200 ^{o}C, this variation becomes visible after about 100 minutes. In all of the test cases, the bed joint (point D) temperatures were lower than those of the head joint (point A). The same behaviour was also noted by Ruvalcaba [67]. This may be attributed to the difference between the mass volume of the bed and head joints, where temperature propagation will occur more rapidly within small mass volumes than in larger ones.

It would be useful to compare the durations of temperature equilibrium obtained in this study with those achieved by Ruvalcaba [67]. This comparison is presented in Table 9.2. The former study [67] had considered the test results at 200 ^{o}C to be unreliable and incorporating an experimental error. It was expected that the result would be much lower if the same experimental methodology used for the other tests had been followed. From Table 9.2, it can be seen that the results of the current study showed up to a 200% improvement in the insulation feature in comparison with those presented in [67].

Table 9.2: A comparison between the results of the equilibrium times of this study and those obtained by Ruvalcaba [67]

Temperature	Duration to reach the state of equilibrium (hours)		
	Results of Ruvalcaba [67]	Results of current study	
		R wallette	M wallette
200 ^{o}C	7	8.25	9.60
300 ^{o}C	-	8.40	9.60
400 ^{o}C	4.3	-	8.75

9.4.3 Structural behaviour of the masonry wallettes

The results obtained for the load-displacement behaviour of both types of masonry wallettes at high temperatures, are shown in Figure 9.12a to 9.12e.

Except for the reference wallettes at 400 ^{o}C, the above figures show minimal reduction in the bearing capacity of both masonry wallettes when exposed to high temperatures. The relative strength at higher temperatures in comparison with that observed at ambient temperature was in the range of 0.8 to 0.9 for the modified wallettes, while it remained at about 1.0 for the reference masonry wallettes. This behaviour reflects the balance between an increase in strength of the cement mortar and the corresponding decrease in the strength values of the lightweight concrete blocks at high temperatures, as explained in Section 9.4.1. Since the total load-bearing capacity of the masonry is governed by the strength of its joints, so the stronger mortar joint compensates for the reduced strength of the concrete block, thereby enabling a higher strength value to be achieved for the masonry wallettes.

At the start of the tests, with the exception of the optimum modified wallettes at 400 ^{o}C, none of the masonry wallettes showed any significant vertical deformation up to a load of about 50 kN. The reason for this could be related to heat effects, which tend to induce relief of the applied mechanical pressure [113]. Beyond a load value of 50 kN, vertical deformation commences. A approximately linear relationship was observed with an increase in the applied loads. Due to the manual mechanism for applying loads, the linear relationship was generally characterised by a wavering form.

The experimental data (except for the modified wallettes at 300 ^{o}C) showed a notable difference between the values of vertical displacement for points 1 and 2. These are located on the top of the masonry wallettes. This difference can be explained by minor imperfections in the masonry wallettes, which cause eccentricity of the applied load. This effect was also mentioned in BS EN 1991-1 [65].

Another important observation is that the maximum vertical displacement of the masonry wallettes when exposed to high temperatures was similar to that obtained at ambient temperature. This means that only a limited thermal strain occurred during the testing. A possible explanation for this may be attributed to the all around heat exposure regime, which results in minimum or zero net thermal expansion effect, associated with the higher strength of the cement mortar joint revealed at high temperatures.

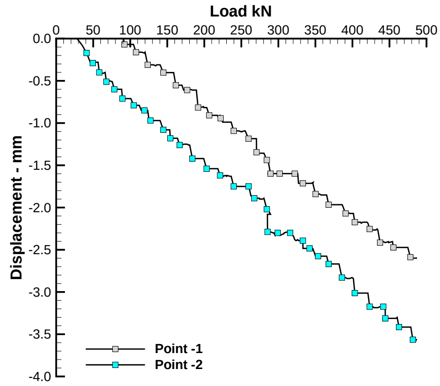

(a) R wallette at 200 ^{o}C

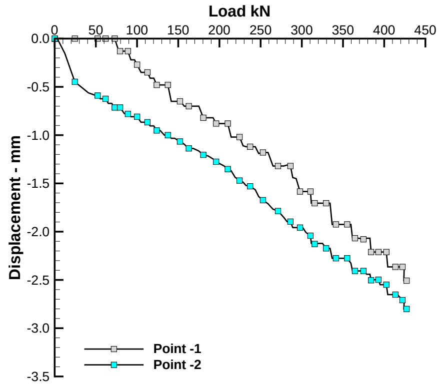

(b) M wallette at 200 ^{o}C

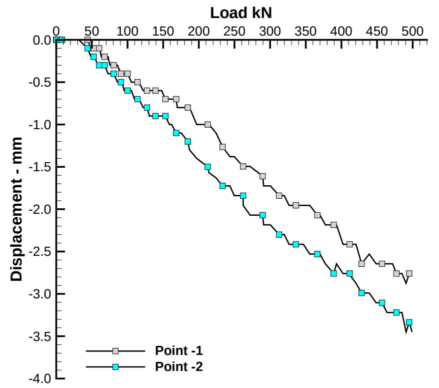

(c) R wallette at 300 ^{o}C

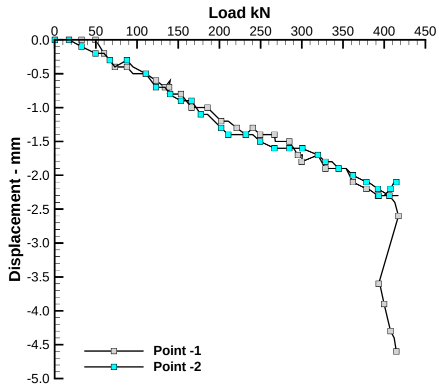

(d) M wallette at 300 ^{o}C

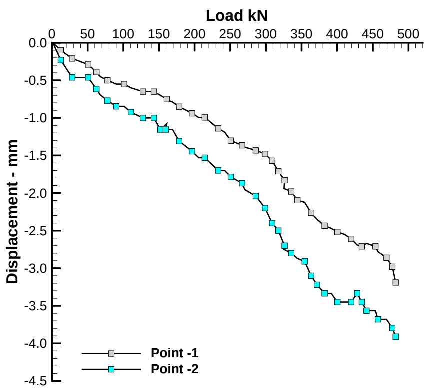

(e) M wallette at 400 ^{o}C

Figure 9.12: Load-displacement curves of both masonry wallettes at different temperature exposure

Previous reference has been made to explosive spalling of the reference wallette samples at temperatures of 400 ^{o}C or more. The first sample of this set of wallettes suffered from severe fragmentation spalling, whilst the second sample failed due to local bursting, as shown in Figures 9.13f and 9.13g. This happened even though the wallette had been dried out for three days at 70 ^{o}C. The reason for this behaviour might be related to the denser micro-structure of this concrete with a reduced permeable network. This would lead to a build-up of steam pressure to a level which exceeded the tensile strength of the specimen [53, 54]. Alternatively, due to their coarse and irregular shapes, the glass particles incorporated within the optimum modified wallettes may have provided more pore space and increased the total permeability of the concrete (see Figure 3.1). This finding supports the idea of improving the concrete performance against spalling at high temperatures by increasing the maximum aggregate particle size as mentioned by Heo et al. [114].

Hertz [43] suggested an expression for predicting the reduction in strength (deterioration) of the concrete elements at high temperatures. He reported that the following formula can be used to represent the strength reduction of any structural member at any specified temperature.

$$\xi(T) = k + \frac{(1-k)}{1 + \frac{T}{T_1} + (\frac{T}{T_2})^2 + (\frac{T}{T_8})^8 + (\frac{T}{T_{64}})^{64}} \tag{9.4}$$

where $\xi(T)$ is the ratio of the material property at temperature T compared to that at 20 ^{o}C and k is the ratio between the minimum and maximum values of the property. In the case of compressive strength, the proposed value of $k = 0$, T_1 to T_{64} are parameters which describe the deterioration curve with temperature. In the case of a rapid heating rate (as with this study) the values of T_1 ,T_2, T_8 , T_{64} are 1500, 580, 520 and 690 respectively.

Using Equation 9.4, a linear relationship is observed for the deterioration feature with temperature. This is inconsistent with the findings of this study, where limited reductions in compressive strength were observed at all exposure temperatures. It is interesting to note that the fourth and fifth terms in the denominator of Equation 9.4 did not show any significant increase in the total value of the deterioration, showing that in practice these terms can be neglected.

Excluding the simplified method which calculates the resistance of walls under the standard fire-temperature curve described in Section 9.2, there is no direct formula given in BS EN 1996-

1-2 [55] for the calculation of the compressive strength at exposure to a specific temperature. In this study, the known strength expression of the masonry walls at ambient conditions has been used to predict the resistance of the wallettes at high temperatures from its constituents by introducing the strength reduction factors for both the block units and the cement mortar due to the effects of high temperatures, as given in Equation 9.5.

$$f_k(T) = K(a\delta f_b)^{0.7}(bf_m)^{0.3} \tag{9.5}$$

where a and b are the ratios of the blocks and mortar strength at temperature T to those at 20 ^{o}C. From the results obtained in this study, the K value is in the range of 0.55-0.6. The highest and lowest limits of K were taken to predict the resistance of both the reference and optimum modified wallettes. The effects of the cylindrical geometry of the concrete and mortar specimens were considered in the calculation of the shape factor (δ) and the equivalent strength to that of cubic geometry was taken as 0.8 [5]. This implies a δ value of 1.1. Table 9.3 shows a comparison between the calculated and the measured results of the load-bearing capacity of both masonry wallettes at different temperatures. Close agreement can be observed between the tested and calculated results. On this basis, it can be said that when the strength reduction factors are incorporated, BS EN 1996-1-1 [65] formula used to predict of the characteristic compressive strength of masonry walls in ambient condition is also valid for use under conditions of elevated temperatures.

Table 9.3: Comparison between the measured and calculated results of the load-bearing capacity $f_k(T)$ for both masonry wallettes

Temperature	$f_k(T)$ of R wallettes (MPa)			$f_k(T)$ of M wallettes (MPa)		
	Test result	Eq. 9.5	(%) difference	Test result	Eq. 9.5	(%) difference
200 ^{o}C	7.25	6.53	9.9	6.37	6.48	1.75
300 ^{o}C	7.44	6.49	12.8	6.18	6.28	1.76
400 ^{o}C	-	-	-	7.19	6.10	14.2

(a) R wallette at 200 ^{o}C

(b) M wallette at 200 ^{o}C

(c) R wallette at 300 ^{o}C

(d) M wallette at 300 ^{o}C

(e) M wallette at 400 ^{o}C

(f) R wallette-1 at 400 ^{o}C

(g) R wallette-2 at 400 ^{o}C

Figure 9.13: Failure modes of both masonry wallettes at exposure to different temperatures

Figures 9.13a to 9.13g show the failure modes of both masonry wallettes when exposed to a combined load-heat effect. As mentioned before, the set of reference wallette samples at 400 ^{o}C showed spalling failure due to heat action without the application of any mechanical load. All of the other wallettes revealed normal failure behaviour. The combination of shearing-compression domain and vertical splitting are the major mechanism governing the failure of the masonry wallettes. It was noted that cracking failure usually initiates from a point underneath the applied load and passes through the concrete block and the head joint, finishing at the toe of the wallette. Other cracking paths were also observed, beginning at the top right or the top left corners and ending in a variety of locations. In general, the critical regions of the failure modes are similar to those observed for the masonry wallettes at ambient temperature (see Figure 8.13). However, the optimum modified wallettes indicated that one more critical region was the heel of the wallette, as shown in Figure 9.13d.

9.4.4 Stress-strain curves and modulus of elasticity of the masonry wallettes

Figure 9.14 shows the stress-strain curves of the masonry wallettes at exposure to different temperatures. Regardless of the heating temperature, it was clear that the trend of stress-strain behaviour is similar to that observed at ambient conditions. This indicates a lower deterioration in the strength value of the wallette samples under the combination of thermo-mechanical action. Almost linear behaviour was observed for all of the tested samples until the failure point.

At the same stress level, both types of masonry wallette showed similar vertical strain values; however, the maximum stress at failure was higher for the reference wallettes in comparison to that for the optimum modified wallettes. This behaviour could be related to the softening phase change of the recycled glass particles at high temperatures, which may have therefore affected the load-bearing capacity of the masonry wallettes.

The moduli of elasticity were calculated using Equation 4.3, which is taken from [89]. Using this approach, both types of masonry wallettes exhibited similar moduli of elasticity to those obtained at ambient temperature, as shown in Table 9.4. This behaviour is consistent with the lesser reduction in strength mentioned earlier.

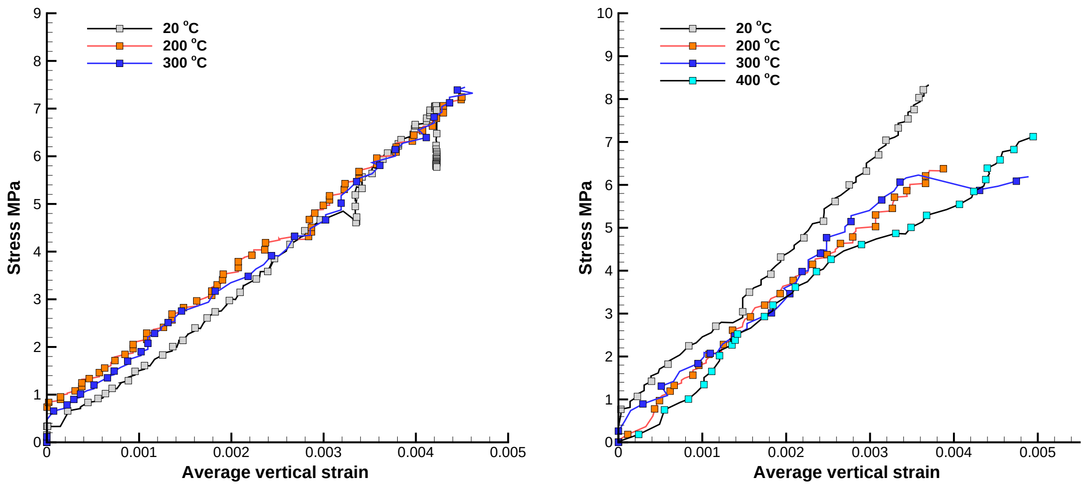

(a) Reference wallette (b) Optimum modified wallette

Figure 9.14: Stress-strain curves of both masonry wallettes at exposure to different temperatures

Table 9.4: Modulus of elasticity values (E) of the masonry wallettes tested in this study and those obtained by Ruvalcaba [67]

Temperature	E of Ruvalcaba [67] (MPa)	E of current study (MPa)	
		R wallettes	M wallettes
20 ^{o}C	697	1375	1795
200 ^{o}C	466	1907.8	1770.28
300 ^{o}C	-	1911.8	1768.73
400 ^{o}C	418	-	1800.9

It is of interest to compare the current results of the stress-strain and modulus of elasticity with those obtained by Ruvalcaba [67]. A comparison of these results is presented in Figure 9.15 and Table 9.4 respectively. From Figure 9.15, It can be seen that the stress values at failure of this study were more than double those obtained by Ruvalcaba, while the corresponding strain values were about half. On the other hand, the percentage increase in the modulus of elasticity was as much as 300% greater than achieved by Ruvalcaba [67]. Such improvements in the thermo-mechanical behaviour are consistent with the superior performance of the lightweight concrete blocks tested in this thesis.

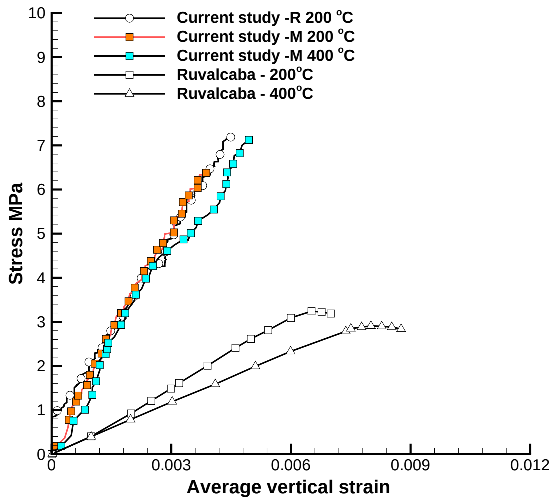

Figure 9.15: Comparison between the stress-strain behaviour of the current study with that obtained by Ruvalcaba [67]

9.5 Summary

The strength ratio at temperature T in comparison with that at 20 ^{o}C for the cylindrical concrete samples was about 0.6-0.7, while the mortar samples exhibited an increase to about 1.2 under the same test conditions. Lower vertical displacements were observed for both types of concrete in this study in comparison with those reported in BS EN 1996-1-2 [55] for pumice lightweight concrete. The values of the modulus of elasticity showed a major reduction for the concrete samples tested under a combined heat-axial load effect. Greater improvements in the duration of heat equilibrium were achieved and the highest values were observed for the optimum modified wallettes, which reached as much as 9.6 hours. The reference wallette samples tested at 400 ^{o}C failed due to explosive spalling without supporting any mechanical load, whereas the optimum modified wallettes seemed to be adequate in the same test conditions. A minimal reduction in the values of compressive strength and modulus of elasticity was observed for both masonry wallettes when exposed to high temperatures. Vertical displacement that was approximately similar to those at ambient temperature was observed for all of the wallettes at high temperatures. If the strength reduction is introduced, the BS EN 5628-1 [103] expression which was suggested to predict the compressive strength of the masonry walls at ambient temperature is also valid for use at elevated temperature conditions.

Chapter 10

Numerical simulation of the thermo-mechanical behaviour of masonry wallettes at ambient and high temperatures

10.1 Introduction

Experimental tests of masonry structures (specifically in this thesis, wallettes) are relatively time consuming and expensive. A logical solution would be to develop a computer-based numerical model of the masonry structure in question and validate it against a number of actual laboratory tests. With a reliable numerical model, a wider range of test parameters could be investigated in a shorter time at lower cost.

To date, only a limited amount of work has been published on the simulation of the thermo-mechanical behaviour of masonry wallettes. This chapter describes in detail the development of a reliable model for the prediction of both structural and thermal behaviour at ambient and high temperatures using the Abaqus/Standard 6.10-1 finite element package. Firstly, approaches of numerical simulation of masonry walls are described, followed by a presentation of the main components of the structural model at ambient temperatures. Thereafter, the model is calibrated and validated against the experimental measurements. The high temperatures structural model is then presented with a detailed discussion of its findings. Finally, the pure thermal modelling of both masonry wallettes is described and discussed.

10.2 Approaches of numerical simulation for the behaviour of masonry walls

As mentioned in Chapter 2, there are two approaches for simulating the structural behaviour of masonry walls: macro and micro-modelling. Micro-modelling comprises two constitutive models: detailed and simplified. Using the macro-modelling approach, the global behaviour of a masonry wall can be predicted. Conversely, the detailed micro-modelling approach is more suitable for predicting the accurate behaviour under different external loading. In the former approach, a continuum element is normally assumed for both concrete blocks and mortar joints. The block-mortar interface, on the other hand, is considered a discontinuum (contact) element (see Figure 2.17c).

Because the actual response of the masonry wallettes is one of the main topics proposed in this study, the detailed micro-modelling technique is considered in order to predict the response of the masonry wallettes at both ambient and high temperatures. Based upon this technique, the structural behaviour was simulated through a developed finite element model described in this chapter.

In the structural response problem which characterised by the stress-strain behaviour, the main components of the finite element model are the element type, material model, mortar-block interaction and the analysis procedure. All of these components are discussed within the context of their place within the Abaqus/Standard finite element package in the following sections.

10.3 Components of the finite element model for the structural behaviour of wallettes at ambient temperature

10.3.1 Element type

To simulate the behaviour of axially loaded masonry walls with a finite element model, a three-dimensional solid (continuum) element was selected for both wallette constituents (concrete blocks and mortar joints). This element is suitable for the formulation of a variety of geometrical shapes and is capable of facilitating the definition of the influence of material nonlinearity throughout the integration points.

The Abaqus/Standard [97] offers a solid elements library. Each element within the library has a specified number of nodes, formulation and method of integration. All of the specified elements have the same number of degrees of freedom at each node. These are three directional translations (displacement), as shown in Figure 10.1a.

In the present study, eight-node linear brick reduced integration (C3D8R) has been selected from the different types of solid elements available. This choice was made in order to reduce both the duration of computational processes and the effect of shear locking which are associated with a full integration solid element. Shear locking makes the element to become highly stiff and usually occurs when the structure is mainly subjected to pure bending. However, the global loading condition in the current study is axial compression.

In C3D8R, all nodes are located at the corners of the element, as shown in Figure 10.1b, and a linear interpolation method is used to account for the stress/displacement at each direction. If the C3D8R element is appropriately meshed, the same efficiency as the second-order solid element would be expected.

In order to define the material properties along the solid elements, a solid homogenous section was employed for both elements of concrete blocks and mortar joints. Because the nodal coordinates are sufficient to completely identify the geometry of the element, there is no need to define any further geometric data.

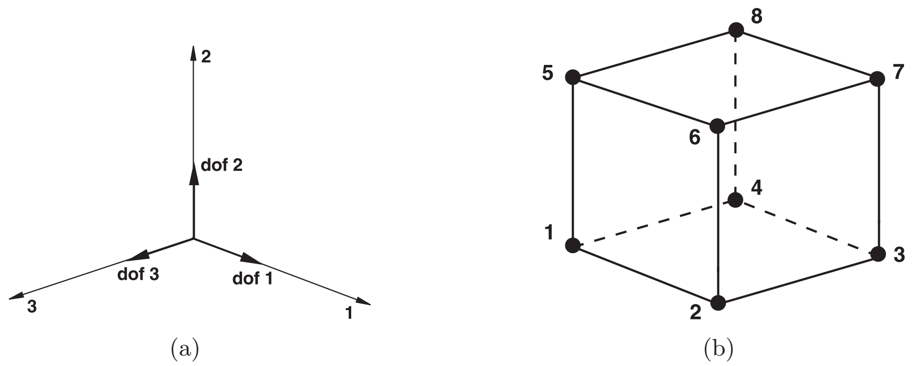

Figure 10.1: Continuum (solid) element: (a) formulation of degree of freedom; (b) geometry of the linear solid element [97]

10.3.2 Material model

As explained in Chapter 2, nonlinear behaviour is the most realistic approach for modelling the material response, thus this behaviour is considered in this study in terms of both the elastic and inelastic regimes under tension and compression states. Figures 10.2a and 10.2b show the typical response of concrete in terms of stress-strain feature.

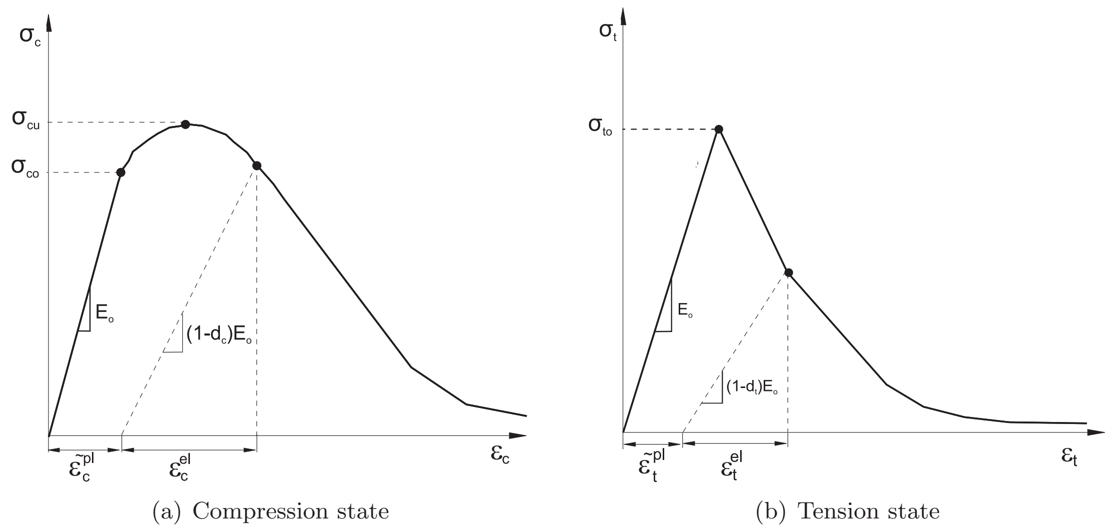

Figure 10.2: Typical stress-strain curve for a concrete in both compression and tension states [75]

Ideally, the Abaqus/Standard addresses the linear elastic region for the isotropic material for both concrete block and mortar joints throughout two simultaneously parameters, namely instantaneous Young's modulus (E_o) and Poisson's ratio (v). These parameters can also have temperature dependencies assigned, thus enabling thermo-mechanical behaviour to be incorporated into the model.

The Abaqus/Standard involves two methods to formulate the inelastic behaviour of concrete, smeared cracking and damage plasticity. Due to the convergence problem (the entire numerical solution cannot achieve), the smeared cracking method is inappropriate for use in the analytical modelling intended in this research. This conclusion was based upon a comparative study between the former methods on the behaviour of reference masonry wallettes at ambient temperature. Except for the inelastic definition which follows the concept of each method, similar data were used for all other modelling parameters, as illustrated in Section 10.6. The results obtained from both modelling methods in terms of the vertical displacements and their corresponding axial loads are presented in Figure 10.3.

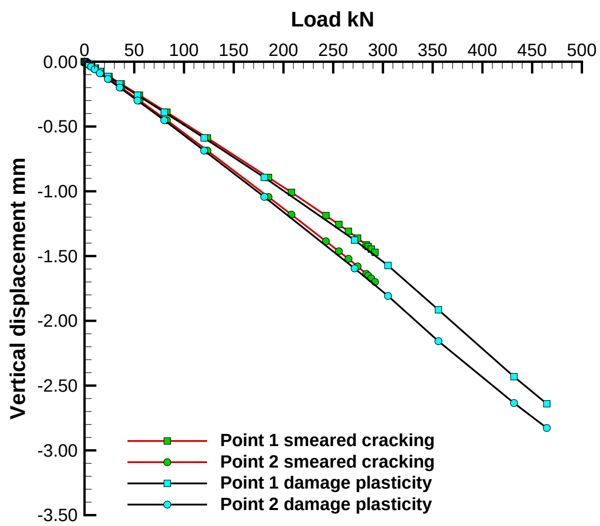

Figure 10.3: Comparison between the smeared cracking and damage plasticity models in terms of load-vertical displacement

From Figure 10.3, it can be seen that the smeared cracking model was unable to capture the total vertical deformation. It was steady at about 63% of the axially applied load. On the other hand, the damage plasticity model was able to handle the full response of the masonry wallette. The same issue was also noted by Abdullah [115]. The observed result of the smeared cracking model may be explained by the absence of the stress component of the first crack from those used to identify the failure surface. The latter surface is the locus of the propagation of the subsequent cracks. As a result, the fixed angle crack model assumed by the smeared cracking method is affected [75]. Based upon the above results, the damage plasticity method is considered for the whole numerical simulation and is described in the next section.

10.3.2.1 Concrete damage plasticity model

In the damage plasticity model, the Abaqus/Standard defines the inelastic behaviour of concrete by three parameters: (1) plasticity which consists of the failure criteria of concrete and flow rule; (2) uniaxial compression behaviour; and (3) uniaxial tensile behaviour. All of the aforementioned parameters can be defined as a function of temperature variation, so the structural behaviour of the masonry wallettes at high temperatures can be satisfactorily predicted.

10.3.2.1.1 Plasticity The failure criterion of concrete is governed by the initiation of cracks, which takes place when the triaxial state reaches a yield surface. The latter can be calculated in terms of the effective stresses under the tension and compression states using Equation 10.1 [75]:

$$(\bar{\sigma}, \tilde{\varepsilon}^{pl}) = \frac{1}{1+\alpha}(\bar{q} - 3\alpha\bar{p} + \beta(\tilde{\varepsilon}^{pl})\left\langle\bar{\sigma}_{max}\right\rangle - \gamma\left\langle-\bar{\sigma}_{max}\right\rangle) - \bar{\sigma}_c(\tilde{\varepsilon}_c^{pl}) = 0 \tag{10.1}$$

where

$$\alpha = \frac{(\sigma_{bo}/\sigma_{co} - 1)}{2(\sigma_{bo}/\sigma_{co} - 1)} \qquad 0 \leq \alpha \leq 0.5 \tag{10.2}$$

$$\beta = \frac{\bar{\sigma}_c(\tilde{\varepsilon}_c^{pl})}{\bar{\sigma}_t(\tilde{\varepsilon}_t^{pl})}(1-\alpha) - (1+\alpha) \tag{10.3}$$

$$\gamma = \frac{3(1-K_c)}{2K_c - 1} \tag{10.4}$$

$\bar{p}$	is the effective hydrostatic stress;
$\bar{q}$	is the Mises equivalent effective stress;
$\bar{\sigma}_{max}$	is the maximum principal effective stress;
σ_{bo}/σ_{co}	is the ratio of initial equibiaxial compressive yield stress to initial uniaxial compressive yield stress (the default value is 1.16);
K_c	is the ratio of the second stress invariant on the tensile meridian, $q(TM)$, to that on the compressive meridian, $q(CM)$, at initial yield for any given value of the pressure invariant p to such a point that the maximum principal stress is negative, $\bar{\sigma}_{max} < 0$; it must satisfy the condition of $0.5 \leq K_c \leq 1$ (the default value is 2/3);
$\bar{\sigma}_c(\tilde{\varepsilon}_c^{pl})$	is the effective compressive cohesion stress;
$\bar{\sigma}_t(\tilde{\varepsilon}_t^{pl})$	is the effective tensile cohesion stress; and
$\tilde{\varepsilon}_c^{pl}$ and $\tilde{\varepsilon}_t^{pl}$	are the hardening parameters that control the evolution of the yield surface.

In order to account for the potential plastic flow of concrete, a non-associated flow was represented by the damaged plasticity approach, based on the Drucker-Prager hyperbolic function [75]. The flow potential (G) is characterised by the following equation:

$$G = \sqrt{(\varepsilon \sigma_{to} \; tan\psi)^2 + \bar{q}^2} - \bar{p} \; tan\psi \tag{10.5}$$

where ψ is the dilation angle measured in the p-q plane at high confining pressure; σ_{to} is the uniaxial tensile stress at failure, taken from the user-defined tension stiffening data; and ε is so-called eccentricity parameter, that defines the rate at which the function approaches the asymptote (the default value is 0.1). When the eccentricity is close to zero, the flow potential tends toward a straight line, as shown in Figure 10.4.

The Abaqus/Standard reported that when the default value of the flow potential eccentricity is used, the material has almost the same dilation angle over a wide range of confining pressure stress values. In this thesis the value for the dilation angle recommended by Mohsin [76] was used, which is 15^o.

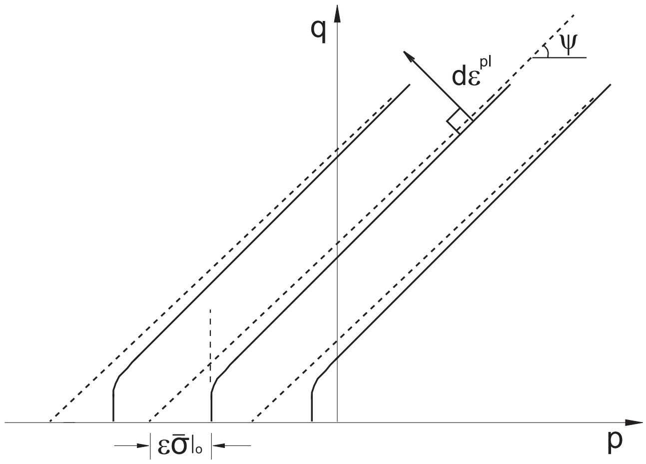

Figure 10.4: Potential flow in the p-q plane [75]

10.3.2.1.2 The unixial compression behaviour The response of concrete to uniaxial compression loading is considered linear until the point of initial yield, as shown in Figure 10.2a. Thereafter, a stress hardening regime takes place, and eventually strain softening behaviour follows after the ultimate stress level (σ_{cu}) is reached. In both the hardening and softening regions, the response of the concrete is defined by the data of stress (σ_c) with their corresponding inelastic strain (ε_c^{in}). The latter can be calculated using the following equation:

$$\varepsilon_c^{in} = \varepsilon_c - \sigma_c/E_o \tag{10.6}$$

The stress-strain data under a uniaxial compression load were experimentally measured for both the concrete blocks and cement mortar at ambient and high temperatures in Chapters 8 and 9. These were presented in a nominal form and then converted to the true form using Equations 10.7 and 10.8 [75]. The nominal form refers to stress or strain resulting from an undeformed area or length respectively.

$$\varepsilon = ln(1 + \varepsilon_{nom}) \tag{10.7}$$

$$\sigma = \sigma_{nom}(1 + \varepsilon_{nom}) \tag{10.8}$$

where σ and ε are the actual stress and strain respectively; σ_{nom} and ε_{nom} are the nominal stress and strain respectively.

10.3.2.1.3 The uniaxial tension behaviour This criterion represents the post-failure behaviour of concrete and allows for the definition of the strain-softening regime of the cracked section, as shown in Figure 10.2b. Two approaches are available in the Abaqus/Standard for running out the uniaxial tension behaviour, namely the stress-strain relationship and stress-fracture energy cracking.

For unreinforced concrete, which is the case in this study, the first approach introduces mesh sensitivity leading to a convergence problem within models. The reason for this is that the mesh refinement shows a narrower crack band. Normally, this problem appears when the cracks are formed at a localised region in the structure [75].

Based upon the approach of Hillerborg [116], the second approach deals with the post-failure behaviour in terms of the fracture energy (G_F) required to open a unit area of crack. This approach can solve mesh sensitivity problems. Essentially, the concept of this approach is to consider the fracture energy as a material property which can be analytically calculated as the area under the stress-displacement curve. The brittle behaviour of the concrete can therefore be characterised by a stress-displacement response rather than a stress-strain response. The implementation of this approach for a finite element model requires the definition of the length associated with the integration point.

Following the recommendation of CEB [117], the concept of crack bandwidth has been used in this study. It is assumed that the crack bandwidth is within the tributary region of an integration point at which cracking occurs. Figure 10.5 shows the stress-crack opening diagram for a uniaxial tension load.

In order to determine the values of crack openings at both W_o and W_1 the following equations can be applied [117]:

$$W_o = \alpha_F \frac{G_F}{f_{ctm}} \tag{10.9}$$

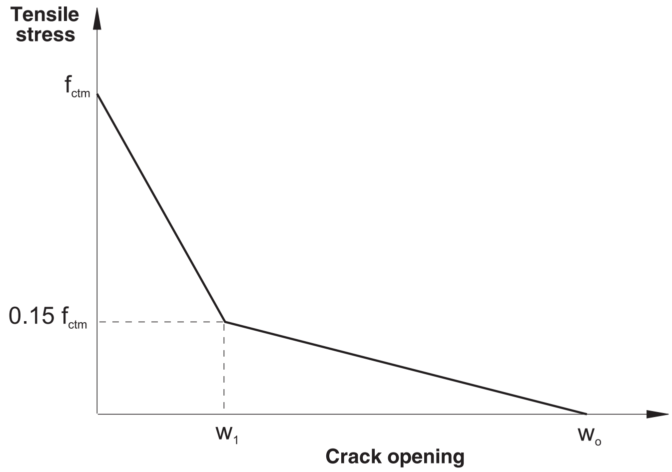

Figure 10.5: The stress-crack opening diagram under a uniaxial tension load [117]

$$W_1 = 2\frac{G_F}{f_{ctm}} - 0.15W_o \tag{10.10}$$

where α_F is a coefficient depending on the value of the maximum size of the aggregate as given in Table 10.1, and G_F can be calculated using Equation 10.11:

$$G_F = G_{Fo}(\frac{f_{ctm}}{f_{cma}})^{0.7} \tag{10.11}$$

in which $f_{cma} = 10$ MPa and G_{Fo} is the base value of fracture energy in (N.mm/mm^2) which depends upon the maximum aggregate size (d_{max}), as given in Table 10.2, and f_{ctm} is the tensile strength (MPa).

Table 10.1: Cofficient of α_F [117]

$d_{max}(mm)$	8	16	32
α_F (-)	8	7	5

10.3.3 Cement mortar-block interaction

As described in Section 10.2, the detailed micro-modelling approach was selected to conduct the finite element analysis of the masonry wallettes. This approach involves the use of interaction surfaces between the individual concrete block and the mortar. Normally, the presence of these

Table 10.2: Base value of fracture energy G_{Fo} [117]

$d_{max}(mm)$	G_{Fo} (Nmm/mm^2)
8	0.025
16	0.030
32	0.058

interaction surfaces increases the nonlinearity of the simulated wallettes. The Abaqus/Standard allows for assigning such interaction by defining the contact method and the physical properties of the interfacial zone between the concrete block and the mortar.

In order to describe the contact pairs, a pure master-slave algorithm was followed, meaning that each contact surface should be either master or slave. In addition, each node on the slave surface cannot penetrate the segments of the master surface. The criteria for choosing a specific surface as a slave surface are that it should be the more finely meshed of the surfaces and also that it should be the softer underlying material surface (if the mesh sizes are similar) [118]. To reflect the actual contact of the constituents of the assembly (concrete blocks and cement mortar), the surface-to-surface contact method was chosen over other types of interaction. This method is suitable for general modelling purposes and permits the definition of the sliding formulation between the contact pairs.

Both tangential and normal behaviours are required to define the interaction properties, because they govern the overall structural behaviour of masonry wallettes. The tangential behaviour represents the friction formulation which is adequately defined by the penalty method. In this method, at the sticking state, some relative motion is permitted between the surfaces. So, in addition to the coefficient of friction, the allowable elastic slip (γ_i) must also be defined. The default value of γ_i (0.005) selected by the Abaqus/Standard gives a reasonable compromise between accuracy and efficiency [118]. The coefficient of friction was taken to be 0.78 in accordance with the results presented by Burnett et al. [119].

Normal behaviour, on the other hand, defines the pressure-overclosure and the constraint enforcement methods between the contact pairs. In practice, when the applied loads are acted normally to the direction of the bed joint (which is the case in this study), the sticking between the concrete blocks and the cement mortar is considered a hard contact. The Abaqus/Standard provides the penalty constraint enforcement formulation as a stiff approximation of the hard contact. In the former method, the contact force is proportional to its penetration distance. Furthermore, some advantages are gained when the penalty method is used. There is an improvement in the efficiency of generating a solution and also a reduction in the number of iterations required for an analysis, due to the elimination of the need to incorporate the effect of overconstraint. The default stiffness for the penalty method is linear, meaning the pressure-overclosure relationship is linear along the contact surfaces. By default, the Abaqus/Standard sets the value of stiffness as 10 times the representative underlying element stiffness ($10EA/l$). However, this value can be scaled to suit the measured results, as discussed in Section 10.5.

10.4 The procedure of the finite element analysis

As previously mentioned, the simulation of masonry wallettes needs to follow the nonlinear regime. Such nonlinearity comes from the material response of the concrete blocks and cement mortar as well as the interfacial joints between them. Occasionally, due to the high nonlinearity of a problem (especially with those containing contact surfaces), an unstable numerical solution takes place. In such cases, the Abaqus/Standard provides automatic stabilisation algorithms to mitigate this effect. One of these algorithms specifies a dissipated energy fraction which is suitable for the general static load-displacement step. The former technique was followed in the numerical analysis by taking the default value of the dissipated energy fraction as 2×10^{-4}.

In order to perform the finite element analysis, the load history of the structural behaviour model was divided into three main steps. These are as follows:

1. Initially, the interaction surfaces were defined as contact pairs.

2. Four boundary conditions were employed as a very small displacement (1E-008) for all of the masonry direction (top, bottom, right and left) to ensure that the contact between each surface pairs is achieved.

3. The boundary conditions of the previous step were then released, then the load and supports were applied to the masonry wallette.

In order to achieve a nonlinear solution, steps 2 and 3 were divided into small increments. The sizes of the initial, minimum and maximum time increments have significant impact upon the simulation results. In such a way, the initial increment must be small enough to take the elastic limit into consideration. When the initial increment size is selected, the Abaqus/Standard automatically adjusts the other increments until convergence is obtained at the end of each increment. This solution technique is based on the full Newton-Raphson equilibrium iterations for determining the stiffness at each increment.

10.5 Calibration of the finite element model

It is of interest to investigate the influence of the model parameters on the overall numerical solution in order to adjust their values. Therefore, a comprehensive study on the parameters of description of the model, penalty stiffness, imperfection effect, mesh size and support formulation was conducted. All of the investigations were carried out based upon the model of the reference masonry wallette at ambient temperature. The data used in this model were 0.00135 for the scale factor of penalty stiffness, $l/900$ for the imperfect value and a mesh size which resulted of $(9 \times 9 \times 4)$ $(l \times h \times t)$ elements for the full concrete block. The values for the above parameters were selected after a calibration strategy for various practical limits, as explained in the next sections.

10.5.1 Description of the model

The masonry wallette was considered non-symmetrical about any direction, due to the sequence of head mortar joints and different boundary conditions. Therefore, all constituents were formulated to match the geometry of the experimental case. Firstly, a uniform distributed load (UD load) was applied on the top surface of the upper cement mortar, as shown in Figure 10.6a. The value of the UD load was determined by dividing the maximum load recorded during the test over the surface area of the cement mortar. However, it was found that the vertical displacements of the wallette ends (points 1 and 2, see Figure 8.6) were similar, as discussed in Section 10.5.3, while an appreciable difference between their displacement values was observed during the experimental work.

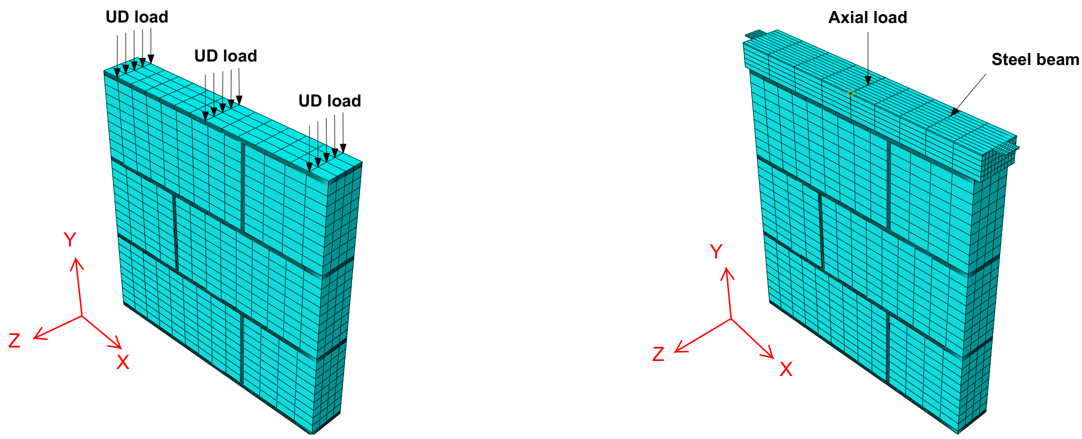

(a) (b)

Figure 10.6: The geometry of the masonry wallette: (a) assembly of the wallette using a UD load; (b) incorporating the effect of the distributed steel beam.

To address this issue, the exact wallette set-up was followed by introducing the loaded (distributed) steel beam, as shown in Figure 10.6b. In this case, the applied load was considered an axial force located at the mid of the distributed steel beam. A contact surface was then defined for the steel beam-cement mortar interaction, in which the coefficient of friction was taken to be 0.2 [119].

10.5.2 Penalty stiffness

The Abaqus/Standard manual [56] states that in most cases, the contact penetration in normal behaviour resulting from the default penalty stiffness does not significantly affect the results obtained. However, an option is available for scaling the value of penalty stiffness. Previous studies [119–121] have mentioned that when the default penalty stiffness is adopted, the value of the interface stiffness is overestimated. This means that the desired compressive strength is obtained with a lower vertical deformation. The former effect was clearly noted in the present numerical analysis. Based upon the results presented by Burnett et al. [119], the penalty stiffness (k) set for unreinforced blockwork walls using LS-DYNA finite element package, is as per Equation 10.12:

$$k = \frac{P_f A^2}{V_e} K \tag{10.12}$$

where P_f is a penalty factor, with a default value of 0.1, A is the area of the master segment, V_e is the element volume and K is the bulk modulus of elasticity, which is equal to:

$$K = \frac{E}{3(1-2v)} \tag{10.13}$$

After a detailed sensitivity analysis, Burnett et al. [119] found that a value of $P_f = 0.05$ gives reasonable results. In contrast, Rots [122] used a large variation in the value of interface stiffness ranging from 10 to 10^6 without clear explanation.

The penalty factor in Equation 10.12 incorporated the modification of Burnett et al. [119] is equivalent to a scale factor of about 0.0035 in the Abaqus/Standard application. This value was used as a guide for scaling the default penalty stiffness. On this basis, a range of selected values between 0.001 and 0.004 were used to verify the analytical results against those measured in the experimental programme, as shown in Figures 10.7a to 10.7d.

From Figures 10.7a and 10.7b, it can be seen that lower vertical and lateral displacements were obtained when the value of scale factor increased. At a lower scale factor value (0.001), the numerical simulation incorporated a convergence problem, as shown in Figure 10.7c. On the other hand, the value of 0.00135 was an adequate scale factor for the penalty stiffness, which can give reasonable numerical results for the case of this study in both vertical and lateral deformations. On this basis, this latter value was used throughout the analytical analysis.

In case of the optimum modified masonry wallette, the value of scale factor was taken to be 0.0016. The latter value is equivalent to the variation in the value of Poisson's ratio between both the reference and optimum modified wallette constituents (concrete blocks).

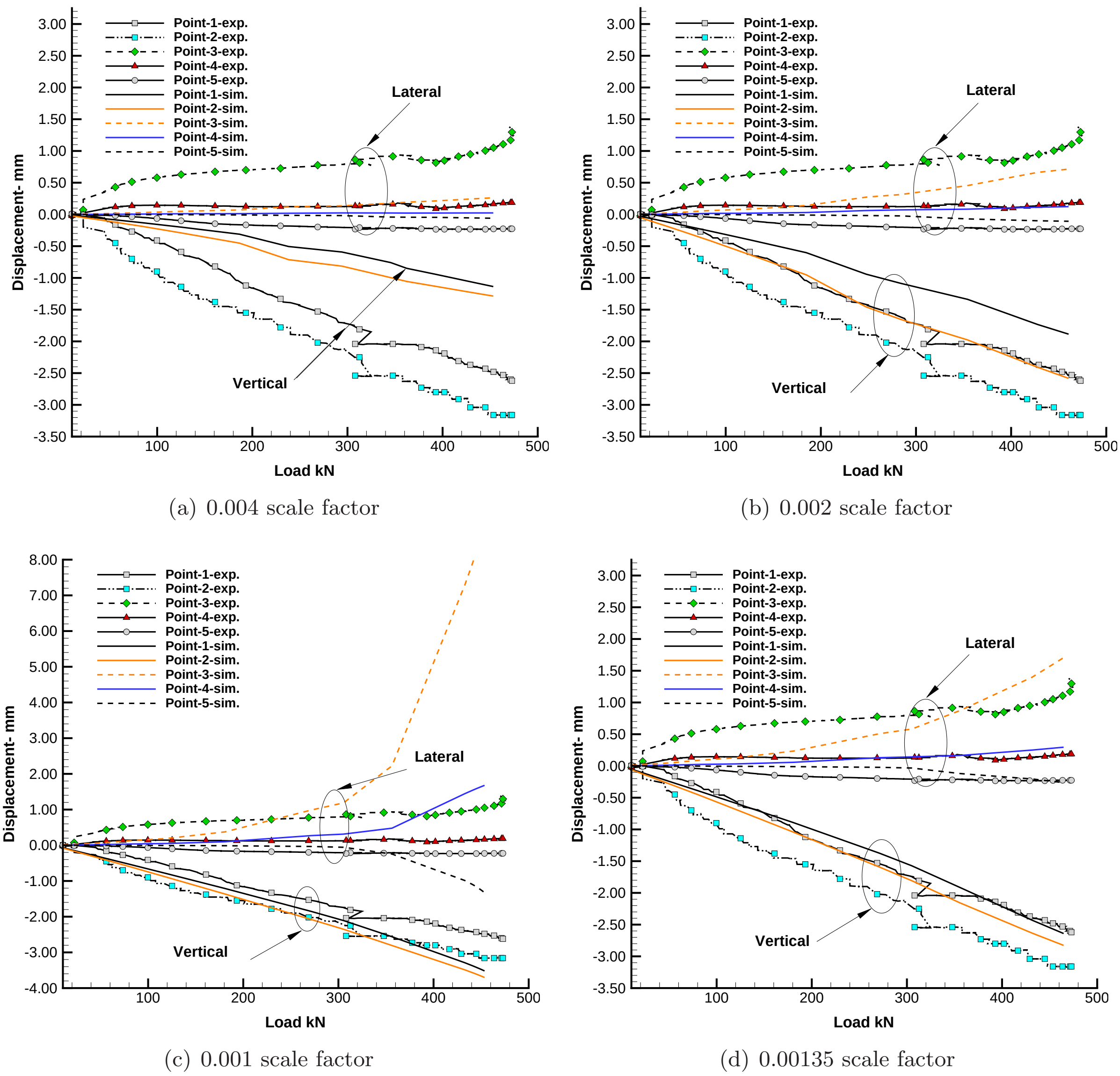

(a) 0.004 scale factor

(b) 0.002 scale factor

(c) 0.001 scale factor

(d) 0.00135 scale factor

Figure 10.7: Effect of the scale factor of penalty stiffness on the structural response of the reference masonry wallettes at ambient temperature

10.5.3 Imperfection effect

Initially, the masonry wallettes were assumed to be under a perfect axial compression load, which allows for converting the applied load to a uniform distributed load upon the top surface, as shown in Figure 10.6a. However, this assumption implies a purely theoretical view and can no longer be accepted if it is compared with the experimental results.

Other studies, for example [74, 120], have reported that in practice and modelling issues, the applied load should involve small eccentricities resulting from the effect of imperfection.

BS EN 1996-1-1 [65] assumes the maximum value of construction or loading imperfection to be $h_{ef}/450$. To introduce such eccentricity, a second approach to the model description was followed by applying an eccentric compression force upon the distributed steel beam, as mentioned in Section 10.5.1. Four imperfection values ranging from 0 to $h_{ef}/450$ were calibrated in terms of the obtained results relative to those measured in the experimental programme, as shown in Figures 10.8a to 10.8d.

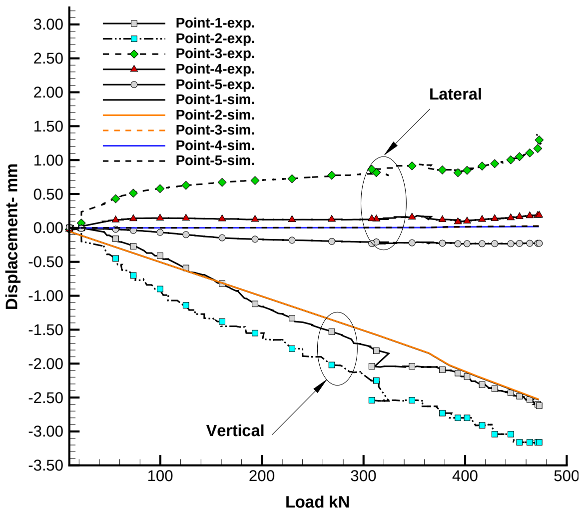

(a) 0% imperfection

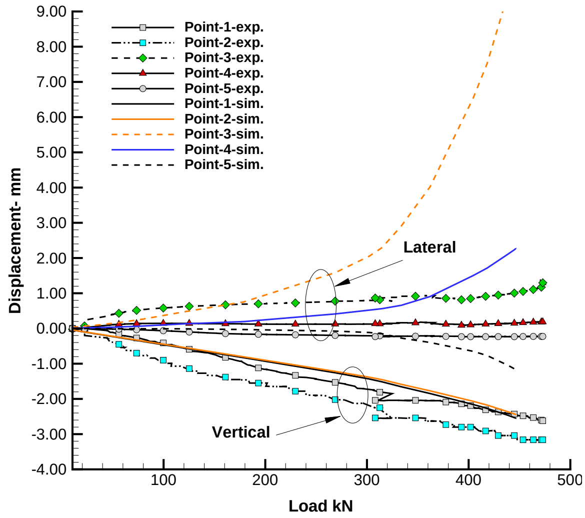

(b) $h_{ef}/450$ imperfection

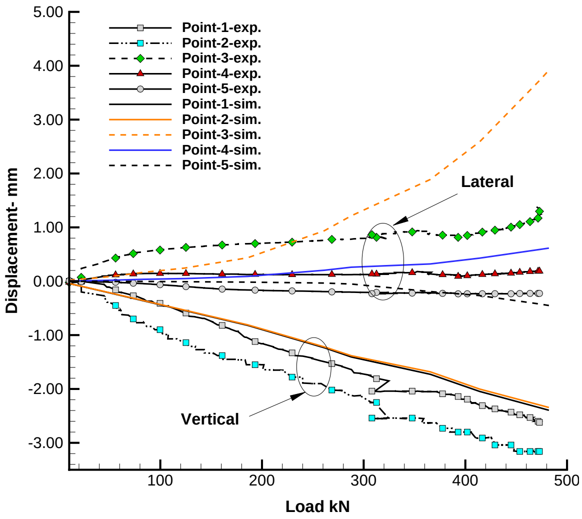

(c) $h_{ef}/900$ imperfection

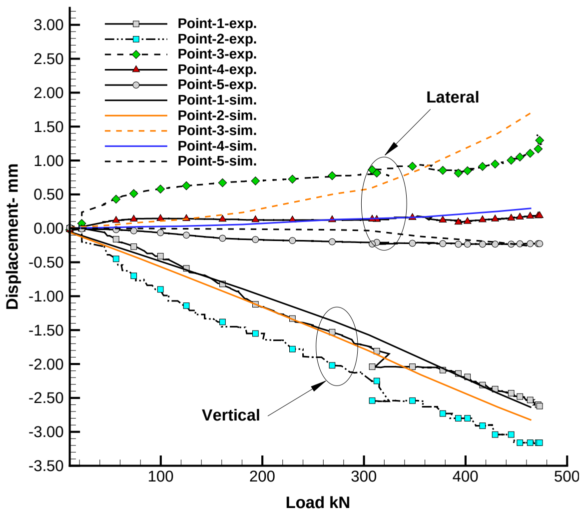

(d) $h_{ef}/1350$ imperfection

Figure 10.8: Imperfection effect on the structural response of the reference masonry wallettes at ambient temperature

It can be seen that the zero imperfection case introduced similar vertical displacement values for both of the wallette edges (points 1 and 2) with minimal lateral displacement, as shown in Figure 10.8a. Among the other cases, the lower eccentricity value ($h_{ef}/1350$) met the overall structural behaviour of the masonry wallettes in terms of both their vertical and lateral deformations, as shown in Figure 10.8d. Consequently, this value of imperfection was considered as an eccentricity for the applied loads throughout the numerical simulation. It should be noted that this small value of imperfection would be indicative of a high level of quality control during the construction process of the masonry wallettes in the experimental programme.

10.5.4 Mesh size

In order to achieve a consistent mesh size, both the elements of the concrete blocks and the mortar joints were divided in a similar manner. Three mesh sizes were selected to perform the mesh sensitivity analysis: these can be classified as coarse, medium and fine. The resulting elements of each full concrete block were $(4 \times 4 \times 2)$, $(9 \times 9 \times 4)$ and $(18 \times 18 \times 8)$ for the coarse, medium and fine mesh sizes respectively. In all of the above cases, the mesh size of the distributed steel beam elements was kept constant and approximately equal to those of the medium mesh size. This is because the distributed steel beam did not show any signs of deformation during the test due to its high stiffness. In addition, the overall failure was covered by the localised cracks within the masonry wallette, so that investigation of the mesh sensitivity was limited to the wallette itself.

Figures 10.9a to 10.9c show the results obtained from the sensitivity analysis for the effects of different mesh configurations. In the case of the coarse mesh size, unstable behaviour leading to a convergence problem has been observed in relative to the measured results, as shown in Figure 10.9a. Both the medium and fine mesh sizes exhibited reasonable results in terms of the vertical and lateral deformations, as shown in Figures 10.9b and 10.9c. However, the fine mesh involved a lot of computational time with little visible improvement. On this basis, the medium mesh size was adopted throughout the analytical simulation work.

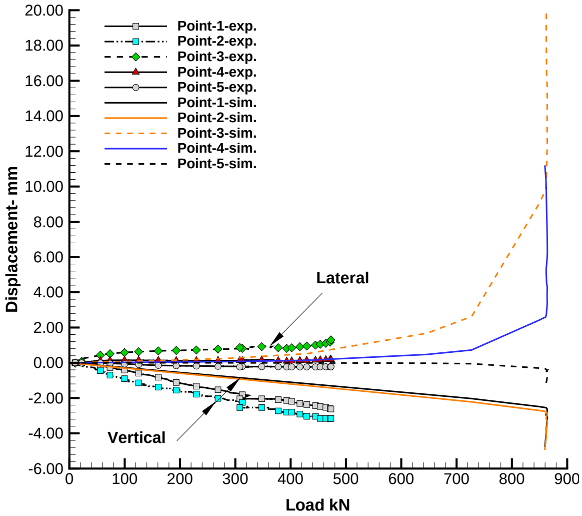

(a) Coarse mesh size

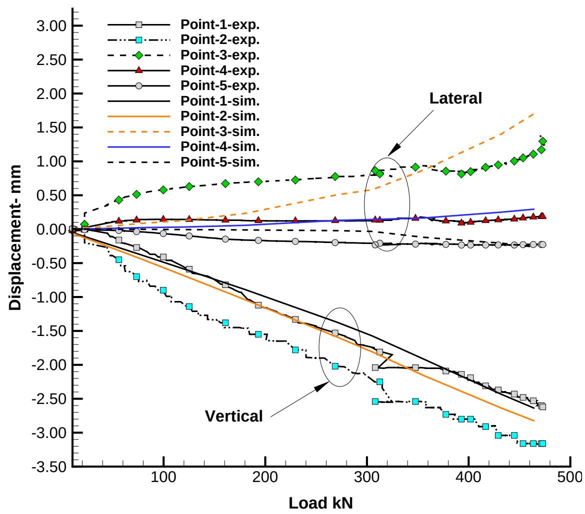

(b) Medium mesh size

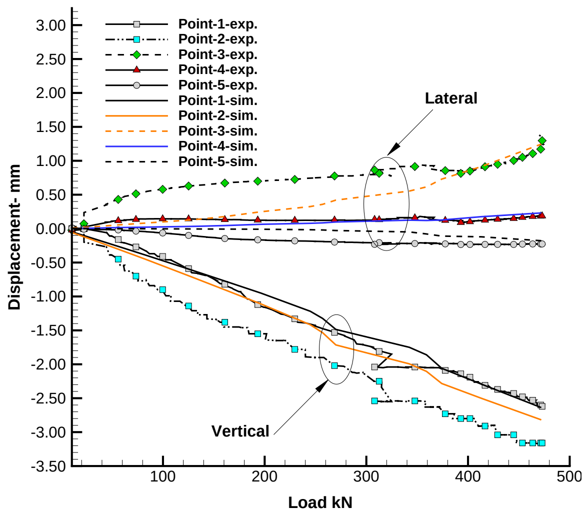

(c) Fine mesh size

Figure 10.9: Effect of mesh size on the structural response of the reference masonry wallettes at ambient temperature

10.5.5 Formulation of the supports

The formulations of the supports at the top and bottom of the wallettes are significant parameters in determining the boundary conditions for modelling. Based upon the test set-up and experimental data previously mentioned in Chapter 8, the wallettes were assumed to behave as cantilever columns. However, further evaluation was needed in order to have a clear understanding of the actual behaviour of bottom support. For this reason, two different cases were considered as possible representations of the response of the bottom support. These were a pin support, involving restriction of movement in all directions (X,Y and Z), and a hinge support, which only restricted the vertical (Y direction) movement. The results obtained are shown in Figures 10.10a and 10.10b.

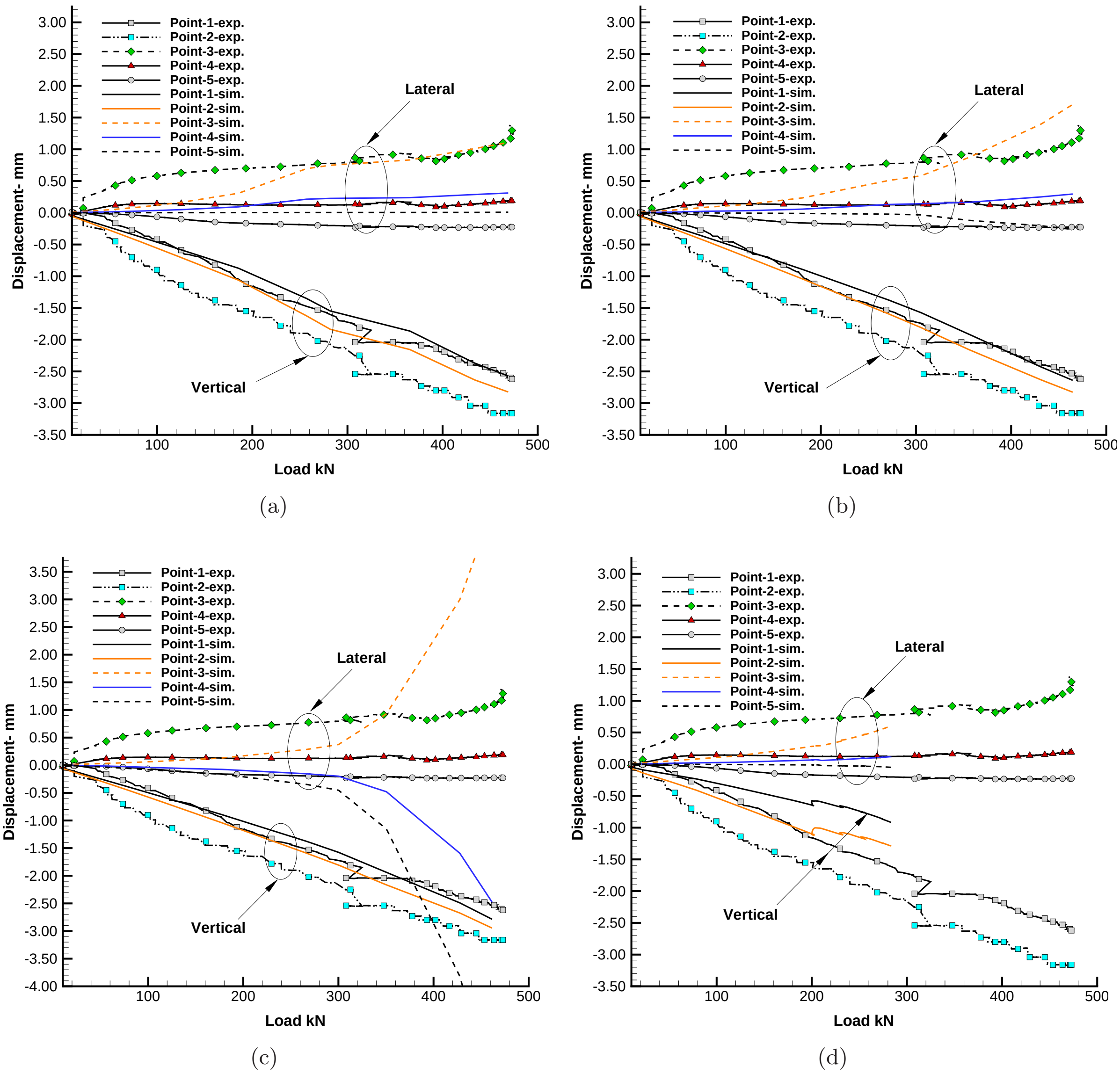

Figure 10.10: Effect of the formulation of the supports on the structural response of the masonry wallettes at ambient temperature: (a) pin support; (b) hinge support with bottom fixed node and top restriction; (c) hinge support without bottom fixed node; (d) hinge support without top restriction

Due to the equilibrium requirements of the masonry wallette, a symmetrical fixed node support located at the bottom centre was incorporated within the formulation of the hinge support. To justify this, the effect of the elimination of the fixed node was also evaluated, as shown in Figure 10.10c.

In the case of the top support, restriction in the X-direction has been assumed in order to give stability against sliding action in both the pin and hinge support cases. Again, this assumption was also checked in the hinge support case by ignoring its effect, as shown in Figure 10.10d.

From Figures 10.10a to 10.10d, it can be seen that the hinge support incorporation a fixed node at the bottom of the wallette with restriction in the X-direction at the top of the wallette is the most appropriate support formulation for achieving good agreement with the experimental results. The other cases either suffered from numerical instability problems (the cases of the hinge support without a bottom fixed node or without a top restriction) or produced incorrect lateral displacement (the pin support case). The latter case showed opposite displacement direction to that of lateral displacement at point 5, as shown in Figure 10.10a.

10.6 Validation of the finite element model for the structural behaviour of the masonry wallettes at ambient temperature

To verify the developed numerical model, a comparison between the measured and simulated results is required. In addition to the values of the calibrated parameters which previously described in Section 10.5, the other parameter data used in the validation of the finite element model are summarised in Table 10.3.

The results obtained for the analytical simulation in relation to those measured in terms of the load-vertical and lateral displacements for both masonry wallettes are presented in Figures 10.11a and 10.11b.

It can be seen that the maximum vertical displacement reaches as much as 3.2 mm for the case of the reference wallettes. The maximum lateral displacement was about 1.8 mm for the case of the optimum modified wallettes. These lower displacement values can be explained by the low slenderness ratio (effective height/effective thickness) of the wallette. The slenderness

Table 10.3: The data used in the numerical simulation

Property	Value			Note
	R blocks	M blocks	Cement mortar	
Dilation angle	15^o	15^o	15^o	From [76]
Modulus of elasticity (GPa)	13.24	14.6	8.27	From test results
Poisson's ratio	0.26	0.30	0.19	From test results
Density (kg/m^3)	1681	1644	1827	From test results
Indirect tensile strength (MPa)	1.95	2.10	1.20	From test results
Coefficient of sliding friction for the block-mortar interface		0.78		From [119]
	Distribution steel beam			
Modulus of elasticity (GPa)		200		From [119]
Poisson's ratio		0.30		From [119]
Density (kg/m^3)		7800		From [119]
Coefficient of sliding friction for the steel-mortar interface		0.20		From [119]

ratio of all of the tested wallette samples was 6.85. Normally, global failure of a short wall is due to the material crushing, so no large deformation would be expected [74].

In general, close agreement between the measured and simulated outputs was observed at all of the lateral measurement points. Even at small displacement values, the analytical model was able to reproduce the actual behaviour of the wallette. The direction of deformation, especially at the base of a wallette (point 5), was identical to that observed in the experimental programme. In this case, the analytical model followed the wallettes bowing from the positive Z-direction to the reverse. The average displacement of the centre of the wallette (point 4) was very close to the simulated value.

At the top of the wallette (point 3), a noticeable variation was observed in the lateral displacement between the measured and simulated values. This variation was more apparent at the beginning of the load application, as shown in Figure 10.11a. After a load value of about 150 kN, a tendency toward convergence was observed for both wallette samples. This behaviour could be related to the imperfection effect in the direction of the wallette bowing. The practical

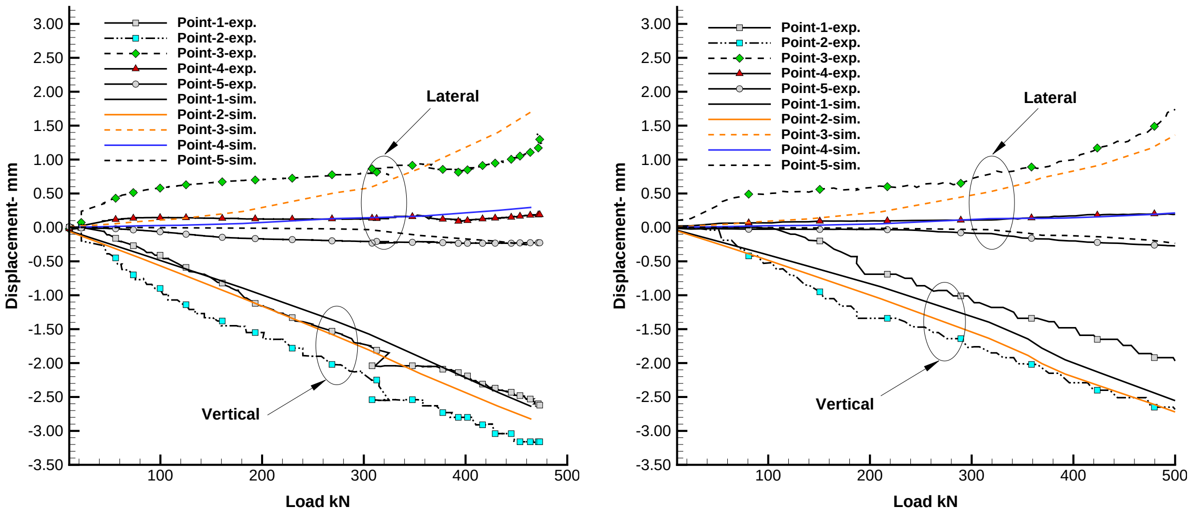

(a) Reference wallettes

(b) Optimum modified wallettes

Figure 10.11: A comparison between the measured and simulated results of the structural behaviour of both types of masonry wallettes at ambient temperature

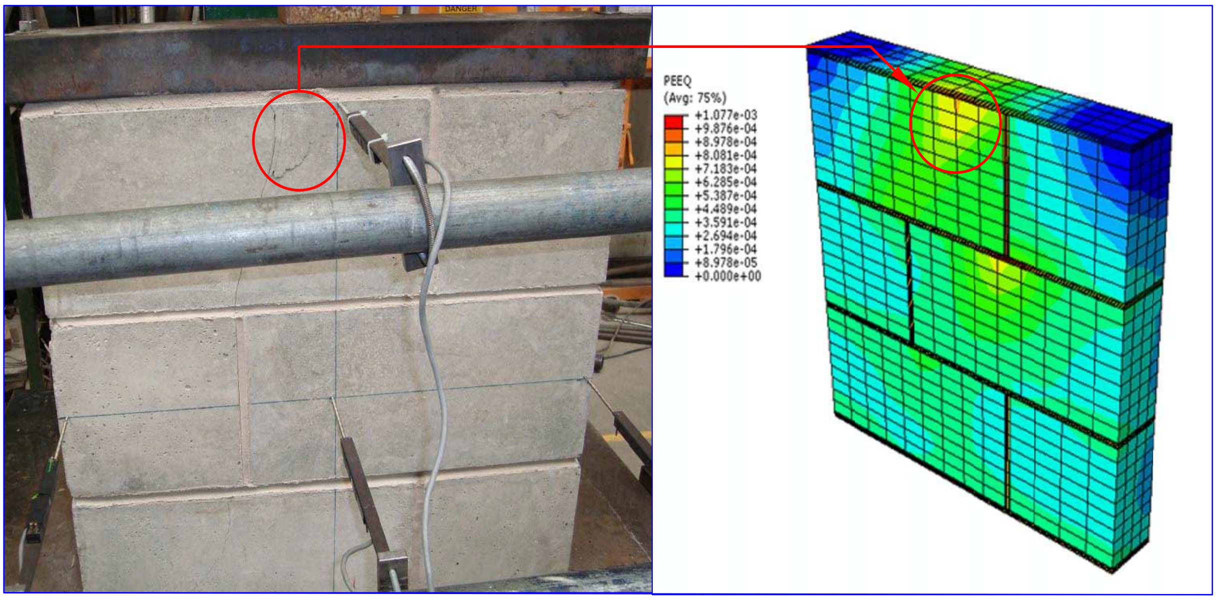

Figure 10.12: Failure modes of the reference masonry wallettes for both experimental measurement and numerical analysis at ambient temperature

codes indicated that this was an accidental effect [65].

In the case of vertical displacement for the reference wallette samples, both simulated values of the vertical edges (points 1 and 2) were close to the measured value of point 1, as shown in Figure 10.11a. This indicates a variation with respect to the measured value of point 2, reaching a value of about 9%. This behaviour might be explained by the increased stiffness of the numerical model, resulting from the hard contact formation. This effect tends to reduce the value of vertical deflection. However, the corresponding values in the case of the optimum modified wallettes were in the range of the mean measured values of points 1 and 2, as shown in Figure 10.11b.

Figure 10.12 shows the failure mode of the reference wallette for both the experimental and numerical phases. It can be seen that the numerical model accurately predicted the location of the critical failure zone. This location was underneath the point of the load application.

10.7 Numerical simulation of the structural behaviour of the masonry wallettes at high temperatures

There are two approaches available to simulate the thermal-stress: namely, fully coupled and sequentially coupled analysis. Sequentially coupled analysis is appropriate for most thermal-stress analysis, in which the stress analysis depends on the thermal results and no exhibits inverse dependency [56]. This approach consists of two analyses: heat transfer analysis, which should be performed first, followed by stress analysis. As a result, the temperature data provided by the thermal analysis model are considered in the mechanical response model.

Unlike the sequentially coupled analysis, both thermal and displacement field solutions are required for the fully coupled analysis. Therefore, the chosen element for this analysis must include degrees of freedom for both temperature and displacement.

If the coefficient of thermal expansion (α) is constant, the Abaqus/Standard calculates the thermal strain (ε_{th}) as follows.

$$\varepsilon_{th} = \alpha(\theta - \theta_1) \tag{10.14}$$

Stress (σ_{el}) and strain (ε_{el}) in the elastic region is calculated using the following equations:

$$\varepsilon_{el} = \varepsilon - \varepsilon_{th} \tag{10.15}$$

$$\sigma_{el} = E_\theta \ \varepsilon_{el} \tag{10.16}$$

As the testing regime of the masonry wallettes was based upon the steady state heat effect from all around of the wallette surfaces, as described in Chapter 9, both of the above approaches are not exactly suited to the case of present study. However, to a certain extent, the sequentially coupled analysis can be applied to predict the thermal stress with some amendments. These amendments are that: (1) no thermal model is required to perform the numerical simulation, and (2) according to BS EN 1996-1-2 [55], if the heat is acting from all around the wall surfaces, the net effect of the thermal expansion can be neglected.

Taking all of these considerations into account, the previous finite element model developed at ambient temperature described in Sections 10.3 to 10.6 can be used to simulate the structural response of the masonry wallettes under high temperatures. All that is needed is a revision of the material model to be temperature-dependent and to incorporate the predefined temperature condition into the ambient structural model. The material model in this case reflects the material response under both compression and tension with a combined load-heat effect. This can be introduced by tabulating the load-displacement data against the temperature variation. The former data were already measured in Chapter 9 for both concrete blocks and cement mortar. The percentage decrease in compressive strength due to the effects of heat and Equation 4.11 were simultaneously used to predict the equivalent decrease in tensile strength at high temperatures. The parameters of the plasticity feature are kept the same for those at ambient temperature. On the other hand, the temperature state was introduced using a predefined file. This effect would take place at step 3, so that all element nodes have the specified test temperature before loads were applied. The results obtained from the numerical simulation were then validated against the experimental measurements, as described in the next section.

10.8 Results and discussion of the analytical simulation of the masonry wallettes at high temperatures

Figures 10.13a to 10.13e show the results obtained from the analytical simulation with their corresponding measurements in terms of the load versus vertical displacement for both masonry wallettes at exposure to different temperatures.

In general, the values of vertical displacement were similar to those obtained at ambient temperature tests. The maximum measured and simulated vertical displacement was about 4 mm for the modified masonry wallettes at 300 ^{o}C, as shown in Figure 10.13d. This behaviour may be related to the use of the all around heat effect and to the increased compressive strength of the cement mortar at high temperatures, as mentioned in Chapter 9. These two factors combined to produce a lower thermal strain component; the variations in total deformation are therefore limited compared with those at ambient temperature.

A linear load-vertical displacement relationship was observed for most of the measured samples. In a similar manner to that of the experimental results, the simulated results behaved in a linear manner until about two-thirds of the total applied load. Eventually, they tended to diverge from the measured results. Similar results were also observed by Nguyen et al. [64]. This behaviour might be explained by local damage in the mortar joint or in the concrete blocks at high temperatures [64].

Except for the optimum modified wallette samples at 300 ^{o}C, the differences between the values of vertical displacement for both wallette edges (point 1 and 2) were clearly visible due to the load or construction imperfection. On this basis, for the purposes of comparison, it would be useful to consider the mean displacement values of point 1 and 2 for both the simulated and measured results. In general, from Figures 10.13a to 10.13e, it can be seen that a good agreement between the measured and simulated results was obtained for both types of wallette

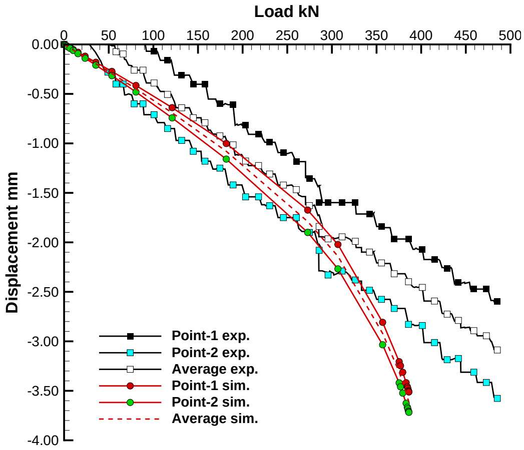

(a) R wallettes at 200 ^{o}C

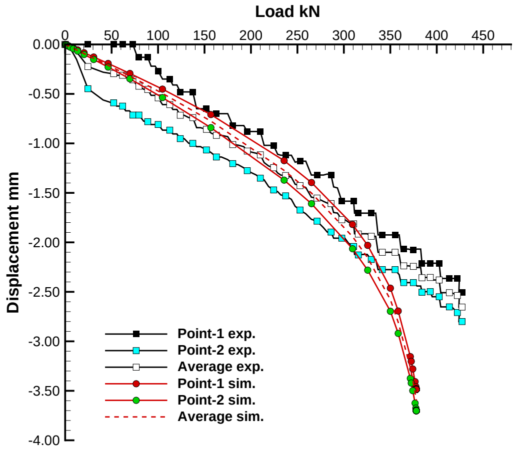

(b) M wallettes at 200^{o}C

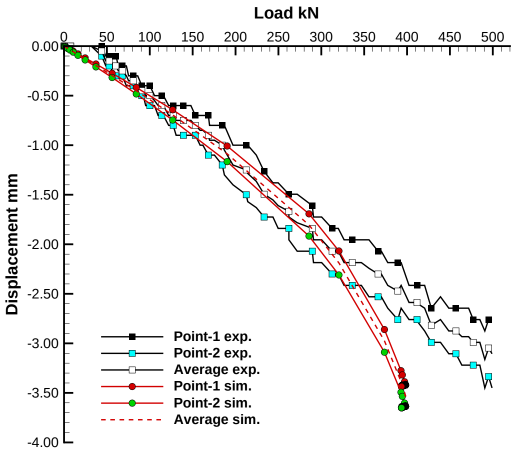

(c) R wallettes at 300 ^{o}C

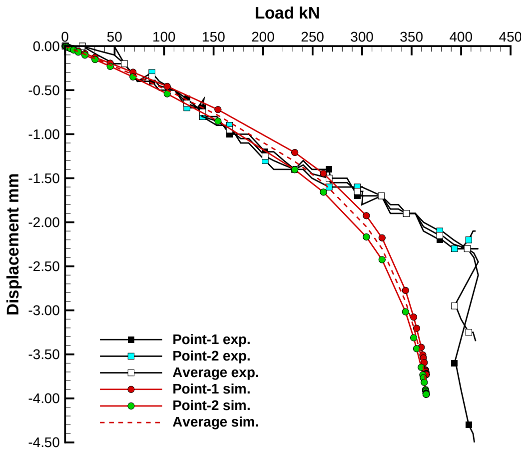

(d) M wallettes at 300^{o}C

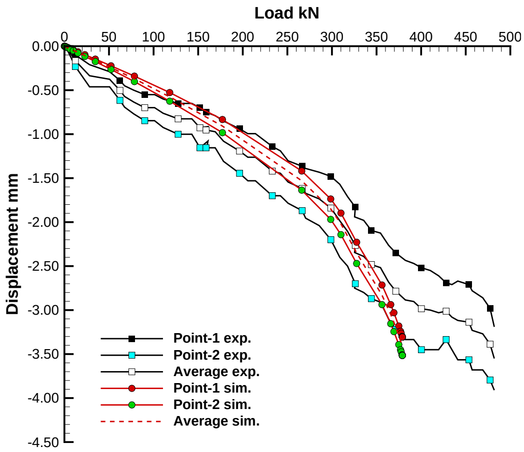

(e) M wallettes at 400^{o}C

Figure 10.13: Load-vertical displacement relationship for both types of masonry wallette samples at exposure to different temperatures

samples at exposure to different temperatures .

10.9 Pure thermal modelling of the masonry wallettes at high temperatures

The thermal model has been explained in detail using the data relating to small specimens of the different lightweight concrete mixtures at high temperatures, as presented in Chapter 6. The differences with the application of masonry wallettes are represented by two parameters: thermal action and thermal contact.

The previous thermal action described in Chapter 6 was consistent with the unidirectional heat flow regime, which implies one hot surface and another cold. The present case of masonry wallettes involved all around heat exposure, meaning that all of the wallette surfaces were hot. The boundary conditions were changed accordingly.

Since only one prism specimen was used to formulate the heat flow test in Chapter 6, the thermal model did not contain any representation of the effects of thermal contact. In reality, the mortar joints result in many thermal contact surfaces for the case of masonry wallettes exposed to high temperatures, which should be addressed in the thermal modelling.

10.9.1 Thermal action

From the beginning of the test unto reaching the steady state condition for a desired testing temperature, a transient heat transfer method was used to simulate the temperature profile of the masonry wallettes. The net heat flux which defines the thermal action consists of both radiation and convection heat transfer components. Emissivity was assumed to be a bulk material property, and was set at the same value as for the previous thermal model (0.85) (see Chapter 6). The coefficient of convection which defines the surface film condition has to be amended to be consistent with the all around hot surface state. The recommended film condition value given by BS EN 1991-1-2 [55] was taken as a benchmark for the thermal action; this was 25 W/m^{2}K. In order to improve the results, the temperature-dependent data of the film condition (h_c) was incorporated. The latter was calculated using the following equation [58]:

$$h_c = 1.32(\frac{\Delta T}{L})^{1/4} \tag{10.17}$$

where L is the thickness of the member. The above equation gave a film condition which ranged from 13 W/m^{2}K to 25 W/m^{2}K. The same approach was also used by Chow and Chan [58].

10.9.2 Thermal contact

The assembly of the wallette constituents incorporated a number of mortar joints which acted as contact surfaces. These surfaces had the same designation mentioned for the contact pairs in the structural model at ambient temperature (Section 10.3.3). As a result, the surface of the cement mortar was treated as a slave surface, while the concrete block surface was considered the master surface. In such a way, a surface to surface contact method was assigned between each contact pairs.

In order to define the properties of the aforementioned contact, the parameters of thermal conductance and radiation are required. Since the heat flux between the (solid) contact surfaces is mainly due to conduction, the radiation effect is considered to be minimal [118]. The Abaqus/Standard determines the conductive heat transfer between two surfaces using the following equation:

$$q = k(\theta_A - \theta_B) \tag{10.18}$$

where q is the heat flux per unit area crossing the interface from point A in one surface to point B on the other; θ_A and θ_B are the temperatures of the points on the surfaces; and k is the gap conductance which depends on the clearance between A and B.

To define the gap conductance, clearance values were tabulated starting from a closed gap (zero clearance) to the maximum gap. However, because the masonry wallettes were exposed to heat action first without mechanical loading in which no debonding took place, the major conductance effect was corresponding to the zero clearance value. The results obtained from the analytical simulation of the pure thermal behaviour were compared with the results of the temperature profile of the masonry wallette samples measured in Chapter 9. These results are presented in the next section.

10.10 Results and discussion of the pure thermal modelling of the masonry wallettes at high temperatures

The results of the time-temperature profiles for both the numerical simulation and experimental measurements for both wallette samples at different temperature exposure are presented in Figures 10.14a to 10.14e. It can be seen that all of the temperature profiles were adequately predicted by the numerical model. Except for points B & C and E, all of the other point temperatures were close to those measured in the experimental programme.

In the case of points B & C and E which are located on the opposite sides of the wallette (see Figure 9.3), identical temperature values were obtained for the front and back surfaces of the wallettes. This behaviour could be explained by the same coefficient of convection being assumed for all of the surfaces of the wallette sample. Indeed, the experimental measurements showed a notable variation between the temperatures of the front and back faces of the masonry wallette. This variation was mainly due to the difference in convection of the furnace when it was occupied by the wallette sample. The latter effect was not considered in the numerical model. A slight variation between the temperatures of the bed and head joints was observed in the numerical model similar to that noted in the experimental measurements.

Figures 10.15a and 10.15b show the temperature distribution thorough the head and bed joints respectively for the case of modified wallette at 200 C^o. A lower interior block temperature was observed in comparison with that of the cement mortar joint. In addition, the residual surface temperature of the concrete blocks was higher than that of the cement mortar joint. This is indicative of the higher insulation criterion of the lightweight concrete blocks used in this study, resulting from their lower thermal conductivity.

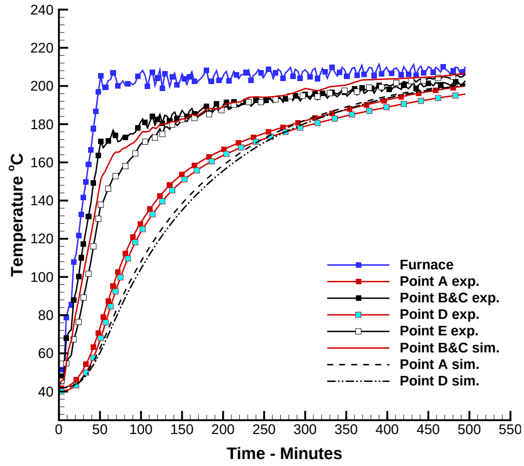

(a) R wallettes at 200 ^{o}C

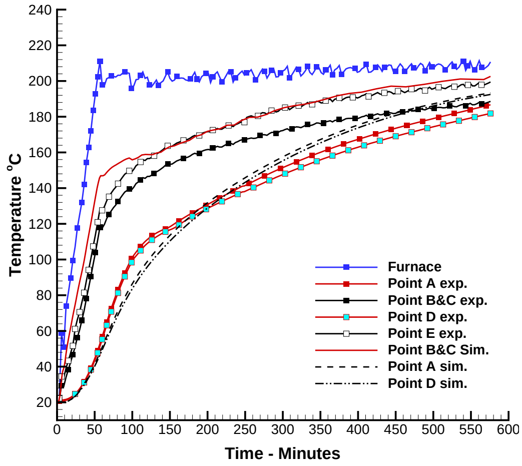

(b) M wallettes at 200^{o}C

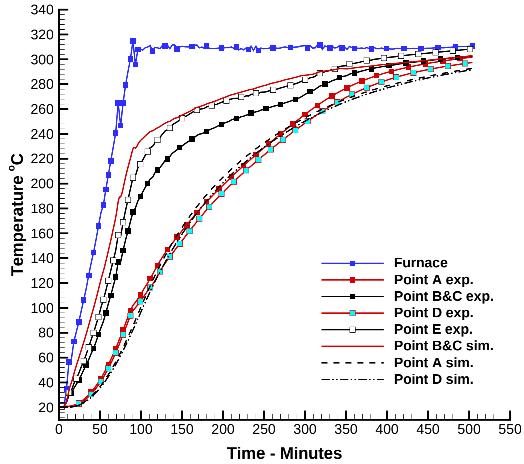

(c) R wallettes at 300 ^{o}C

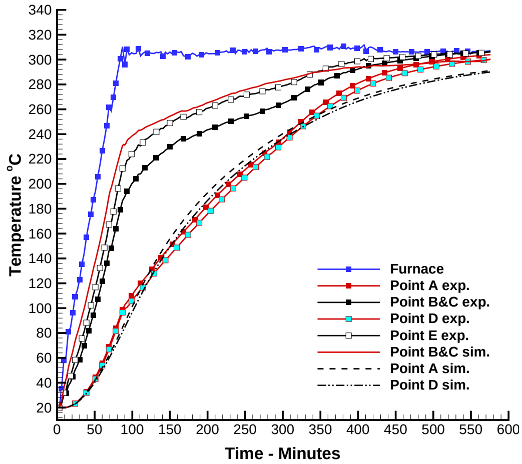

(d) M wallettes at 300^{o}C

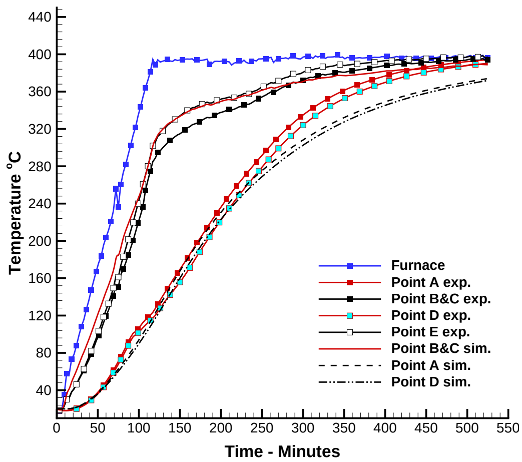

(e) M wallettes at 400^{o}C

Figure 10.14: Time-temperature profiles of both masonry wallettes at exposure to different temperatures

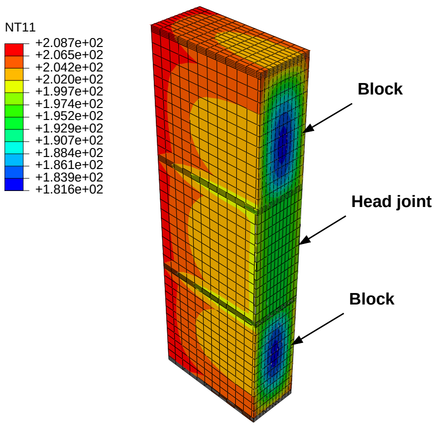

(a) Section through the head joint

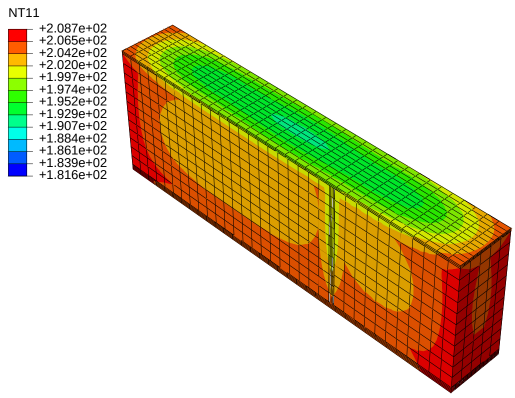

(b) Section through the bed joint

Figure 10.15: Temperature distributions (^{o}C) through the head and bed cement mortar joints

10.11 Summary

A detailed description for the developed structural and thermal finite element models of the masonry wallettes at ambient and high temperatures was presented in this chapter. Among the different constitutive modelling approaches, the detailed micro-model was selected to give an accurate numerical result in terms of the load-deformation criteria. The smeared cracking technique was inappropriate to perform the structural numerical modelling for the case of this study due to the issue of convergence. Conversely, the damage plasticity method showed a reliable prediction for this kind of modelling. The calibration study showed that the penalty stiffness has a major effect on the results of numerical simulation. This requires adjustment using a scaling factor to reflect the actual tendencies of the masonry wallettes. The appropriate scale factors for the penalty stiffness were 0.00135 and 0.0016 for the reference and optimum modified masonry wallettes respectively. Imperfections resulting from the construction of the wallette and/or applied loads had a remarkable influence on the results of the structural model. The best value was found to be one third of that recommended by BS EN Standards [65]. The medium mesh size implying $(9 \times 9 \times 4)$ elements for the full concrete block met the requirements of a compromise between computational accuracy and processing speed. By considering the material-temperature dependence and specifying the temperature value, the structural numerical model at ambient temperature can be adequately used to predict the structural behaviour of masonry wallettes at high temperatures. Development of the pure thermal model described in Chapter 6 was carried out by means of incorporating the effect of contact surfaces and thermal action on the thermal behaviour of masonry wallettes. In general, close agreement between the simulated and measured results in all cases was obtained for both structural models at ambient and high temperatures as well as the pure thermal model.

Chapter 11

Conclusions and future studies

11.1 Conclusions

This study was undertaken to evaluate the thermo-mechanical behaviour of new combinations of lightweight concrete mixes containing different percentages of recycled glass and metakaolin in conjunction with expanded clay. The structural applications of these lightweight concrete mixes as masonry walls was also evaluated under axial compression loads at ambient and high temperatures. Both experimental and numerical simulation approaches were used as part of these evaluations. The conclusions regarding the detailed objectives of this study were given at the end of their respective chapters. The main significant findings may be summarised as follows:

1. The required strength level for structural lightweight concrete can be achieved when recycled glass materials are used in conjunction with the additions of metakaolin and expanded clay aggregate.

2. The key parameter which affects the mechanical strength of the modified lightweight concrete mixes is the ratio of metakaolin to recycled glass. The increase in compressive strength is equivalent to sufficient coating the glass particles with metakaolin.

3. The metakaolin additions improved the durability of the modified lightweight concrete mixes under condition of high temperatures and the highest enhancement was seen for the concrete mix containing 10% metakaolin.

4. Significant reductions in thermal conductivity can be achieved at ambient and high temperatures when recycled glass and metakaolin are added to the composition of the reference lightweight concrete mixes. This implies a marked increase in the value of the thermal insulation criterion. The magnitude of the improvement achieved depends upon the recycled glass and metakaolin contents.

5. The optimisation analysis showed that the concrete mix of (30%G+10%MK) is the modified lightweight concrete mix which best met the requirements of using more by-product materials and improving both mechanical and thermal properties.

6. The finite element model of the thermal behaviour supported the suggestion of omitting the thermal radiation effect on the unexposed surface of the concrete sample. Conversely, the combined influence of the convection and radiation phenomena satisfied the heat transfer between the furnace environment and the exposed surface of the sample.

7. The value of the coefficient of thermal convection had the most influential role on the insulation criterion among the different investigated parameters which may affect the overall thermal behaviour.

8. Under the combined effect of axial load and high temperatures, both the reference and modified lightweight concrete mixes exhibited lower vertical displacements compared with those reported in BS EN 1996-1-2 [55] for the pumice lightweight concrete.

9. At ambient temperatures, greater load-bearing capacity was achieved by using the by-product materials in producing the modified masonry wallettes compared with the reference wallette samples. At high temperatures, minimal reduction in the value of load-bearing capacity was observed for both types of masonry wallettes.

10. In general, the failure mode of the masonry wallettes under axial compression load was due to the combined compression-shear effect, leading to splitting failure. The critical path of the progression of failure usually started from underneath the load point and passing through the concrete blocks and head joint to reach the toe of the wallette.

11. The expressions given by BS EN standards [65, 103] to predict both the characteristic compressive strength and modulus of elasticity of masonry walls require modification in order

to be applicable for use with the masonry wallettes investigated in this study.

12. Explosive spalling was observed for the reference wallette samples at 400 ^{o}C with no applied load, while the optimum modified wallettes showed a normal failure mode under the same conditions and failed under axial compression load of about 480 kN.

13. The formula suggested by BS EN 1996-1-1 [65] to predict the characteristic compressive strength of the masonry walls at ambient temperature can be adapted for use for conditions of elevated temperatures by introducing a term which accounts for the ratio of strength reduction due to exposed for such conditions.

14. Penalty stiffness and the effect of imperfections had the most influence on the results of the structural finite element model. These parameters require adjustment by means of using scale factor and an appropriate imperfection value respectively. The suitable values of scale factors for the reference and optimum modified masonry wallettes were found to be 0.00135 and 0.0016 respectively. The reliable value of imperfection effect was one third of that recommended by BS EN 1996-1-1 [65].

11.2 Future studies

Any research work is normally set out according to specific limitations; consequently the obtained outcomes will follow these conditions. As mentioned before, this study incorporated some limitations which are either related to the sake of simplification considerations or else to comply with the intended research objectives. These include ignoring the effect of mass transport of fluid and the variation of furnace convection in developing the pure thermal finite element models of the lightweight concrete samples and masonry wallettes respectively. A steady state heat transfer regime was assumed in order to evaluate the behaviour of the masonry wallettes under the combined effects of mechanical load and heat exposure; the heat exposure ranged between temperatures of 20 ^{o}C and 400 ^{o}C. On this basis, in order to obtain detailed results for the behaviour of these kinds of lightweight concrete samples and masonry wallettes, the aforementioned points should be taken into consideration.

Since this study was not previously conducted, it forms a constitutive issue for a wide scope of further research. Some relevant topics which may be undertaken in the future are summarised as follows:

1. The mechanical properties of lightweight concrete mixes were investigated at sample ages ranging from 7 to 180 days. Such an investigation is sufficient for the purposes of structural design which is usually specified by the strength value at 28 days age. However, from the viewpoint of durability, more knowledge of the long-term behaviour is required to build up a broader view of the performance of the lightweight concrete mixes developed in this study.

2. In order to develop more understanding of the physical and chemical changes associated with the addition of by-product materials and with exposure to high temperatures, a study of the microstructure is recommended.

3. Investigation of alternative materials to expanded clay to be used as a coarse aggregate in the concrete mixes, such as recycled waste brick, would be beneficial.

4. Evaluation of the thermo-mechanical behaviour of lightweight concrete mixes when finer particle size of metakaolin powder is used as a partial replacement for the Portland cement. In the extreme, such an approach might involve particles at the nano size range.

5. Extending the present study with a theoretical approach to derive some mathematical formulae for the thermal behaviour of the modified lightweight concrete samples at ambient and high temperatures.

6. Performing a comprehensive parametric study for the application of the developed structural finite element model of the masonry wallettes to evaluate different geometries and load conditions.

7. Extending the present study by deriving some theoretical approaches in order to determine the behaviour of masonry wallettes under an axial load at both ambient and high temperatures conditions.

8. Evaluation of different formulations of masonry wallettes, such as cavity and composite, with hollow lightweight concrete blocks at both ambient and high temperature conditions.

9. Investigation of the enhancement of the load-bearing capacity of masonry wallettes at ambient temperature using steel and/or plastic fibre reinforcement with different percentages.

10. Using different load considerations such as shear, bending and dynamic loads to evaluate the behaviour of developed masonry wallettes at ambient or high temperature in combination with the former load conditions.

11. Investigation of the beam-wall connection behaviour using the developed lightweight concrete at different heat exposure conditions.

12. Investigation of the behaviour of a composite steel-modified lightweight concrete structural member under an axial load and at both ambient and high temperatures.

Appendix A

Journal and conference papers

This appendix shows the first page of the journal and conference papers published/ submitted during the period of this study.

Construction and Building Materials 31 (2012) 157–167

Contents lists available at SciVerse ScienceDirect

Construction and Building Materials

journal homepage: www.elsevier.com/locate/conbuildmat

Mechanical and thermal properties of novel lightweight concrete mixtures containing recycled glass and metakaolin

Adnan Al-Sibahy *, Rodger Edwards

School of Mechanical, Aerospace and Civil Engineering, The University of Manchester, PO Box 88, Manchester M60 1QD, United Kingdom

A R T I C L E I N F O

Article history:
Received 29 August 2011
Received in revised form 12 December 2011
Accepted 23 December 2011
Available online 25 January 2012

Keywords:
Lightweight concrete
Metakaolin
Recycled glass
Expanded clay
Mechanical behaviour
Thermal behaviour

A B S T R A C T

The aim of this study was to investigate the behaviour of a new type of lightweight concrete which would be suitable for use as a load-bearing concrete masonry unit. Different ratios of by-product materials which consist of metakaolin (MK) and recycled glass were used in conjunction with expanded clay to produce the lightweight concrete mixtures. The short and long-term mechanical properties and thermal criteria were measured using a total of 208 specimens with different geometries. Some statistical analysis was conducted and the obtained results were compared with the standard expressions.

The tests results showed that it is possible to produce a structural lightweight concrete possessing good thermal properties using by-product materials. Compressive and splitting tensile strengths, as well as the modulus of elasticity, increased with an increase in the metakaolin content, whilst a counteractive behaviour was recorded for the density. Clear improvements in thermal conductivity and insulation criteria were observed in comparison with conventional lightweight concrete mixtures. The measured thermal conductivity values ranged from 0.092 W/m K to 0.177 W/m K, and the insulation criterion reached up to 110.25 min for 29 mm concrete member thickness.

1. Introduction

Huge amounts of waste glass are produced worldwide every year. Each year in the UK, households throw away over 29.1 million tonnes of waste, 4.2% of which is glass [1]. Recycling of glass therefore makes an important contribution to overall sustainability. In the case of construction, there are several options for making use of glass waste and other by-product materials in concretes.

In particular, the inclusion of crushed or ground glass in concrete mixes as an entire or partial replacement for aggregate is of growing interest. This operation reduces the demand on the natural resources for construction materials and provides multiple alternatives to the traditional ingredients of concrete mixes [2–5].

In making innovations of this nature, it is important that the mechanical properties of the concrete mixes produced are not inferior to the traditional ones. It is also important that resistance to the effects of fire and heat is not adversely affected, as this would have serious implications for safety.

Glass aggregates are granular particles with a smooth surface texture and a very low ability to absorb water. These characteristics contribute to the reduced strength of the concrete as well as reduced drying shrinkage [5–9].

There is a slight increase in the expansion of glass aggregate concrete compared with normal aggregate concrete. This is due to the alkali–silica reaction ASR [1–9]. However, this reaction can be reduced by using appropriate mineral additives with pozzolanic properties [5,9]. Previous studies [10–18] have reported that the metakaolin MK is a versatile mineral admixture which can be used to improve both strength and durability of concrete mixes.

Metakaolin is manufactured by the calcination of kaolinitic clay ($Al_2Si_2O_7$) at 650–800 °C [10–12] or the calcinations of waste sludge from the paper recycling industry [13]. It has a specific surface area about 15 times that of Portland cement with a specific gravity of 2.4 g/cm^3 [10,16]. The major role of the metakaolin material in concrete mix formulation is to reduce the amount of $Ca(OH)_2$ released during the hydration of cement. $Ca(OH)_2$ is responsible for the promotion of the alkali–silica reaction [10–18].

The use of lightweight concrete has increased sharply and its consumption grows every year on a global basis [19]. Energy can be saved in buildings by using lightweight concrete to provide improved thermal insulation and fire resistance. Lightweight concrete units have found their way into the construction market due to their many advantages, which include a reduction in building dead load, which minimises the dimensions of structural members; the production of lighter and smaller pre-cast elements with inexpensive casting, handling and transportation operations; the provision of more space due to the reduction in size of the structural members' dimensions; a reduced risk of earthquake damage and

* Corresponding author. Tel.: +44 (0)1613064250.
E-mail addresses: Adnan.hassan@postgrad.manchester.ac.uk, Adnan_flayih@yahoo.com (A. Al-Sibahy), Rodger.edwards@manchester.ac.uk (R. Edwards).

0950-0618/$ - see front matter Crown Copyright © 2011 Published by Elsevier Ltd. All rights reserved.
doi:10.1016/j.conbuildmat.2011.12.095

Construction and Building Materials 31 (2012) 174–187

Contents lists available at SciVerse ScienceDirect

Construction and Building Materials

journal homepage: www.elsevier.com/locate/conbuildmat

Thermal behaviour of novel lightweight concrete at ambient and elevated temperatures: Experimental, modelling and parametric studies

Adnan Al-Sibahy *, Rodger Edwards

School of Mechanical, Aerospace and Civil Engineering, The University of Manchester, PO Box 88, Manchester M60 1QD, United Kingdom

A R T I C L E   I N F O

Article history:
Received 16 September 2011
Received in revised form 15 December 2011
Accepted 23 December 2011
Available online 25 January 2012

Keywords:
Lightweight concrete
Metakaolin
Recycled glass
Expanded clay
Thermal properties
Fire resistance
Finite element

A B S T R A C T

This paper reports a study based upon experimental investigation and analytical simulation which assesses the behaviour of a new type of lightweight concrete at both ambient and elevated temperatures. Different ratios of by-product materials, including recycled glass and metakaolin, were used in conjunction with expanded clay to produce the lightweight concrete mixes. Their fundamental mechanical properties of compressive and splitting tensile strengths were determined at ambient temperature. In order to characterise their overall thermal behaviour, their density, thermal conductivity and specific heat characteristics were first measured at ambient and high temperatures. A heat flow test was then carried out using a unidirectional heat flow regime and the results obtained were analytically simulated in terms of the time–temperature aspect. A parametric study was conducted using a simulation model to identify the most influential factors governing the thermal behaviour of this type of concrete.

The results showed improvements in mechanical and thermal properties in comparison with conventional types of lightweight concrete. Compressive strength exceeded the value required for structural lightweight concrete by about 11%, whilst superior performance was recorded for the modified concrete mixes in terms of thermal conductivity, with percentage decreases reaching 42% at ambient temperature. The best resistance to the effects of high temperatures was observed for concrete mixes containing 15% and 30% recycled glass with 10% metakaolin. Close agreement was obtained between the simulated and measured results. The parametric study showed that the coefficient of thermal convection had the most influential role on the insulation criterion.

1. Introduction

In the event of a fire, thermal stresses play an essential role in the deterioration of concrete structures and the outcome is significantly affected by the thermal properties of the concrete being used. In order to reduce such deterioration, attention has been paid to the issue of fire protection.

Previous studies have described the physical and chemical changes in concrete when it is exposed to elevated temperatures [1–7]. Free water evaporates at around 100 °C and is completely removed at 120 °C. Above approximately 150 °C, there is a loss of the water chemically bound in hydrated calcium silicate, with a peak rate of loss at 270 °C [2,3]. The propagation of micro-cracks begins after 300 °C and mechanical strength and thermal conductivity are degraded at this stage, with some associated expansion taking place [4]. Between 400 °C and 600 °C, complete desiccation occurs and crystals of calcium hydroxide decompose into their original components (calcium oxide and water), producing weakened concrete [1]. Further decomposition of hydrated calcium silicate takes place above 600 °C, and spalling behaviour is observed. The cement paste is transformed into a glass phase above 1150 °C [2].

Spalling reduces the integrity of concrete members and may cause the complete collapse of a structure. It occurs at elevated temperatures when the pore pressure and thermal stresses exceed the tensile strength of the concrete. The most influential parameters governing this phenomenon are the permeability of the concrete and the continuity of its pore system. If the concrete has a low permeability with a close pore network, the pore pressure begins to build up. This increasing pressure produces stresses on the interior structure of the concrete. The intensity of pore pressure increases with an increase in temperature [8–12].

Because of their high density and lower permeability, high strength concrete and (to a lesser degree) normal concrete have a greater tendency toward explosive spalling than lightweight concrete [8,12,13].

One of the most effective approaches to increasing the duration of fire resistance is the use of lightweight concrete in producing structural elements [14].

* Corresponding author. Tel.: +44(0)1613064250.
E-mail addresses: Adnan_flayih@yahoo.com, Adnan.hassan@postgrad.manchester.ac.uk (A. Al-Sibahy), Rodger.edwards@manchester.ac.uk (R. Edwards).

0950-0618/$ - see front matter Crown Copyright © 2011 Published by Elsevier Ltd. All rights reserved.
doi:10.1016/j.conbuildmat.2011.12.096

Engineering Structures 48 (2013) 193–204

Contents lists available at SciVerse ScienceDirect

Engineering Structures

journal homepage: www.elsevier.com/locate/engstruct

Behaviour of masonry wallettes made from a new concrete formulation under combination of axial compression load and heat exposure: Experimental approach

Adnan Al-Sibahy *, Rodger Edwards

School of Mechanical, Aerospace and Civil Engineering, The University of Manchester, Manchester M13 9PL, United Kingdom

ARTICLE INFO

Article history:
Received 3 June 2012
Revised 24 July 2012
Accepted 13 September 2012

Keywords:
Masonry wallettes
Lightweight concrete
Metakaolin
Recycled glass
Load-bearing capacity
Thermal behaviour

ABSTRACT

This study was undertaken to evaluate the thermo-mechanical behaviour of masonry wallettes constructed using blocks made from lightweight concretes of experimental compositions under an axial compression load combined with heat exposure. A comprehensive experimental investigation was carried out on two different types of masonry wallettes at temperature levels ranging from 20 °C to 400 °C. The wallettes were produced using two types of lightweight concrete blocks, the first incorporating expanded clay and the second using by-product materials which consisted of recycled waste glass and metakaolin. The vertical deformation, load-bearing capacity and failure modes were determined experimentally. Furthermore, the modulus of elasticity was determined for both types of wallette and their constituent concrete blocks and cement mortar.

The results obtained showed that the percentage decrease in the strength of both lightweight concretes when exposed to various temperatures compared to that at ambient temperature reached almost 30%. In contrast, the cement mortar exhibited an increase in strength of approximately 20%. A significant reduction in the value of modulus of elasticity was observed for the constituents of wallette, whilst the entire masonry wallettes showed a minimal reduction for both types. Clear improvements in thermal behaviour were observed for both types of masonry wallettes. The masonry wallettes formulated using expanded clay lightweight concrete blocks exhibited failure due to explosive spalling at 400 °C with no mechanical load, whereas the second type of masonry wallettes (the modified wallettes) did not show such behaviour.

1. Introduction

In the event of a major fire, some masonry walls are exposed to heat from all sides. This eventuality poses the most serious risk of deterioration. If such an exposed wall is load-bearing, then the combined effect of load and temperature will govern its overall behaviour. To satisfy fire safety requirements, the wall should maintain its ability to provide structural support under applied loads throughout the period of exposure to heat [1,2]. In recent years, there has been an increasing interest in the issues of fire protection and enhancement of wall strength under such conditions.

Practice codes define the requirements for the behaviour of load-bearing masonry walls at high temperatures by specifying the minimum wall thickness necessary to resist the effects of fire for a specific period of time [1]. The period of fire resistance of a given wall element depends upon several parameters such as the type of masonry unit, the type of mortar, the density of the units, the type of wall construction, the slenderness ratio of the wall and the eccentricity of the load. All of these parameters are relevant to the standard fire test described in BS EN 1365-1 [3], in which the heat exposure applied to the test sample is assumed to be unidirectional in nature.

A simplified calculation model is also developed for predicting the load-bearing capacity of a wall element depending on the limit state condition. For other cases of heat exposure, the practice code [1] reported that the assessment of masonry walls should be addressed by the results of experimental tests.

Special consideration is needed when attempting to evaluate the behaviour of masonry walls under the combined effect of load and high temperatures because the complexity of the interaction between the two factors. For example, Russo and Sciarretta [4] performed an experimental investigation to evaluate the behaviour of masonry walls made from a hand-made clay bricks under effect of two temperature levels, namely 300 °C and 600 °C, for about an hour. In general, it was found that the load-bearing capacity of masonry walls decreased with increasing temperature and the intensity of deterioration became more accentuated at higher temperatures. A similar reduction was also observed for the mod-

* Corresponding author. Tel.: +44 1613064250.
E-mail addresses: Adnan.hassan@postgrad.manchester.ac.uk, Adnan_flayih@yahoo.com (A. Al-Sibahy), Rodger.edwards@manchester.ac.uk (R. Edwards).

0141-0296/$ - see front matter © 2012 Elsevier Ltd. All rights reserved.
http://dx.doi.org/10.1016/j.engstruct.2012.09.028

This paper has been submitted to the Journal of Engineering Structures

Behaviour of masonry wallettes made from a new concrete formulation under compression loads at ambient temperatures: Testing and modelling

Adnan Al-Sibahy*, Rodger Edwards

School of Mechanical, Aerospace and Civil Engineering, the University of Manchester, Manchester, M13 9PL, United Kingdom

Abstract

This paper presents an experimental investigation and analytical simulation which aim to assess the behaviour of a new type of masonry wallette under conditions of an axial compression load at ambient temperature. Two different masonry wallettes were produced using two types of lightweight concrete blocks, the first incorporating expanded clay and the second using by-product materials which consisted of recycled waste glass and metakaolin. Both vertical and lateral deformations were measured at different positions on the wallette specimens. The load-bearing capacity was also determined. The measured results obtained were compared with analytically simulated results produced by the Abaqus/Standard finite element package.

The experimental results showed that the maximum axial loads at failure were 474 kN and 558 kN for the reference and modified wallettes respectively implying corresponding bearing capacities of 7.1 MPa and 8.3 MPa. The critical path of the failure mode was similar for all of the wallettes tested and normally began underneath the load point, then passed through the concrete blocks and head joint to reach the wallette toe.

The most influential factors on the analytical model are the value of penalty stiffness and imperfect wallette construction. A close agreement between the measured and simulated results has been observed, suggesting that finite element analysis provides a reliable alternative to further laboratory measurements.

Keywords: Masonry wallettes, lightweight concrete, metakaolin, recycled glass, load-bearing capacity, finite element

---

* Corresponding author. Tel:+441613064250

Adnan.hassan@postgrad.manchester.ac.uk ; Adnan_flayih@yahoo.com (A. Al-Sibahy)

Rodger.edwards@manchester.ac.uk (R. Edwards)

SPARC / The University of Salford May 2012

Structural behaviour of new developed lightweight concrete masonry walls

Adnan Al-Sibahy and Rodger Edwards

Adnan.hassan@postgrad.manchester.ac.uk

Keywords: Masonry walls, Finite element, Structural behaviour, By-product materials

Masonry walls normally act as structural members to resist the massive floor and (in some cases) beams loads. Axial compression forces form a significant part of the total live and dead loads applied upon the masonry walls. In order to improve the bearing capacity, a new type of masonry wall was formulated using by-product materials. An appropriate experimental programme was designed to investigate the structural behaviour of two different small scale walls (wallettes) produced with developed lightweight concrete blocks. Both vertical and lateral deformations were measured at different positions. The results obtained were analytically simulated using the Abaqus/Standard finite element package.

The result showed that the maximum axial loads at failure were 474 kN and 558 kN for the reference and optimum modified wallettes respectively, which imply corresponding bearing capacity of 7.1 MPa and 8.3 MPa. The critical path of the failure mode was approximately similar for all tested wallettes and normally starts from underneath the load point and passing through the concrete blocks and head joint to reach the wallette toe. The most influential factors on the analytical model are the value of penalty stiffness, imperfect wallette construction and mesh size. Close agreement between the measured and simulated results has been observed. These findings have important implications for enhancing the strength of masonry walls and mitigating the effect of waste materials.

Structural behaviour of new masonry lightweight concrete wallettes at high temperatures

Adnan Al-Sibahy, Rodger Edwards
Adnan.Hassan@postgrad.manchester.ac.uk

Introduction

In fire situations, thermal stresses play an essential role in the deterioration of concrete structures and the outcome is significantly affected by the thermal properties of the concrete being used. To reduce such deterioration, attention has been paid to the issue of fire protection. One of the most effective approaches to increasing the duration of fire resistance is the use of lightweight concrete in producing structural elements.

The most common application for the lightweight concrete units is the construction of masonry walls. In the case of fire action, masonry may involve both structural contribution and separation function or be restricted to fulfil the separation role only. This study deals with the first section which intended to support the applied loads and providing the insulation criterion.

Despite much attention being paid in improving the thermo-mechanical behaviour of construction materials at ambient and high temperatures, qualify the effects of using by-product materials in lightweight concrete masonry units needs more research. In this study a new type of lightweight concrete unit was experimentally evaluated in terms of thermo-mechanical properties and its structural behaviour as a masonry wallettes was then measured and analytically simulated using the finite element approach.

Description of Research

Two types of lightweight concrete blocks were produced using different percentages of by-product materials including recycled glass, metakaolin and/or expanded clay. The first set of concrete blocks were referred as ''modified'', while the second set were so-called ''reference''. In order to characterise overall thermal behaviour of concrete blocks, their modulus of elasticity, density, thermal conductivity and specific heat characteristics were first measured at ambient and high temperatures. The thermo-structural response of axially loaded masonry wallettes was then measured. The wallettes dimensions were 670 × 685 mm constructed with three courses. Each course contains one and a half solid lightweight concrete block. The deformations due to the axial compression loads were measured at five points, as indicated in Figure1. In case of elevated temperature, a steady state with all around heat exposure regime was followed. A detailed nonlinear micro-modelling scenario was used to simulate the masonry structure. The unit-mortar interface stiffness was calculated using the following Equation.

$$k = \frac{P_f A^2}{V} K$$

Where P_f is a penalty stiffness factor and K is the bulk modulus of elasticity.

Description of Industrial Relevance/Impact

Improvements in both thermal and load-bearing characteristics were achieved when recycled glass and metakaolin materials in conjunction with expanded clay are partially replacing the traditional ingredients of concrete. The maximum load at failure of the modified wallettes was around 55 Tonnes at ambient temperature. The thermal conductivity reached about 0.1 W/m.K .Good resistance to heat, at test temperature up to 400^0C was observed for the modified masonry wallettes which failed under 45 Tonnes compression load, as shown in Figure 3.On the other hand, reference masonry wallettes showed type of explosive spalling at 400^0C without supporting any mechanical load, as show in Figure 4. Close agreement between the measured and simulated results at ambient temperature have been observed, as shown in Figures 5 and 6.

31st Cement and Concrete Science Conference **Paper Number: PP8**
Novel Developments and Innovation in Cementitious Materials
12-13 September 2011
Imperial College London, United Kingdom

Thermo-mechanical behaviour of a new combination of lightweight aggregate concrete mixtures

Adnan Al-Sibahy and Rodger Edwards
School of Aerospace, Mechanical and Civil Engineering, the University of Manchester

ABSTRACT

This paper summarizes the results of an experimental investigation of the thermo-mechanical behaviour of a newly developed lightweight concrete. The essential objective was to improve both thermal properties and achieve the increased strength in structural lightweight concrete. The main components of the lightweight concrete mixes were expanded clay as a coarse aggregate, two ratios of metakaolin MK material (5% and 10%) as a partial replacement for the Portland cement and three ratios of recycled waste glass (15% , 30% and 45%) as a partial replacement for the natural sand. Mechanical and thermal measurements were conducted to evaluate the overall behaviour of the lightweight concretes produced.
The results obtained show that it is possible to produce structural lightweight concrete possessing good thermal properties using by product materials. Adding the metakaolin improves the compressive strength and unit weight of the concrete mixes. The compressive strength increases with an increase in the metakaolin content, while a counteractive behaviour was recorded for the unit weight aspect. Clear improvements in thermal conductivity and insulation properties have been observed compared with other conventional concrete materials. The measured thermal conductivity values ranged from 0.092 W/m.K to 0.177 W/m.K, while the insulation criterion reached up to 110.25 minutes for 29 mm concrete member thickness.

1. INTRODUCTION

In recent years, there has been an increasing interest in improving the thermo-mechanical properties of lightweight concrete. Improvements to the strength and, in a parallel pathway, thermal insulation criterion are the major keys to improving the performance of lightweight concrete. The strength characteristic represents the load bearing capacity of concrete to support the applied load.
Whilst, the insulation criterion refers to the ability of structural element to maintain its separation function when it is subjected to elevated temperatures (BS/EN1996-1-2, 2005).
The orientation mentioned above has also associated with environmental aspects in the construction processes. From that point, the idea of environmental friendly construction has grown up during the last few decades.
Due to the negative effect of waste glass and their existence with massive amounts in the worldwide every year, crushed or ground glass aggregate is an effective environmental re-use such materials. The general properties of glass aggregates are granular particle shape, smooth surface texture and very low tendency to absorb mixing water. These characteristics produce a dry consistency and lower strength concrete mix. Further, there is a slight increase in alkali–silica reaction of glass aggregate concrete compared with the normal concrete. However, this reaction can be overcome by using mineral by product materials like metakaolin MK in the mixtures (Miao L., 2011 and Chen CH, et al, 2006).
The physical and chemical changes in concrete when it is exposed to elevated temperatures are described in many studies, for example (Md A. and Y. Wang, 2011 and K. D. Hertz, 2005).Free water evaporates at around 100˚C and it is completely removed at 120˚C. Above approximately 150˚C, loss of the chemically bound water of hydrated calcium silicate takes place with a local peak at 270˚C. Propagation of micro-cracks begins after 300˚C. At this stage mechanical strength and thermal conductivity are degraded, with some associated expansion. Between 400˚C to 600˚C, complete desiccation occurs, and crystals of calcium hydroxide decompose into the original components. Further decomposition of hydrated calcium silicate takes place above 600˚C with spalling behaviour observed.
The spalling phenomenon at elevated temperatures reduces the integrity of concrete members, and may cause an entire collapse of a structure. It occurs when the pore pressure and thermal stresses exceed the tensile strength of concrete. The most influential parameters governing the spalling phenomenon are the permeability of concrete, the continuity of the pores system and moisture content (Faris A., et al., 2010 and Samir N. Shoukry, et al., 2011).
Although recent developments in field of construction materials have emphasized the importance of improving thermo-mechanical behaviour of concrete elements, it has heightened the need for more research in this aspect. In this study, a new type of lightweight concrete has been produced using by product materials and then experimentally evaluated in terms thermo-mechanical behaviour.

Computational Methods and Experimental Measurements XV 85

Mechanical behaviour of high metakaolin lightweight aggregate concrete

A. Al-Sibahy and R. Edwards
Department of Mechanical, Aerospace and Civil Engineering, University of Manchester, UK.

Abstract

The work described in this paper forms part of a much larger investigation of the behaviour of a new developed type of lightweight aggregate concrete which would be suitable for use as a load bearing concrete masonry units. The experimental work investigated the effect of high metakaolin (MK) content on the mechanical behaviour of newly modified lightweight aggregate concrete.15% metakaolin and waste glass were used as a partial replacement for both ordinary Portland cement and natural sand. A medium grade expanded clay type Techni Clay was used as a coarse aggregate in the concrete mixes. Equal amounts of waste glass with particles sizes of 0.5-1 and 1-2 mm were used throughout this study. Unit weight, compressive and splitting tensile strengths were measured at various ages in accordance to the relevant British/ EN standards. Fresh concrete properties were observed to justify the workability aspect. An assessment was carried out to indentify the pozzolanic activity of metakaolin material. The tests results were compared with the obtained results of controlled and lower metakaolin contents concretes which were previously studied. The tests results showed that metakaolin material had an explicit role in improving the strength and unit weight of modified lightweight concrete mixes. Compressive and splitting tensile strengths increase with an increase in the metakaolin content, while a counteractive behaviour was recorded for the unit weight aspect. The metakaolin material showed higher pozzolanic activity which was overcame the reduction of compressive strength due to the negative effect of glass aggregate. However, the workability of concrete mixes degraded at higher metakaolin inclusion.

Keywords: lightweight aggregate concrete, metakaolin, waste glass, mechanical behaviour.

A new method of producing lightweight aggregate concrete

Adnan Al-Sibahy

Adnan.hassan@postgrad.manchester.ac.uk

This study investigated the possibility of developing a new type of lightweight aggregate concrete which would be suitable for use as a load bearing concrete. The research work proposed a lightweight concrete containing an aggregate made from a process by product material. It was proposed to use expanded clay as a coarse aggregate and recycled waste glass aggregate as a partial replacement to the natural sand with ratios of 15%, 30% and 45%. Metakaolin material was used as a partial replacement to Portland cement with ratios of 5% and 10%. The density and compressive strength of this type of concrete was investigated in accordance with the relevant BS EN standards. A total of 84 cube specimens were tested to measure the fundamental properties at ages of 7 and 28 days.

The results revealed that all density and compressive strength values lie within the range appropriate for structural lightweight concrete. The use of recycled waste glass aggregate decreased the density of concrete mixes and increased the compressive strength at the later ages. Metakaolin material had explicit role in improving the strength and reduction the density of concrete.

References

[1] Kayali O. Fly ash lightweight aggregates in high performance concrete. *Construction and Building Materials*, 22:2293–2399, 2008.

[2] Rita N. and Zsuzsanna J. Strength of lightweight glass aggregate concrete. *Material in Civil Engineering*, 5(18):710–714, 2006.

[3] Unal O., Uygunoglu T., and Yildiz A. Investigation of properties of low-strength lightweight concrete for thermal insulation. *Building and Environment*, 42(2):584–590, 2007.

[4] http://www.bis.gov.uk/analysis/statistics/construction-statistics/building-materials. 2012.

[5] Neville A. *Properties of concrete*. Pearson Education Limited, Edinburgh: England, 4th edition, 2002.

[6] Petrella A., Petrella M., Boghetich G., Petruzzelli D., Calabrese D., Stefanizzi P., Napoli D., and Guastamacchia M. Recycled waste glass as aggregate for lightweight concrete. *Proceedings of the ICE -Construction Materials*, 160(4):165–170, 2007.

[7] http://www.recycle-more.co.uk/nav/page2129.aspx. 2012.

[8] Chi S.L., Chi S. P., and Dixon C. Enhancing the performance of pre-cast concrete blocks by incorporating waste glass-ASR consideration. *Cement and Concrete Composites*, 29:616–625, 2007.

[9] Miao L. Incorporating ground glass in self- compacting concrete. *Construction and Building Materials*, 25:919–925, 2011.

[10] Parande A., Chitradevi R. H., Thangavel K., Karthikeyan M. S., Ganesh B., and Palaniswamy N. Metakaolin: a versatile material to enhance the durability of concrete an overview. *Structural concrete*, 7(1):125–138, 2009.

[11] Siddique R. and Klaus J. Influence of metakaolin on the properties of mortar and concrete: A review. *Applied Clay Science*, 34(3):392–400, 2009.

[12] Dong O., Weiting X., Tommy Y. L., and Janet F.C. S. Increasing mortar strength with the use of activated kaolin by products from paper industry. *Construction and Building Materials*, 25:1537–1545, 2011.

[13] Al-Sibahy A. and Edwards R. Mechanical and thermal properties of novel lightweight concrete mixtures containing recycled glass and metakaolin. *Construction and Building Materials*, 31:157–167, 2012.

[14] Al-Sibahy A. and Edwards R. *Mechanical behaviour of high metakaolin lightweight concrete mixtures*. International Conference of Computational Methods and Experimental Measurements XV. Wessex Institute of Technology, May 2011.

[15] Al-Sibahy A. and Edwards R. Thermal behaviour of novel lightweight concrete at ambient and elevated temperatures: Experimental, modelling and parametric studies. *Construction and Building Materials*, 31:174–187, 2012.

[16] Al-Sibahy A. and Edwards R. *Thermo-mechanical behaviour of new combination of lightweight aggregate concrete mixtures*. 31st Cement and Concrete science Conference (Novel Developments and Innovations in Cementitious Materials), September 2011.

[17] Al-Sibahy A. and Edwards R. *Structural behaviour of new masonry lightweight concrete wallettes at high temperatures*. Postgraduate Research Conference. The University of Manchester, December 2012.

[18] Al-Sibahy A. and Edwards R. *Structural behaviour of new developed lightweight concrete masonry walls*. 12th SPARC Conference. The University of Salford, May 2012.

[19] Al-Sibahy A. and Edwards R. Behaviour of masonry wallettes made from a new concrete formulation under combination of axial compression load and heat exposure: experimental approach. *Engineering Structures*, 48:193–204, 2013.

[20] Teychenne' D.C., Franklin R.E., and Erntroy H.C. *Design of normal concrete mixes*. Building Research Establishment Ltd, Garston:Watford, 2th edition, 1988.

[21] Chen H.J., Yen T., Lia T.P., and Huang Y.L. Determination of the dividing strength and its relation to the concrete strength in lightweight aggregate concrete. *Cement and Concrete Composites*, 21:29–37, 1999.

[22] Miled K., Sab K., and Roy R. L. Particle size effect on EPS lightweight concrete compressive strength: Experimental investigation and modelling. *Mechanics of Materials*, 39:222–240, 2007.

[23] Ke Y., Beaucour A.L., Ortola S., Dumontet H., and Cabrillac R. Influence of volume fraction and characteristics of lightweight aggregates on the mechanical properties of concrete. *Construction and Building Materials*, 23(8):2821–2828, 2009.

[24] Tommy Y.L., Tang W.C., and Cui H.Z. The effects of aggregate properties on lightweight concrete. *Construction and Building Materials*, 42:3025–3029, 2007.

[25] Rossignolo J. A., Agnesini M. V.C, and Morais J. A. Properties of high-performance lwac for precast structures with brazilian lightweight aggregates. *Cement and Concrete Composites*, 25:77–82, 2003.

[26] Smadi M. and Migdady E. Properties of high strength tuff lightweight aggregate concrete. *Cement and Concrete Composites*, 13(2):129–135, 1991.

[27] Limbachiya M.C. Bulk engineering and durability properties of washed glass sand concrete. *Construction and Building Materials*, 23:1078–1083, 2009.

[28] Ismail Z. and Al-Hashmi E. Recycling of waste glass as a partial replacement for fine aggregate in concrete. *Waste Management*, 29:655–659, 2009.

[29] DD 249:1999. *Testing aggregates-Method for the assessment of alkali-silica reactivity - Potential accelerated mortar-bar method*. British Standards, 2011.

[30] Xie Z., Xiang W., and Xi Y. ASR potentials of glass aggregate in water-glass activated fly ash and portland cement mortars. *Material in Civil Engineering*, 15(1):67–74, 2003.

[31] Maraghechi A., Shafaatian S.M.H., Fischer G., and Rajabipour F. The role of residual cracks on alkali silica reactivity of recycled glass aggregates. *Cement and Concrete Composites*, 34:41–47, 2012.

[32] Ganesh K. and Dinakar P. Strength efficiency of metakaolin in concrete. *Structural Concret*, 7(1):27–31, 2006.

[33] Paulo C., Ana L. V., and Fernando R. Effect of Portuguese metakaolin on the hydraulic lime concrete using different curing conditions. *Construction and Building Materials*, 24:71–78, 2010.

[34] Wild S., Khatib J.M., and Jones A. Relative strength, pozzolanic activity and cement hydration in superplasticised metakaolin concrete. *Cement and Concrete Research*, 26(10):1537–1544, 1996.

[35] Vejmelkova K., Pavlikova M., Keppert M., Kersner Z., Rovnankova P., Ondracek M., Sedlmajer M., and Cerny R. High performance concrete with Czech metakaolin: Experimental analysis of strength, toughness and durability characteristics. *Construction and Building Materials*, 24:1404–1411, 2010.

[36] Batis G. and Pantazopoulou P. The effect of metakaolin on the corrosion behavior of cement mortars. *Cement and Concrete Composies*, 27:125–130, 2005.

[37] Kim H.S., Lee S. H., and Moon H. Y. Strength properties and durability aspects of high strength concrete using korean metakaolin. *Construction and Building Materials*, 21:1229–1237, 2007.

[38] Justice J., Kennison L.H., Mohr B.J., and Wiggins B. Zhang Z.Z. Kurtis K.E. Beckwith S.L., McCormick L.E. *Comparison of two Metakaolins and a silica fume used as supplementary cementituous materials*. Seventh International Symposiumon Utilization of High strength/ High performance concrete-Washington D.C, 2005.

[39] Demirboga R. and Gul R. The effects of expanded perlite aggregate, silica fume and fly ash on the thermal conductivity of lightweight concrete. *Cement and Concrete Research*, 33(5):723–727, 2003.

[40] Demir I. and Serhat B. M. effect of silica fume and expanded perlite addition on the technical properties of the fly ash lime- gypsum mixture. *Construction and Building Materials*, 26:1299–1304, 2008.

[41] Demirbas A. A discussion of the paper:the effects of expanded perlite aggregate, silica fume and fly ash on the thermal conductivity of lightweight concrete by Ramazan Demirboga and Rustem Gul. *Cement and Concrete Research*, 34(4):725–725, 2004.

[42] Othuman M.A and Wang Y.C. Elevated temperature thermal properties of lightweight foamed concrete. *Construction and Building Materials*, 25:705–716, 2011.

[43] Hertz K. D. Concrete strength for fire safety design. *Magazine of Concrete Research*, 25(8):445–453, 2005.

[44] Formosa J., Chimenos J.M., Lacasta A.M., Haurie L., and Rosell J.R. Novel fire-protecting mortars formulated with magnesium by-products. *Cement and Concrete Research*, 41:191–196, 2011.

[45] Kong F.K., Evans R. H., Cohen E., and Roll F. *Handbook of structural concrete*. Pitman Books Limited: London, 1983.

[46] BS EN 1992:1-2 Eurocode 2. *Design of concretestructures. General rules - structural fire design*. British Standards, 2004.

[47] Tanyildizi H. and Coskun A. The effect of high temperature on compressive strength and splitting tensile strength of structural lightweight concrete containing fly ash. *Construction and Building Materials*, 22(11):2269–2275, 2008.

[48] Sullivan P. and Labani J. Flexural behaviour of plain and reinforced lightweight aggregate concrete beams up to 600 ^{o}C. *Cement and Concrete Research*, 4:231–237, 1974.

[49] Fletcher I. A., Welch S., Torero J. L., Carvel R. O., and Usmani A. Behaviour of concrete structures in fire. *Thermal Science*, 11:37–52, 2007.

[50] Bailey C. Holistic behaviour of concrete buildings in fire. *Structures and Buildings*, 152(3):199–212, 2002.

[51] Malhotra H.L. *Spalling of concrete in fires*. Construction Industrial Research and Information Association (CIRIA), 1984.

[52] Khoury G. and Anderberg Y. *Concrete spalling review*. Fire Safety Design AB (FSD), Swedish National Road Administration, 2000.

[53] Ali F.A., Connolly R., and Sullivan P. J. E. Spalling of high strength concrete at elevated temperatures. *Applied Fire Science*, 6(1):3–14, 1996.

[54] Kodur V.K.R. and Phan L. Critical factors governing the fire performance of high strength concrete system. *Fire Safety Journal*, 42:482–488, 2007.

[55] BS EN 1996-1-2 Eurocode 6. *Design of masonry structures: Part 1-2: General rules structural fire design*. British Standards, 2005.

[56] Abaqus 6.10. *Abaqus Analysis User's Manual*, volume 2. Simulia, 2010.

[57] Incropera F. P. and DeWitt D. P. *Fundamental of heat and mass transfer.* John Wiely Sons: New York 61-68, 5 edition, 2002.

[58] Chow W. K. and Chan Y.Y. Computer simulation of the thermal fire resistance of building materials and structure elements. *Construction and Building Materials*, 10:131–140, 1996.

[59] BS 476-20. *Fire tests on building materials and structures. Method for determination of the fire resistance of elements of construction (general principles)*. British Standards, 1987.

[60] OConnor D.J., Silcock G.W.H., and Morris B. Furnace heat transfer process applied to a strategy for the fire testing of reduced scale structural models. *Fire Safety Journal*, 27:1–22, 1996.

[61] Oliveira D. V. *Experimental and numerical analysis of blocky masonry structures under cyclic loading*. PhD thesis, The University of Minho, 2003.

[62] Drysdale R. G. and Hamid A. A. *Masonry structures behavior and design*. The Masonry Society, 3rd edition, 2008.

[63] Hendry A. W., Sinha B.P., and Davies S.R. *Design of masonry structures*. E and FN Spon, an imprint of Chapman, London, UK, 3 th edition.

[64] Nguyen T., Meftah F., Chammas R., and Mebarki A. The behaviour of masonry walls subjected to fire: Modelling and parametrical studies in the case of hollow burnt-clay bricks. *Fire Safety Journal*, 44:629–641, 2009.

[65] BS EN 1996-1-1 Eurocode 6. *Design of masonry structures: Part 1-1: Common rules for reinforced and unreinforced masonry structures*. British Standards, 2005.

[66] Phipps M. E, Mirza S.A., Bell A. J., Fettit G.J.L., Ormesher M., and Lewis N.G. Characteristic compressive strength of concrete block masonry. *The Structural Engineer*, 23/24:31–38, 2001.

[67] Ruvalcaba F. *Mechanical properties and structural behaviour of masonry at elevated temperatures*. PhD thesis, The University of Manchester, 2010.

[68] Brencich A. and Felice G. D. Brickwork under eccentric compression: Experimental results and macroscopic models. *Construction and Building Materials*, 23:1935–1946, 2009.

[69] Lourenco P.B., Vasconcelos G., Medeiros P., and Gouveia J. Vertically perforated clay brick masonry for loadbearing and non-loadbearing masonry walls. *Construction and Building Materials*, 24:2317–2330, 2010.

[70] BS EN 1363-1. *Fire resistance test-part 1: general requirements*. British Standards, 1999.

[71] Russo S. and Sciarretta F. Experimental and theoretical investigation on masonry after high temperature exposure. *Experimental Mechanics*, 52:341–359, 2012.

[72] Lourenco P.B. *Computational strategies for masonry structures*. PhD thesis, The University of Proto, 1996.

[73] Gabor A.and Ferrier E., Jacquelin E., and Hamelin P. Analysis and modelling of the in-plane shear behaviour of hollow brick masonry panels. *Construction and Building Materials*, 20:308–321, 2006.

[74] Sandoval C., Roca P., Bernat E., and Gil L. Testing and numerical modelling of buckling failure of masonry walls. *Construction and Building Materials*, 25(12):4394–4402, 2011.

[75] Abaqus 6.10. *Abaqus Analysis User's Manual*, volume III. Simulia, 2010.

[76] Mohsin E. *Support stiffness effect on tall load bearing masonry walls*. PhD thesis, The University of Alberta, 2005.

[77] EN BS 197-1. *Cement, Part 1: Compositions, specification and conformity criteria for common cements*. British Standards, 2000.

[78] http://www.plasmor.co.uk/html/company/expanded-clay. *technical paper, 8-5R medium grade*, 2011.

[79] http://www.specialistaggregates.com. 2011.

[80] http://www.whitchem.co.uk/adhesives.htm. technical paper of metastar 501. 2011.

[81] BS EN 206-1. *Concrete: Specification, performance, production and conformity*. British Standards, 2000.

[82] Chandra S. and Berntsson L. *Lightweight aggregate concrete Science, Technology, and Applications*. William Andrew Publishing. Norwich, New York: U.S.A, 1st edition, 2000.

[83] BS EN 5075-3. *Concrete admixture, Part 3: Specifications for superplasticizer admixture*. British Standards, 1985.

[84] BS EN 12390-1. *Testing hardened concrete, Part 1: Shape, dimensions and other requirements for specimens and moulds*. British Standards, 2000.

[85] BS EN 12390-2. *Making and curing specimens for strength test*. British Standards, 2009.

[86] BS EN 12390-7. *Testing hardened concrete, Part 7: Density of hardened concrete*. British Standards, 2009.

[87] BS EN 12390-3. *Testing hardened concrete, Part 3: Compressive strength of test specimens*. British Standards, 2009.

[88] BS EN 12390-6. *Testing hardened concrete, Part 6: Splitting tensile strength of test specimens*. British Standards, 2009.

[89] BS ISO 1920-10. *Testing of concrete, Part 10: Determination of static modulus of elasticity*. British Standards, 2009.

[90] Courard L., Darimont A., Schouterden M., Ferauche F., Willem X., and Degeimbre R. Durability of mortars modified with metakaolin. *Cement and Concrete Research*, 23:473–1479, 2003.

[91] BS EN 1992-1-1. *Eurocode 2: Design of concrete structures: Part 1-1: General rules and rules for buildings*. British Standards, 2004.

[92] Qian X. and Li Z. The relationships between stress and strain for high-performance concrete with metakaolin. *Cement and Concrete Research*, 31:1607–1611, 2001.

[93] Demirel B. and Kelestemur O. Effect of elevated temperature on the mechanical properties of concrete produced with finely ground pumice and silica fume. *Fire Safety Journal*, 45:385–391, 2010.

[94] BS EN 993-15. *Methods of test for dense shaped refractory products, Part 15: Determination of thermal conductivity by the hot wire (parallel) method*. British Standards, 2005.

[95] Borhan T. M. Properties of glass concrete reinforced with short basalt fibre. *Materials and Design*, 42:265–271, 2012.

[96] http://www.tpl.fpv.ukf.sk/engl$_v ers/hot_w ire.htm.$ 2011.

[97] Abaqus 6.10. *Abaqus Analysis User's Manual*, volume IV. Simulia, 2010.

[98] BS EN 1991-1-2. *Eurocode 1: Actions on structures: Part 1-2: General actions-actions on structures exposed to fire.* British Standards, 2002.

[99] Viskanta R. and Grosh R.J. Effect of surface emissivity on heat transfer by simultaneous conduction and radiation. *International Journal of Heat and Mass Transfer*, 5(8):729–739, 1962.

[100] BS 6073-1. *Precast concrete masonry units: Part 1: Specification for precast of concrete masonry units.* British Standards, 1981.

[101] BS EN 771-3. *Specification for masonry units Part 3: Aggregate concrete masonry units (dense and light-weight aggregates).* British Standards, 2003.

[102] BS EN 772-1. *Methods of test for masonry units: Part 1: Determination of compressive strength.* British Standards, 2000.

[103] BS 5628-1. *Code of practice for the use of masonry: Part 1: Structural use of unreinforced masonry.* British Standards, 2005.

[104] BS EN 1052-1. *Methods of test for masonry: Part 1: Determination of compressive strength.* British Standards, 1999.

[105] Ali S. and Page A. W. Concentrated loads on solid masonry walls- a parametric study and design recommendations. *Instn Civ. Engrs*, 2(85):271–289, 1989.

[106] BS EN1365-1. *Fire resistance tests for loadbearing elements: Part 1: walls.* British Standards, 1999.

[107] BS EN 1094-1. *Insulating refractory products: Part 1: Terminology, classification and methods of test for high temperature insulation wool products.* British Standards, 2008.

[108] Shoukry S. N., William G.W., Downie B., and Riad M.Y. Effect of moisture and temperature on the mechanical properties of concrete. *Construction and Building Materials*, 25:688–696, 2008.

[109] Poon C-S., Azhar S., Anson M., and Wong Y.L. Comparison of the strength and durability performance of normal- and high-strength pozzolanic concretes at elevated temperatures. *Cement and Concrete Research*, 31(9):1291–1300, 2011.

[110] Nadjai A., O'Garra M., Ali F. A., and Laverty D. A numerical model for the behaviour of masonry under elevated temperatures. *Fire and Materials*, 27:163–182, 2003.

[111] Nadjai A., O'Garra M., and Ali F. A. Finite element modelling of compartment masonry walls in fire. *Computers and Structures*, 81:1923–1930, 2003.

[112] Aydn S. and Baradan B. Effect of pumice and fly ash incorporation on high temperature resistance of cement based mortars. *Cement and Concrete Research*, 37(6):988–995, 2001.

[113] Aydn S., Yazc H., and Baradan B. High temperature resistance of normal strength and autoclaved high strength mortars incorporated polypropylene and steel fibers. *Construction and Building Materials*, 22(4):504–512, 2008.

[114] Heo Y.-S., Jay G., Sanjayan J. G., Han C.-G., and Han M.-C. Relationship between inter-aggregate spacing and the optimum fiber length for spalling protection of concrete in fire. *Cement and Concrete Research*, 42:549–557, 2012.

[115] Abdullah A. *Analysis of Repaired/Strengthened R.C. Structures Using Composite Materials: Punching Shear*. PhD. Thesis, The University of Manchester, 2010.

[116] Hillerborg A., Modeer M., and Peterson P.E. Analysis of crack formation and crack growth in concrete by means of fracture mechanics and finite elements. *Cement and Concrete Research*, 6(6):773–782, 1976.

[117] CEB. *RC elements under cyclic loading*. 1996.

[118] Abaqus 6.10. *Abaqus Analysis User's Manual*, volume V. Simulia, 2010.

[119] Burnett S., Gilbert M., Molyneaux T., Beattie G., and Hobbs B. The performance of unreinforced masonry walls subjected to low-velocity impacts: Finite element analysis. *International Journal of Impact Engineering*, 36:1433–1450, 2007.

[120] Porto F. D., Guidi G., Garbin E., and Modena C. In-plane behaviour of clay masonry walls: Experimental testing and finite-element modelling. *Journal of Structural Engineering*, 136(11):1379–1392, 2010.

[121] Senthivel R. and Lourenco P.B. Finite element modelling of deformation characteristics of historical stone masonry walls. *Engineering Structures*, 31:1930–1943, 2009.

[122] Rots J.G. *Structural masonry: an experimental/ numerical basis for practical design rules*. Rotterdam, 1997.